UNIVERSITY OF
KWAZULU-NATAL

School of Chemical Engineering
Howard College Campus
Durban

PRODUCTION AND HIGH TEMPERATURE TREATMENT OF SYNGAS

By:

Martin Francis Botha

BScEng (Chemical)

March 2010

Abstract

Gas cleaning is an essential step in many chemical processes. The reason for cleaning is to remove components that can damage equipment or inhibit further reactions. The treatment can include the removal of particulates, removal of one or more chemical species, or the conversion of one species to another. The gases include natural gases, combustion gases or synthesis gas (syngas).

Of particular importance is the hot gas desulphurization (HGD) of syngas after gasification. This method of treatment offers potential energy and raw material savings to traditional 'wet' gas cleaning methods, such as physical or chemical absorption.

Syngas is a valuable intermediate product because it can be processed into a number of different chemicals. These range from hydrocarbon chains (Fischer-Tropsch reactions), methanol, and ammonia (from hydrogen in the syngas). Methanol and ammonia are important raw materials to produce other chemicals. Syngas can be used for production of electricity via gas turbines in an Integrated Gasification Combined Cycle (IGCC) plant.

In this study, a laboratory scale gasification and desulphurization unit was designed and constructed for removal of hydrogen sulphide (H_2S) from syngas. The gasifier operates at moderately high temperature (700-900 °C) and low pressure (1-3 bar g) to produce syngas containing H_2S (1-6 mol %) from a liquid hydrocarbon fuel mixture and oxygen. Desulphurization occurs in a fixed bed isothermal reactor (300-600 °C) whereby H_2S is removed by chemical reaction with a sorbent. The fuel used was a mixture of methanol and *i*-propanethiol and the sorbent chosen was zinc oxide.

The apparatus was tested to obtain a reliable experimental method. A series of experiments were conducted to determine two results: Firstly, to see the performance of the unit during repeated sorbent testing (i.e. a systematic experimental run programme). Secondly, to determine the effect of some process variables (temperature, flowrate and particle size) on the conversion of sorbent.

GC analysis of the syngas showed consistent gas composition during the experiment, an important result which justifies this new method of syngas production from a liquid fuel. The final conversions from ZnO to ZnS ranged from 2-12 mole %. However, there was some variation under repeated conditions, which showed the need for additional method development.

~ Statement of Authorship ~

The work presented in this dissertation was undertaken at the School of Chemical Engineering, University of KwaZulu-Natal, Howard College Campus in Durban, South Africa, from February 2008 until December 2009.

The work was supervised by Professor Milan Carsky.

This dissertation represents the full requirement for the degree of Master of Science in Engineering (Chemical).

All work presented is this dissertation is original unless otherwise stated. It has neither in whole nor part been submitted previously to any other University or Institute as part of a degree.

_____

Martin Francis Botha

As the candidate's supervisor, I have approved this dissertation for submission.

_____

Professor Milan Carsky

~ *Acknowledgements* ~

Technically

- Professor Milan Carsky, for his dedicated help, guidance and faith.
- Professor Mathew Starzak, for his help with the reactor modelling and discussions on optimization.
- Doctoral student, Mr David Lokhat, for invaluable advice on the GC operation and general help in laboratory.
- Mr Kevin Wickee, for his help with the GC installation, modifications and operation.
- Mr James Wesley-Smith and Ms Sharon Eggers at Electron Microscope Unit at UKZN for helping me to use the scanning electron microscope.
- The UKZN School of Chemical Engineering workshop team: In particular Mr Les Henwood for discussions on the design of the reactors and Danny, Mr Ken Jack, Mr Kelly Robertson, Patrick and Elliot and Mrs Rekha Maharaj and Mr Sadha Naidoo.

Financially

- The National Research Foundation (NRF)
- ESKOM

Personally

- Professor Milan Carsky, for providing many new opportunities to make my post-graduate experience at UKZN really worth all the long, lonely hours in the laboratory. This included some external work on thermal engineering design, being taken to two conferences in Johannesburg and Somerset West and a visit to the Czech Academy of Sciences in Prague.

- My father and mother, Paul and Kieran, and my sister Caitlin, for their faith and tolerance of the 'reactor' and 'engineering' jargon. They always provided support and patience that I may not have noticed at the time, but certainly helped me to continually be moving forward.

- The staff and students at UKZN. In particular, Mrs Niri Naidu for chats in the office and my office companion Ms Letšabisa Lerotholi for her advice and encouragement.

- Professor Peter Leach, for continual encouragement and suggestions. His positive attitude about everything is inspiring.

- Mr Mike Oliver, for the opportunity of real engineering design work and mentoring.

Always remember to *Carpe Diem*.

Table of Contents

List of Figures

List of Tables

Nomenclature

Symbol	Definition	Dimension
a_{ik}	number of atoms of *k* per molecule species *i*	[-]
A_g	surface area of grain	m^2
A_p	surface area of pellet	m^2
b	stoichiometric coefficient of gas gas solid reaction	[-]
C_{Ab}	concentration of gaseous reactant *A* in bulk gas stream	$mol.m^{-3}$
C_{Cb}	concentration of gaseous product *C* in bulk gas stream	$mol.m^{-3}$
C_{H_2S}	molar concentration of H_2S in gas	$mol.cm^{-3}$
C_B^o	molar concentration of ZnO solid (initial)	$mol.cm^{-3}$
D_{AB}	diffusion coefficient: solute *A* in solvent *B*	$m^2.s^{-1}$
D_c	diffusion coefficient: combined	$m^2.s^{-1}$
D_e	diffusion coefficient: effective	$m^2.s^{-1}$
D_K	diffusion coefficient: Knudsen	$m^2.s^{-1}$
E_a	activation energy	kJ.mol-1
F_g	grain factor: equal to 1, 2 or 3 for a slab, cylinder or sphere	[-]
F_p	particle factor: equal to 1, 2 or 3 for a slab, cylinder or sphere	[-]
g_{fp}	grain function defined by Equation (5.10)	[-]
$\Delta G_{f,i}^o$	Gibbs energy of formation of component *i*	$J.mol^{-1}$
ΔG_{rxn}^o	Gibbs energy of reaction at standard conditions	$J.mol^{-1}$
$GHSV$	gas hourly space velocity	hr^{-1}
ΔH_{rxn}^o	standard heat of reaction	$kJ.mol^{-1}$
HHV	higher heating value	$kJ.kg^{-1}$
k_0	frequency factor	$m.s^{-1}$
k_g	mass transfer coefficient	$m.s^{-1}$
k_s	surface reaction rate constant	$m.s^{-1}$
K_E	equilibrium constant	[-]
L	characteristic length	m
m	reaction order with respect to ZnO	[-]
$\dot{m}_f$	fuel feed flow	$kg.s^{-1}$
m_{tot}	total mass at end of experiment	g
m_{ZnO}	mass of ZnO at start of experiment	g
M_{ZnO}	molar mass of ZnO	$g.mol^{-1}$
M_{ZnS}	molar mass of ZnS	$g.mol^{-1}$
n	reaction order with respect to H_2S	[-]

Symbol	Definition	Dimension
n_0	moles total system at start	mol
N_A	single particle reaction rate of *A*	mol.s^{-1}
N_B	single particle reaction rate of *B*	mol.s^{-1}
n_{H_2S}	molar flow of H_2S	mol.min^{-1}
n_{i0}	moles component *i* at start	mol
$n_{i\text{-}p}$	molar flowrate of *i*-propanethiol	mol.min^{-1}
n_B^o	moles of solid *B*, initial	mol
n_B	moles of solid *B*, final	mol
N_{Re}	Reynolds number	[-]
N_{Sc}	Schmidt number	[-]
N_{Sh}	Sherwood number	[-]
p_{fp}	particle function defined by Equation (5.11)	[-]
P	pressure	atm
P^o	standard pressure (1 atm)	atm
P_d	delivery power	kW
Q	volumetric flowrate at temperature *T*	m^3.min^{-1}
Q_{STP}	volumetric flowrate at standard conditions	m^3.min^{-1}
R_0	initial molar reaction rate of ZnS formation	mol.cm^{-2}.s^{-1}
R	radius of spherical particle	m
R_C	radius of reacted core	m
R_g	gas constant	J.mol^{-1}.K^{-1}
SV	space velocity	hr^{-1}
t	time of reaction	min
t^*	dimensionless time, defined by Equation (5.12)	[-]
T	temperature	K
u	superficial fluid velocity	m.s^{-1}
$\bar{u}$	mean molecular velocity	m.s^{-1}
V	reactor volume	m^3
V_g	volume of grain	m^3
V_{inj}	volume of sample injected into GC	m^3
V_p	volume of solid (non-porous) spherical particle	m^3
X	conversion of solid	[-]
y	mole fraction of H_2O and H_2S in gas phase	[-]
Z	compressibility factor	[-]
Z_v	ratio: molar volume of the product formed to the molar volume of the reactant	[-]
ε_b	porosity of pellet	[-]
ε_j	extent of reaction *j*	mol

Symbol	Definition	Dimension
$\beta(X)$	conversion function, defined by Equation (A.6.23)	$m^3.mol^{-1}.s^{-1}$
$\Gamma(X)$	conversion function, defined by Equation (5.19)	[-]
ε_p	particle porosity	[-]
η	thermal efficiency	%
κ	constant, defined by Equation (5.16)	$m^3.mol^{-1}.s^{-1}$
λ_k	Lagrange multiplier for element *k* of total *E* elements, defined by Equation (A.1.5)	$J.mol^{-1}$
μ	fluid viscosity	Pa.s
ξ	constant, defined by Equation (5.21)	$mol.m^{-4}.s^{-1}$
ρ_c	molar density of the pore-free solid reactant (crystalline density)	$mol.m^{-3}$
ρ_p	molar density of a particle (including pores)	$mol.m^{-3}$
σ	reaction modulus, defined by Equation (5.8)	[-]
$\hat{\sigma}$	reaction modulus, defined by Equation (5.8)	[-]
$\hat{\sigma}_s$	'shrinking core ' reaction modulus, defined by Equation (5.7)	[-]
τ	space time	hr
τ_p	particle tortuosity	[-]
τ_R	time for complete reaction	s
υ_i	stoichiometric coefficient of component *i*	[-]
$\upsilon_{i,j}$	stoichiometric coefficient of component *i* in reaction *j* of *R* total reactions	[-]
υ_j	overall stoichiometric coefficient for reaction *j*	[-]
φ_i	fugacity coefficient of *i*	[-]

Chapter 1

Introduction

1. A brief background to syngas treatment

Gasification is one of the most important chemical engineering processes in the world. The reason for this grand statement is that the gasification process takes an energy containing raw material, such as coal, and converts it (by reaction at high temperatures) into a more useful form of energy, or type of fuel, or into chemicals. This is achieved by reacting the product gases (named synthesis gas or 'syngas') to form hydrocarbon fuels (alkanes and alcohols), or hydrogen, or even to produce electricity. The chemical products are also important raw materials for other chemicals, such as ammonia from hydrogen.

The syngas consists of hydrogen and carbon monoxide as its major components. Traditionally this was formally defined as H_2 to CO in a ratio of 2:1, but over the years this definition has been 'relaxed' to be any product gas mixture from a gasification reaction.

Before processing the raw syngas, the gas must be cleaned of impurities present from the original fuel source. One of the treatment steps is the removal of hydrogen sulphide, H_2S. It is an unavoidable product of gasification reactions involving any fuel source that contains sulphur. Practically, this means all fuel sources: coal, natural gas, oils and biomass. It is the amount of sulphur present in a specific fuel that varies.

The three primary reasons for H_2S removal via a gas treatment step are:

- Poisoning of catalysts in downstream gas reactors: H_2S present in very small concentrations (<10 ppm) can cause deactivation of catalytic sites.
- Corrosion of process equipment: H_2S is highly corrosive, especially in the presence of water.
- Controlling the sulphur emissions: for environmental compliance. The emissions are usually as SO_2 after combustion.

Each reason by its own right justifies the gas cleaning step, as each situation simply cannot be accepted from a chemical processing perspective.

Modern chemical plants strive for the most efficient use of raw materials and energy to process their chemical products. On full scale plants, small improvements to reduce both chemical and energy consumption translate into large savings, not just on a financial level, but on the ever important environmental level. For example, reducing energy consumption reduces fossil fuel consumption and hence carbon dioxide emissions during electricity generation.

The most widely used 'traditional' approach to H_2S removal is by absorption (chemical or physical) in a solvent. It has been shown that for certain applications, the removal of H_2S by reaction at high temperatures has significant advantages over the absorption processes. These will be detailed in due course.

2. Area of research

This dissertation presents a study into the gas-solid reaction of H_2S and a metal oxide, namely zinc oxide, at high temperature to remove the H_2S from a syngas mixture and hence treat the syngas. It must be stressed that this was a non-catalytic reaction and note that unless specified, the term 'desulphurization' is to be understood as H_2S removal.

3. Importance of the study

The increased capability of computers over the last two decades has brought engineers a tool for complex calculations and simulations. Fluid mechanics, heat and mass transfer, multiphase reacting systems can be modelling and solved with relative ease. However, the models cannot replace the value of accurate experimental data. In addition, the data may always be used as a basis to check the simulation results.

This study develops working equipment to carry out experiments into the characteristics of the gas-solid reaction of H_2S-ZnO. The effects of process conditions on a sorbent's performance in an industrially representative environment were investigated. Performance is understood to be the conversion of the zinc oxide to zinc sulphide and the corresponding outlet concentration of H_2S as a function of time.

The apparatus was versatile enough to simulate a variety of different conditions. The results could be supplied to industry (where applicable) or used for testing and evaluating new technology such as new sorbents. As mentioned, small improvements in reaction engineering can translate into significant savings on large plants.

4. Objectives of the study

The primary objectives of the study were:

- Design and construct apparatus, at a laboratory scale, for production of syngas with H_2S and subsequent desulphurization
- Develop an experimental method for the operation of the apparatus
- Develop an experimental programme and conduct experiments to investigate optimal conditions for desulphurization

One novel feature of this study was to use liquid hydrocarbons as a fuel source for gasification. To the author's best knowledge, this method of laboratory syngas production had not been reported in literature. Thus the secondary objectives were:

- Evaluate the method of syngas production from liquids
- Investigate methods for syngas gas composition analysis
- Investigate the modelling of gas-solid reactions

5. Scope of the study

There has been significant research into H_2S-metal oxide gas-solid reactions where the reaction has been with a single solid particle. There has been less research into gas-solid reactions in a packed or fluidized bed, especially with a bed diameter greater than 1 cm. There has been even less research where the desulphurization reaction has been preceded by a gasification step, as occurs in industry.

This study has *not* been concerned with the reaction as a part of a *process*. This means that other operations such as regeneration of the solid, final treatment of the sulphur species as a gas and the integration of the units (such as heat exchangers and other gas treatment steps) at a process level were not considered.

Most researchers have investigated the effects of process variables (temperature, pressure, particle size etc.); however, there has been limited investigation into their interaction effects, i.e. if one process variable (such as temperature) dominates the system's performance. This implies the importance of an analysis of the interaction effects.

This study has excluded single particle reaction analysis. This means that accurate data (for rate constants, mass transfer coefficients and effective diffusivity) cannot be directly measured. In addition, this study has been constrained to one type of sorbent (namely pure zinc oxide) and low pressures of below 1.5 bar (absolute).

Lastly the study has not examined either the preparation of the sorbent or its regeneration after the reaction. While the importance of each is discussed, it has not been included in the experimental work.

6. Outline of the dissertation

The project was divided into four general phases:

- Research of the topic: literature review and the theoretical background, covered in Chapters 2 to 5.
- Design and procurement of the equipment: covered in Chapters 6 and 7
- Commissioning of the equipment: covered in Chapters 8 and 9
- A formal experimental programme: covered in Chapters 8 and 9

These phases did overlap, but they had individual aims to achieve before progressing to the next step. The discussion of each phase forms the basis of this dissertation.

With the research step, the goal was to find out how to build such apparatus in the laboratory. This included operating conditions, raw materials, construction materials, experimental variables and a procedure. The important results that other researchers have obtained were noted and, significantly, areas where there has been less focus were identified. This may provide scope for some new developments.

This naturally lead to the equipment design and construction to physically perform the reaction under controlled conditions. The commissioning of the equipment also included the development of an experimental method. Lastly, the experimentation programme was aimed at testing the apparatus over an extended time and allowed for some work into optimisation of the reactor.

Chapter 2

Literature Review: Gasification

1. Introduction

In 1812, Westminster Bridge in London was lit by a gas produced from coal. By 1826, gas plants had been built for street lighting in New York and Boston. By 1875, gas was available for domestic lighting. By the early 1900s, the gas was used to manufacture chemicals and even hydrogen. By 2000, there are over 468 industrial 'gasifiers' in current operation with many being designed or constructed. But what is this 'gas' and why is it so important nearly 200 years later?

The 'gas' described above was some mixture of combustible components, primarily methane, hydrogen and carbon monoxide. The above instances were taken from Rezaiyan and Cheremisinoff (2005). The process of gasification took a feedstock containing some form of hydrocarbons and converted it into these combustible gases.

More formally, the gasification process is a reaction of a carbonaceous material (mostly containing compounds with the elements C, H, O, S, N) in an environment that converts the material to a gas mixture of H_2, CO, CO_2, CH_4, H_2O, H_2S, COS, N_2, NH_3 and HCN. This occurs at high temperatures (>600 °C), and may involve injections of air, oxygen or steam. Note that the process is not combustion, where the material would be reacted with *excess* oxygen to form combustion products of CO_2, H_2O, SO_2, SO_3, NO and NO_2.

Today, gasification is a major industrial process used in a variety of applications. In a world that is facing both an energy and an environmental crisis, the imperative to use the available energy resources more efficiently is an ever-increasing challenge for chemical engineers. The gasification process provides some key solutions, as discussed below.

2. Industrial applications and advantages

The reason for the major development of gasification is that the product gases can be used in a variety of applications. Traditionally, the name of the 'syngas' was given to a gas mixture consisting of H_2 and CO in a ratio of 2:1. This has been relaxed over time and syngas is any gas mixture resulting from gasification.

The main fuel sources for gasification are:

- Natural gas
- Coal
- Petroleum coke
- Biomass
- Organic wastes

Each fuel source would have a specific composition of C, H, O, S and N. The remainder would be inorganic elements such as rocks or salts which would form an ash when gasified.

From a reaction viewpoint, the gasification process 'breaks down' the feedstock into simpler compounds, i.e. the syngas. The energy required for the conversion comes from the partial combustion of some of the feed. These components, notably H_2 and CO, still have a high energy content which can be subsequently utilised.

There are two general options for syngas processing: energy production or chemical production. With energy, the gas would be combusted in a gas turbine to produce electricity. Compared to combustion, it is possible to achieve a higher efficiency, since higher combustion temperatures can be reached and steam is not necessarily used as a working fluid. With chemical production, syngas can be made into many chemicals, which in turn are building blocks for others. This includes the production of liquid fuels. Some chemical products have been given in Figure 2.1.

Syngas can be classified into four classes, determined by the gasifier system configuration, fuel, gasification agent and operating conditions. These are shown in Table 2.1.

Another advantage of gasification is the ability to use 'waste' products from other processes (as opposed to incineration of the waste). This includes agricultural wastes, municipal wastes and biomass. Some fuels are simply not suited for direct combustion, such as those with a high moisture contact and low carbon content. Instead, they could be converted into combustible gas (i.e. syngas).

Lastly, emissions of sulphur and nitrogen could be significantly reduced. The reason is that syngas must be treated to remove these components before further processing of the gas. Hence, the final gas released is generally free of, or at least contains very little, sulphur and nitrogen components. It is also possible to recover sulphur as pure sulphur or produce sulphuric acid.

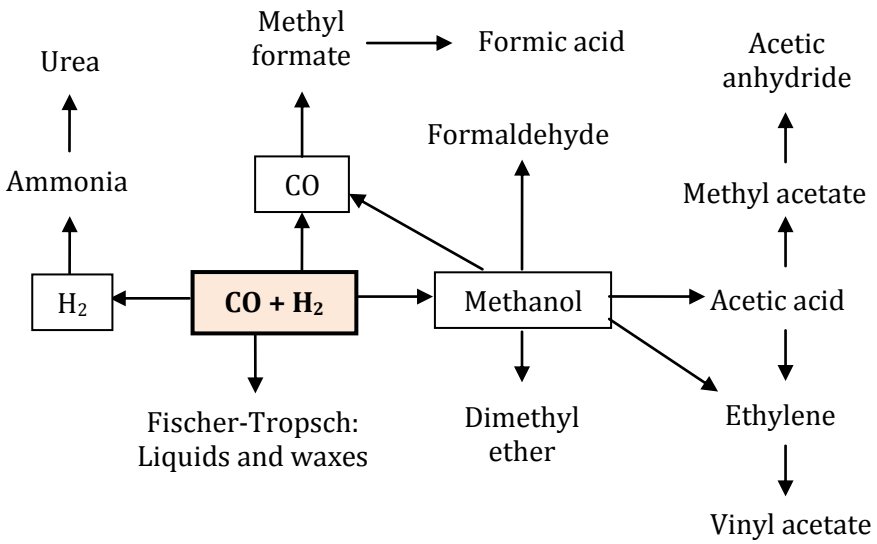

Figure 2.1: Some chemical products from syngas, adapted from Wender (1996)

Table 2.1: Types of syngas and their applications, adapted from Rezaiyan and Cheremisinoff (2005)

Type	**Energy content / MJ.m^{-3}**	**Application**	**Gasification Agent**
Low heating value gas	3.5 - 10	Gas turbine fuel (IGCC). Boiler fuel for steam. Fuel for smelting and iron ore reduction.	Air Air and steam
Medium heating value gas	10 - 20	Gas turbine fuel (IGCC). Hydrogen production. Chemical and fuel synthesis.	Oxygen and steam
High heating value gas	20 - 35	Gas turbine fuel (IGCC). Hydrogen production. Fuel cell feed. Chemical and fuel synthesis.	
Synthetic natural gas (SNG)	> 35	Natural gas replacement. Hydrogen and chemical production. Fuel cell feed.	Hydrogen and hydrogenation

A recent industrial development has been the Integrated Gasification Combined Cycle (IGCC) power plant, described briefly in Wender (1996) and Engelbrecht *et al.* (2008). Here, syngas is combusted in a gas turbine to produce electricity. The hot combustion product gas is subsequently sent to a waste heat boiler to create steam. This is then used in steam turbine to produce electricity again. The IGCC plant offers significant improvements in power plant efficiencies. However, they are more expensive to construct.

The thermal efficiency η of a power plant is defined by Equation (2.1):

$$\eta[\%] = \frac{P_d}{\dot{m}_f \times HHV} \times 100 \qquad (2.1)$$

η	thermal efficiency	[%]
P_d	delivery power	[kW]
HHV	higher heating value [1]	[kJ.kg^{-1}]
$\dot{m}_f$	fuel feed flow (usually coal)	[kg.s^{-1}]

Engelbrecht *et al.* (2008) give some recent figures for the thermal efficiency of power plants:

Traditional Coal Power:	33-38 %
Ultra super critical pulverised coal combustion:	45-47 %
IGCC:	45-55 %

These efficiencies are in accordance with figures from Cal *et al.* (2000 a). They report that current IGCC plants operate with an efficiency of about 43 % compared to a maximum of 35 % for conventional coal-fired power plants. "With improved gas turbine technology and high temperature coal gas cleanup, efficiencies exceeding 50 % are possible". This refers to changing from "cold gas cleanup at temperatures of 100-150 °C" to hot gas cleanup at 400-650 °C for on overall improvement of about 3 % in thermal efficiency.

3. Types of gasifiers

There are a variety of types of gasifiers. Their design depends primarily upon the type of feed (for example, coal, natural gas, biomass etc.) and the desired syngas composition (for example, H_2 rich syngas).

It is important to understand how the technology works in order to apply/improve it in further applications. This forms the basis for constructing of a bench scaled based gasifier for this study. The following information is taken from Nowacki (1981), McKendry (2002) and Rezaiyan and Cheremisinoff (2005) and describes common gasification processes.

Fixed Bed Gasifiers: Here, the reactive gases pass in a co- or counter-current flow to the solids. These are also known as up draft and down draft gasifiers, respectively, or a generic term "moving bed" gasifier. The name "fixed bed" is used as the bed is essentially stationary compared to the higher gas flowrate. In general, counter-current gasifiers are predominant.

Coal enters from the top of the reactor, and as it flows downward it passes through different zones: drying, devolatilization, gasification, combustion and finally the ash bed. Air or oxygen

[1] The higher heating value is the heat of combustion with all components at a reference of 25 °C, where water is a *liquid* product of the reaction.

and steam are added at appropriate points. The top exit gas temperature is about 420-650 °C, and the combustion zone is about 925-1425 °C.

Advantages include a high thermal efficiency, a long residence time (thus high carbon conversion) and it is an established technology. The disadvantages include low capacity (limited gas flow rates), a specific size of coal particles and the low temperature reaction results in a more complex gas cleanup.

Commercial units: British Gas/Lurgi (BGL), Lurgi, BHEL.

Fluidized Bed Gasifiers: A stationary bed of coal is lifted by gasifying agents moving through the bed, expanding the bed to cause random particle movement and thus excellent gas-solid mixing. Characteristics include: smaller sized coal and higher temperatures (815-1040 °C) compared to the fixed bed. The reactor is almost isothermal with temperature variations of less than 50 °C. These gasifiers can handle higher coal feed rates than fixed beds, although there is more solid carryover (entrainment). There is less tar and soot production, but more unreacted carbon in the ash. Current developments include the circulating fluidized bed gasifiers, where the solids are carried by the gas into large cyclones, and returned via standpipes.

Commercial units: High Temperature Winkler (HTW) Process, Integrated Drying Gasification Combined Cycle (IDGCC), Kellog Rust Westinghouse (KRW). Circulating fluidized beds: KBR Transport reactor, Foster Wheeler.

Entrained Bed Gasifiers: Here, the coal particles are carried (entrained) by the reactant gases, as opposed to being fixed (moving bed) or suspended (fluidised bed). This has the highest capacity per unit volume of all gasifiers. Reactants enter co-currently at high velocity through nozzles known as burners. The reactions occur at high temperatures of 1200-1500 °C, with exit gas at 350-700 °C depending on the process. The ash is usually removed as a liquid, as slag. The high temperatures require a higher use of oxygen, meaning more CO_2 is produced. In addition, the gasifier requires advanced control systems and very small particles.

Commercial units: Hitachi, Shell Coal Gasification Process (SCGP), Mitsubishi Heavy Industries (MHI), Texaco (now GE Energy), Koppers Totzek, Babcock Borsig Power (BBP), E-Gas, Siemens, Conoco Phillips.

Table 2.2: Comparison of gasifier types, adapted from Rezaiyan and Cheremisinoff (2005)

	Moving Bed	**Fluidized Bed**	**Entrained Bed**
Exit gas temperature (°C)	420-650	920-1050	350 – 700 °C
Coal feed size	< 50 mm	< 6 mm	< 100 mesh
Ash conditions	Dry/slagging	Dry/agglomerating	Slagging

4. Modelling of gasification processes

The modelling of gasification processes is very complicated. There are a number of different reactions at different parts of the gasifier. There are heat and mass transport phenomena and flow patterns (that depend on reactor geometry) to account for and the solid particle characterisation. Models, for example, for fixed-bed coal gasification, have been published (Hobbs *et al*. 1992).

The composition of the exit gas depends upon the following:

- Feedstock
  - Composition
  - Preparation
  - Particle size
- Reactor type
  - Flow geometry
  - Feed type: slurry / dry
  - Heat transfer system: direct / indirect
  - Mineral removal system: dry ash / slag
  - Temperature and pressure
- Residence time
- Syngas cleanup system

The complete gasifier reactor modelling was outside the scope of this study.

4.1 Typical gasification reactions

The gasification reactions are endothermic. The heat required for them to occur comes from the combustion of some of the fuel. The typical gasification reactions are given in Table 2.3, where the primary reactions are given by an asterisk, *.

The oxygen added to the gasifier is for the combustion reactions. General reaction trends are as follows (from equilibrium considerations, refer to Figure 7.7 and 7.14 in Chapter 7).

- CH_4 formation decreases with increasing temperature.
- CH_4 formation increases with increasing pressure.

- CO and H_2 formation increases with increasing temperature.

- CO_2 formation decreases (sharply) with increasing temperature.
- CO_2 formation increases with increasing pressure.

- Reducing oxygen/steam ratio: increases H_2 and CH_4 formation.
- Increasing oxygen/steam ratio: increases CO and CO_2 formation.

Table 2.3: Typical gasification reactions

Reaction	**Name**	**$\Delta H°_{rxn}$ / kJ.mol^{-1}**	**Comment**
$C + O_2 \rightarrow CO_2$	Combustion	- 393.7	Provides heat for drying solid, breaking chemical bonds, maintain reaction temperature.
$C + ½O_2 \rightarrow CO$	Incomplete combustion	- 110.6	
$H_2 + ½O_2 \rightarrow H_2O$	Combustion	- 285.8	
$C + H_2O \rightarrow CO + H_2$	* Water-gas	131.4	Principle gasification reactions favoured by high temperature and low pressure.
$C + 2H_2O \rightarrow CO_2 + 2H_2$	* Water-gas	90.3	
$C + CO_2 \rightarrow 2CO$	* Boudouard	283.1	Relatively slow.
$CO + H_2O \rightarrow H_2 + CO_2$	* Water-gas shift	- 41.1	Allows for adjustment of H2/CO ratio.
$C + 2H_2 \rightarrow CH_4$	* Methanation	-74.5	Slow at low temperatures.
$CO + 3H_2 \rightarrow CH_4 + H_2O$	* Methanation	-205.8	

More recently, biomass gasification has been investigated in detail. Biomass is more difficult to characterise than coal or natural gas since it can consist of a wide variety of materials, such as wood, crops, paper, rice husks, almond shells, municipal wastes and bagasse. Hence, it is usually described by ultimate analysis, i.e. the mass percent of each element (C, H, O, N and S) on a dry basis (excluding the water content), and the higher heating value (HHV).

4.2 Equilibrium models for predicting syngas composition

The use of equilibrium models has been investigated, whereby the composition of the fuel has been used to predict the syngas composition. The principle of the method is that at equilibrium, the total Gibbs free energy of the system is at a minimum value. From a mass balance, it is thus possible to calculate the composition subject to this constraint.

This has application for this study because the treatment of the feed would be set in terms of chemical composition. However, a key difference is that with biomass, the feeds are solids, or at least in slurry form. Hence there is some sort of residue left over after gasification. In this study, the feed was to be liquid and it was anticipated that very little solid residue would remain.

The model works on the thermodynamic principle that at equilibrium, the total Gibbs Energy of a system is at a minimum value. Please refer to the Appendix, Section A.1 for a more detailed review of the thermodynamics theory. The principle advantage is that the mass balance can be solved, subject to the minimization criterion, without a knowledge of the actual reactions. However, all the product species must be known and the reactor conditions (temperature and pressure) must be set.

Ruggiero and Manfrida (1999) presented a very simple equilibrium model based upon Gibbs energy minimization method. It was tested against different fluidized beds and an entrained bed, with a total of 4 data sets. The results varied from good agreement (2-4 mol %) with some poor agreement (with maximum absolute difference of 15 mole %).

Zainal *et al*. (2001) used equilibrium modelling in a downdraft gasifier using wood as a fuel. They presented a detailed computation scheme and reported that the predicted values compared "reasonably well" with experimental data. The maximum composition error was a 6 mol % over-estimate of H_2. However, general agreement was within 4 mol %.

Li *et al*. (2001) considered five elements (C, H, O, N and S) with 44 different species in the gas and solid phase. They introduced a kinetically modified equilibrium model and included carbon formation boundaries on C-H-O ternary diagrams as a function of temperature. Their results were good with comparison to 8 operating conditions of a circulating fluidized bed reactor, with a mean error of 16.6 %. The error was defined as $\Sigma(y_{eq} - y_{exp})^2$. From their information, the gas had a mean residence time of about 1 second under STP conditions.

Altafini *et al*. (2003) note that the application of equilibrium models was especially good at high temperatures above 1500 K (1227 °C). However, it was commented that perhaps at temperatures less than 1000 K (727 °C) kinetic theory would be better suited to describe the reactions. However, their equilibrium model gave fairly good results compared to experiments at 800 °C in a fixed-bed downdraft gasifier with sawdust as the fuel. The model over-predicting the H_2 mole percent by 6 % and under-predicting CH_4 by 2.5 %.

Melgar *et al*. (2007) extended the chemical equilibrium model to include thermo-chemical processes. They use an energy balance to predict the outlet gas temperature. There was excellent agreement (less than 1 mol % error) with experimental data from the gasification of rubber wood.

The conclusions here were that the equilibrium models would:

- Provide a reasonable indication of syngas composition
- Indicate general trends, for example, the influence of temperature, pressure, feed composition.
- Not require complicated rate data that would be dependent upon the reactant type and reactor conditions.

However, a major piece of information that was missing from the studies was some reference to the gasifiers' residence times. In other words, when model data was compared to experimental data, a discussion of how closely the gasifier operated to the "equilibrium point" was not examined. The reasonable agreement between the data sets suggested that the answer was that operation was fairly close to the equilibrium point.

The criteria for assuming thermodynamic equilibrium were:

- The residence time of the reactants was high enough to 'reach' chemical equilibrium.
- Ideal gas behaviour (which is reasonable at high temperature and low pressure)
- The influence of chemical structure in favouring a specific reaction pathway towards a specific component (i.e. a reaction mechanism) was ignored.
- All carbon was gasified: no formation of charcoal as pure C.

An interesting paper was published by Kuramochi *et al*. (2005) where they examined the predicted behaviour of H_2S and HCl released during the gasification of residual biomass fuels, using equilibrium models. Their results showed the distribution of sulphides as a function of temperature. The important result was that for temperatures above 1023 K (750 °C), H_2S was greater than 95 % and COS typically less than 5 % of all the sulphur components.

5. Gasification in the laboratory

Gasification on a laboratory scale is rather unusual. Research is typically conducted on 'pilot plant' scale. The reason for this is mainly due to the feedstock, which is usually coal or biomass. Since the feeds were large particle sizes, the equipment should be larger, with higher gas flows and solids handling. There were many gasification experiments in the literature with coal and biomass gasification. The ones detailed below are to give an indication for fuel flow rate and operating conditions.

Cook *et al*. (1992) detail their studies into gasification and desulphurization. Their apparatus, located at GE Corporate Research and Development in New York, had a fixed bed air blown gasifier followed by a moving bed desulphurization reactor. The feed was coal at 816 $kg.hr^{-1}$ and 19.3 barg at 538-621 °C. This was certainly not laboratory sized. This was an important study because it combined both gasification and hot gas desulphurization in the pilot plant.

Gil *et al*. (1997) used a fluidized bed gasifier, 15 cm diameter, and 3.2 m high. It was fed with pine wood chips (flow rates of 5-20 $kg.hr^{-1}$), at bed temperatures of 780-890 °C and atmospheric pressure. The pilot plant was at the University of Saragossa, Spain.

Lucas *et al.* (2003) worked on a batch, fixed bed gasifier with 12 mm diameter wood pellets (12 mm in diameter). The total mass was 20 kg per run. The temperature gasifier varied during the reaction from 600-1100 °C at atmospheric pressure.

Engelbrecht *et al*. (2008) used the fluidized bed pilot plant gasifier at the CSIR, which was reactor 0.2 m square (area 0.04 m^2). The bed height was 0.6 m. The coal feed was 20 – 30 $kg.hr^{-1}$ with particle sizes of 5 mm. Gasification was at 900-950 °C and at atmospheric pressure. Krameiter *et al*. (2008) performed experiments using a fixed bed, twin fired gasifier with wood chips as a fuel. The capacity of the gasifier was 125 kW (thermal) and used over 150 kg per run of 15 hours (~ $10kg.hr^{-1}$). The gas exited at about 650 °C and atmospheric pressure.

Information on how to *design* a laboratory scale gasifier was not found. In addition, there was no report of the gasification of liquids for laboratory studies.

6. The need for gas treatment

One of the major challenges facing syngas processing is the gas cleaning treatment step. Due to the feedstock containing a number of elements in small amounts, these are present in the resulting syngas in different species. The impurities include compounds containing sulphur and nitrogen, and to a lesser extent chlorine and alkali and heavy metals such as mercury. The remainder would be particulates and tars. The removal of these species is a limiting step from both a process and economic point of view.

By far the greatest concern is sulphur removal, and discussion will be limited to this. After gasification with a sulphur containing feedstock, the syngas would have H_2S, COS and trace amounts of CS_2, mercaptans and thiophenes. The reasons that they have to be removed are due to:

- Chemical process: the sulphur components will contaminate and deactivate catalysts. They will also corrode process machinery. H_2S is especially corrosive in the presence of water.
- Environmental emissions: total sulphur emissions (usually as SO_2) must be below local limits.

On the process side, the tolerance of various contaminants for some catalytic processes is very small. The main catalytic processes are methanol synthesis and Fischer-Tropsch reactions. Horazak *et al*. (2005) gives contaminant limits for methanol synthesis from syngas for a plant operating under "future standards", as shown in Table 2.4. Torres *et al.* (2007) obtained contaminant levels from various references and these are shown in Table 2.5.

Lastly, Leibold *et al.* (2008) also give some gas cleaning requirements for the Fischer-Tropsch Process, from various references and have been presented in Table 2.6. It was noted that the specified limits below were general, and "do not refer to special catalysts, process temperatures or syngas compositions."

Table 2.4: Contaminant limits for methanol syngas, adapted from Horazak *et al*. (2005)

Contaminant	**Limit**
Total sulphur	60 ppb
Total halide	10 ppb
NH_3	10 ppm
HCN	10 ppb
Metal carbonyls	100 ppb
Particulates	0.1 ppm (mass)
Hg	95 % removal

It is clear that the tolerance levels were extremely low. The total sulphur content of the gas of course depends upon the feedstock. It could range from 500 ppmv range to 0.5 – 3 mol %. With higher concentrations, the desulphurization becomes a major process in its own right.

Table 2.5: Contaminant limits for different syngas processes, adapted from Torres *et al.* (2007)

Process	**Contaminant**	**Limit**
Internal combustion systems	"Tars"	< 10 mg.Nm^{-3}
		< 30 mg.Nm^{-3}
PEM fuel cells	H_2S	< 1 ppm
Methanol synthesis	"Tars"	< 0.1 mg.Nm^{-3}
	CH_4	< 3 %
	NH_3	10 ppm
	HCN	0.01 ppm
	Total sulphur	0.5 ppm
	Halides	0.001 ppm

Table 2.6: Limits for different Fischer-Tropsch process, adapted from Leibold *et al*. (2008)

Contaminant	**Sasol**	**Reference 1**	**Reference 2**	**Reference 3**
CO_2	< 10 %	n.s.	< 5 %	< 5 %
Particulate	n.s.	< 0.1 ppm	n.s.	< 0.1 ppm
HCN	< 20 ppb	< 10 ppb	< 20 ppb	< 1 ppm
NH_3	n.s.	< 10 ppm	n.s.	n.s.
H_2S	< 10 ppb	< 60 ppb	< 10 ppb	< 1 ppm
COS	n.s.	n.s.	n.s.	n.s.
HCl	< 10 ppb	< 10 ppb	< 10 ppb	< 10 ppb
Br, F	n.s.	n.s.	n.s.	< 10 ppb
Alkalis	< 10 ppb	n.s.	< 10 ppb	< 10 ppb
Tars	n.s.	n.s.	below dew point	below dew point

n.s.: not specified

Quin *et al.* (2004) looked at the effect of trace contaminants for methanol synthesis. They found that the rate of methanol production was "adversely affected" by the following components, investigated separately: 1.91 ppm phosphine (PH_3), 2.75 ppm carbonyl sulfide (COS), 2.07 ppm carbon disulfide (CS_2), 1.61 ppm thiophene (C_4H_4S), 2.14 ppm methyl thiocyanate (CH_3SCN), 2.01 methyl chloride (CH_3Cl), and 2.55 methyl fluoride (CH_3F). However, the nitrogen-containing contaminants hydrogen cyanide (HCN), acetonitrile (CH_3CN), and methylamine (CH_3NH_2) "had no effect on catalyst activity." Note that this applies to the type of catalyst used, which was a "standard copper, zinc oxide, and alumina catalyst".

To conclude, the desulphurization step of syngas treatment is unavoidable. It is thus an area that can be improved, as small improvements here can have a major effect on the operation and efficiency of the plant. The remaining questions are: what is the best way to perform hot gas desulphurization and how can this be determined?

Chapter 3

Literature Review: Desulphurization

1. Existing desulphurization technologies

There are different types of methods to remove sulphur components from gas streams. Most of the methods employ some mechanism to transfer the sulphur out of the gas phase. The sulphur is then (usually) removed from the transfer phase in a regeneration step. The material on desulphurization technologies has mostly been compiled from Kohl and Riesenfeld (1979). The general methods can be broadly classified into 3 categories:

- Absorption into a liquid
- Adsorption on a solid
- Chemical conversion to another compound

Focus is placed on the absorption processes as they are the predominant method of sulphur removal in industry. An equally important aspect to discuss is the fate of sulphur once it is removed from the gas streams. This will be touched on briefly as it is not directly related to this study.

It should be stated at the start that the treatment of a H_2S rich gas for conversion to sulphur is a standard process, namely the Claus Process. Thus, the general problem is the selective removal of H_2S from a gas mixture into a separate stream of appropriate composition for this processing. If, however, H_2S is removed from the gas and converted to SO_2, a different process would be required, such as the production of H_2SO_4.

1.1 Physical absorption in a liquid

The basic process of *physical* absorption of a gas component(s) is to contact it with a liquid (usually at low temperature and high pressure), transfer the liquid to a flash vessel (usually a stripper) where the pressure is reduced and the absorbed components are stripped out of the liquid. The clean liquid is then recycled back to the absorber. There are a number of

processes based upon this physical principle. Some of the processes can remove CO_2 in addition to sulphur species and separate them due a difference in their relative solubilities.

i. Rectisol Process: Developed by Lurgi, from Lurgi (2009)

This process can reduce the total sulphur content of the gas to 0.1-1 ppm, primarily as H_2S and COS, and reduce CO_2 to 10-50 ppm. Absorption occurs in methanol at low temperatures (-10 to -40 °C). Application of Rectisol was focussed on synthesis gases. A very pure CO_2 stream with 5 ppm H_2S is also possible in the process design. In addition, trace components such as CS_2, NH_3, HCN, Hg and organic sulphur compounds are removed. The H_2S rich gas is suitable for a Claus Process.

The advantages were that there was lower energy consumption compared to absorption in water or ethanolamines, excellent removal of all undesirable components in a single process and the product gas has a low water content. The difference of solubility between H_2S and CO_2 in methanol allow for selective recovery of the gases. The disadvantages included the complex flow scheme and solvent loss.

ii. Fluor-Solvent Process: Developed by Fluor, from Kohl and Riesenfeld (1979)

This uses a propylene carbonate solvent and has been used for the processing of natural gas.

iii. Purisol Process: Developed by Lurgi, from Lurgi (2009)

This uses *n*-methyl-2-pyrrolidone (NMP) as a solvent and has been used for the processing of natural gas and for hydrogen cleaning. The solvent has an exceptionally high solubility for H_2S and is selective for H_2S in the presence of CO_2. The lower limits are a few ppm for H_2S and 0.1 mol % for CO_2.

iv. Selexol Process: Developed by UOP, from UOP (2009)

This uses a dimethyl ether of polyethylene glycol as a solvent. Along with H_2S, the process also removes COS, mercaptans, ammonia, HCN and metal carbonyls. CO_2 can be removed or retained in the product gas. It is possible to reach ppm levels for sulphur removal. Application is for both natural gas and syngas.

v. Sulfinol Process: Developed by Shell, from Kohl and Riesenfeld (1979)

This uses a combination of chemical and physical solvents. The presence of the physical solvent allows a higher solution capacity of sulphur species. The solvent consists of di-iso-propanolamine (DIPA), sulfolane (tetra-hydrothiopene dioxide) and water.

vi. Other processes, from Kohl and Riesenfeld (1979)

Lesser known or used processes include the Estasolvan Porcess, the Methylcyanoacetate Process and the Amisol Process (which is similar to Sulfinol). Lastly, water absorption of H_2S is possible although industrially not important from a commercial viewpoint. It was, however, proved to be technically possible.

1.2 Chemical absorption in a liquid

Chemical absorption involves a *chemical reaction* of a particular species in the gas with the liquid. With these processes, H_2S reacts with the absorbing liquid to form a new product compound, under the absorption conditions. The process would be reversed during regeneration to strip the H_2S out of the liquid into the gas phase.

i. Ethanolamines: The Glycol-Amine Process, from Kohl and Riesenfeld (1979)

Monoethanolamine (MEA), diethanolamine (SEA), methyldiethanolamine (MDEA) are selective solvents for H_2S in the presence of CO_2. The classic process is the Glycol-Amine Process which uses di- or tri-ethylene glycol as a solvent with MEA. Aqueous solutions of the ethanolamines can also be used. The typical reaction is: $2R\text{-}NH_2 + H_2S \leftrightarrow (R\text{-}NH_3)_2S$.

The glycol-amine solution could be stripped almost completely of H_2S and CO_2. The problems included corrosion in heat exchangers and high vaporization loss of the solvent. This could be reduced by including a water or glycol wash of the stripped gas. The aqueous solutions have been used for refinery gas (which contain high amounts of COS and CS_2 in addition to H_2S and CO_2).

ii. Alkaline salt solutions, from Kohl and Riesenfeld (1979)

This is a solution containing sodium and potassium cations, with a particular anion to give the solution a pH of 9-11. Sodium and potassium carbonate have been used. The processes include: The Seaboard Process, The Vacuum Carbonate Process and the Tripotassium Phosphate Process. UOP (2009) has developed the Benfield Process. This process uses hot potassium carbonate for natural gas and syngas processing and has been used in ethylene oxide and ammonia plants.

1.3 Solid Adsorption Processes

i. Adsorption on molecular sieves, from Kohl and Riesenfeld (1979)

It is possible to selectively adsorb H_2S from a mixture also containing CO_2 using molecular sieves (zeolites). Type 13X was the preferred adsorbent for natural gas processing to completely remove all sulphur compounds. However, in general, there were problems with disposing the sulphur rich regeneration gas.

1.4 Liquid Phase oxidation of H_2S and/or Neutralization

The oxidation of H_2S to elemental sulphur could be achieved by oxygen carriers dissolved or suspended in aqueous or non-aqueous liquids. The following could be used as oxygen carriers (either as suspensions or solutions). There are a number of different processes associated with them, from Kohl and Riesenfeld (1979):

- Polythionates
- Iron oxide (for example, the Ferrox Process)
- Thioarsenates
- Iron-cyanide complexes
- Organic compounds (alone or in conjunction with heavy metal salts)
- Sulphur dioxide
- Potassium permanganate and sodium or potassium dichromate
- Ammonia

1.5 Catalytic Conversion

This is usually associated with organic sulphur compounds that are catalytically converted to H_2S. They are hydrogenation and hydrolysis reactions and include, from Kohl and Riesenfeld (1979):

- The Carpenter Evans Process
- The Peoples Gas Company Process
- The Holmes-Maxted Process (extensively used)
- British Gas Council Process

The treatment of H_2S tailgas can make use of the Beavon Process or SCOT Process. These processes can treat dilute gas streams containing H_2S or SO_2 and recycle them back to a Claus Plant as H_2S. They involve catalytic reactors.

The Claus Process, as mentioned, was for production of sulphur from H_2S. This occurs in two steps: a partial oxidation at high temperature and then a series of catalytic reactors. Conversion of H_2S is usually between 97 and 99%, depending upon the number of catalytic stages.

1.6 Oxidation Processes

These can be classified into two types: oxidation to sulphur or oxidation to oxides of sulphur. With oxidation to sulphur, the rates of reaction are too low at normal temperatures. The temperature must thus be raised, or a catalyst or oxygen carrier used to make the reaction industrially viable. Also from Kohl and Riesenfeld (1979):

i. The iron oxide process: also known as “dry box purification”.

The reaction of H_2S with Fe_2O_3 occurred in beds or "boxes" at ambient temperatures. This process was used in many applications, and is one of the oldest methods for removing sulphur species.

ii. The activated carbon process

H_2S was oxidised in activated carbon beds. Very pure sulphur was obtained using regeneration by extraction with aqueous ammonium sulphide solution. However, the carbon suffered from rapid deactivation due to depositions of tars and particulates.

iii. The Sulfreen Process

This was another extension to a Claus Plant to react H_2S and SO_2 at lower temperatures than the Claus process, below the dew point of sulphur. As such, the sulphur collected on the catalyst and was removed by vaporization at a later stage.

1.7 Oxidation to Oxides of Sulphur, from Kohl and Riesenfeld (1979)

i. The Katasulf Process: H_2S and a portion of the organic sulphur are oxidized catalytically to SO_2.

ii. The North Thames Gas Board Process: organic sulphur compounds are oxidized catalytically to SO_2.

iii. The Iron-Soda process: where organic sulphur compounds are converted to SO_2 and SO_3.

iv. The Appleby-Frodingham Process: where H_2S and organic sulphur compounds are removed by absorption on iron oxide in a continuous fluidized bed at 350 °C. Regeneration was with air at 600 °C.

1.8 The fate of sulphur

Once sulphur has been removed from the syngas, natural gas etc. it exists in various phases, depending on how it was removed. Ideally, this could be converted into a useful product.

The main products are pure sulphur or sulphuric acid. From a process perspective, there are a number of ways to achieve this, and this has been the focus of much recent research.

H_2S rich gas stream:	Claus plant:	sulphur
SO_2 rich gas stream:	Contact process:	sulphuric acid
Metal sulphide solid:	regeneration:	SO_2 or S directly

These have been looked at by Gangwal *et al*. (1998) and Wheelock *et al.* (2003). However, the sulphur recovery was not related to this study.

2. Hot gas desulphurization technology

Hot gas desulphurization (HGD), as the name suggests, is the removal of sulphur species at high temperatures, generally above 300 °C. As such, they are considered 'dry' processes compared to "wet" processes like absorption. In general, HDG refers to the gas-solid reaction of H_2S or other sulphur species with a solid sorbent. The sorbent is typically a solid that can be reduced by H_2S, and as will be shown, many transition metal oxides have favourable properties.

The principle idea behind the development of HGD is that the temperature of syngas from gasification is typically above 600 °C and treating the gas in this condition would save energy. For conventional sulphur removal by absorption, the temperature of the gas is reduced to ambient or even lower temperatures. The next step in the process is usually a catalytic step at high temperature. Both methanol and Fischer-Tropsch reactions occur at over 200 °C. The gas must thus be reheated and energy is consumed.

The reheating may be possible via gas compression. This of course depends upon the process: does the gasifier operate at high pressure or does compression occur before the main synthesis reactor? The point is that there is the potential to *save energy* by not cooling and reheating the gas. This would increase the thermal efficiency of a plant. Lastly, it will be shown that the actual process of HGD has economic advantages over the wet processes in terms of capital and operating costs.

2.1 Type of desulphurization

This is broadly classified into bulk desulphurization or gas polishing, and whether the sorbent is disposable or can be regenerated. From Gangwal *et al.* (1995):

"Typically, disposable sorbents are calcium based (limestone, dolomite or lime). They react with H_2S in a gasifier to form first CaS and then $CaSO_4$. However, only 80-90 % of the H_2S would be removed and thus a polishing step would still required. The $CaSO_4$ would be removed with the ash."

Regeneration of sorbents with steam, air or oxygen is possible to produce either S or SO_2. The challenge is for this to occur in industrially feasibly conditions. The challenges include: sorbent structure integrity over multi-cycle runs and temperature control, as the regeneration reaction is highly exothermic.

2.2 The basic reactions

The reactions of H_2S with metal oxides (MO) to metal sulphides (MS) are well established. The first major study of hot gas desulphurization was conducted by Westmoreland and Harrison (1976), where they identified potential desulphurization metal oxide candidates. These were the oxides of iron, zinc, molybdenum, manganese, vanadium, calcium, strontium, barium, cobalt, copper and tungsten. The general reactions are:

Sulphidation	$MO + H_2S \leftrightarrow MS + H_2O$	(3.1)
Regeneration	$MS + (3/2)O_2 \leftrightarrow MO + SO_2$	(3.2)

The metal oxide sorbent has been the subject of much research and development. The gas-solid reaction can occur in a fixed, moving or fluidized bed. A very useful diagram was developed by Westmoreland and Harrison (1976) and is shown in Figure 3.1 below. It shows where the stable sulphides (from sulphidation) and oxides or carbonates (from regeneration) of various transition metals can be formed *as a function of temperature*. Note that the formation of these compounds were thermodynamically favoured.

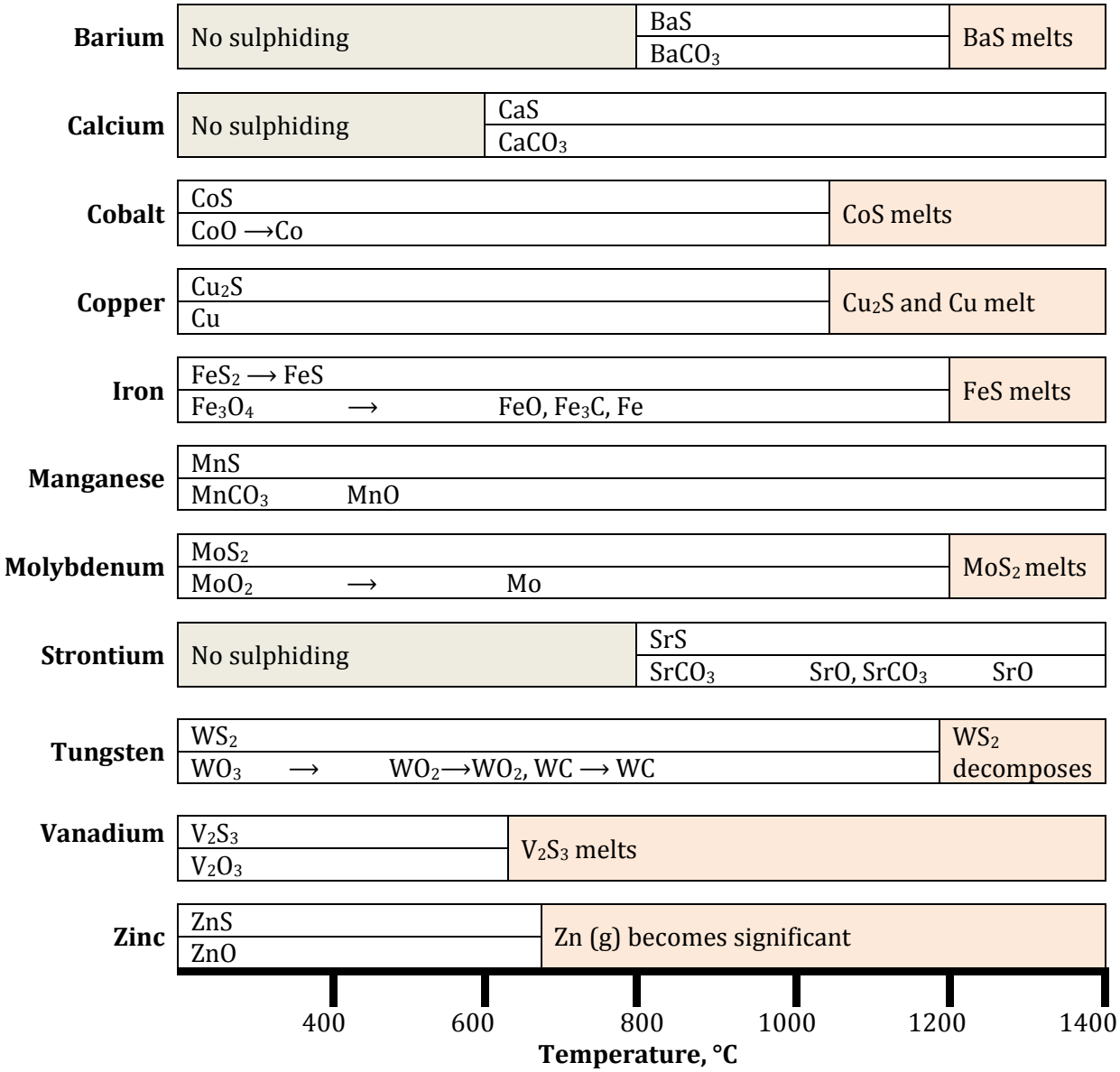

Figure 3.1: Stable transition metal sulphides and oxides as a function of temperature. Adapted from Westmoreland and Harrison (1976)

2.3 Economics

Studies into the cost of implementing HGD using sorbents were conducted to establish the economic feasibility. Even if the thermal efficiency improved, implementing the process design would ultimately come down to the *cost* of the technology, both capital and operation.

Gangwal *et al*. (1995) reported a net thermal efficiency increase from 42.75 % to 45.14 % of a nominal 800 MW (electrical) Texaco gasifier based IGCC plant using hot gas cleanup at 350 °C. In addition, the capital cost and cost of electricity decreased by 6 % and 2 % using hot gas cleanup at 350 °C.

The study by Horazak *et al*. (2005), conducted a commercial evaluation of an IGCC plant and methanol synthesis plant (with electric power co-production). They compared conventional, low-temperature dry-gas cleaning technology of the same plant with a 'novel' high temperature gas cleaning process. While the actual values are applicable to the specific processes they presented, it shows an indication of the cost and energy savings from HGD. These are shown in Table 3.1.

Table 3.1: Cost comparison for traditional and HGD processes, adapted from Horazak *et al*. (2005)

	IGCC Plant			**Methanol Plant with Electric Power Co-generation**		
	Traditional	Novel Gas Cleaning	Change (%)	Traditional	Novel Gas Cleaning	Change (%)
Net plant power generated (MW)	285.2	302.5	+ 6.07	288.3	309.1	+ 7.21
Plant net efficiency (%, LHV)	40.56	43.03	+ 2.47	35.20	37.77	+ 2.57
Cost of acid gas removal (k$)	21,831	15,635	- 28.38	30,562	21,514	- 29.61
Total capital requirement (k$)	427,748	428,179	+0.10	516,316	483,723	- 6.31
Acid gas removal of plant cost (%)	5.10	3.65	- 1.45	5.92	4.45	- 1.47
Total capital requirement ($/kW)	1,500	1,415	- 5.67	1,791	1,565	- 12.62
Cost of electricity (US cents/kWh)	6.56	6.34	- 3.35	5.55	5.06	- 8.83

In the study, the sulphur content of the hot gas was ~10 000 ppm. Bulk desulphurization occurred in a transport reactor at 549 °C and 23 bar g with zinc oxide-titanate to reduce the sulphur content to less than 50 ppm. The gas then enters a polishing reactor where the sulphur content is reduced to sub ppm levels.

2.4 Process considerations and type of reactor

Horazak *et al.* (2005) also provide useful comparisons between the different types of industrial desulphurization reactors. These were namely fixed beds, moving beds, transport reactors or a filter-reactor.

A major consideration was the sorbent's attrition resistance if fluidized beds were being considered. Sometimes, this can be advantageous if the product ash on a particle is broken down to expose the unreacted core due to the fluidization dynamics. Secondly, the ability of the sorbent to undergo repeated sulphidation-regeneration cycles while maintaining its structural integrity is important. For example, the formation of $ZnSO_4$ during regeneration can be a problem as $ZnSO_4$ is nearly three times the molar volume of ZnO.

Lastly the resulting SO_2 tailgas, which is usually dilute, must be treated to meet local environmental emission requirements. The options are: to recycle back to the gasifier for reaction with calcium based sorbent (if possible), conversion of SO_2 to S or H_2SO_4. Conversion to H_2SO_4 is not always feasible.

3. Hot gas desulphurization studies

As mentioned, the first study into thermodynamic feasibility of HDG was by Westmoreland and Harrison (1976). After this, there were a number of experiments into the high temperature reaction of H_2S and a metal oxide sorbent. Many of these have been presented in Table 3.2. The aim here was to give an idea of experimental scope (range of conditions). In general, the research varied:

- Sorbent type
- Sorbent preparation method
- Reactor type
- Reactor size and hence gas flowrates
- Gas composition
- H_2S initial concentration

The following important points were made. A discussion on reaction kinetics will be given in the next section. The modelling of the reaction is treated in Chapter 5.

Westmoreland *et al.* (1977) found that zinc oxide sorbents had an upper temperature limit of about 750 °C. At this temperature, the zinc was reduced by hydrogen and vapourized. Zinc was thus deposited outside of the reactor bed. Lew *et al.* (1989) reported this temperature to be as low as 600 °C.

To solve this problem, it was found that the addition of titanium 'stabilized' the sorbent. The general reaction was now:

$$Zn_xTi_yO_{x+2y\,(s)} + xH_2S_{\,(g)} \rightarrow xZnS_{\,(s)} + yTiO_{2\,(s)} + xH_2O_{\,(g)} \qquad (3.3)$$

Lew *et al*. (1989) found no effect of hydrogen gas concentration on the sulphidation kinetics of zinc oxide and zinc titanate sorbents for temperatures in the range of 400-800 °C. A higher percentage of titanium was needed in order to decrease the reduction rate. This would be at the expense of sulphur loading. Their conclusions were:

"(1) Zinc titanates exhibit lower rates of zinc loss than zinc oxide during reduction-sulfidation of the sorbents at 650 °C in a simulated fuel gas atmosphere. (2) Zinc titanates have comparable intrinsic sulfidation kinetics to zinc oxides at 650 °C. (3) Zinc titanates have similarly high hydrogen sulphide removal efficiency as zinc oxides. (4) Sulphided zinc titanate sorbents are fully regenerable under the regeneration conditions employed in this work. (5) Incomplete sulfidation of zinc titanates is mainly due to slow diffusion through the product layer. (6) Zinc titanate sorbents prepared from chloride-containing precursors can be sulphided completely."

Li *et al*. (1997) used a ZnO-MnO sorbent at 200-400 °C and found "the reaction rate was controlled, at lower temperatures, by the grain surface reaction rate and at higher temperatures by the rate of intrapellet diffusion...". However, note that 400 °C is not necessarily a very high temperature compared to other studies.

Cal *et al*. (1999) suggested that carbon based sorbents have the potential to be less expensive than metal oxides.

Elseviers and Verelst (1999), with zinc based sorbents concluded that the fuel gas composition did not have a large influence on the desulphurisation performance, except for the minimum residual H_2S level which could be obtained.

Sánchez *et al*. (2005) studied a commercial sorbent, Z-Sorb III, and concluded that the presence of H_2, CO, and H_2O did not have a detrimental effect on sorbent performance.

Sánchez-Hervás *et al.* (2005) studied the sorbent Z-Sorb III. And concluded that gas residence time had a strong effect on sorbent utilization. At higher gas velocities (3500 h^{-1}), the sulphidation reaction proceeds isothermally to complete conversion of ZnO. Further increase in space velocity to 5000 h^{-1} leads to lower sorbent utilization, which was typical of diffusion-limited gas–solid heterogeneous reactions.

Table 3.2: Summary of experimental studies into Hot Gas Desulphurization, given in chronological order. TGA is thermogravimetric reactor, i.d. is internal diameter.

Authors	Year	Sorbents studied	Reactor	Modelling	Conditions		
Westmoreland *et al* (1977)	1977	MnO, CaO, ZnO, and V_2O_3. Size: -100 mesh	TGA	kinetics	Temperature	°C	300-800
					Pressure	atm	1.00
					Gas flow	[-]	n/a
					Composition	mol %	1.9-7.0 H_2S, H_2 at 5 times H_2S, balance N_2
Yumura and Furimsky (1985)	1985	CaO, ZnO and Fe_2O_3. Size: 1.5 mm pellet, 2g	fixed bed	n/a	Temperature	°C	600-800
					Pressure	atm	1.00
					Gas flow	LPM	0.1
					Composition	mol %	0.7-2.0 H_2S, H_2, bal N_2
					Reactor i.d.	cm	1
Tamhankar *et al*. (1986)	1986	ZnO, CuO, ZnO-Fe_2O_3, CuO-Fe_2O_3, CuO-Al_2O_3 and CuO-Fe_2O_3-Al_2O_3. Size: -10 +40 mesh	fixed bed	n/a	Temperature	°C	538-600
					Pressure	atm	1
					Gas flow	hr^{-1}	2000
					Composition	mol %	0.2-1.0 H_2S, 0-20 H_2, 7-25 H_2O, balance N_2
					Reactor i.d.	cm	1
Bagajewicz *et al.* (1988)	1988	V_2O_3. Size: -35 +45 mesh, 3-6 g	fixed bed	n/a	Temperature	°C	500-800
					Pressure	atm	1.00
					Gas flow	hr^{-1}	2600
					Composition	mol %	150-2000 ppm H_2S, 0-20 H_2, balance N_2
					Reactor i.d.	cm	1
Woods *et al.* (1990)	1990	ZnO, zinc-oxide titanate: Size: 0.32-0.48 cm pellets	TGA	n/a	Temperature	°C	650-760
					Pressure	atm	1-10
					Gas flow	[-]	n/a
					Composition	mol %	0.25-2.5 H_2S, balance N_2
					Reactor i.d.	cm	n/a

Jothimurugesan amd Harrison (1990)	1990	ZnO, zinc-oxide titanate: Size: 0.32-0.48 cm pellets	TGA	shrinking core model	Temperature	°C	650-760
					Pressure	atm	1-10
					Gas flow	[-]	n/a
					Composition	mol %	0.25-2.50 H_2S, balance N_2
Lew *et al.* (1989)	1989	ZnO, zinc titanates: Size: 20-35 µm (fixed bed), bed height 4-6 cm. 115-170 mesh (TGA)	TGA and fixed bed	kinetics	Temperature	°C	600-650
					Pressure	atm	1.00
					Gas flow	hr^{-1}	2000
					Composition	mol %	1 H2S, 13 H_2, 19 H_2O, balance N_2
					Reactor i.d.	cm	1.5
Lew *et al.* (1992 a)	1992	ZnO, zinc titanates. Size: 90-125 µm, 1-3 mg	TGA	kinetics	Temperature	°C	400-800
					Pressure	atm	1.00
					Gas flow	cm^3/min STP	350
					Composition	mol %	1 H_2S, 13 H_2, 19 H_2O, balance N_2
					Reactor i.d.	cm	n/a
Wakker *et al.* (1993)	1993	MnO or FeO on γ-Al_2O_3. Mass: 3g	fixed bed	n/a	Temperature	°C	402-602
					Pressure	bar	1-5
					Gas flow	µmol/min	67.5
					Composition	mol %	1 H_2S, 0-40 H_2, 0-70 CO, 0-15 H_20, 0-10 hydrocarbons, 0-1 HCl, 0-1 COS, balance N_2.
					Reactor i.d.	cm	1.2
Abbasian *et al.* (1994)	1994	zinc titanate based	fluidized bed	n/a	Temperature	°C	750
					Pressure	atm	20.00
					Gas flow	SLPM	maximum 600
					Composition	mol %	5000 ppm H_2S, 10 H_2, 10 H_2O, balance N_2
					Reactor i.d.	cm	2.5 to 7.5

Sasaoka *et al.* (1994)	1994	Zinc oxide with additions of ZrO_2, TiO_2, and Al_2O_3. Volume: 0.5 cm^3 sorbent	fixed bed	n/a	Temperature	°C	600
					Pressure	atm	1.00
					Gas flow	cm^3/min STP	300
					Composition	mol %	500 ppm H_2S, 12.5 H_2, 11.9 H_2O, balance N_2
					Reactor i.d.	cm	1.5
Sasaoka *et al.* (1995)	1995	Zinc ferrite ($ZnFe_2O_4$). 0.2 cm^3 sorbent (fixed bed), 0.1 g (TGA)	TGA and fixed bed	kinetics (soot formation)	Temperature	°C	450-600
					Pressure	atm	1.00
					Gas flow	cm^3/min STP	200
					Composition	mol %	10-200 ppm H_2S, 20 H_2, 30 CO, 10 CO_2. 9.4 H_2O, balance N_2
					Reactor i.d.	cm	0.65
Li *et al*. (1997)	1997	ZnO-MnO	TGA	apparent kinetics, SCM and grain model	Temperature	°C	200-400
					Pressure	atm	1.00
					Gas flow	cm^3/min STP	600
					Composition	g/Nm^3	5.41-19.25 H_2S, balance N_2
Jothimurugesan and Gangwal (1998)	1998	Zinc titanate trade names. 1 g (fixed bed), 18 g, -50 +140 mesh (fluidized)	fixed bed and fluidized bed	n/a	Temperature	°C	400-500
					Pressure	bar	1.00
					Gas flow	[-]	2500 hr-1 (fixed), 15 SLPM (fluidized)
					Composition	mol %	1 H_2S, 10 H_2, 15 CO, 5 CO_2, 15 H_2O, balance N_2
					Reactor i.d.	cm	1 (fixed), 2.5 (fluidized)
Gangwal *et al.* (1998)	1998	Zinc ferrite ($ZnFe_2O_4$)	fluidized bed	n/a	Temperature	°C	Simulations
					Pressure	atm	
					Gas flow	[-]	
					Composition	mol %	
					Reactor i.d.	cm	

Harrison *et al.* (1998)	1998	Fe_2O_3 and CeO_2	TGA and fixed bed	n/a	Temperature	°C	Focussed on regeneration of sorbents
					Pressure	bar	
					Gas flow	[-]	
					Composition	mol %	
Elseviers and Verelst (1999)	1999	Zinc titanate	fixed bed	n/a	Temperature	°C	500-600
					Pressure	atm	1.00
					Gas flow	[-]	n/a
					Composition	mol %	0.325-0.483 H_2S, 47.8 H_2, 21.3 CO, 18.3 CO_2, balance Ar
					Reactor i.d.	cm	0.7
Rajagopalan and Amiridis (1999)	1999	Perovskite based: $LaMnO_3$, $LaCoO_3$, $LaFeO_3$, La_2CuO_4. Size: 100-120 mesh	fixed bed	n/a	Temperature	°C	500
					Pressure	atm	1.00
					Gas flow	$cm^3.min^{-1}$ STP	250
					Composition	mol %	3000 ppm H_2S, balance N_2
					Reactor i.d.	cm	n/a
Cal *el al.* (2000 a)	2000	Activated carbon, with varoius activators. 5.5 g sorbent	fixed bed	n/a	Temperature	°C	550
					Pressure	atm	1.00
					Gas flow	hr-1	1700-2000. 200 cm^3/min STP
					Composition	mol %	0.5 H_2S, 13 H_2, 21 CO, 7.5 CO_2, 8.5 H_2O, balance N_2
					Reactor i.d.	cm	1.2
Pineda *et al.* (2000)	2000	Zinc oxide based sorbents doped with CuO or TiO_2. 15 g	fixed bed	n/a	Temperature	°C	600
					Pressure	atm	1.00
					Gas flow	hr^{-1}	2600. 500 cm^3.min-1 STP
					Composition	mol %	1 H_2S, 8 H_2, 15 CO, 15 H_2O, balance N_2
					Reactor i.d.	cm	1

Slimane and Abbasian (2000 a)	2000	Copper based. 425-850 µm	fixed bed	n/a	Temperature	°C	350-550
					Pressure	atm	1.00
					Gas flow	hr^{-1}	2000
					Composition	mol %	2 H_2S, 10 H_2, 20 CO, 10 CO_2, 10 H_2O, balance N_2
					Reactor i.d.	cm	n/a
Slimane and Abbasian (2000 b)	2000	Cu, Fe, Mn, Zn based with minor additives. 180-425 µm	fixed bed	n/a	Temperature	°C	350-550
					Pressure	atm	1.00
					Gas flow	hr^{-1}	2000
					Composition	mol %	1.5 H_2S, 10 H_2, 20 CO, 10 CO_2, 10 H_2O, balance N_2
					Reactor i.d.	cm	2.5
Alonso *et al.* (2001)	2001	Zinc oxide with graphite as pore-modifer additive. 10 mg (TGA)	TGA and fixed bed	n/a	Temperature	°C	550-600
					Pressure	atm	1.00
					Gas flow	cm^3/min STP	200 (TGA), 6000 hr^{-1} (fixed bed)
					Composition	mol %	0.5-1.0 H_2S, 10 H_2, 15 CO, 5 CO_2, 15 H_2O, balance N_2
					Reactor i.d.	cm	2.3
Jun *et al.* (2001)	2001	Improved Zn/Ti-Based Desulfurization Sorbents with Co_3O_4. 1 g sorbent, 200-300 mesh	fixed bed	n/a	Temperature	°C	480-650
					Pressure	atm	1.00
					Gas flow	hr^{-1}	5000. 50 cm^3/min STP
					Composition	mol %	1.5 H_2S, 11.7 H_2, 9.6 CO, 5.2 CO_2, balance N_2
					Reactor i.d.	cm	1
Huiling et al. (2002)	2002	ZnO	TGA	Apparent kinetics, equivalent grain model	Temperature	°C	200-320
					Pressure	atm	1.00
					Gas flow	ml/min	800
					Composition	mol %	8.73 g/Nm^3 H_2S, 20 H_2, balance N_2

Kwon *et al.* (2003)	2003	AHI-1 sorbent: 20 % Fe_2O_3, 10% ZnO, 70 % spent FCC catalyst. 0,05 g, 130 µm	TGA		Temperature	°C	450-600
					Pressure	bar	1.25
					Gas flow	ml/min	250-750 (25°C)
					Composition	mol %	1000-4000 ppm H_2S, 0-20 H_2, 0-20 H_2O, bal N_2
Zhang *et al.* (2003)	2003	MnO, Fe_2O_3, ZnO on γ-Al_2O_3	fixed bed	n/a	Temperature	°C	500-650
					Pressure	atm	1.00
					Gas flow	hr^{-1}	2000-5000
					Composition	mol %	0.2-0.6 H_2S, 12 H_2, 20 CO, 7 CO_2, balance N_2
					Reactor i.d.	cm	1
Turton *et al.* (2004)	2004	ZnO sorbents. 3 mg (TGA)	TGA and transport (pilot plant)	kinetics	Temperature	°C	482-593
					Pressure	atm	1.00 (TGA); 20.23 (transport)
					Gas flow	cm^3/min STP	140 (TGA); 1350 (transport)
					Composition	mol %	0.5-2.0 H_2S, bal N_2 (TGA); 1 H_2S balance N_2 (transport)
					Reactor i.d.	cm	0.84 (11.54m long transport)
Ryu *et al.* (2004)	2004	Zinc titanate modified with cobalt oxide, molybdenum oxide and iron hydroxide. 130-300 µm	fixed bed		Temperature	°C	480
					Pressure	atm	1.00
					Gas flow	cm^3/min STP	250
					Composition	mol %	1 H_2S, 11.7 H_2, 19 CO, 6.8 CO_2, 10 H_2O, balance N_2
					Reactor i.d.	cm	1

Feng *et al.* (2005)	2005	Activated Carbon Fibers. 1 g	fixed bed		Temperature	°C	23 (low temperature)
					Pressure	atm	1.00
					Gas flow	cm^3/min STP	150
					Composition	ppm	200 ppm in N_2
					Reactor i.d.	cm	1
Karayilan *et al.* (2005)	2005	Mn-Cu and Mn-Cu-V mixed oxides. 0.2 g	fixed bed	n/a	Temperature	°C	627
					Pressure	atm	1.00
					Gas flow	cm^3/min STP	275
					Composition	mol %	1.0 H_2S, 10 H_2, balance He
					Reactor i.d.	cm	0.6
Park *et al.* (2005)	2005	ZnO deposited on activated carbon. 3 g	fixed bed		Temperature	°C	480
					Pressure	atm	1.00
					Gas flow	cm^3/min STP	250
					Composition	mol %	50 ppm H_2S, 11.7 H_2, 19 CO, 6.8 CO_2, 10 H_2O, balance N_2
					Reactor i.d.	cm	2.1
Sánchez *et al.* (2005)	2005	Z-Sorb III: zinc oxide and a promoter (nickel oxide) are supported on a proprietary matrix, 2500 g	fixed bed		Temperature	°C	250-650
					Pressure	atm	2-20
					Gas flow	hr^{-1}	3500-10000
					Composition	mol %	1 H_2S, 20 H_2, 56 CO, 4 CO_2, 10 H_2O, balance N_2
					Reactor i.d.	cm	8
Sánchez-Hervás *et al.* (2005)	2005	Z-Sorb III: zinc oxide and a promoter (nickel oxide) are supported on a proprietary matrix, 2500 g	fixed bed		Temperature	°C	400-500
					Pressure	atm	10-20
					Gas flow	hr^{-1}	1000-5000
					Composition	mol %	1 H_2S, 20 H_2, 56 CO, 4 CO_2, 10 H_2O, balance N_2
					Reactor i.d.	cm	8

Jung *et al.* (2006)	2006	$ZnO–Al_2O_3$ (ZA) sorbent with 5–10 wt.% additives such as iron (Fe_2O_3), cobalt (Co_3O_4), nickel (NiO) and cerium oxide (CeO_2)	fixed bed	SCM	Temperature	°C	480-580
					Pressure	atm	1.00
					Gas flow	hr^{-1}	5000. 50 cm^3/min STP
					Composition	mol %	1.5 H_2S, 11.7 H_2, 9.6 CO, 5.2 CO_2, balance N_2
					Reactor i.d.	cm	1
Bu *et al*. (2007)	2007	zinc titanate-based: trade names G-201 and G-202. Micro: 4 g, 0.2-0.4 mm. Large: 3 litre, 4 mm	Micro: packed bed, Larger: packed bed		Temperature	°C	450-800
					Pressure	bar	1.01 (micro), 8 (large)
					Gas flow	[-]	3000 hr^{-1} (micro), 10 m^3/hr (large)
					Composition	mol %	10 g/m^3 H_2S, 36-44 H_2, 28-36 CO, 23 CO_2, 1.3 CH_4, balance N_2
					Reactor i.d.	cm	1.4 (micro), 9.6 (large)
Ko *et al*. (2007)	2007	Zn–Mn based sorbents supported on SiO2, γ-Al2O3 and ZrO2	fixed bed		Temperature	°C	500-700
					Pressure	atm	1.00
					Gas flow	$ml.hr^{-1}.g^{-1}$	2000 WHSV
					Composition	mol %	1 H_2S, 15 H_2, 25 CO, balance N_2
					Reactor i.d.	cm	1.6
Sun *et al*. (2007)	2007	Zinc oxide. G72-E. 0.165g, -200 mesh (-75μm)	fixed bed	kinetics	Temperature	°C	350
					Pressure	bar	1.20
					Gas flow	cm^3/min STP	300
					Composition	mol %	50 ppm H_2S in N_2 with CH_4
					Reactor i.d.	cm	0.95
Tsukada *et al*. (2008)	2008	Composite sorbents based on iron oxide and zinc ferrite	fixed bed	SCM	Temperature	°C	400
					Pressure	bar	1.00
					Gas flow	LPM	2 (20 °C)
					Composition	mol %	1000 ppm H_2S, 2 H_2, balance N_2
					Reactor i.d.	cm	2

Yasyerli (2008)	2008	Ce-Mn sorbents. 0.2g	fixed bed	n/a	Temperature	°C	500-700
					Pressure	atm	1.00
					Gas flow	cm^3/min STP	100
					Composition	mol %	1-2.5 H_2S, 10 H_2, balance He
					Reactor i.d.	cm	n/a

3.1 Influence of soot formation during the reaction

It was apparent from a number of studies that there was a possibility of soot forming due to the gas composition. Soot is essentially pure carbon, effectively some small remainder of the carbon fuel source which can form under certain conditions, as given below. This was relevant to this study as the syngas mixture would be made from a gasification reactor. The influence of soot formation has been documented below:

Soot formation on zinc ferrite sorbents decreased with the increase of reaction temperature. This soot formation was inhibited by H_2O and CO_2 and accelerated by H_2 and CO according to Sasaoka *et al.* (1995).

Elseviers and Verelst (1999) found that in a CO and CO_2 containing atmosphere, soot formation can occur.

Lastly, Sánchez-Hervás *et al.* (2005) measured values of carbon content up to 18 % in the solid from the sulphidation runs carried out at 1000 h^{-1} of gas hourly space velocity.

3.2 Kinetics of the ZnO-H_2S reaction

These have been published by a number of authors and are compared and discussed below. In general, the rate law was given by:

Arrhenius Relationship:
$$k = k_0 \exp\left\{\frac{-E_a}{R_g T}\right\} \tag{3.4}$$

Rate Law:
$$R_0 = kC_{H_2S}^{n} C_{ZnO}^{m} \tag{3.5}$$

R_0	initial molar rate of ZnS formation per unit surface area of the solid reactant	[$mol.cm^{-2}.s^{-1}$]
C_{H_2S}	molar concentration of hydrogen sulphide in gas	[$mol.cm^{-3}$]
C_{ZnO}	molar concentration of ZnO solid	[$mol.cm^{-3}$]
E_a	activation energy	[$kJ.mol^{-1}$]
R_g	gas constant	[$kJ.mol^{-1}.K^{-1}$]
T	reaction absolute temperature	[K]
k_0	frequency factor	[$cm.s^{-1}$]
n	reaction order with respect to H_2S	[-]
m	reaction order with respect to ZnO	[-]

Westmoreland *et al.* (1977) and Lew *et al.* (1992 a) found the reaction order to be 1 (n=1), i.e. first order with respect to H_2S and zero order for ZnO (m=0). The results for k_0 and E_a are given in Table 3.3, all at 1 atm pressure.

Table 3.3: Kinetics of ZnO-H_2S reaction by various researchers, all at 1 atm pressure

Researchers	Temperature Range	Activation Energy, E_a	Frequency factor, k_0	Conditions	Comment
	°C	kJ.mol^{-1}	cm.s^{-1}		
Westmoreland *et al.* (1977)	300-750	30.3	1.22	H_2S: 1-9 mol %. H_2 at 5 times the H_2S mol %. Balance N_2.	
Lew *et al.* (1992 a)	400-800	43.1	1.31	H_2S: 2 mol %, H_2 1 mol %, balance N_2	
Turton *et al.* (2004)	482-593	31.4	0.333	H_2S: 0.5-2 mol %, balance N_2	24.5-38.2 kJ.mol^{-1} 95% confidence interval for E_a.
Li *et al.* (1997)	200-400	11.84	0.0044	H_2S: 5.41-19.25 g.Nm^{-3}, balance N_2. 4 mm pellet	(ZnO-MnO ratio 9:1) Apparent kinetics
Huiling *et al.* (2002)	200-320	15.85	0.21	H_2S: 8.73-16.4 g. Nm^{-3}, H_2 20 mol %, balance N_2. 3-3.5 mm sphere	Apparent kinetics in presence of H_2.
Huiling *et al.* (2002)	200-320	19.32	0.08	H_2S: 8.73-16.4 g. Nm^{-3}, balance N_2. 3-3.5 mm sphere	Apparent kinetics.

Westmoreland *et al.* (1977) explain that to measure the intrinsic rate constant, the experiment must be in conditions where there are no effects of external mass transfer and pore diffusion limitations. They neglected the diffusion resistance since the *initial* reaction rate was calculated (hence, negligible product ash layer). They found the range of external mass transfer limitations by reducing the ratio of sample size (i.e. particle radius) to flowrate until reaction rate constant did not change.

Lew *et al.* (1992 a) also state that the gas flow, particle size and quantity of sample were varied to ensure that external mass transfer and pore diffusion limitations were absent, in order to measure the reaction rate.

The researchers have thus calculated the *intrinsic* reaction kinetics. These are independent of the pellet used. When the reaction rate is based upon specific experimental conditions (for example, a specific sorbent), this is termed the *apparent* kinetics. Fogler (2006) notes that when internal diffusion limitations are present, the apparent reaction order and activation energy would primarily be measured.

Turton *et al.* (2004), in a more recent study, also took care to conduct experiments at high gas flow rates to eliminate external mass transfer resistances. They also found that n=1 and m=0. While good agreement with the activation energy was found with Westmoreland *et al*. (1977), they do not offer an explanation as to the lower frequency factor compared to both Westmoreland *et al*. (1977) and Lew *et al.* (1992 a)

The work of Li *et al.* (1997) looked at a 4 mm sorbent pellet of 90 % ZnO, 10 % MnO. Huiling *et al.* (2002) determined the effect of hydrogen on the apparent kinetics of a 3 mm ZnO pellet. The results are included in Table 3.3 for comparison.

3.3 General trends of the H_2S-metal oxide reaction

Most researchers looked at the effect of changing some operation conditions on the reaction. These were primarily temperature, pressure, pellet size, flowrate, gas concentration and to a lesser extent gas composition. The following two tables, Table 3.4 and Table 3.5, give a summary of their findings. Although some are not for zinc oxide as a sorbent, the trends are important and applicable to this study.

4. Summary of literature review

This chapter has reviewed the existing literature on desulphurization. The existing technologies and processes were broadly classified into absorption into a liquid (by chemical or physical means), adsorption onto a solid (such as using molecular sieves) or chemical conversion. The chemical conversion could be a liquid phase reaction, a catalytic reaction, or an oxidation reaction. The use of a sorbent is generally an oxidation-reduction reaction with H_2S.

The use of certain transition metal oxides showed excellent potential to selectively react with H2S. Since the reactions could occur at high temperature, economic studies showed the financial viability from both a capital and operational point of view.

Table 3.2 detailed a number of experimental studies in the literature, including the experimental conditions and Table 3.3. presented some of the reaction kinetics that have been published.

Lastly, Table 3.4 showed the general trends found when changing process variables, according to specific researchers. It is difficult to make a general statement regarding the trends, as it is dependent upon the sorbent type, experimental conditions and the goal of the work (for example, noting the breakthrough time, or the conversion of the sorbent, or the minimum outlet concentration achieved). However, the table provides useful indicators that can be used in the experimental design.

This leads to an examination of gas-solid reaction theory and the associated mathematical modelling.

Table 3.4: The effect of temperature and pressure on the H_2S reaction with a sorbent. Note that TGA is a thermogravimetric reactor.

Researcher	**Sorbent**	**Reactor Type**	**Temperature**	**Pressure**
Yumura and Furimsky (1985)	ZnO	TGA	Increasing the temperature from 600-800 °C had little effect on sulphur removal capacity of the sorbent.	-
Woods *et al.* (1990)	Zinc titanate	TGA	For low temperatures (< 400 °C), the reaction rate was very slow. As the temperature increased to 650 °C, the reaction rate increased considerably. However, from 650-750 °C, there was almost no dependence of the reaction rate upon temperature.	An increase in pressure from 1-10 atm at 705 °C caused a decrease in reaction rate, attributed to a decrease in the transfer coefficients with the increase in pressure. This was at constant H_2S concentration.
Lew *et al.* (1992 b)	ZnO	TGA	The reaction rate for zinc oxide increased significantly from 400-600 °C and then only slightly to 700 °C.	-
Turton *et al.* (2004)	ZnO	TGA	The reaction rate increases from 482-593 °C	-
Sánchez *et al.* (2005)	Z-Sorb III	fixed bed	There was little influence in solid adsorption capacity in 400-650 °C and minor differences in breakthrough time. However, at 250 °C, breakthrough occurred at after half the time of the 400 °C result.	Conditions: 1 mol % H_2S at 400 °C, pressure: 2-20 atm. At higher pressures, the sulphur loading values were considerably higher, reaching estimated values as high as 97 % of the maximum loading capacity at 20 atm. At 2 atm, sorbent utilization was only 52 % of the maximum capacity. Possibly, the diffusion of H_2S to the interior of the pellet is enhanced at higher pressure.

Table 3.5: The effect of pellet size, space velocity and H_2S inlet concentration on the H_2S reaction with a sorbent. Note that TGA is a thermogravimetric reactor.

Researcher	**Sorbent**	**Reactor Type**	**Pellet Size**	**Space Velocity**	**H_2S inlet concentration**
Woods *et al.* (1990)	Zinc titanate	TGA	The smaller pellets (3.2 mm) reacted appreciably faster than larger pellets (4.8 mm). Similar results were obtained at other temperatures.	-	Concentration was varied from 0.25-2.5 mol % at 1 atm and 705 °C. As expected the global rate increased with increasing H2S concentration.
Lew *et al.* (1992 b)	ZnO	TGA	[Inlet concentration only] Concentration was varied from 1-3 mol % at 1 atm and 500 °C. The reaction rate increased with increasing H2S concentration.		
Li *et al.* (1997)	ZnO-MnO	TGA	[Pellet size only] The initial and final reaction rates were significantly increased with a decrease in the pellet size from 4mm to 3.3mm.		
Turton *et al.* (2004)	ZnO	TGA	[Pellet size only] No difference in reaction rate between size fractions from 37-137 μm.		
Sánchez *et al.* (2005)	Z-Sorb III	fixed bed	[Space velocity only] Conditions: 10 atm, 400 °C, gas space velocities of 3500 h^{-1} to 10 000 h^{-1}. At higher velocity, sulphur uptake by the sorbent is lower. In addition to diffusion resistance, a possible explanation would be that, at the higher velocity, the bed length might be shorter than the absorption front. Breakthrough of the higher velocity occurred at about one third of the lower velocity result.		

Chapter 4

Gas-solid Reaction Theory

1. Introduction

It is important to understand the theory of non-catalytic gas-solid reactions to be able to design experiments and interpret their results. The analysis of a typical gas-solid reaction is well covered in the texts by Szekely *et al*. (1976) and Levenspiel (1979 and 1999) and Doraiswamy and Sharma (1984). The theory is introduced before developing the mathematical models to describe these processes.

The gas-solid general reaction is:

$$aA_{(g)} + bB_{(s)} \rightarrow cC_{(g)} + dD_{(s)} \qquad (4.1)$$

Doraiswamy amd Sharma (1984) classify these into five types:

Type A:	$a, b, c, d \neq 0$	(Reduction and roasting of ores)
Type B:	$c = 0$	
Type C:	$a = 0$	(Decomposition reactions)
Type D:	$d = 0$	(Oxidation/chlorination of ores)
Type E:	a and $d = 0$	(Gasification reactions)

The H_2S-ZnO reaction is Type A.

2. General reaction mechanism

Szekely *et al*. (1976) describes the general mechanism for a reaction-diffusion system. A generalized model would be able to mathematically describe the following processes, accounting for chemical and structural change. This is also shown in Figure 4.1.

1. Gas phase mass transfer of the gaseous reactant from the bulk of the gas stream to the external surface of the solid particle.

2. Gas movement in the particle:

   (i) Diffusion of the gaseous reactant through the pores of the solid matrix, which would consist of a mixture of solid reactants and products.
   (ii) Adsorption of the gaseous reactant on the surface of the solid matrix.
   (iii) Chemical reaction at the surface of the solid matrix.
   (iv) Desorption of the gaseous product from the surface of the solid matrix.
   (v) Diffusion of the gaseous product through the pores of the solid matrix.

3. Gas phase mass transfer of the gaseous product from the external surface of the solid to the bulk of the gas stream.

For exothermic or endothermic reactions, the diffusional and reaction steps will also be accompanied by heat transfer processes, which affect the temperature:

- Convective (and possibly radiative) heat transfer between the gas stream and the surface of the solid particle.
- Conduction heat transfer within the solid reactant-product matrix.

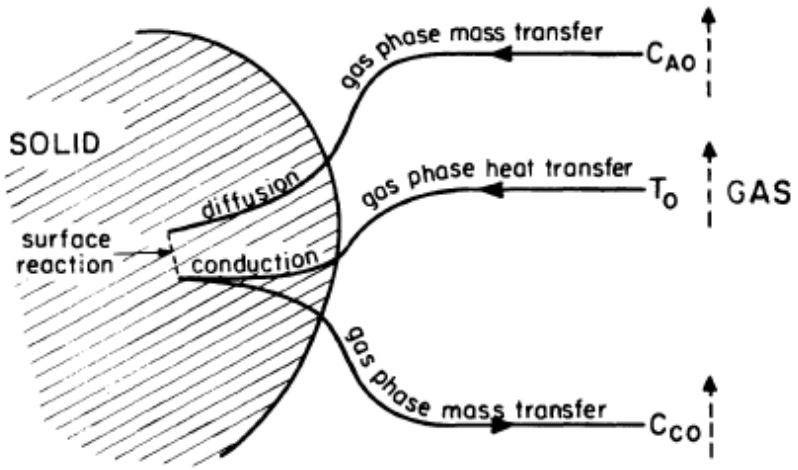

Figure 4.1: The transport processes occurring in a gas-solid reaction. From Szekely *et al*. (1976)

Lastly, there would be the structural changes of the solid to consider, such as sintering, swelling, cracking or softening. This could change the pore sizes which could affect the overall reaction rate.

3. Mass transfer effects

The process of mass transfer from one phase to another is well understood and an enormous subject area in chemical engineering. The transfer process can be described and quantified by a mass transfer coefficient, determined by flow and physical characteristics of the species in the system.

For gas-solid reactions, in a fixed bed, the mass transfer of interest is the reactant species in the bulk gas onto the surface of the solid stationary particles, through a layer of gas film. The solid may be porous or non-porous. The mass transfer coefficient is available from a number of correlations. For the flow of fluid past a single particle, the correlations are of the form:

$$N_{Sh} = A + BN_{Sc}^{m} N_{\mathrm{Re}}^{n} \tag{4.2}$$

For example, the Ranz and Marshall Equation for N_{Re} 0-200 was given by both Szekely *et al*. (1976) and Levenspiel (1999).

$$N_{Sh} = 2 + 0.6N_{Sc}^{1/2} N_{Re}^{1/3} \tag{4.3}$$

$$N_{Sh} \equiv \frac{k_g L}{D_{AB}} \tag{4.4}$$

$$N_{Sc} \equiv \frac{\mu}{\rho D_{AB}} \tag{4.5}$$

$$N_{Re} \equiv \frac{u\rho L}{\mu} \tag{4.6}$$

N_{Sh}	Sherwood number	[-]
N_{Sc}	Schmidt number	[-]
N_{Re}	Reynolds number	[-]
k_g	external mass transfer coefficient	[$m.s^{-1}$]
L	characteristic length (diameter for a sphere)	[m]
D_{AB}	diffusion coefficient	[$m^2.s^{-1}$]
ρ	fluid density	[$kg.m^{-3}$]
μ	fluid viscosity	[Pa.s]
u	superficial fluid velocity	[$m.s^{-1}$]

Szekely *et al*. (1976) discussed the importance and difficulties associated with calculating (or measuring) the gas diffusion coefficient, D, of the system. They also stressed that Equation (4.3) gives almost identical Sherwood numbers compared to other correlations in the range of practical interest for gas-solid reactions. Levenspiel (1999) noted that if a particle changes size during the reaction (for example, gasification), the mass transfer coefficient would change as well since N_{Re} and N_{Sh} are dependent upon a characteristic length.

4. Chemical reaction effects

The chemical reaction can be described by a series of steps. There is adsorption of the gas onto an 'active site', the chemical reaction itself, and the subsequent desorption. Briefly, there are two types of adsorption: *physical adsorption* and *chemisorption*. Physical adsorption is governed by longer range van der Waals (or dispersion) forces and the gas molecules can form multiple layers on the solid. With chemisorption, the forces are much stronger, and are short range (due to being associated with chemical bonds). However, there is only one layer of molecules formed on the surface.

Chemical reaction is usually associated with chemisorption. The adsorption process is characterized by an equilibrium isotherm. This is an expression to determine the amount of gas adsorbed when the rate of adsorption and desorption are equal (in equilibrium).

The chemical reaction could also be viewed from a kinetic point of view. Here, the reaction takes place in three reversible steps: the adsorption of the gas with the surface to form a complex, the actual reaction, and then the desorption step. Note these steps would not be in equilibrium.

The expressions for either an equilibrium or kinetic model can become very complicated and result in a number of kinetic parameters that can only be found by regression using experimental data. With so many parameters, the sensitivity of the model is compromised.

As a result, most work has resulted in a simple rate expression, such as an empirical power law (based on gas concentration or partial pressure) or equilibrium expression such as Langmuir-Hinshelwood-Hougan-Watson (LHHW) type. The rate constant would thus be expressed as moles A reacted per surface area per time. The rate constant would usually have temperature dependence given by an Arrhenius type of equation, with a pre-exponential (frequency) factor and activation energy.

5. Pore diffusion effects

Pore diffusion is the movement of the gas within the pores of a solid particle, due to a variation of chemical potential. This is required for the reactant gas to come into contact with some solid surface, and for the product gas to travel to the surface of the particle and be removed, as shown in Figure 4.2

There are two types of diffusion: ordinary (or molecular) diffusion and Knudsen diffusion. Ordinary diffusion applies when the gas molecules are predominantly in contact (colliding) with each other. Knudsen diffusion occurs when the gas molecules collide with the solid surface more than with each other. This occurs when the radius of the pores becomes very small (radius of 10-1000Å) or the pressure becomes very low. At low pressure, there is a larger 'free path' for the gas molecules.

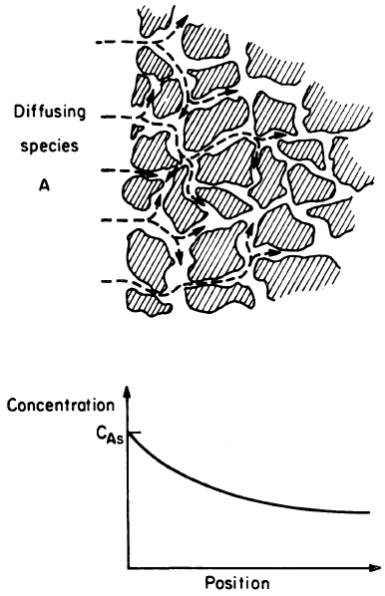

Figure 4.2: The process of gas diffusion through a solid particle. From Szekely *et al*. (1976)

Especially at low pressures, the pressure drop across a particle would not be sufficient to force the gas reactant into the particle for reaction in the pores. The mass transfer must thus occur by diffusion. In reaction engineering, for both catalytic and non-catalytic reactions, an effective diffusivity is used to take the following factors into account, as given in Szekely *et al*. (1976), Fogler (2006) and Seader and Henley (2006):

- The diffusion paths are tortuous (i.e. not a straight line).
- The pores have varying cross sectional area.
- All the surface area may not be available for reaction.
- There may be a pressure gradient in the solid.

The diffusion coefficient characterises the rate of the gas movement of a solute species (A) in another species (B), expressed as D_{AB}. There are a number of different models to express the effective diffusivities depending upon the physical system. A common method is as follows, from Seader and Henley (2006):

$$D_e = D_c\left(\frac{\varepsilon_p}{\tau_p}\right) \tag{4.7}$$

$$D_c = \left[\frac{1}{D_{AB}} + \frac{1}{D_K}\right]^{-1} \tag{4.8}$$

$$D_K = d_p\frac{\overline{u}}{3} \tag{4.9}$$

$$\overline{u} = \left[\frac{8R_gT}{\pi M_r}\right]^{0.5} \tag{4.10}$$

ε_p	particle porosity	[-]
τ_p	particle tortuosity	[-]
D_c	combined diffusion coefficient	[$m^2.s^{-1}$]
D_e	effective diffusion coefficient	[$m^2.s^{-1}$]
D_{AB}	diffusion coefficient of solute *A* in solvent *B*	[$m^2.s^{-1}$]
D_K	Knudsen diffusion coefficient	[$m^2.s^{-1}$]
$\bar{u}$	mean molecular velocity	[$m.s^{-1}$]
M_r	molecular mass	[$g.mol^{-1}$]
T	absolute temperature	[K]
R_g	gas constant	[$J.mol^{-1}.K^{-1}$]

The effective diffusivity, D_e, is found by taking into account the sorbent structure, the tortuosity, τ_p and porosity, ε_p. Then, D_c is a 'combined' diffusion term consisting of ordinary and Knudsen diffusion coefficients. Usually one term, D_{AB} or D_K would be much higher than the other.

The tortuosity has experimental values ranging from 1.5 to 10. A popular estimate is that $\tau_p = 1/\varepsilon_p$. This is known as the 'random pore model'. D_{AB} can be found from experiments in many tables and calculated standard equations, for example, in Seader and Henley (2006), Perry and Green (1999), and in particular Poling *et al*. (2001), along with various mixing rules for multi-component mixtures.

There are more complex methods to describe the pore diffusion process (for example, to account for a distribution of pore sizes); they are outside the scope of the study. Szekely *et al*. (1976) note that most of the work on pore diffusion is for heterogeneous catalysis and molecular sieve adsorption. In both cases the solid structure does not change (significantly) with time. With gas-solid reactions, however, the solid structure does change with the course of reaction.

6. Application to experiments

If the reaction kinetics of a gas-solid reaction are to be measured, it is imperative to conduct the experiment where the reaction is indeed being controlled by chemical reaction. Likewise, if it is found that the rate controlling step is mass transfer from the gas, one should design a reactor to try and minimise this effect. It is thus very important to understand how the general gas-solid reaction mechanism fits the reaction being studied.

6.1 Experiments for mass transfer controlling the reaction

According to Szekely *et al*. (1976), to establish whether a process is mass transfer limiting, a series of identical experiments using different gas velocities must be conducted. These would be single particle experiments and the conversion as a function of time would be given by Equation (4.11)

$$X = \frac{bk_g\left(C_{Ab} - C_{Cb}/K_E\right)}{\left(1-\varepsilon_p\right)\rho_c}\left(\frac{A_p}{V_p}\right)\frac{K_E}{1+K_E}t \qquad (4.11)$$

b	stoichiometric coefficient of gas species A reacting	[-]
k_g	external mass transfer coefficient	[m.s^{-1}]
C_{Ab}	concentration of gaseous reactant A in bulk gas stream	[mol.m^{-3}]
C_{Cb}	concentration of gaseous product C in bulk gas stream	[mol.m^{-3}]
K_E	equilibrium constant	[-]
ε_b	porosity of pellet	[-]
ρ_c	molar density of the pore-free solid reactant (crystalline density)	[mol.m^{-3}]
A_p	surface area of pellet	[m^2]
V_p	volume of pellet	[m^3]
t	time of reaction	[s]

From Equation (4.11), if the process is mass transfer controlling, there should be a linear relationship between the conversion and the time, since all the terms in the equation should remain constant. This assumes the particle does not change in size.

Szekely *et al*. (1976) gave a word of caution that the experiment must be carried out with high enough velocities so that the solid is not 'starved' of gas. If sufficient portion of the gas has reacted, the solid is not contacted with the bulk concentration, but rather with a lesser value.

6.2 Experiments for the chemical reaction controlling the reaction

This can only be investigated when mass transfer resistance and pore diffusion are minimized. This means that at low temperatures, with very small pellet diameters (to minimize pore diffusion) and high gas velocities (to minimize mass transfer). The point where mass transfer and diffusion limitations are negligible can be found by reducing the ratio of sample size to flowrate until reaction rate constant does not change.

Levenspiel (1979) noted that usually the sensitivity to temperature is apparent for the reaction step compared to either diffusion step. However, should the solid structure change due to the temperature (for example, by sintering), then the resistance to diffusion can change dramatically with temperature.

6.3 Experiments for the diffusion controlling the reaction

If the particle is non-porous, there is only diffusion of the reactant gas through the product layer to the unreacted surface. If the particle is porous, there is diffusion through both the ash layer and possibly through the unreacted solid pores.

According to Szekely *et al*. (1976), it would be preferable to perform independent measurements to determine the pore diffusion coefficient.

Levenspiel (1979) noted that the resistance to diffusion through the ash layer was usually greater than through the gas film, so whenever an ash layer was present, the resistance to diffusion through the gas film could be neglected.

The relationship between the time of reaction, *t*, and the particle size (usually radius, *R*), has been developed, for example, by Levenspiel (1999). These can be used to determine the reaction controlling mechanism.

Film diffusion controls	$t \propto R^{1.5–2}$	(4.12)
Ash diffusion controls	$t \propto R^2$	(4.13)
Chemical reaction controls	$t \propto R$	(4.14)

Levenspiel (1999) offers a cautionary note for using different particle sizes:

- It is unsafe to extrapolate reaction control to larger particles, but one can to smaller particles.
- It is safe to extrapolate ash diffusion control to larger particles, but not to smaller particles.

The ranges of the different controlling regimes have been shown schematically in the Figures below.

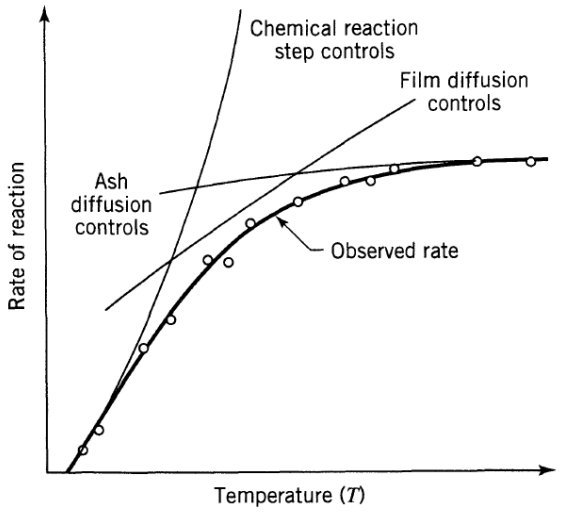

Figure 4.3: The effect of temperature on overall reaction rate. From Levenspiel (1999)

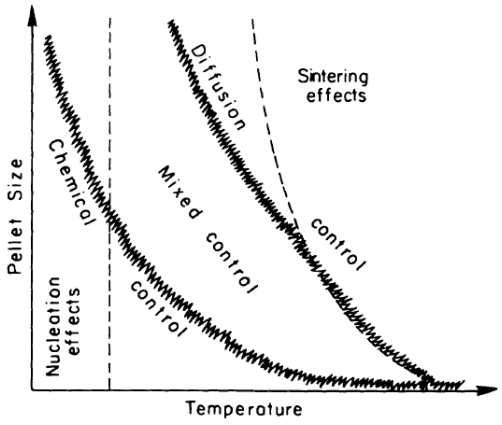

Figure 4.4: The reaction controlling regime in terms of temperature and pellet size. From Szekely *et al*. (1976)

6.4 Typical values of diffusion and mass transfer coefficients for design

The important aspect is to determine what range of values that the mass transfer and diffusion coefficients can be expected to be in, from previous studies.

From Szekely *et al*. (1976), D_{AB} for H_2O in O_2 at 450 K is 0.59 $cm^2.s^{-1}$ or 0.6×10^{-4} $m^2.s^{-1}$. A reasonable range is thus 10^{-4} $m^2.s^{-1}$. From Seader and Henley (2006), all quoted binary diffusivities were above 400 K range from 0.61 – 4.86×10^{-4} $m^2.s^{-1}$. The diffusion coefficient has been reported to be proportional to $T^{1.75}$ (absolute scale), for example, from Seader and Henley (2006) using the Chapman-Enskog equation . Hence at 500 °C a realistic value to use would be 1.17 – 9.66×10^{-4} $m^2.s^{-1}$. However, the gas viscosity would also change with temperature.

From Equation (4.7), along with the random pore model and neglecting Knudsen diffusion, D_e can be defined as $D_{AB}\times\varepsilon_p^2$, it most likely be smaller than D_{AB} by two orders of magnitude since ε_p would be between 0 and 1. Hence, D_e is approximately 10^{-6} $m^2.s^{-1}$.

For the external mass transfer coefficient, k_g, there was limited data available as most researchers had conducted their experiments outside the mass transfer limiting conditions. A value range of k_g = 0.004 – 0.06 $m.s^{-1}$ was used in Jothimurugesan and Harrison (1990).

However, a minimum value can be found using the Ranz and Marshall correlation, Equation (4.3). Assuming there is no flow, then N_{Sh} = 2. With D_{AB} = 10^{-4} and a particle diameter of 1 mm, this gives a value of k_g = 0.2 $m.s^{-1}$. This is much greater than 0.004-0.06 $m.s^{-1}$ and suggests that the reaction would not be mass transfer limiting and the effect of ash diffusion would be far more significant.

6.5 Conditions for isothermality

According to Szekely *et al*. (1976), the thermal conductivity in a porous solid is not well understood. Hence, an 'effective' thermal conductivity is used to describe the heat transfer. During a reaction, the particle is considered isothermal if:

The heat generated / consumed by the reaction =
enthalpy transport through the particle and to / from the bulk stream. (4.15)

This is likely to occur if the heat of reaction is small and the thermal conductivity is large. Otherwise, it is likely that a temperature gradient will exist through the particle.

Chapter 5

Gas-solid Reaction Modelling

1. Introduction

The modelling of a gas-solid reaction was found to be quite an extensive subject area in its own right. The goal of this chapter of the study was to research reactor modelling in order to:

- Determine the conversion of the solid in a packed bed reactor after a pre-determined reaction time.
- Determine the outlet concentration of the reacting gas as a function of time (i.e. a breakthrough curve).

As will be covered, there are many models to describe the reaction of a single particle with a gas. These are, by definition, unsteady state reactions because the conversion of the solid changes with time. A result of a model was the conversion of the solid as a function of time. The extension of describing the reaction of a single particle to a multi-particle packed bed situation was not a trivial procedure.

The discussion on models was taken from Levenspiel (1979 and 1999), Szekely *et al.* (1976) and Doraiswamy and Sharma (1984) and various papers.

2. Single particle models

It is noted that the different names, variations and developments of the models make it a confusing subject area. Doraiswarmy and Sharma (1984) and Levenspiel (1979 and 1999) present a number of possible gas-solid reaction models.

1. Shrinking core model
2. Homogeneous model, also known as the volume reaction model
3. Finite reaction zone model
4. Grain model

These models do not account for structural change of the solid. However, there have been many extensions to the models above. They include application for non-isothermal effects, decomposition and gasification reactions and application for porous and non-porous specific solids. Other extensions include the overlapping grain model and diffuse interface shrinking core model.

The models that do account for the structural change are termed 'modified', as given below:

1. Modified shrinking core model
2. Modified homogenous model
3. Modified grain model
4. Single pore model
5. Distributed pore model
6. Sintering effects

There have been numerous papers that have developed these structural models in one form or another. The important research has summarized in Table 5.1.

Table 5.1: Important developments of gas-solid reaction models

Authors	**Year**	**Title**	**Comment**
Ishida and Wen (1968)	1968	Comparison of Kinetic and Diffusional Models for Solid-gas Reactions	Similarities and differences of the unreacted core and homogenous model are examined in terms of the rate controlling factors, and their correct application to experimental data. An important work.
Wen (1968)	1968	Non-catalytic Heterogeneous Solid Fluid Reaction Models	Combination of two stages for the shrinking core model incorporating a homogeneous model and critical evaluation of experimental data.
Szekely and Evans (1970)	1970	A structural model for gas-solid reactions with a moving boundary	Introduction of the pore model and grain model
Ishida and Wen (1971)	1971	Comparison of zone-reaction model and unreacted-core shrinking model in solid-gas reactions - I Isothermal analysis	Extension of 1968 work to include diffuse zone models like the Grain Model
Szekely and Evans (1971)	1971	A structural model for gas-solid reactions with a moving boundary - II The effect of grain size, porosity and temperature on the reaction of porous pellets	Development of the grain model for pellet structural effects

Sohn and Szekely (1972)	1972	A structural model for gas-soild reactions with a moving boundary - III A general dimensionless representation of the irreversible reaction between a porous solid and a reactant gas	Development of the grain model for different pellet and grain geometries
Ramachandran and Smith (1977)	1977	A Single-Pore Model for Gas-Solid Noncatalytic Reactions	A "single pore model" to account for structural changes occurring with the reaction.
Ranade and Harrison (1979)	1979	The Grain Model Applied to Porous Solids with varying structural properties	Application of the grain model to account for structural changes in the solid
Do (1982)	1982	On the validity of the shrinking core model in gas solid reaction	The shrinking core model was rigorously justifies as a special case of the homogenous model when the reaction rate is much faster than the diffusion rate
Prasannan *et al*. (1985)	1985	A model for gas-solid reactions with structural changes in the presence of inert solids	The grain model with structural changes and the presence of inert solids
Sotirchos and Yu	1985	Mathematical Modelling of Gas-Solid Reactions with Solid Product	Random pore structural models that use a pore size distribution
Sotirchos and Yu	1987	A Generalized Pore Model for Gas-Solid Reactions Exhibiting Pore Closure	Gas solid reaction exhibiting pore closure for pore structure evolution model. Very complicated.
Sotirchos and Yu	1988	Overlapping Grain Models for Gas-Solid Reactions with Solid Product	Extension of the grain model
Khan and Bowen (1992)	1992	A theoretical analysis of reaction zone thickness and concentration profile in non-catalytic, gas-solid reactions	Testing of linear, sigmoidal and exponential concentration profiles in the diffuse interface model. The sigmoidal and exponential were more realistic
Villa *et al*. (1992)	1992	The shrinking core model for non-catalytic gas-solid reactions with arbitrary order with respect to the gaseous reactant and general boundary conditions	Generalization of the shrinking core model.
Efthimiadis and Sotirchos (1993)	1993	A Partially Overlapping Grain Model for Gas-Solid Reactions	Further development of Overlapping Grain Model.

Lastly, Levenspiel (1979) lists some miscellaneous gas-solid models and accounts for some specific reaction scenarios. These were:

- Crackling core model
- Nucleation model
- Solid catalyzed gas-solid reactions
- Reaction between solids proceeding through gaseous intermediates
- Consecutive reactions
- Reaction of two gases with the same solid
- Reaction of two solids
- Delayed diffusion in solids
- Thermal decomposition models
- Phase change models

This study will focus on the shrinking core model, the homogenous model (briefly) and the grain model.

3. The shrinking core model

In the model, the three processes of mass transfer of the reactant from the gas, chemical reaction and pore diffusion are treated as individual steps. The *assumptions* of the model are:

- The particle is initially non-porous.
- The particle size does not change during reaction.
- The particle is isothermal.
- The reaction occurs on the surface of the particle. As the surface reacts, the reaction front moves towards the centre.
- The effective diffusivity is constant.
- The surface area remains constant.
- The mass transfer coefficient is constant.
- There is equi-molar counter diffusion of gases.
- The reaction is of the first order.
- The pseudo-steady state assumption.

Doraiswarmy and Sharma (1984) explained that "the physical significance of the pseudo-steady state assumption is that the reaction interface can be assumed to remain stationary at any time, while a steady-state diffusion flux is calculated to find the concentration profile." It is valid for $C_{Ab}M_B/\rho_p < 10^{-3}$. It almost always holds for gas-solid, but not always for liquid-solid reactions. Some of the other assumptions have been accounted for by variations to the basic model, for example, non-isothermal, size changes and different reaction orders.

The reactant gas firstly moves through a gas film onto the surface of the particle. It then reacts on the surface. The solid product is called the 'ash layer' and is porous. Subsequent to the initial surface reacting, the reactant gas must now diffuse through the ash layer to reach

the unreacted core. By writing mass balances over the gas film, for the chemical reaction and for diffusion through the pores, the following expressions are obtained. They are standard solutions, applicable to spheres, from Levenspiel (1999).

Mass Transfer Controls
$$t = \left[\frac{\rho_p R}{3bk_g C_{Ab}}\right] X \qquad (5.1)$$

Ash Diffusion Controls
$$t = \left[\frac{\rho_p R}{6bD_e C_{Ab}}\right]\left(1 - 3(1-X)^{2/3} + 2(1-X)\right) \qquad (5.2)$$

Reaction Controls
$$t = \left[\frac{\rho_p R}{bk_s C_{Ab}}\right]\left(1 - (1-X)^{1/3}\right) \qquad (5.3)$$

X	conversion of solid	[-]
ρ_p	molar particle density (note particle is non-porous)	[mol.m^{-3}]
R	radius of spherical particle	[m]
b	stoichiometric coefficient of gas species A reacting	[-]
C_{Ab}	concentration of gaseous reactant A in bulk gas stream	[mol.m^{-3}]
k_s	surface reaction rate constant	[m.s^{-1}]
k_g	mass transfer coefficient	[m.s^{-1}]
D_e	effective diffusion coefficient	[m^2.s^{-1}]
t	time of reaction	[s]

This reaction process can be represented by a very useful diagram, given by Doraiswamy and Sharma (1984).

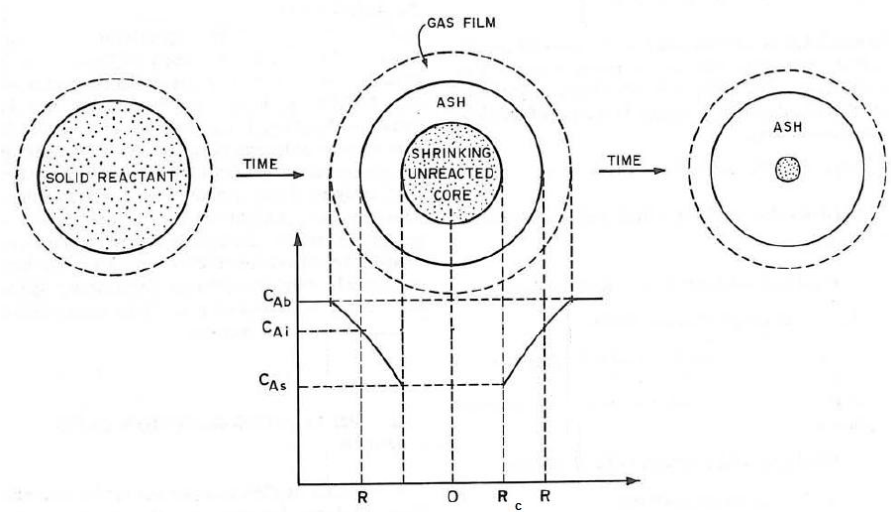

Figure 5.1: The shrinking core model for a particle of unchanging size. Adapted from Doraiswamy and Sharma (1984)

The model results in the following conversion-time normalized profiles, for a sphere:

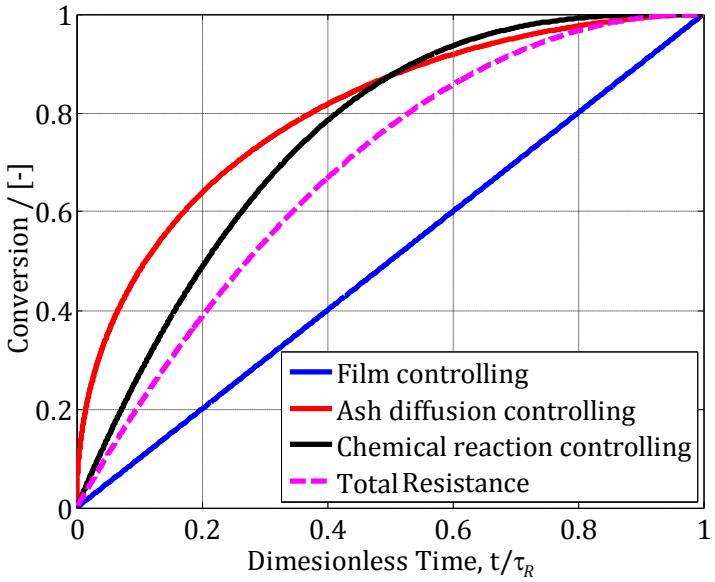

Figure 5.2: Relative effect of film, ash and chemical reaction controlling effects on a gas-solid reaction with the shrinking core model in a sphere, where τ_R is the time for complete reaction (all available solid has reacted). This is equal to the term in square brackets of Equations (5.1), (5.2) and (5.3).

The extension to particles of changing size was covered by Szeleky *et al.* (1976). A factor Z was defined as the ratio of the molar volume of the product formed to the molar volume of the reactant. The equations, for a sphere with the shrinking core model, with volume change are given below.

$$t^+ = 3\left\{\frac{Z_v - \left[Z_v + (1-Z_v)(1-X)\right]^{2/3}}{Z_v - 1} - (1-X)^{2/3}\right\} \tag{5.4}$$

$$t^+ = \frac{t^*}{\sigma_s^2} \tag{5.5}$$

$$t^* = \left(\frac{bk_s C_{Ab}}{\rho_p R}\right) t \tag{5.6}$$

$$\sigma_s^2 \equiv \left(\frac{k_s}{2D_e}\right)\left(\frac{V_p}{A_p}\right)\left(1 + \frac{1}{K_E}\right) \tag{5.7}$$

Z_v	ratio: molar volume of the product formed to the molar volume of the reactant	[-]
A_p	surface area of pellet	[m^2]
V_p	volume of pellet	[m^3]

Note that σ_s is called the 'shrinking core reaction modulus' and is used to describe the combined effect of chemical reaction and diffusion.

4. Practical application of the shrinking core model

There are two main cases where the model is *limited*. The first case is if the reaction has a 'diffuse' reaction front (for example, if the reactant particle is porous). Secondly, should there be a large heat of reaction, it may cause a significant temperature gradient in the particle. Wen (1968) and Ishida and Wen (1971) address the problem of a diffuse reaction front by combination with the homogenous model.

There are two cases where the model does not apply: a slow reaction in a very porous particle and if the solid is converted *without contact* with a gas, for example, decomposition upon the application of heat.

Jothimurugesan and Harrison (1990) explain that for a porous reactant, the unreacted core model can reasonably be applied *only* when the transport resistances (external mass transfer from the bulk gas to pellet surface and diffusion through the porous product layer) control the global rate. If the surface reaction resistance is important, the reaction in a porous solid will occur in a zone of finite radial thickness and the basic requirement of a reaction surface is not satisfied.

Now the transport control condition is most likely to be satisfied at high reaction temperatures. This is because there is greater temperature dependence of the rate constant k_s than either mass transfer coefficient, k_g or effective diffusion coefficient D_e.

This is echoed by Szekely *et al.* (1976). The concentration of the fluid reactant would be constant throughout the particle (when chemical reaction presents the major resistance). The reaction would then occur uniformly throughout the solid. Hence, to summarize:

- Reaction control: The gas reactant would be in the entire solid and a diffuse reaction zone exists. The shrinking core model cannot be used. It applies to porous solids or slow reactions.

- Mass transfer and diffusion control: The reaction occurs in a narrow boundary between the unreacted and the completely reacted zones. The diffusion controlled shrinking core model can be used.

The shrinking core model can be used to determine the rate limiting step by conducting a single particle experiment under different operating conditions, as discussed in Chapter 4.

5. The homogenous model

This model applied to porous solids when the rate of diffusion would be rapid. Physically, the gas would diffuse into the solid instantaneously, and have a (near) constant concentration

profile. The reaction occurs throughout the solid as a whole. The model equations for a sphere have been documented in Doraiswamy and Sharma (1984) and Ishida and Wen (1968). It can be shown the shrinking core model is a limiting case of the homogenous model.

6. The grain model

The grain model was developed by Szekely and Evans (1970), Szekely and Evans (1971) Sohn and Szekely (1972) and finally comprehensively in Szekely *et al.* (1976). It was a major advancement in gas-solid reaction modelling.

The model divided up the solid particle into sub-particles or grains. The grains could be assumed to be spheres, cylinders or slabs. It then assumed that the shrinking core model applied to each grain, which was essentially non-porous. The solution was quite complicated. For some limiting cases, analytical 'asymptotic' solutions have been found. For cases between the asymptotic solutions, numerical techniques were required to solve the equations. However, later some numerical approximations were developed by Evans and Ranade (1980) to simplify the general solution.

The particle could be considered a slab, cylinder or sphere, and likewise the grains could also be those shapes. This method was thus quite flexible to describe the solid structure. Usually the grains would be identified by images from a scanning electron microscope.

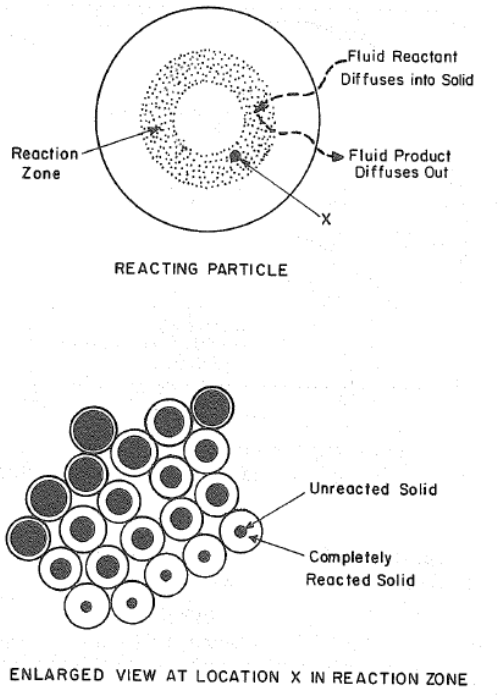

Figure 5.3: Schematic representation of the grain model. From Ranade and Evans (1980)

The gas-solid reaction was characterised by a reaction modulus, σ or $\hat{\sigma}$. This value was a measure of the relative magnitude for the rate of chemical reaction and rate of diffusion in

the particle. By evaluating this value, it could help determine which solution to use, depending upon a dominant controlling mechanism. Szekely *et al.* (1976) defines the modulus as:

$$\hat{\sigma} \equiv \frac{\sigma}{\sqrt{2F_g F_p}} \equiv \frac{V_p}{A_p}\sqrt{\frac{(1-\varepsilon_p)k_s F_p}{2D_e}\left(\frac{A_g}{F_g V_g}\right)\left(1+\frac{1}{K_E}\right)} \qquad (5.8)$$

F_g	grain factor: equal to 1, 2 or 3 for a slab, cylinder or sphere	[-]
F_p	particle factor: equal to 1, 2 or 3 for a slab, cylinder or sphere	[-]
ε_p	particle porosity	[-]
A_g	surface area of grain	[m^2]
V_g	volume of grain	[m^3]

The solutions to the grain model were presented by Szekely *et al*. (1976), however, the solution was complex. Asymptotic solutions were available. For high values of $\hat{\sigma}$, there could either be a fast chemical reaction ($k_s \rightarrow \infty$) or slow pore diffusion ($D_e \rightarrow 0$). This means that the process would be controlled by the diffusion rate. Alternatively, For low values of $\hat{\sigma}$ < 0.3, the pore diffusion offers negligible resistance ($D_e \rightarrow \infty$) and the chemical reaction controls the process.

For all other values of $\hat{\sigma}$, a numerical solution would be required. However, Evans and Ranade (1980) provide a very useful approximation which can be used. This is given as:

$$t^* = g_{F_g}(X) + \hat{\sigma}^2 p_{F_p}(X) + (0.21X - 0.31X^2)(1+\hat{\sigma}^2)\exp\left\{-0.9\left[\ln\frac{\hat{\sigma}}{1.08}\right]^2\right\} \qquad (5.9)$$

$$g_{F_g}(X) = 1-(1-X)^{1/3} \qquad (5.10)$$

$$p_{F_p}(X) = 1-3(1-X)^{2/3}+2(1-X) \qquad (5.11)$$

$$t^* = \left(\frac{bk_s C_{Ab}}{\rho_p}\frac{A_g}{F_g V_g}\right)t \qquad (5.12)$$

Note that for spheres, particles and grains: $F_g = F_p = 3$, hence, $A = 4\pi R^2$, $V = 4/3\,\pi R^3$, where R is the radius of the particle or grain.

Equation (5.9) is plotted in Figure 5.4, with different values of $\hat{\sigma}$ and compared to the Shrinking Core model in Figure 5.5

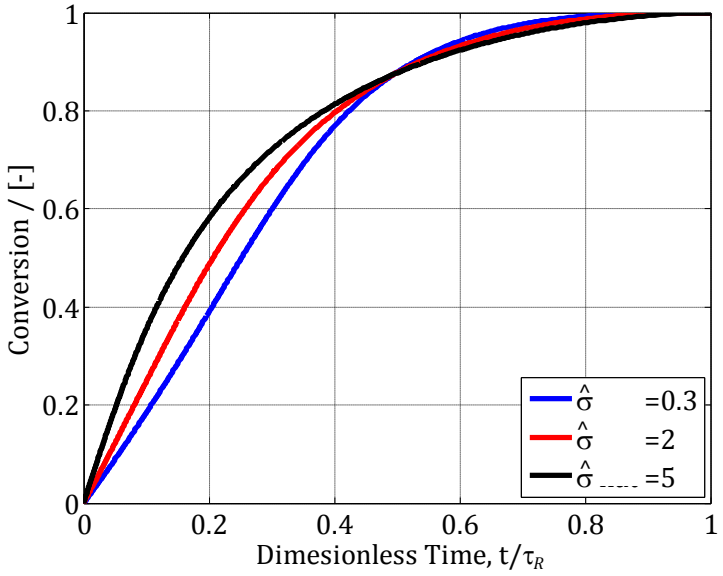

Figure 5.4: Approximate solution for the grain model as a function of $\hat{\sigma}$

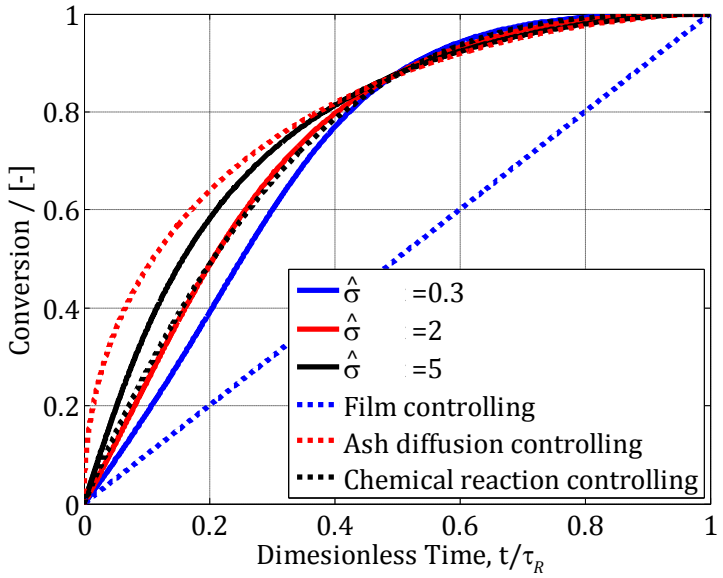

Figure 5.5: A comparison of the grain model (solid lines) with the shrinking core model (dotted lines) under different controlling regimes

7. Application to this study

In order to apply the reaction models to this study, the single particle models must be extended to a fixed bed. This is explained by Szekely *et al.* (1976) following the paper by Evans and Song (1974). Szekely *et al.* (1976) incorporate the grain model into a fixed bed reactor model while Doraiswamy and Sharma (1984) incorporate the shrinking core model. The problem, however, was that the computation was difficult, due to non-linear partial differential equations arising from the mass an energy balances. There have been relatively

few studies relating the solid particle models described for single particles to packed beds and even fewer studies comparing packed bed reactor results to a model.

Ranade and Evans (1980) applied the grain model to a packed bed reactor. Here, the reaction was the reduction of iron oxide with hydrogen. The grain model used the simplifications presented by Evans and Ranade (1980). It was noted that the reactor was non-isothermal. The agreement of the model and simulation was good.

Park *et al*. (1984) presented an interesting approach, where the relationship between the conversion and time of a single particle was incorporated directly into the packed bed model. The model was applied successfully to the reaction of oxidation of iron using stream.

Sotirchos and Zarkanitis (1989) used a second order equation to describe the mass transfer through the bed, including an axial dispersion coefficient for the bed. They used models based upon pore structure and grain structure to simulate the packed bed behaviour. Their simulation results showed that the form of the pore or grain size distribution strongly influenced the performance of the reactor. No comparison to experiments was made.

Mutasher *et al.* (1989) studied the reduction of copper sulphate with hydrogen. They used the diffuse interface model to describe the individual particles. The bed was non-isothermal and included an energy balances with heat transfer from the solid by conduction and radiation. The simulated results showed good agreement with the experiments.

7.1 Development of packed bed model for this study

In this study, a procedure was developed by the author to apply a specific form of conversion-time expression for a single particle, to a packed bed. The specific form was in fact quite generalized. Here, the shrinking core model and grain model were applied.

From single particle experiments, conversion-time profiles can be found. These profiles are usually fitted with a model, either using some fitting parameters (such as effective diffusivity, mass transfer coefficients etc.) or completely predicted from previous work.

The full solution has been detailed in the Appendix, Section A.6. The shrinking core model uses Equations (5.1) – (5.3) and the grain model uses Equations (5.9) – (5.12) to describe the conversion-time profile. The assumptions of both models were explained in Sections 3 and 6.

With the assumptions of plug flow, no axial dispersion and isothermal conditions, the standard equation for a packed bed of particles is derived in the Appendix A.6, Section 3.

$$\varepsilon_b \frac{\partial C_{Ab}}{\partial t} + u \frac{\partial C_{Ab}}{\partial z} = -\hat{r}_A \qquad (5.13)$$

ε_b	voidage of reactor bed	[-]
C_{Ab}	concentration of gaseous reactant *A* in bulk gas stream	[mol.m^{-3}]

C_B^o	rate of reaction of *A* per volume reactor per time	[mol *A*.m^{-3}.s^{-1}]
u	superficial gas velocity	[m.s^{-1}]
t	time of reaction	[s]
z	bed depth	[m]
$\hat{r}_A$	rate of reaction of *A* per volume reactor per time	[mol *A*.m^{-3}.s^{-1}]

It can be shown (Appendix, Section A.6) that the reaction rate of *A* is

$$-\hat{r}_A = \frac{(1-\varepsilon_b)}{-b} C_B^o \frac{dX}{dt} \tag{5.14}$$

Pseudo-steady state in the gas phase was assumed. Hence Equation (5.13) becomes

$$u\frac{dC_{Ab}}{dz} = \frac{(1-\varepsilon_b)}{-b} C_B^\circ \frac{dX}{dt} \tag{5.15}$$

An expression is required for dX/dt. This is available from the single particle studies and will be implemented in Section 7.2. Usually, they will be of the form:

$$t = \frac{1}{\kappa C_{Ab}} f(X) \tag{5.16}$$

The method described below will work for any single particle model taking the above form. Note κ is constant and will be some combination of particle density, rate constant, radius etc. and that $f(X)$ is an arbitrary function describing the conversion. Differentiating Equation (5.16) with respect to time, implicitly:

$$\frac{d}{dt}(t) = \frac{1}{\kappa C_{Ab}} \frac{d}{dt}(f(X)) \tag{5.17}$$

$$1 = \frac{1}{\kappa C_{Ab}} \left(g(X) \frac{dX}{dt} \right) \tag{5.18}$$

Rearranging

$$\frac{dX}{dt} = \kappa \Gamma(X) C_{Ab} \tag{5.19}$$

Where $\Gamma(X)$ is a re-arranged form of $g(X)$ and that $g(X)$ depends upon the differentiation of $f(X)$. This can now be applied to the overall balance, i.e. Equation (5.15).

$$\frac{dC_{Ab}}{dz} = \frac{(1-\varepsilon_b)}{-bu} C_B^\circ \kappa \Gamma(X) C_{Ab} \tag{5.20}$$

Let
$$\xi = \frac{(1-\varepsilon_b)}{bu} C_B^\circ \tag{5.21}$$

Integrating
$$\int_{C_{Ab}^o}^{C_{Ab}} \frac{dC_{Ab}}{C_{Ab}} = -\xi\kappa \int_0^z \Gamma(X)dz \tag{5.22}$$

$$C_{Ab} = C_{Ab}^\circ \exp\left\{-\xi\kappa \int_0^z \Gamma(X)dz\right\} \tag{5.23}$$

This expression for C_{Ab} can be inserted into the conversion Equation (5.19).

$$\frac{dX}{dt} = \kappa\,\Gamma(X) C_{Ab}^\circ \exp\left\{-\xi\kappa \int_0^z \Gamma(X)dz\right\} \tag{5.24}$$

This equation, when solved, will give the conversion as a function of time and position in the bed. To apply it, it is only necessary to evaluate the expressions for κ and $\Gamma(X)$. Note that this solution is quite complex and is developed in the Appendix, Section A.6. Essentially, Equations (5.19) and (5.20) are treated as coupled partial differential equations and solved simultaneously using a numerical technique.

7.2 Application of Packed Model to the Shrinking Core and Grain Model

Consider the *reaction controlled* shrinking core model. The specific conversion time relationship required as Equation (5.16) has been given in Section 3.

Reaction Controls
$$t = \frac{\rho_p R}{b k_s C_{Ab}}\left[1-(1-X)^{1/3}\right] \tag{5.3}$$

Thus, for Equation (5.16)
$$\kappa_{SCM} = \left[\frac{\rho_p R}{b k_s}\right]^{-1} \tag{5.25}$$

$$f_{SCM}(X) = 1-(1-X)^{1/3} \tag{5.26}$$

Note the Equation (5.3) can be easily differentiated and re-arranged to find κ and $\Gamma(X)$.

$$\frac{dX}{dt} = \frac{3bk_s C_{Ab}}{\rho_p R}\left[(1-X)^{-2/3}\right] \tag{5.27}$$

$$\frac{dX}{dt} = 3\kappa(1-X)^{-2/3} C_{Ab} \tag{5.28}$$

And
$$\Gamma_{SCM}(X) = 3(1-X)^{-2/3} \tag{5.29}$$

Consider the grain model:

$$t = \frac{\rho_B}{bk_s C_{Ab}} \frac{F_g V_g}{A_g} \left[g_{F_g}(X) + \hat{\sigma}^2 p_{F_p}(X) + \left(0.21 - 0.31X^2\right)\left(1 + \hat{\sigma}^2\right) \exp\left\{ -0.9 \left[\ln\left(\frac{\hat{\sigma}}{1.08} \right) \right]^2 \right\} \right] \tag{5.30}$$

Where for spherical grains and pellets:

$$g_{F_g}(X) = 1 - (1 - X)^{1/3} \tag{5.31}$$

$$p_{F_p}(X) = 1 - 3(1 - X)^{2/3} + 2(1 - X) \tag{5.32}$$

Thus,

$$\kappa_{GM} = \left[\frac{\rho_B}{bk_s} \frac{F_g V_g}{A_g} \right]^{-1} \tag{5.33}$$

$$f_{GM}(X) = g_{F_g}(X) + \hat{\sigma}^2 p_{F_p}(X) + \left(0.21 - 0.31X^2\right)\left(1 + \hat{\sigma}^2\right) \exp\left\{ -0.9 \left[\ln\left(\frac{\hat{\sigma}}{1.08} \right) \right]^2 \right\} \tag{5.34}$$

Thus, this model can also be used. The differentiation and re-arrangement of Equation (5.30) is slightly more tedious.

8. Summary of gas-solid reaction modelling

With gas-solid reaction modelling, there has been major focus by researchers upon the modelling of single particles. With time, new models with certain applications were developed whilst others were generalized and become increasingly more mathematically complex. Perhaps the two models that received the most attention were the shrinking core model (for its simplicity) and the grain model (for its physical meaning).

There was far less literature on the application of these single particle models to a packed bed reactor. The author presented a procedure that used a generalized method, suitable for computer implementation that allowed for easier application of the single particle models, provided that they could be arranged into a suitable form.

The shrinking core model will be compared to the experimental results. These results would be duly obtained from a laboratory scaled fixed bed gas-solid reactor. The design and commissioning of this reactor unit is now presented in Chapters 6, 7 and 8.

Chapter 6

Experimental Design

1. Introduction

The objective of the study was to conduct high temperature desulphurization of syngas. Hence, two main units would be required in the apparatus: the gasifier (to produce syngas with H_2S) and the desulphurization reactor (to remove the H_2S). Both units would be high temperature reactors. In addition, it was known that the feed would consist of a hydrocarbon liquid mixture as a fuel and an oxidizing agent. Desulphurization would be by reaction with a solid at high temperature.

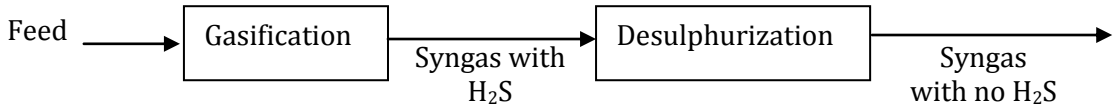

Figure 6.1: Basic block diagram of process for experimental apparatus

Before proceeding into the detailed design of the system, the experiment was planned. This was done to determine exactly what data was desired from an experiment, how it was going to be obtained from the apparatus and how it achieves and applies to the goals of the study. Once this information was set, the design and construction of the apparatus could commence accordingly.

The following experimental design has been adapted from the "Professional Reference Shelf" support material from Fogler (2006). The independent and dependent variables are introduced. These allowed the experimental objectives to be clearly defined and subsequently the necessary measurements required to achieve the objectives.

The concept of optimizing the reactor's performance is then discussed. Lastly, the actual experiments are detailed, along with the statistical analysis that was recommended.

2. Independent experimental variables

An independent variable is defined as a manipulated variable in an experiment or study whose presence or degree determines the change in the dependent variable. The independent variables must be identified and set to a known value (not necessarily constant) at the start of an experiment. It was anticipated, but not guaranteed, that a change in each variable (provided the others remained constant) would cause a change in the outcome of the experiment. This could be a large or small change.

An important experimental decision was to decide upon the *range* over which the effect of an independent variable would be examined. In addition, in some instances, it could be possible to group experimental variables into dimensionless groups, which could shorten experimental runs and measurements. This was not the case with this gas-solid reaction study.

For the gasification and desulphurization experiments, the main variables were temperatures, pressures, compositions and flowrates. The independent variables are given below. These are set directly for each experiment and, for this study, should remain constant throughout the course of the experiment.

- System pressure: gasification and desulphurization reactors
- Gasification temperature
- Desulphurization temperature
- Space velocity
    - In gasifier: determined by flowrate of feed species and reactor volume
    - In reactor: determined by flowrate of syngas (from gasifier) and the volume of sorbent in the bed
- Species flowrates into gasifier
    - Fuel composition (mixture of organic compounds)
    - Fuel flowrate
    - Oxidizer composition
    - Oxidizer flowrate
- Sorbent
    - Type and preparation method
    - Particle size
- Time of reaction: also determined by the mass of sorbent loaded into the reactor.
- Mass of sorbent used: influenced by the time of the experiment for the reaction to take place.
- Sorbent type. sorbents differ due to variation in their:
    - Chemical composition: On a mass basis, simply what species are present, including the presence of inert species.
    - Physical structure: The type of solid phase (if applicable) and the structural characteristics. This is also determined by preparation of the sorbent (below).

- Preparation of the sorbent: This influences the structural characteristics, such as pore size distribution, grain size and shape, surface area, density, distribution of active sites on support material (if applicable).

The process of setting each of the above variables to a specific value defined the *operating condition* of the apparatus. Hence, changing an independent variable changed the system's operating condition.

Note that the preparation of the sorbent was very important, with many of the studies explaining in depth their experimental procedures. This was, however, outside the scope of the study.

3. Dependent experimental variables

These were the quantity or properties that 'responded' in the system, due to the interactions of the independent variables. Not all these variables would necessarily be measured.

- Syngas composition: determined by gasification temperature and species flowrates.
- Inlet gas concentration to desulphurization reactor: determined by temperature and pressure, or volumetric flow.
- The conversion of zinc oxide to zinc sulphide (i.e. the desulphurization reaction)
- The outlet concentration of H_2S: determined by the extent of reaction.

4. Experimental objectives

For each experiment, under a particular operating condition, the objectives were to find:

- The sulphur loading of the sorbent (how much sorbent that had reacted compared to the theoretical amount that should have reacted).
- The degree of desulphurization (the minimum H_2S outlet concentration achieved).
- Time of H_2S breakthrough (the time taken for the outlet concentration reach a certain maximum value, such as 100 ppm). This could be determined by the measuring instrument's detection limit.

For all the experiments, there was the aim of optimization to try and achieve the 'best' reacting system. This is discussed in due course.

5. Experimental measurements to achieve objectives

For each experimental run, the following information would be measured, under a set of controlled experimental operating conditions, to achieve the above objectives:

- The conversion of the sorbent after the experiment.
- The outlet concentration of H_2S as a function of time during the experiment.

It was proposed that the conversion could be found from the change in mass of the sorbent and the outlet H_2S concentration by gas analysis using gas chromatography. The reliability of success of these methods will be duly discussed in Chapter 10.

6. System sampling for analysis

Sampling from the experimental system is critical for accurate data to be obtained for subsequent measurement and it thus has an important influence on the reactor design. The sampling is required for some form of analysis. For gas-solid reactions, this was usually sampling for the composition analysis of the gas phase.

For the solid and gas phase, the sample taken must be: representative of the process stream (gas) or bed (solid); should minimize the disturbance to the process with respect to the operating conditions (temperature, pressure, flowrate) and should be repeatable.

Practically, gas sampling is straightforward whereas solid sampling is difficult, especially at high temperatures.

7. Sorbent performance in a gas-solid reactor: the goal of optimization

Reactor design strives to achieve optimal conditions to achieve the 'best' result from the reactor unit. For any optimization analysis, criteria that define the 'optimal point' must be established first. In other words, *what* will operating at the optimal point actually achieve? The next question is, how can the corresponding combination of settings (of independent variables) be found to achieve this?

For a gas-solid reaction process, the function of the unit is strongly dependent upon the physical limitations of the reaction and the role of the unit in the overall process of a plant. These constraints provide the boundary limits of any possible optimization procedure.

The ideal reactor is presented before looking at certain constraints that are imposed on the reactor, and how these affect the breakthrough time and conversion of the sorbent.

7.1 The ideal fixed bed gas-solid reactor

For the ideal case, all the sorbent would react with the gas instantaneously. The result is that there is no gas species in the outlet until all the sorbent has reacted. Hence, the mass of sorbent required would be found from a mass balance with the inlet H_2S concentration, C_{H2S} and flowrate, Q and time.

$$m_{ZnO} = n_{H_2S} \times M_{ZnO} \times t = C_{H_2S} \times Q \times t \qquad (6.1)$$

m_{ZnO}	mass zinc oxide required	[g]
n_{H2S}	molar flowrate of H_2S	[mol.min^{-1}]
M_{ZnO}	molar mass of ZnO	[g.mol^{-1}]

C_{H2S}	concentration of H_2S at temperature T	[$mol.m^{-3}$]
Q	volumetric flowrate at temperature T	[$m^3.min^{-1}$]
t	time of reaction	[min]

The ideal breakthrough curve (H_2S concentration as a function of time) is shown below in Figure 6.2.

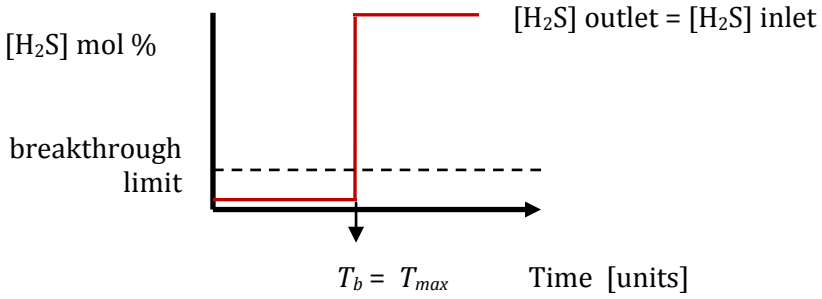

Figure 6.2: Ideal breakthrough curve of H_2S from a packed bed

T_b is the breakthrough time (time to reach a set maximum concentration level).
T_{max} is the maximum time (when all the sorbent has theoretically reacted, according to a mass balance).

Practically, it is almost impossible to achieve this type of operation due to physically limiting steps of the reaction and, as a direct consequence, the associated process requirements.

7.2 Physical limitations

For identifying the constraints of optimization, one must firstly look at the physical limitations of the actual gas-solid reaction. This has been discussed in Chapter 4 and 5. The equilibrium constant for a gas-solid reaction is available from thermodynamics, by calculating the Gibbs energy of the reaction, from the Gibbs free energy of each reactant, as a function of temperature and gas composition. This is an absolute limit to the outlet concentration of the gas, meaning that further reaction simply cannot occur under the current set of operating conditions.

Secondly, the reaction mechanism and the relative resistance of each reaction step contributes to the overall rate of reaction (hence conversion) of the particle as a whole. The mathematical treatment of the mechanism and its complexity differ depending upon the type of model used, for example, the shrinking core model or grain model. In general, there the overall rate of reaction could be determined by:

- The external mass transfer of reactant gas species through the gas film and internal diffusion through any product ash formed.
- The actual reaction rate between the gas and solid.

Usually, the external mass transfer through the gas film is negligible (although this could be the rate limiting step in liquid-solid reactions, for an analogous analysis). The reaction rate is usually described by a power law or a Langmuir-Hinshelwood-Hougan-Watson (LHHW) expression.

Thirdly, there could be some unconstrained variables that pose physical limits on the reaction, for example, reactor temperature. According to the rate law described by an Arrhenius equation, the reaction rate increases exponentially with an increase in temperature. However, the temperature must be limited. Very high temperature equipment is expensive, the structure of the sorbent may change as temperature is increased and it would ultimately melt.

To summarize, the type of sorbent and the physical mechanism associated with the gas-solid reaction will limit the conditions for optimal reactor operation.

7.3 Process limitation: Exit H_2S concentration

Due to the above physical limitations, all the mass of sorbent will not react. Hence, an exit concentration limit, or breakthrough limit must be defined. This consideration would depend upon whether the unit is to be used for bulk H_2S removal from the gas (i.e. reduce the concentration from percent levels to, say, the 100 ppm level) or as a 'polishing' or 'guard bed' (i.e. to ensure the concentration was below, say, the 1 ppm level).

For the bulk removal of a gas species, it would seem sensible to aim for the greatest possible sulphur loading, where the maximum outlet concentration was not set too low (say, 100 ppm). Here the breakthrough time would be very close to the maximum time available for total conversion of the sorbent and it is similar to the ideal reactor and is shown in Figure 6.3.

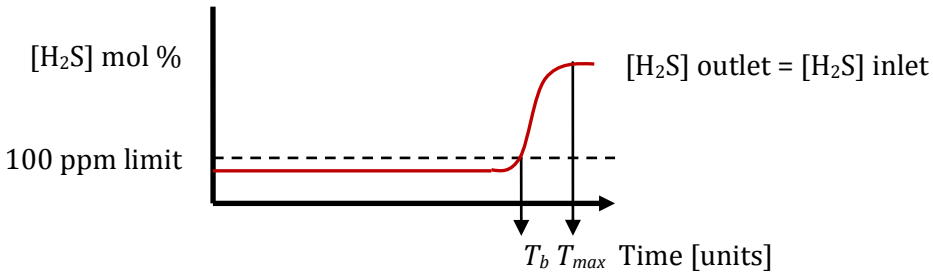

Figure 6.3: Bulk desulphurization reactor

For the polishing step of a guard bed, where near complete removal is desired, it would seem sensible to aim for the smallest possible outlet concentration, where sulphur loading is not the main concern. Here the breakthrough time would be significantly shorter than the time available for total sorbent conversion, as it would be more important to maintain a low exit H_2S concentration. The breakthrough curve is shown in Figure 6.4.

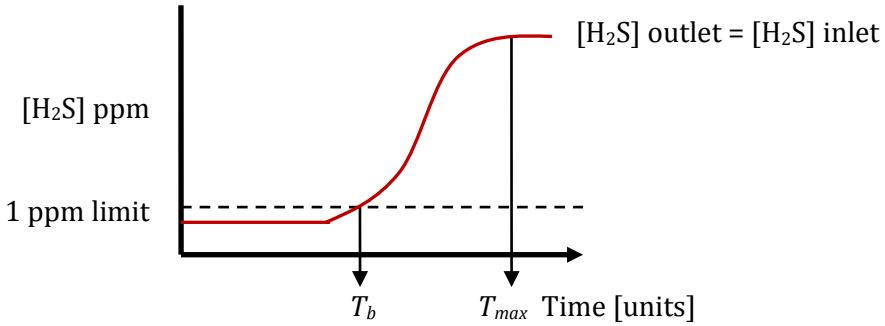

Figure 6.4: Desulphurization reactor operating as a polishing step (guard bed)

7.4 Process limitation: Sorbent sulphur loading

The final consideration was the desired conversion of the sorbent, or in other words, to what extent must the solid react? This would be important as it has implications on process design. The sulphur captured in the sorbent would be released during a regeneration step, either as pure sulphur or SO_2. The sizing of this equipment and its performance would be influenced by the amount of sulphur that can be expected to be 'released' from the sorbent. The discussion on regeneration of the sorbent was outside the scope of the project, but should always be kept in mind.

The breakthrough curve would be similar to Figure 6.3, where most of the sorbent has reacted, but the outlet concentration of the gas is not necessarily very low.

7.5 Criteria for optimization

The combination of the above three factors, namely the physical limitations, the exit gas concentration and the sulphur loading, represent the criteria for optimization. The specific objective function would be subject to actual process requirements. In order to understand how the optimization would proceed, one must look at the process variables that are *available* to be changed.

The last factor to mention, of course, is the cost of the various technologies. This would be determined by implementing the technology on an industrial basis. The cost analysis would include the cost of regeneration of the sorbent and possibly the cost of further processing of the tail gas from the regeneration step. It may be found that the best operating point would be too costly to achieve in practice.

The goal of optimization is thus: what combination of independent reaction variables gives the best result, under the limitations discussed, with respect to the desired function of the reactor? The extreme cases would be:

Infinite mass transfer, diffusion and reaction rate: H_2S reacts immediately with the solid.

$T_b = T_{max}$. For $t < T_b$, $C_{H2S,\,out} = 0$. For $t > T_b$, $C_{H2S,\,out} = C_{H2S,\,in}$.

Infinite bed of sorbent: H_2S that enters the bed ultimately reacts to give a zero (or at least equilibrium level) concentration in the exit gas stream. However, the conversion would have the limit tending to zero.

$m_{ZnO} \rightarrow \infty$, $C_{H2S,\,out} \rightarrow 0$, $X_{ZnO} \rightarrow 0$.

Infinite time of reaction: All the sorbent reacts. However, it is likely that the inlet and outlet concentrations are now the same.

As $t \rightarrow \infty$, $C_{H2S,\,out} \rightarrow C_{H2S,\,in}$, $X_{ZnO} \rightarrow 100\%$.

The limiting factors could be conveniently represented In Figure 6.5. On each vertex there is one maximum possible value. Practically, the optimal point (for a defined objective function) would lie in the triangle by some set of independent variables that define the reactor's operating condition.

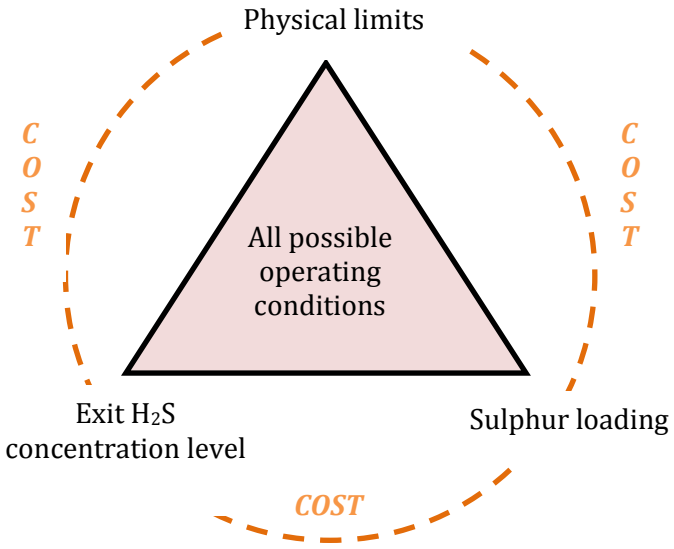

Figure 6.5: Optimization of gas-solid reactor design

Of course the interesting aspect would be the comparison of the experimental results to those calculated from the gas-solid reactor models.

The combined optimization of more than one outcome (for example, maximum conversion and maximum time until H_2S breakthrough) is very complicated. The remaining discussion will be limited to a single outcome for simplicity and application on the experiments. This is namely to try and achieve the maximum conversion of sorbent.

Now that the question of what was going to be optimized has been addressed, the subsequent question was *how* to achieve this experimentally? One needs to look at the reactor design and plan the experiments needed to be conducted. This planning would show what independent variables to change, to try and determine the optimal operating point.

8. Factorial experiment design

The mathematical modelling of gas-solid reactions is complex, as detailed in Chapter 5. The major problem of using the models is that they rely on accurate evaluation of physical properties of solids and gases, reaction kinetics and system geometry. The model would provide a basis to form an objective function to allow for optimization, but how would this represent the actual physical system? If there is doubt, optimization should be carried out in terms of experiments, whereby each variable was changed to try and see where the best operating point would be.

The method of optimization by 'random variable changing' could be extremely tedious. Fortunately, there are recommended procedures to follow to minimize the number of experiments without sacrificing the possible loss of information.

The use of a factorial experimental design has been recommended for experimental outcomes that are determined by a number of input variables. This is fully developed in standard statistics books, such as Montgomery and Runger (1999) or Devore and Farnum (2005). A 'full factorial' experimentation design simply takes all the input variables, at certain discrete values (called levels), and conducts one experiment per discrete value per input in order to test a certain outcome. This is best illustrated by example.

Assume that there were 4 possible variables. Typically, each variable would be tested against each other at a high and low value, which is known as a two level factorial design. Thus, there would be $2^4 = 16$ experiments to gauge a certain outcome. This means that every combination of the 4 variables at the high and low level was tested, and there would be 16 corresponding results of the single outcome.

How could these results be used? One needs to employ some basic statistical analysis, and the following results could be found:

1. The 'best' (optimized) solution. The conditions of the experiment that gave the best results, i.e. the experimental conditions with the highest conversion of sorbent.

2. The relative effect of a certain variables: This would show if there was a variable that had a dominating influence on the outcome of the experiment compared to the other input variables.

3. The interaction effects of certain variables: This would show whether two or more variables acting together had an influence on the outcome of the experiment.

4. Modelling: The experimental data can be regressed to give a basic, empirical model of the system. Thus, given the input variable values (providing they were in the *same range* as the experiment), an estimate of the outcome can be found.

It must be noted that the so called optimized solution found from a factorial experiment design is only in the *range* of the experimental values tested. Another method of optimization is the simplex method. This is favourable because it does not rely on a model, it is robust and could be easily adapted for experiments.

The principle of this method is to compare (n+1) experimental results, where n is the number of variables, and 'move away' from the least desirable result.

Again, this is best illustrated by example. Suppose there are two variables that affect the *conversion* of a reactant: temperature and pressure. Three experiments were performed in the 'expected range' of the best conversion. When plotted, they were points A, B and C on Figure 6.6. Now these three results are compared, using the red triangle, and the suggested move is away from the lowest point B, to point D. The experiment is performed under these new conditions and this result is compared to B.

If it is indeed a better result, point B is discarded and the new points are the blue triangle ADC. The lowest point is A, and a new point E is suggested. Now the new triangle to consider is the green CDE.

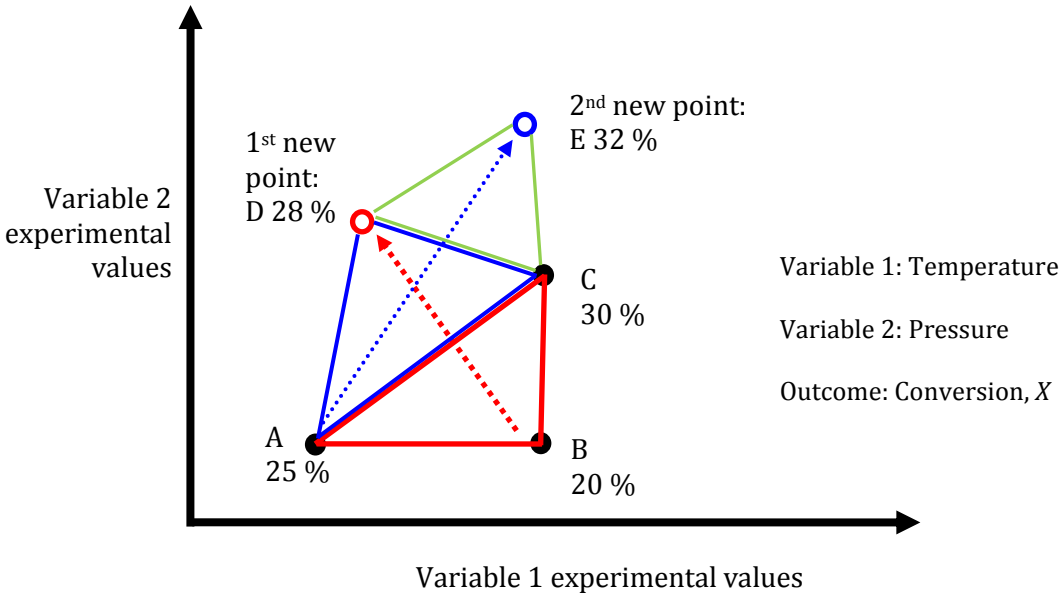

Figure 6.6: Simplex method example, showing 2 possible moves

The procedure continues until a lower value is found. This is shown in Figure 6.7. Suppose that D was in fact smaller than A, B and C. Now, the magnitude of the step move must be lowered to limit the move, and a better value could be found.

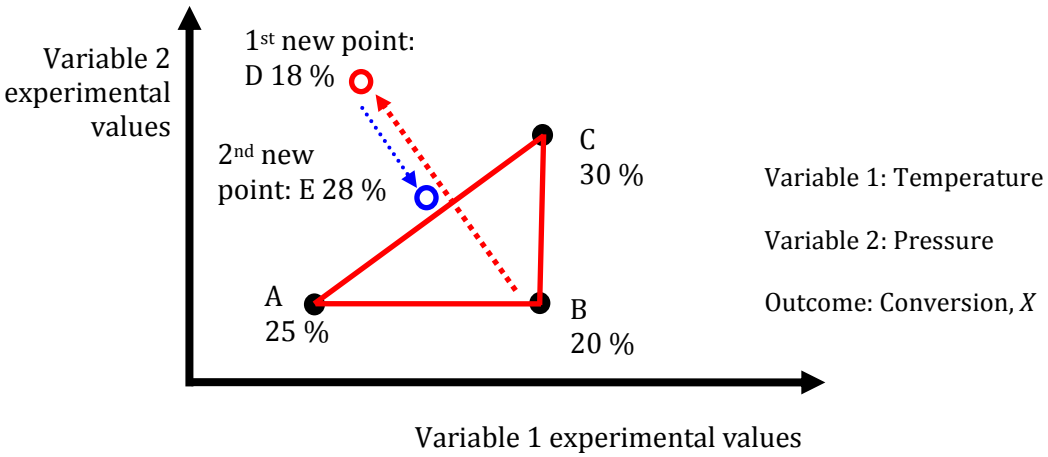

Figure 6.7: Simplex method example, showing 2 alternate moves

This example shows the method with two variables, but it can easily be applied to more input variables. With two variables, the simplex is a triangle in a plane, with three, it is a pyramid in space, and with more variables, one needs to think in multi-dimensional space.

The 2-level factorial experiments could be used in conjunction with a simplex type procedure as a form of optimization. The factorial experiments would determine which variables were important (i.e. the main effects in the experiment) and the simplex method could then be utilized to determine their 'best' combination to produce the optimal result.

This assumes of course that the reproducibility of the experiment is satisfactory. In addition, some variables may be constrained to certain values (be they single or discrete values). For example, the reaction has to occur at 350 °C, or only particle sizes of 1, 3 and 5 mm are available.

9. Optimization application to this study

It had been identified in the literature survey that few experiments have been performed that investigated the interaction of the process variables. For example, it was known (Woods *et al*. 1992) that increased rate of sulphur loading of a single pellet occurred faster with smaller particle diameters (1/8 in compared to 3/16 in), at 1 atm. However, the 3/16 in pellets also showed an increased rate at higher pressure. The 1/8 in pellet was not tested at the higher pressures.

This study has the aim of addressing this issue, by examining the interaction of some variables. For simplification of the desulphurization reaction, the following variables were held constant:

- Pressure
- Gasification temperature
- Sorbent type

- Gas composition (notably H_2S and H_2O concentration), as a result of constant feed composition
- Time of reaction
- Mass of sorbent

The following were varied:

- Desulphurization temperature
- Space velocity (i.e. gas flowrate)
- Particle size

To relate this back to the optimization triangle: it will be shown (Chapter 7) that the thermodynamic limit of the reaction was 200 ppb to 1 ppm, and the reaction was not expected to be mass transfer limiting. An outlet concentration limit of 100 ppm would ideally be set as the breakthrough point, and conversion (sulphur loading) could then be found.

The best sorbent and associated operating conditions, as mentioned, would have the highest loading and the longest breakthrough time. However, to start with, only the conversion outcome was used as the objective function, which should be maximized. An example of the experimental simplex has been illustrated in Figure 6.8.

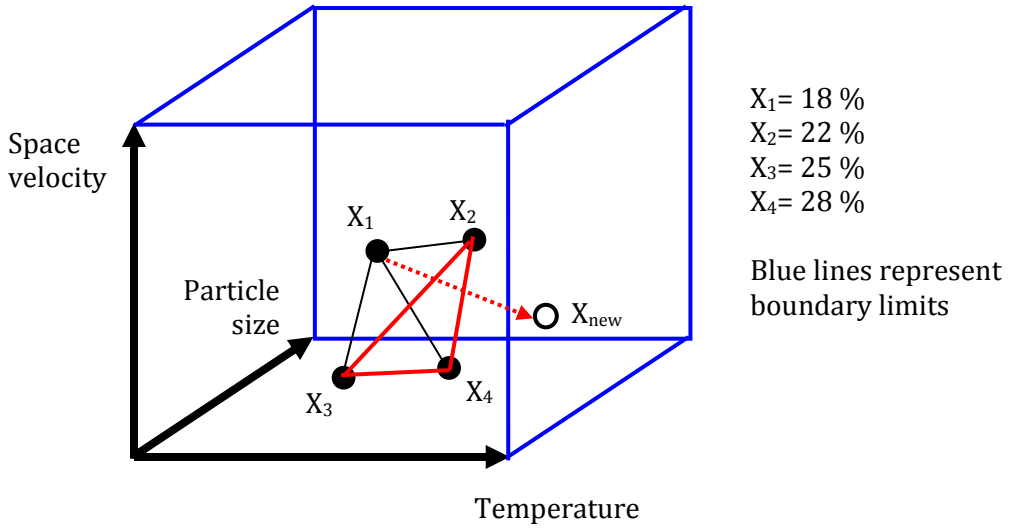

Figure 6.8: Simplex method for 3 input variables in the experiment

To conclude, a form of optimization of this gas-solid reaction consists of the following:

1. The main experimental effects should be determined by a factorial experiment design.
2. The number of variables could then be simplified and the range of optimization would be better defined.
3. The constraints of input variables would then be determined (for example, particle sizes, high temperature to prevent vaporization of zinc).
4. The objective function to maximize (or even minimize) would now be defined.
5. Use simplex method to optimize.

Perhaps reaction models could be used as guidelines. In Chapter 7, the equipment is designed and constructed in order to perform the actual reactions.

The extent of optimization would obviously depend upon the success of the experimental unit's performance. However, at least the procedure discussed above would be available for future implementation once all the experimental problems have been solved.

Chapter 7

Equipment Design

1. Introduction

This chapter details how the equipment was designed and constructed. It identifies the problems encountered and how they were addressed in order to actually build a working experimental unit. As mentioned, the important units were the gasifier reactor and the desulphurization reactor.

There were two main design aspects: sizing of the reactor vessels and their physical integration. This was essentially the spatial layout of the reactors and the associated fittings for piping, instrumentation and sampling.

The Chapter presents the different types of industrial and laboratory gas-solid reactors, along with selection criteria to determine the most appropriate reactor type. This gave guidance for the laboratory design to be representative of industrial reactors.

The reactants were selected. This led to a degree of freedom analysis of the gasifier. The desulphurization reactor was designed according to specific space velocities given in literature. The gasifier reactor was then designed using an equilibrium model to match the flowrate required for desulphurization. Both reactors were subject to constraints such as available furnace diameters.

The auxiliary equipment was everything apart from the reactors, including the instrumentation and control. Safety issues were also addressed. Lastly, photographs of the final equipment have been included as well as the mass balance.

Note that one of the aims of the study was to simulate industrial conditions as best as possible. The two main implications of this were to include the gasification reactions prior to desulphurization and the use of relatively large reactors, particles and bed size.

2. Selection of an industrial gas-solid reactor

One of the most important decisions to take in the study of this gas-solid reaction is the *type* of reactor to utilize. The type is affected by many factors, and obviously depends upon the reaction itself. The types of industrial gas-solid reactors will be briefly discussed to provide the guidance for selection of a suitable the laboratory reactor.

According to Szekely *et al*. (1976), the extension of the many single particle gas-solid reaction studies to multi-particle assemblies is highly desirable "because most systems of practical interest consist of multi-particle assemblies". There are three main problem areas with extending the experimental studies, as these effects cannot be found from the single particle studies:

1. Physical nature of the (reactor) assembly: gas pressure drop, minimum fluid flow rate, minimum fluidisation velocity and temperature (radiation effects).

2. Contact time or residence time in the reaction environment: an *average* time may have to be used.

3. The effect of spatially variable gas composition: the gas composition is well controlled and constant in single particle studies. For multi-particle, both composition and temperature may vary depending on the reactor type.

In order to select the most appropriate reactor to use, Szekely *et al*. (1976) recommend considering the following aspects of a particular reaction first.

1. Thermodynamics: The calculation of an equilibrium constant, and the heat of reaction, would show whether a reaction would actually occur. This would then give an indication for the need for reactant, product or heat addition (or removal). For example, a highly exothermic reaction would require a reactor that can accommodate rapid heat removal to maintain a thermodynamic driving force for the reaction, and for safety reasons.

2. Kinetics: It is stressed that kinetics cannot be calculated, and must be measured., Szekely *et al*. (1976) explained that great caution must be exercised in the use of kinetic data reported in the literature for design purposes. This was due to the possible diversities in experimental conditions, experimental arrangements, and possible differences in the physical state of the solid reactants. Systems that were found to be mass transfer controlled could perhaps be an exception.

3. Selection of the equipment of the gas-solid reaction system: This could depend upon:

- Hold up (fraction of packed bed in reaction zone)
- Mean residence time
- Distribution of residence time

- Pressure drop
- Degree of fluid-solid contacting
- Influence of temperature gradients on the reaction, the solid and the equipment

The conclusion here was that the type of reactor selected has to be made with all these factors considered. There may be one over-riding feature of the reaction that points to a certain reactor type. However, as with most engineering designs, there would probably be a trade off between conflicting issues, be they chemical, thermal, process or even mechanically related.

3. Types and selection of a laboratory gas-solid reactor

The next question would be, how to relate the industrial reactor to laboratory reactor? This is an age-old question in chemical engineering. Then extract below was from Fogler (2006).

"The successful design of industrial reactors lies primarily with the *reliability of the experimentally determined parameters used in the scale-up*. Consequently, it is imperative to design equipment and experiments that will generate accurate and meaningful data."

The criteria for reactor design were specifically for catalytic reactors, where the catalyst was a solid. However, there are numerous similarities between cathalytic and non catalytic gas-solid reactors: the nature of the fluid-solid contact, the effect of external mass transfer through the fluid (gas) film and thermal effects of the reaction and gas-fluid contacting.

Criteria used to evaluate laboratory reactors are:

1. Ease of sampling and product analysis
2. Degree of isothermality
3. Effectiveness of contact between catalyst (solid) and reactant
4. Handling of catalyst decay
5. Reactor cost and ease of construction

Note that point (4) can be interpreted as 'stability of solid reactant/product' in the reactor environment. For example, what happens if there was no/little solid product (for example, combustion) or does the solid product suffer from attrition?

Fogler (2006) discussed the reactor types focusing on catalytic reactors. Note that the primary goal would be to determine catalytic reaction kinetics. Refer to Tables 7.1 and 7.2 for different types of laboratory reactors and some of their advantages and disadvantages.

The notable exception from Fogler's analysis was the thermo-gravimetric reactor, which of course is suitable for single particle studies.

Table 7.1: Different types of laboratory reactors

Type of Reactor	**Principle of Operation**
Differential	There is a thin 'wafer' of solid. Gas has a very small, but detectable, conversion. The rate of reaction is considered constant through the bed.
Integral (fixed bed)	The catalyst is a fixed bed through which the reactants pass.
Stirred batch	The catalyst is dispersed as a slurry and continuously stirred.
Stirred-containing solids	The catalyst particles are contained in paddles that rotate at high speeds to minimize external mass transfer effects.
Continuous-stirred tank	Fresh catalyst is fed to the reactor along with the fluid feed and the catalyst leaves the reactor in the product stream at the same rate that it is fed.
Straight through transport	Either an inert gas or the reactant itself transports the catalyst through the reactor.
Recirculating transport	Recirculating the gas and catalyst through the transport reactor.

Table 7.2: Summary of reactor ratings for laboratory use

Type	**Sampling and Analysis**	**Iso-thermality**	**Fluid-Solid Contact**	**Decaying Catalyst**	**Ease of Construction**
Differential	P-F	F-G	F	P	G
Integral (fixed bed)	G	P-F	F	P	G
Stirred batch	F	G	G	P	G
Stirred-containing solids	G	G	F-G	P	F-G
Continuous-stirred tank	F	G	F-G	F-G	P-F
Straight through transport	F-G	P-F	F-G	G	F-G
Recirculating transport	F-G	G	G	F-G	P-F

G = good, F = fair, P = poor

It was decided to use a fixed bed for the study. The reasons for this were:

- Ease of construction: the fixed bed is the simplest to construct.
- Industrially representative: the fixed bed is a well established reactor type in industry and there could be direct applications.
- Fluidized beds have operational challenges, especially at high temperatures.
- Transport reactors could also be very difficult to operate.

4. Selection of chemicals

The decision to use pure hydrocarbon liquid fuels was taken for the following reasons:

- A simple, gas system comprising the compounds of the elements C, H, O and S (and possible N). This would be free of trace contaminates such as metals and ash.
- Simple flow control of liquid feed, compared to a bank of rotameters or mass flow controllers which would be very expensive.
- Reduced rate of chemical consumption.
- The process as a laboratory method of hot gas desulphurization as not been previously documented and hence the effectiveness of using a liquid fuel can thus be ascertained.

Methanol (CH_3OH) and *i*-propanethiol (C_3H_7SH) were selected since they are miscible and have low normal boiling points of 64.7 °C (methanol) and 59 °C (*i*-propanethiol). Importantly, methanol has a high H:C ratio. The atomic ratio of H:C:S in the feed was important because it, along with the temperature, would determine the composition of the gas, and hence the H_2:CO ratio, and H_2S mole fraction. In addition, methanol was readily available at relatively low cost.

A mixture of ~87 wt % methanol and ~13 wt % *i*-propanethiol would be used. Oxygen would be used as the oxidising agent. This was available from a standard gas cylinder. Alternatively, air could be used. It was decided not to include water into the fuel mixture. This simply complicated the experiment and was not necessary at this stage. Note that the water could dissolve in both methanol and *i*-propanethiol.

Finally, zinc oxide had already been selected as a sorbent. It is also worth noting that a local supplier of zinc oxide titanate could not be found.

5. Degree of freedom analysis

A useful tool for mass balancing was to look at the degrees of freedom of the system. In general, direct measurement of a composition or flow is preferable, but the analysis helps to determine the minimum number of measurements before the others could be found by calculations. The degree of freedom analysis was performed over the gasifier and a schematic is shown below:

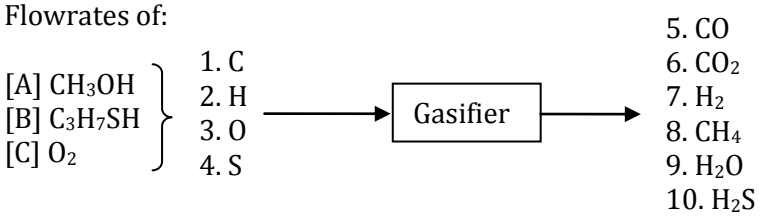

Figure 7.1: Flow of reactants and products for the gasifier

The actual reactions were essentially unknown, although they would be based upon those presented in Table 2.3. However, since the gaseous products species were known, or at least assumed, an element balance could be performed.

The flowrates and compositions of the feed were set.

Number of independent variables:	4 inlet + 6 outlet = 10
Number of independent balances:	4 elemental balances
Number of specified compositions:	3 independent flows on inlet
Number of subsidiary relations:	0
Degree of freedom	10-4-3 = 3

Thus, a minimum of 3 measurements are required for the above system.

- Measurement of a specific molar flow of a component in the product gas
- Measurement of a specific mole fraction of a component in the product gas
- Measurement of the total molar flow of the product

A basis cannot be used as the elements have been specified at their respective composition flows already.

It would turn out that the 3 possible measurements were the mole fractions for CH_4, H_2S and the molar flow of H_2O. However, the measurement of molar flow of water was only developed at a late stage into the project and is subject to saturation considerations. The solution was as follows. It could be adapted at a later stage if different measurements were available.

The 4 element balances are:

Carbon balance:	$n_C = n_{CO} + n_{CO2} + n_{CH4}$
Hydrogen balance:	$n_H = 2\ n_{H2} + 4\ n_{CH4} + 2\ n_{H2O} + 2\ n_{H2S}$
Oxygen balance:	$n_O = n_{CO} + 2\ n_{CO2} + n_{H2O}$
Sulphur balance:	$n_S = n_{H2S}$

The 7 known components are:

Initial element flowrates:	n_C, n_H, n_O and n_S
Measured mole fractions:	y_{CH4} and y_{H2S} (or n_{CH4}/n_T and n_{H2S}/n_T)
Molar flows:	n_{H2O}

This left 4 equations with 4 unknowns of n_{CO}, $n_{CO2,}$ n_{H2} and the total flow of the outlet, n_T, which was required for evaluating the mole fractions. Noting that $y_i = n_i/n_T$, the above equations were divided by n_T for convenience, yielding mole fractions:

$n_C/n_T = y_{CO} + y_{CO2} + y_{CH4}$
$n_H/n_T = 2\ y_{H2} + 4\ y_{CH4} + 2\ y_{H2O} + 2\ y_{H2S}$
$n_O/n_T = y_{CO} + 2\ y_{CO2} + y_{H2O}$
$n_S/n_T = y_{H2S}$

n_T could be calculated immediately from the last equation: $n_T = n_S/y_{H2S}$

y_{H2O} was found from the water flowrate, n_{H2O}: $y_{H2O} = n_{H2O} / n_T$.

This left the top 3 equations, with 3 unknowns: y_{CO}, y_{CO2}, y_{H2}. This could be readily solved by matrix inversion or successive substitution. The algebra is:

$$\begin{bmatrix} 1 & 1 & 0 \\ 0 & 0 & 2 \\ 1 & 2 & 0 \end{bmatrix} \begin{bmatrix} y_{CO} \\ y_{CO_2} \\ y_{H_2} \end{bmatrix} = \begin{bmatrix} n_C/n_T - y_{CH_4} \\ n_H/n_T - 4y_{CH_4} - 2y_{H_2O} - 2y_{H_2S} \\ n_O/n_T - y_{CO} - 2y_{CO_2} - y_{H_2O} \end{bmatrix} \quad (7.1)$$

With the solution:

$$\begin{bmatrix} y_{CO} \\ y_{CO_2} \\ y_{H_2} \end{bmatrix} = \begin{bmatrix} 2 & 0 & -1 \\ -1 & 0 & 1 \\ 0 & 0.5 & 0 \end{bmatrix} \begin{bmatrix} n_C/n_T - y_{CH_4} \\ n_H/n_T - 4y_{CH_4} - 2y_{H_2O} - 2y_{H_2S} \\ n_O/n_T - y_{CO} - 2y_{CO_2} - y_{H_2O} \end{bmatrix} \quad (7.2)$$

This analysis was only valid for the 6 components assumed in the product gas. Note that as more components are added, more measurements would be necessary. The solution method would still be applied. If there were more measurements available than needed, the analysis becomes over-specified. The results using the method above could be compared to equilibrium model, which will be shown in due course.

An energy balance could be added. If the inlet temperature of the feed was known, and any heating / cooling effects can be accounted for, the outlet temperature can be found from the energy balance given below. This would require a computer solution, due to the non-linearity in the heat capacities. The energy balance is:

$$\Delta H_{\text{react}} + Q_{in} = \Delta H_{\text{prod}} - Q_{out} \quad (7.3)$$

If the system is adiabatic, then there is no heat transfer from the reactor. The energy balance becomes:

$$\sum_{i=1}^{M} n_i \Delta H^o_{f,i}(T_R) + \sum_{i=1}^{M} n_i \left(\int_{T_R}^{T^{IN}} C_{P,i}(T) dT \right) = \sum_{j=1}^{N} n_j \Delta H^o_{f,j}(T_R) + \sum_{j=1}^{N} n_j \left(\int_{T_R}^{T^{OUT}} C_{P,j}(T) dT \right) \quad (7.4)$$

The reactants are components *i=1*:*M* and the products *j=1*:*N*.

n_i	molar flow of reactant *i*	[mol.s^{-1}]
n_j	molar flow of product *j*	[mol.s^{-1}]
$\Delta H^o_f(T_R)$	standard heat of formation at T_R	[J.mol^{-1}]
C_P	heat capacity	[J.mol^{-1}.K^{-1}]
T^{IN}	inlet temperature	[K]
T^{OUT}	outlet temperature	[K]
T^R	reference temperature (usually 298 K)	[K]

6. General design constraints

The following were a list of some constraints that had to be factored into the design:

- Gas space velocity: From the literature as given in Table 3.2, other researchers have used space velocities in the range of 2000-10 000 hr^{-1} measured at STP. Space velocity is defined in Section 6.7.

- Sorbent particle diameter: Froment and Bischoff (1990) recommend to have a reactor to particle diameter ratio greater than 10. This is to reduce the so called wall effects of the reactor. This was particularly important for heat transfer and fluid flow in the packed bed.

- Sorbent availability: Zinc oxide was available as 4.5 mm diameter extrusions (cylinder shape) of different lengths from Sud-Chemie. Unfortunately, this meant a relatively large reactor diameter of 45 mm. Smaller pellets were available from M.R. Zinc (pty) Ltd., but they were various sizes and were quite soft particles (disintegrated into powder easily).

- Furnace diameter: The availability and sizes of laboratory tube furnaces had to be considered.

- Time of reaction: The reaction had to occur within a reasonable time frame of hours, rather than days.

- Safety: The equipment design had to be safe to operate.

Lastly, the equipment has the interesting property that half of the apparatus would be at steady state (the gasifier), while the other half would be at unsteady state (the desulphurization reactor).

7. Desulphurization reactor: Application of a process model

The model presented in Chapter 5 could be applied to the reactor design. The model gives the solid conversion as a function of the bed depth and reaction time. However, it relies upon a number of parameters that must be found from measurements, previous studies or estimated.

The model parameters have been given in Table 7.3 along with possible sources of the information. The poor evaluation of just one of these many parameters would have a significant effect on the result of the model. This makes the use of the model very difficult; however, it could be useful for the initial design. Bear in mind that this model incorporated the shrinking core model, which was based upon the assumption of non-porous solids. The sorbent available was porous.

Table 7.3: Parameters required to implement a gas-solid reaction model

Parameter	**Symbol**	**Unit**	**Source**
Stoichiometric coefficient	ν	[-]	Reaction equation
Molecular mass	M_B	g.mol^{-1}	Reaction equation
Diffusion coefficient	D_e	m^2.s^{-1}	Measure or suitable correlation or from literature
Mass transfer coefficient	k_g	m.s^{-1}	Measure or suitable correlation or from literature
Surface reaction rate constant	k_s	m.s^{-1}	Specific kinetic experiments or from literature
Initial reactant gas bulk concentration	$C°_{Ab}$	mol.m^{-3}	Measure: determined by experimental conditions
Density solid, molar (non-porous)	ρ_s	mol.m^{-3}	Measure: determined by sorbent
Radius sorbent	R	m	Measure: determined by sorbent
Bed porosity	ε_b	[-]	Measure: determined by sorbent
Initial reactant solid concentration	$C°_B$	mol.m^{-3}	Measure: determined by sorbent
Superficial velocity	u	m.s^{-1}	Measure: determined by experimental conditions

It was useful to check the equilibrium constant of the reaction. Treating the gas as ideal (low pressure, high temperature), the relationship between the equilibrium composition and Gibbs energy is given, from Smith *et al.* (2001),

$$ZnO_{(s)} + H_2S_{(g)} \rightarrow ZnS_{(s)} + H_2O_{(g)} \tag{7.5}$$

$$K_p = \frac{y_{H_2O}}{y_{H_2S}} = \exp\left\{\frac{-\Delta G^o_{rxn}}{R_g T}\right\} \tag{7.6}$$

$$\Delta G^o_{rxn} = \sum \nu_i \Delta G^o_{f,i}$$
$$\Delta G^o_{rxn} = \Delta G^o_{f,H_2O} + \Delta G^o_{f,ZnS} - \Delta G^o_{f,H_2S} - \Delta G^o_{f,ZnO} \tag{7.7}$$

K_p	equilibrium constant	[-]
y	mole fraction of H_2O and H_2S in gas phase	[-]
ΔG°_{rxn}	Gibbs energy of reaction at standard conditions	[J.mol^{-1}]
$\Delta G^\circ_{f,i}$	Gibbs energy of formation of component *i*	[J.mol^{-1}]
ν_i	stoichiometric coefficient of component *i*	[-]
R_g	gas constant	[J.mol^{-1}.K^{-1}]
T	absolute temperature	[K]

It was found that the equilibrium concentration of H_2S can be down to the 100 ppb levels at temperatures of 200 °C. Lower limits are possible, but they depend upon the type of sorbent, gas composition and operating conditions. However, the reaction rates at low temperatures were low and the temperature must thus be increased or a larger reactor would be required.

For H_2S-ZnO reaction, the equilibrium composition is shown below in Figure 7.2 at different mole fractions of H_2O. Gibbs energies of formation for calculating ΔG°_{rxn} were taken from Perry and Green (1999).

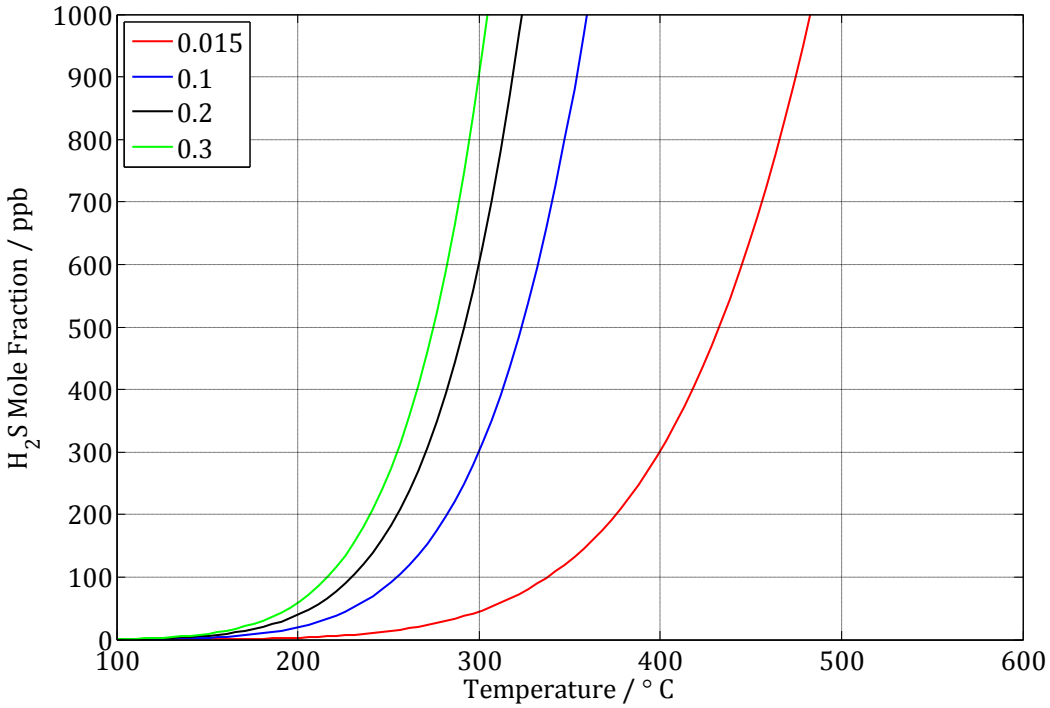

Figure 7.2: Equilibrium composition of the H_2S-ZnO system at various H_2O mole fractions

8. Desulphurization reactor: Process design and sizing

8.1 Range of reactor process conditions

- Temperature range: 300-600 °C. Note that higher temperatures were possible if different sorbents (such as zinc titanates) were being tested. A realistic temperature range was 350-550 °C.

- Pressure: 1-2 bar absolute. This is effectively atmospheric pressure. The main pressure drop of the gas flow would be due to valves and other fittings rather than the reactor bed.

- Gas composition: A 'typical' syngas composition consisting primarily of H_2 and CO, with CO_2, H_2O, CH_4 and H_2S. The important concentration was H_2S in a range of 1-4 mol %. It was anticipated that the H_2O concentration may have an effect on the reaction. However, this was outside the scope of the study and the gas composition, once set, would be constant through all experiments.

- Gas flowrate: A space velocity of 2000-5000 hr^{-1} at STP has been recommended.

- Sorbent size and type: Zinc oxide, spherically shaped, sieved into size ranges of 500-710 μm, 1000-1400 μm and 1400-1700 μm.

8.2 Chemical Reactions

Fortunately, there would be only one main reaction, namely the reduction of zinc oxide to zinc sulphide by hydrogen sulphide:

$$ZnO_{(s)} + H_2S_{(g)} \rightarrow ZnS_{(s)} + H_2O_{(g)} \qquad (7.5)$$

There were some minor reactions to acknowledge:

- SO_2 formation and reaction: this reaction would be minimized due to the reducing environment of the gasifier.

- Sulphur formation: this could be from the formation of SO_2, namely the Claus reaction reacting with H_2S. Note that S could be an allotrope from S_1 to S_8.

$$2H_2S_{(g)} + SO_{2\,(g)} \rightarrow 3S_{(g)} + 2H_2O_{(g)} \qquad (7.8)$$

- Zinc reduction and vaporization: in the presence of hydrogen at temperatures greater than 600 °C, as determined by Westmoreland and Harrison (1976).

$$ZnO_{(s)} + H_{2\,(g)} \rightarrow Zn_{(g)} + H_2O_{(g)} \qquad (7.9)$$

- COS formation and reaction, for example, from Sánchez *et al.* (2005);

$$H_2S_{(g)} + CO_{(g)} \leftrightarrow COS_{(g)} + H_{2\,(g)} \qquad (7.10)$$

$$H_2S_{(g)} + CO_{2\,(g)} \leftrightarrow COS_{(g)} + H_2O_{(g)} \qquad (7.11)$$

8.3 H_2S reaction: mass balance

It was assumed that all the sulphur entering the gasifier formed H_2S. This was a reasonable assumption since: the equilibrium model gave a minimal amount of COS and SO_2 formation.

In addition, the amount of oxygen added was to be extremely small compared to the amount of carbon and hydrogen, again favouring H_2S formation over SO_2.

Hence, the molar flowrate of H_2S was taken as equal to the molar flowrate of *i*-propanethiol. If a certain reaction time was set, the amount of sorbent required could be found easily from the stoichiometric of Equation (7.5) as it is equimolar:

$$m_{ZnO} = n_{i-p} \times M_{ZnO} \times t \qquad (7.12)$$

m_{ZnO}	mass of zinc oxide required	[g]
$n_{i\text{-}p}$	flowrate of *i*-propanethiol	[mol.min^{-1}]
M_{ZnO}	molar mass of zinc oxide	[g.mol^{-1}]
t	reaction time	[min]

This would be an ideal case. In reality, there would be transport and kinetic limitations and the conversion would be less than this, along with breakthrough of H_2S from the bed. This would thus provide a *maximum* time for the reaction for a set mass. As will be seen, an important experimental decision was to set the combination of the sorbent mass and reaction time. One did not want an extremely long experiment, but it had to relate to the actual flowrate available.

8.4 Sizing: Equipment Constraints

It was found that a furnace was available for purchase, manufactured by Carbolite (UK). This furnace had an inner diameter of 38 mm, was 400 mm long and could achieve an operating temperature of 1000 °C. In addition, according to the operating manual, it had a constant heating zone of 100 mm. It was anticipated that this was large enough to achieve the aims of the study.

The furnace was horizontal. Note that the orientation of the reactor makes minimal difference to the study of the reaction, as the gas would simply be flowing through the bed, regardless of direction. It only affects the physical design of the reactor layout.

Working with an available diameter of 38 mm, a reactor tube (Stainless Steel 316 pipe) with a corresponding inner diameter of 27 mm was selected as the reactor.

It was known that zinc oxide was available from M.R. Zinc (pty) Ltd. as spherical pellets in a range of sizes from a powder up to 2 mm diameter. The largest size fraction was 1-1.4 mm. This gave a minimum reactor to particle diameter ratio of $27/1.4 \approx 19$, well above the required 10 to ensure negligible wall effects.

8.5 Sizing: the measurement of particle density

Care was taken with the measurement of the sorbent's density. The sorbent particle is made up of the solid and voids (or pores). Similarly, the bed of sorbent is made up of the solid particles and the inter-particle voids.

- Crystalline density: The density considering only the solid phase of the sorbent. This was referenced as 5.47 $g.cm^{-3}$, from Perry and Green (1999). Measurement requires specialist equipment.

- Particle density: The density of one whole particle. Since the particle can be extremely porous, this density can be significantly less (up to 90%) than the crystalline density. This value has to be measured experimentally because it depends upon the preparation method of the sorbent. This measurement also requires specialist equipment.

- Bulk bed density: This is the total mass of the sorbent bed dividing by its corresponding volume. It includes the void areas between the particles. This can be measured to a fair degree of accuracy in the laboratory. The measured bulk density of the sorbent packed in the bed was 1.07 $g.cm^{-3}$.

The particle density was also measured. This was ρ_p = 1.50 $g.cm^{-3}$, ± 0.25 $g.cm^{-3}$. Here, the diameter of a single pellet was measured using vernier callipers and this particle was then weighed on a mass balance to 0.001 g. This was repeated for over 30 particles.

If it is assumed that all the particles were the same size and spherical, a bed voidage of ε_b = 0.4 can be used.

8.6 Other solid physiochemical properties

As mentioned, sorbent preparation has received considerable attention in other studies. The sorbent's surface area, pore volume and its associated distribution is an extremely important. Large pore sizes provide 'easier' diffusion paths. The measurement for this is usually by a mercury porosimeter. The Brunauer-Emmett-Teller (BET) surface area is found using physical absorption of nitrogen (m^2/g) and the chemisorption surface area by the absorption of ammonia (cm^3 ammonia/g). These are by specialist instruments. In addition, there are instruments that give particle size distributions and bulk density.

The question of whether a large surface area (for a surface reaction) is preferable for the H_2S-ZnO reaction compared to the gas diffusion through the product ash layer to reach the unreacted solid has not been formally addressed. It would be interesting to prepare sorbents of the same chemical composition and diameter with varying internal surface areas.

Although not as relevant for this first study into the reaction (which has been equipment focussed), these sorbent properties will be required for more detailed investigations in the future.

8.7 Sizing: Gas flowrate specifications and space velocity

From the literature, it appeared that the preferred method of characterising the gas flowrate was using space velocity. Some articles published more information than others about flowrates. In general, the experimental conditions were reported by some combination of: space velocity, volumetric flowrate (sometimes corrected to STP, or unspecified) and superficial velocity. However, they were generally poorly defined. Other information such as reactor diameter, sorbent mass, density and volume of the sorbent used may also have been given. The problem was with the definition of these terms and a discussion is worthwhile.

Space velocity: is generally defined as the inverse of *space* time. Space time is also called the holding time or mean residence time and is the "time necessary to process one reactor volume of fluid based on entrance conditions" according to Fogler (2006).

With the space velocity for gases, the flowrate is corrected to STP and it is usually expressed as a 'gas hourly space velocity' basis or GHSV with units hr^{-1}. The confusion arises with the definition of the reactor volume.

$$\tau = \frac{V}{Q} \tag{7.13}$$

$$SV = \frac{Q_{STP}}{V} \tag{7.14}$$

τ	space time	[hr]
SV	space velocity	[hr^{-1}]
V	reactor volume	[m^3]
Q	volumetric flowrate	[$m^3.hr^{-1}$]
Q_{STP}	volumetric flowrate at standard conditions	[$m^3.hr^{-1}$]

For homogenous reactions in the gas or liquid phase, the volume *is* the reactor volume. For gas-fluid reactions, technically, the volume spent by the fluid in the reactor is that of the voids between particles. In addition, what about the voids of the particles? For catalysis, the space velocity can be in terms of catalyst mass, with the units of $m^3.kg^{-1}.hr^{-1}$.

However, some articles specifically define the volume as the volume of the sorbent in the reactor, for example Sánchez *et al*. (2005) and Cal *et al.* (2000). Others give no definition at all. Hence, it is assumed that this was applied in general, and will be used in these calculations. Thus, the 'volume' is found by dividing the mass of sorbent by the particle density, ρ_p.

A bed 10 cm long in the 2.7 cm reactor diameter gave a bed volume of 57.26 cm^3. Using the bulk density, the total mass required of the sorbent is 57.26 $cm^3 \times 1.07\ g.cm^{-3}$ = 61.27 g. The actual volume of particles was thus 61.21 g/1.5 $g.cm^{-3}$ = 40.81 cm^3. For the required space velocities, the gas flowrate (STP) would be:
GHSV = Q/V, Q = 2000 $hr^{-1} \times 40.81\ cm^3$ = 81 620 $cm^3.hr^{-1}$ = 22.67 $cm^3.s^{-1}$

GHSV = Q/V, Q = 5000 hr^{-1}×40.81 cm^3 = 204 050 $cm^3.hr^{-1}$ = 56.68 $cm^3.s^{-1}$

These flowrates were quite high and would result in a large consumption of chemicals.

It was decided to reduce the bed length to about 5 cm, or work with 30 g sorbent. Now the particle volumes was 30 g / 1.5 $g.cm^{-3}$ = 20 cm^3. The flowrates were thus:

GHSV = Q/V, Q = 2000 hr^{-1}*20 cm^3 = 40 000 $cm^3.hr^{-1}$ = 11.11 $cm^3.s^{-1}$
GHSV = Q/V, Q = 5000 hr^{-1}*20 cm^3 = 100 000 $cm^3.hr^{-1}$ = 27.77 $cm^3.s^{-1}$

This was more reasonable, but possibly still too high. Once the volumetric flow at STP was established, this allowed for determining the size of the gasifier and the flowrates of the reactants. The flowrate of the *i*-propanethiol could then be used to give an estimated reaction time.

8.8 Sizing: Change of mass of sorbent

Lastly, it was important to have a significant change in mass of the sorbent in order to calculate the conversion without working in the micro-gram range. The total expected mass change is given in Table 7.4.

Table 7.4: Expected mass changes of ZnO to ZnS given a starting mass of ZnO

Initial Mass ZnO	**With complete conversion to ZnS**	**Change in mass**
g	**G**	**g**
20	23.95	3.95
30	35.92	5.92
40	47.90	7.90

9. Desulphurization reactor: Mechanical design

Since the solid sorbent was a reactant, the reactor has to be loaded with fresh sorbent for each experiment. Thus, it was critical that the reactor assembly aided the ease of this inevitable loading and unloading process.

9.1 Reactor Tube

For assembly of the reactor in the furnace, the following were some design problems that had to be addressed:

- The reactor's diameter had to be smaller than the tube furnace's diameter (to allow it to slide down the furnace tube).

- The reactor had to connect to the gas inlet and outlet piping, (effectively fixed points).

- The reactor tube had to be open, at least on one end (to allow for the sorbent to be added and removed after each experiment).

- Gas sample points on the inlet and exit of the reactor.

- Temperature measurement of the sorbent bed.

- Some means of support for the sorbent to stabilise the bed.

The materials of construction were of initial concern due to the corrosiveness of H_2S in the presence of water. The high temperature would also cause some thermal expansion and affect the mechanical strength of the material. For the corrosion reasons, Stainless Steel 316 was preferable. Since operation would be at near atmospheric pressure and there would not be any significant weight to support, the mechanical strength was not an important factor. This included the reactor's minimum wall thickness.

The simplest design was to use a metal pipe as the reactor tube. This had sockets that could be screwed onto each end to provide both the gas seal and connection fittings to the inlet and outlet piping. The reactor was thus supported by resting on the sockets in the furnace.

There would be one thermocouple extending co-axially into the sorbent bed. Should the thermocouple extend from the gas inlet and outlet and would there be a difference? Since the thermocouple diameter was 6 mm and the reactor diameter 27 mm, it would not have a major effect on the nature of the gas flow. It would thus be simpler to include it with the fittings on the gas inlet side.

9.2 Pressure Drop

The Ergun equation was used to calculate the pressure drop across a packed bed. With some simplifications (for example, using a particle diameter of 0.5 mm and flowrate of 3 200 $cm^3.min^{-1}$ at reaction conditions), a maximum pressure drop of 30 Pa was calculated across the bed. This was negligible. Refer to the Appendix, Section A.5, for the full calculation.

9.3 Inlet and Exit Connections

The inlet socket had four connection points:

- Gas inlet flow connection.
- Thermocouple connection for the reactor inlet temperature.
- Thermocouple connection for the reactor bed temperature
- Connection for gas sampling.

When connecting the socket to the tube, the mesh grid would already be fixed onto the sorbent bed thermocouple, which was also fixed onto the socket. The outlet socket had simple fittings to connect to the piping on the apparatus.

A cross section of the inlet socket looked as follows (not to scale):

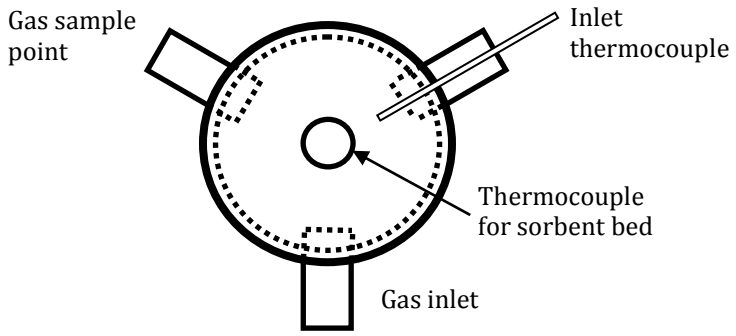

Figure 7.3: Cross section of inlet reactor socket

9.4 Sorbent support and temperature measurement

A thermocouple was used to measure the temperature in the centre of the sorbent bed. It was also used as a connection point to hold a wire mesh grid to support the sorbent. The thermocouple had to be 6 mm thick to avoid possible warping caused by repeated exposure to high temperatures.

The sorbent's mesh grid support design was important and complicated. The support had to have the following properties:

- Porous: the gas must pass through the mesh grid easily. However, it cannot be larger than the expected particle size. In addition, the system could not afford large pressure drops through an effective 'filter'.
- Non-reactive: with the gas (including corrosion resistance to H_2S).
- Non-reactive: with the sorbent (it must not physically adhere to the sorbent).
- Shape integrity: maintain its shape under high temperature.
- Flow distribution: to avoid possible channelling of the gas flow into the sorbent bed.
- Sealing with the reactor wall: to prevent the sorbent from either getting stuck or slipping past.

The mesh grid would be attached to the thermocouple, and preferable be adjustable to allow for different bed lengths.

An associated problem was the sorbent support on the other end of the bed. Since the reactor was horizontal, there needed to be some kind of structure to keep the bed fixed. It was proposed to insert a simple 'spacer' with the same mesh on one side to hold up the bed. The

spacer was a smaller tube that fitted snugly into the main reactor tube. It had the same thick wire grid welded onto one end, with the fine wire mesh sewed on top of it, like the other support. There was a hook on the other end so that the spacer could be removed easily by pulling it out with some wire.

The mesh grid consisted of two parts: a thick piece of stainless steel 'grid' plate (3mm thick). This was welded to a fitting that could slide up and down the thermocouple and be fixed by a grub screw. A much finer mesh was then attached to the grid. The mesh was approximately 300 µm, also stainless steel and literally sewed on by using its own thread.

The thick grid provided the support, the thin mesh allowed for a decent gas distribution. Since it was also quite a smooth surface, it was expected that the sorbent would not stick to it. For the seal with the reactor, the mesh was 'folded' back over the sides of the grid. When the socket with thermocouple was screwed on, the mesh would slide up the reactor sides easily, and the seal would be complete. The only problem was when the socket was unscrewed, the reactor mesh could be bent out of shape. This could of course be fixed for the next experiment. The sorbent support has been shown in Figure 7.4.

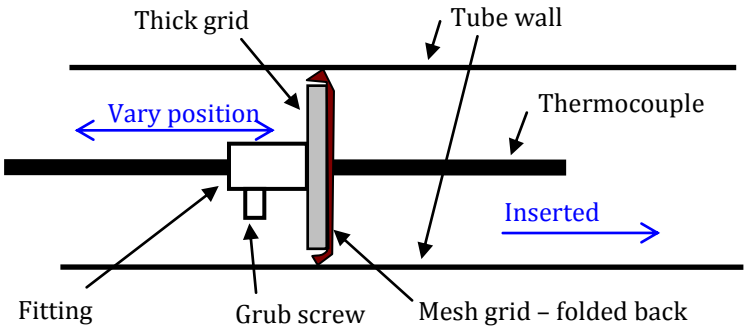

Figure 7.4: Cross section of sorbent support (not to scale)

9.5 Final Reactor Design

The final reactor design has been shown in Figure 7.5.

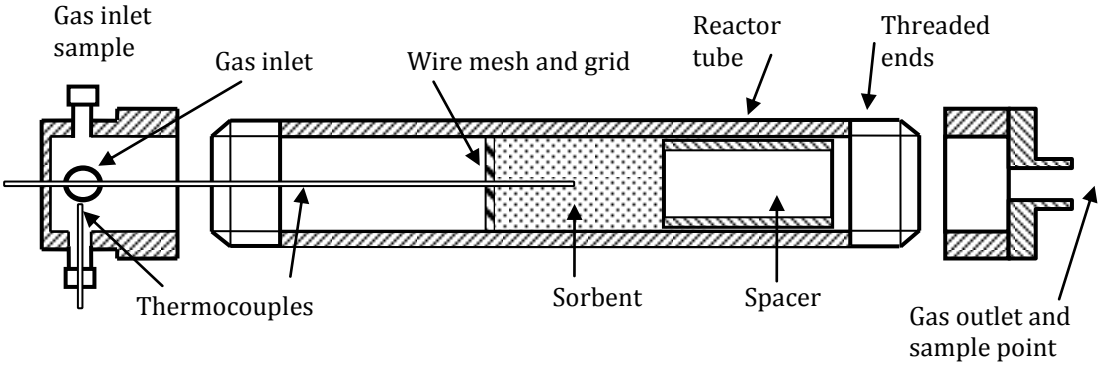

Figure 7.5: Desulphurization reactor design

10. Desulphurization reactor: Gas sampling and analysis

10.1 Gas syringe sampling

It was initially proposed to use a gas tight syringe to sample from the system and inject into the GC to determine the composition of the gas. This simply required a septum to be connected to the system. The syringe's needle would then be inserted into the bulk flow of gas and a sample withdrawn. This meant that the needle from the syringe had to *reach* the bulk flow, and there could not be any 'dead' volumes nearby in the system.

It was hoped, at the initial stage, that a later modification would allow the GC to be directly connected to the apparatus, to enable online sampling and analysis. The fittings chosen provided for this. Upon inquiring about the type of septa available, the maximum temperature was about 400 °C. This provided another problem if the gas was to be very hot (as in 600 °C after leaving the gasifier).

There was significant work performed in order to obtain a reliable result from the gas sample and GC analysis. The details of this work have been given elsewhere in the Appendix, Section A.4. The important points of the work have been summarized below:

- The GC had a packed column and FID detector.
- The FID allowed for detection of hydrocarbons and limited H_2S to about 0.1 mole %.
- Different detectors would be required: A TCD for H_2, CO, CO_2 and H_2S (accuracy about 0.1 mole %) and an FPD for low H_2S concentrations (down to 200 ppb).
- The presence of water in the mixture had an impact on the column selection. In addition, all sample lines had to be heated to prevent condensation of the water.
- An absolute calibration method would be employed since all components could not be detected. This also reduced the number of calibration mixtures required.
- The absolute calibration method required that the measurement of temperature, pressure and volume of the sample injected. This allowed for the calculation of the total number of moles injected into the GC, using the ideal gas equation.

10.2 GC Sampling Valve

At a later stage in the project, a sampling valve was installed due to the unreliability and difficulties of the gas syringe. A sample of gas was taken from a gas stream by a special 6 port valve that included a 1 mL sample loop. By switching the valve, the 1 mL sample would be sent to the GC.

This is shown in Figure 7.6 below. The sample had to be heated to above 100 °C to prevent water condensation and the temperature was measured by a thermocouple placed on the sample loop. The pressure of the line would be given by a pressure gauge placed just before the valve.

Position A: The process stream is flowing through the sample loop.
Position B: The carrier gas is flowing through the sample loop, taking the sample to the GC.

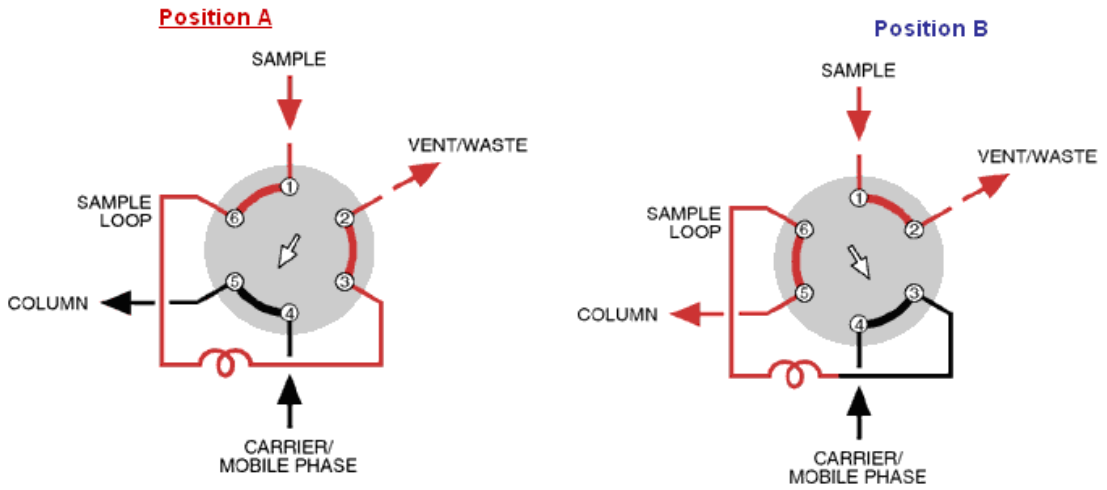

Figure 7.6: Valve positions for sample collection (Position A) and sample analysis (Position B). From Valco Instruments Co. Inc. (2009).

Due to the installation of the sample valve, a more complicated valve scheme was required to sample the gas from both the inlet and the outlet of the reactor.

10.3 Bypass lines and valves

There were two bypass lines: one to bypass the desulphurization reactor and the other to bypass the sampling loop of the GC. The gas sampling for the GC required careful design of valves and gas flows to prevent backflows, blockages and for safe venting.

The valve scheme designed has been shown in Figure 7.7, along with the corresponding valve settings given in Table 7.5.

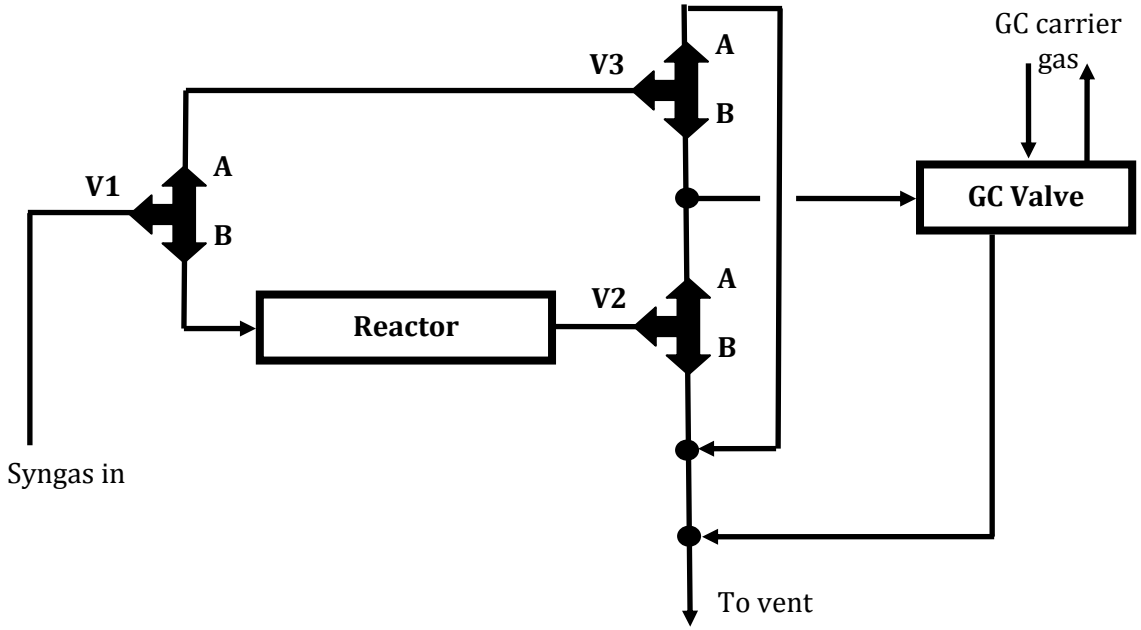

Figure 7.7: Valve scheme for gas sampling to the GC

Table 7.5: Valve positions for different samples or functions

Action	**V1**	**V2**	**V3**
To bypass reactor and vent gas	A	Closed	A
To sample inlet gas	A	Closed	B
To vent gas after reactor	B	B	Closed
To sample exit gas	B	A	Closed

On the inlet side, it was straightforward: the gas either went to the reactor and sorbent or was bypassed to the vent. This also provided a sample point for the inlet. On the outlet side, the gas could either be sampled, or it could be vented. It was important that the right valve combination was used.

10.4 Combustion Gas Analyzer

A combustion gas analyser was also available. It was a Bacharach ECA-450 Portable Combustion Gas Analyzer. It could be used to detect O_2 (range of 0.0-20.9 mol %), and SO_2 (range 0-5000 ppm). Unfortunately, the other readings such as CO were out of the instrument's range of 0-10 000 ppm and the CO_2 reading was calculated based upon the fuel being combusted. The O_2 and SO_2 readings would be useful, as both would be expected as zero.

11. Gasifier design

The problem here with the reactor design was that both the actual reactions and their corresponding reaction rate kinetics were essentially unknown. The aim of the gasifier reactor was to produce syngas with a H_2S concentration of about 1-6 mol % at a flowrate of about 10-30 $cm^3.s^{-1}$ at STP.

11.1 Equilibrium Model

It was decided to use the gasification equilibrium model (refer to the Appendix Section A.1) to determine the correct flowrates and composition to feed to the gasifier. In terms of sizing, research was done to establish a reasonable residence time for the gases in order to "reach equilibrium". As discussed in Chapter 2, Section 4.2, the models provided decent accuracy (~5 mol %). It was assumed that equilibrium was reached almost immediately.

A computer program was written in MATLAB to calculate the equilibrium, given the inlet atomic composition, pressure and temperature. Further details are also in the Appendix, Section A.1. Using trial and error, a suitable molar ratio of C:H:O:S was found to give a gas composition of H_2:CO ratio close to 2:1 and a mole fraction of about 2 mol % for H_2S.

A snapshot of the program is shown in Figure 7.8. It can also be seen that a good temperature for the gasifier would be above 800 °C, as there was no further significant change in composition above this temperature. This shows that a ratio of C:H:O:S of about 100:375:100:6 gave a mole fraction for H_2S of 2 mol %. Interestingly, it shows that the mole fraction of H_2S was an extremely weak function of temperature, especially above 600 °C (i.e. the mole fraction of H_2S barely changed with temperature).

Once the molar ratio was found, this had to be related into the actual chemicals, namely a specific combination of methanol, *i*-propanethiol and oxygen. A suitable combination is shown in Table 7.6 below.

Table 7.6: Relating the atomic molar flows to actual chemical compounds

	Moles	**C**	**H**	**O**	**S**
CH_3OH	85	1	4	1	0
C_3H_7SH	6	3	8	0	1
O_2	9	0	0	2	0
Total	100	**103**	**388**	**103**	**6**

At 830 °C and 1 atm, with feed mole percents: 85 % CH_3OH, 6 % C_3H_7SH, and 9 % O_2. The last question was to find the correct flowrate. This was again by trial and error, by changing the inlet flowrate until the correct range was found. The program made this very straightforward. Table 7.7 shows the linear relationship between the flow of reactants and the volumetric flowrate of the product gas.

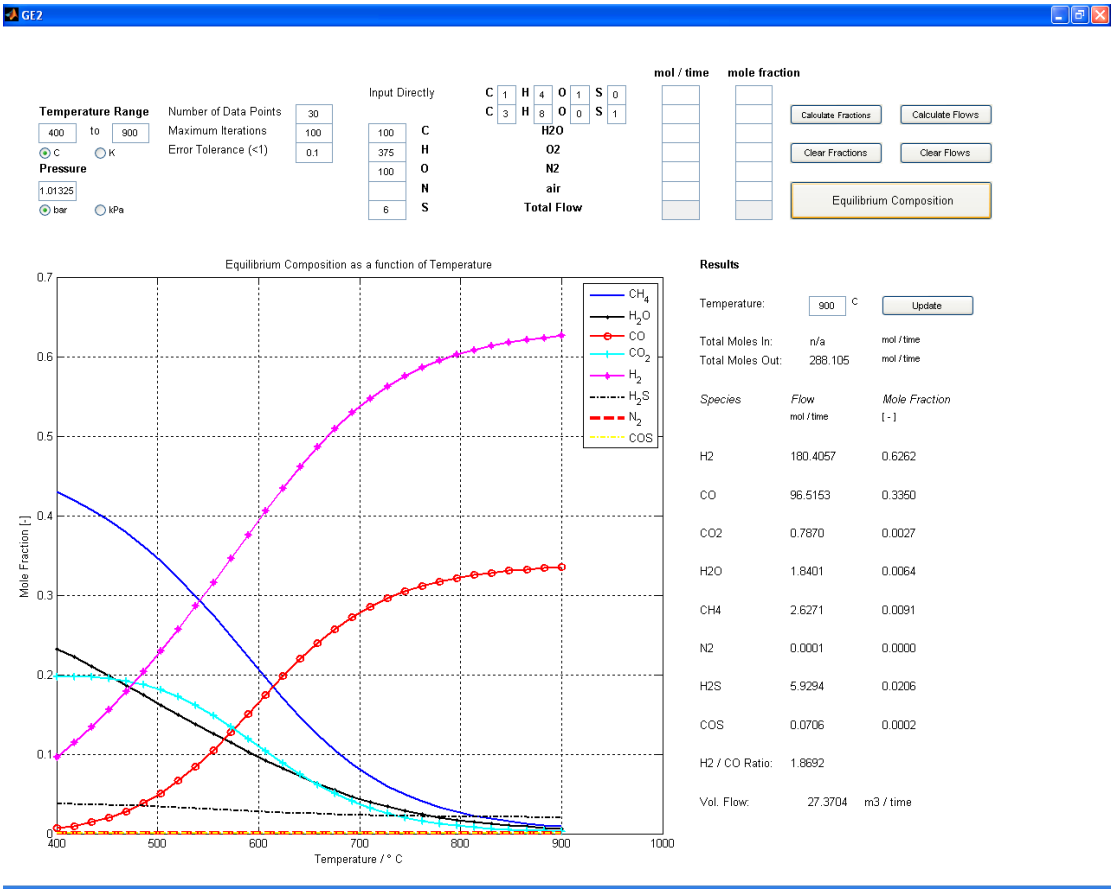

Figure 7.8: Snapshot of the MATLAB program Graphical User Interface (GUI) to calculate the equilibrium composition given an initial molar composition and temperature

Table 7.7: Variation of syngas flowrates according to the flow of reactants

Total Flow In	Total Flow Out	Volumetric Flow at temperature	Volumetric Flow at STP	
$mol.s^{-1}$	$mol.s^{-1}$	$m^3.s^{-1}$	$m^3.s^{-1}$	$cm^3.s^{-1}$
1	2.9179	0.2607	0.0645	64517
0.001	2.918×10^{-3}	2.607×10^{-4}	6.452×10^{-5}	64.52
0.0004	1.167×10^{-3}	1.043×10^{-4}	2.581×10^{-5}	25.81

As highlighted, a flow of 0.0004 $mol.s^{-1}$ was suitable. This matched the upper flowrate required for desulphurization at a space velocity of about 5000 hr^{-1}. This result allowed calculation of the actual inlet fuel flowrates, as shown in Table 7.8.

The oxygen inlet flow was equal to 0.026 SLPM (standard litre per minute). Table 7.8 made it possible to now select a liquid pump and a gas mass flow controller. A mass flow controller with a range of 0-1.0 SLPM for O_2 would be required.

Table 7.8: Final composition and flowrates of reactants

	Mole fraction	**Flowrate at STP**		
	[-]	$mol.s^{-1}$	$g.min^{-1}$	$cm^3.min^{-1}$
CH_3OH	0.85	3.40×10^{-4}	0.6537	0.8297
C_3H_7SH	0.06	2.40×10^{-5}	0.1097	0.1316
O_2	0.09	3.60×10^{-5}	0.0346	26.4059
Total	**1.00**	**4.00×10^{-4}**	**0.8022**	**27.3672**

A reactor tube with internal diameter of 42 mm was available. Assuming a length of 600 mm, this gave a total volume of about 831.27 cm^3. This would give the following residence times:

Flow at STP: 25.81 $cm^3.s^{-1} \rightarrow \tau$ = 32.2 s
Flow at 830 °C: 104.3 $cm^3.s^{-1} \rightarrow \tau$ = 8.0 s

It was noted that the reactor was unlikely to be isothermal and the constant heating zone was not yet established.

11.2 Mechanical Design

The first mechanical issue was how to vaporize the feed. It turned out that the surface of the gasifier, once it had been built, still became very hot despite the insulation, approximately 110 °C. Since the boiling points of both fuels were well below this temperature, the fuel lines were wrapped around the gasifier to transfer the heat to the pipes for vaporization. This worked well, especially after even more insulation was added. Refer to the photographs in Section 15 of this Chapter.

The gasifier would have to have custom end sockets to allow for thermocouples and for gas to pass through. Again, the material of construction was Stainless Steel 316 to prevent corrosion and the low pressure operation meant that a minimum tube thickness was not an issue to be considered. The diagram in Figure 7.9 shows the end sockets.

Note that the gas inlet consisted of a mixture of the vapourized liquid fuel and oxygen.

11.3 Further equipment information

Please refer to the Appendix, Section A.5 for further details upon equipment related information. It includes the calibration and operating principles of the pump, mass flow controller, gas analyzer, heating wire and the pressure drop calculation.

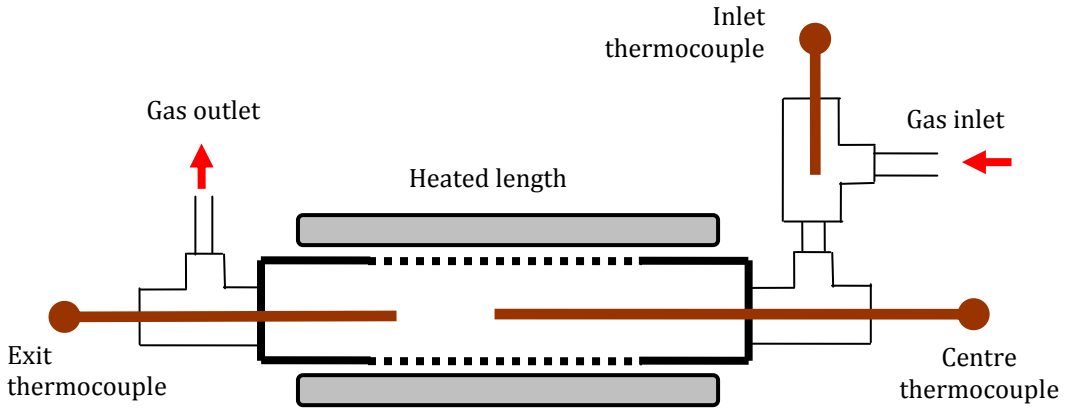

Figure 7.9: Schematic diagram of gasifier inlet and outlet fittings, not to scale

12. Auxiliary equipment

12.1 Liquid storage tanks and fuel changeover

One anticipated problem was the *time* that it would take to establish a consistent gas composition from the gasifier during the 'start up' from the apparatus. There were two reasons for this: firstly, any previous liquid mixture had to be cleared from the piping and secondly the time for 'thermal equilibration' i.e. reaching a temperature steady state.

Gas could not flow over the sorbent until the gas composition and inlet temperature was stable, as this would mean variable experimental conditions. Once some H_2S had reached the sorbent, of any concentration, the experiment would have effectively started. There was thus the need for a gas bypass line around the desulphurization reactor.

While it would not take a long time (30 minutes) to establish consistent gas composition, achieving steady state temperatures could take hours. This was because of the relatively slow conduction of heat through the apparatus, and the relatively fast heat loss by convection to the surroundings due to the large difference in temperature (>500°C to 25 °C).

It was thus decided to start up the equipment using H_2S free syngas ('clean' syngas). The mercaptan, *i*-propanethiol, added to the fuel mixture was relatively expensive compared to methanol (it was 25 times more expensive) and hence it could not be unnecessarily wasted.

To do this, two fuel tanks were necessary: one for pure methanol and other for the methanol-mercaptan mixture. These were made of two 'pots' (from PVC tubing) and were approximately 3 litres in volume. They had lids which were sealed using a sealant and a small hole to break the vacuum formed under pumping. The mercaptan tank had clear flexible tubing as side glass to use as a level gauge in the tank.

The experimental procedure would include some 'changeover' of the fuel mixtures. This had to be thought through carefully. The experiment could be broken down into the following phases.

Table 7.9: Experimental phases

Phase	Gas	Gas Source	Flow path	Function	Time
Heat up	Nitrogen	N_2 Cylinder	Reactor	Heating to temperature	2 hours
Start up 1	Clean syngas	Tank 1 and O_2 cylinder	Bypass	Check no H_2S	30 minutes
Start up 2	Clean syngas	Tank 1 and O_2 cylinder	Reactor	Bring reactor to steady state	30 minutes
Start up 3	Syngas with H_2S	Tank 2 and O_2 cylinder	Bypass	Constant gas composition with H_2S.	30 minutes
Experiment	Syngas with H_2S	Tank 2 and O_2 cylinder	Reactor	Experiment	2 hours
Shutdown 1	Clean syngas	Tank 1 and O_2 cylinder	Bypass	Remove any sulphur gas components	30 minutes
Shutdown 2	Nitrogen	N_2 Cylinder	Bypass	Purge	30 minutes

12.2 Flow control of liquid feeds

A peristaltic pump was available with a range of 0-99 rpm.

12.3 Flow control of gaseous feeds

For the gas feeds, a pump was not required since the gas cylinder was already under pressure. A gas mass flow controller with a range of 0-1.024 SLPM was installed.

12.4 Flow meter of gaseous product

In order to measure the flowrate of the syngas, a simple bubble flow meter was installed before the gas was vented. The major advantage was that the flow meter was independent of gas composition. The minor disadvantage was that sometimes the flow was not suited for the range of the tube (for example, the flow is above 50 $cm^3.s^{-1}$). The flow was on a water free basis, as the water was condensed by the knock out pot.

12.5 Heating lines

Due to the presence of water in the gas sample, all gas lines had to be heated to above 100 °C to prevent condensation. This was fairly straightforward to implement. In addition, the 6 port sample valve was heated and the temperature was measured.

12.6 Knock out pot

A conical flask was placed just before the bubble flow meter. It was partially filled with water to act as a Dreschel bottle to serve two purposes: the bubbles gave a quick visual representation as to whether gas was flowing. Secondly, it cooled the gas and condensed water. This was to prevent significant condensate in the outlet pipes and water flowing backwards. The bubbling would also result in the outlet gas being saturated with water.

13. Flow diagram

The flow diagram for the apparatus is shown below in Figure 7.10. The GC sampling lines have been omitted for clarity.

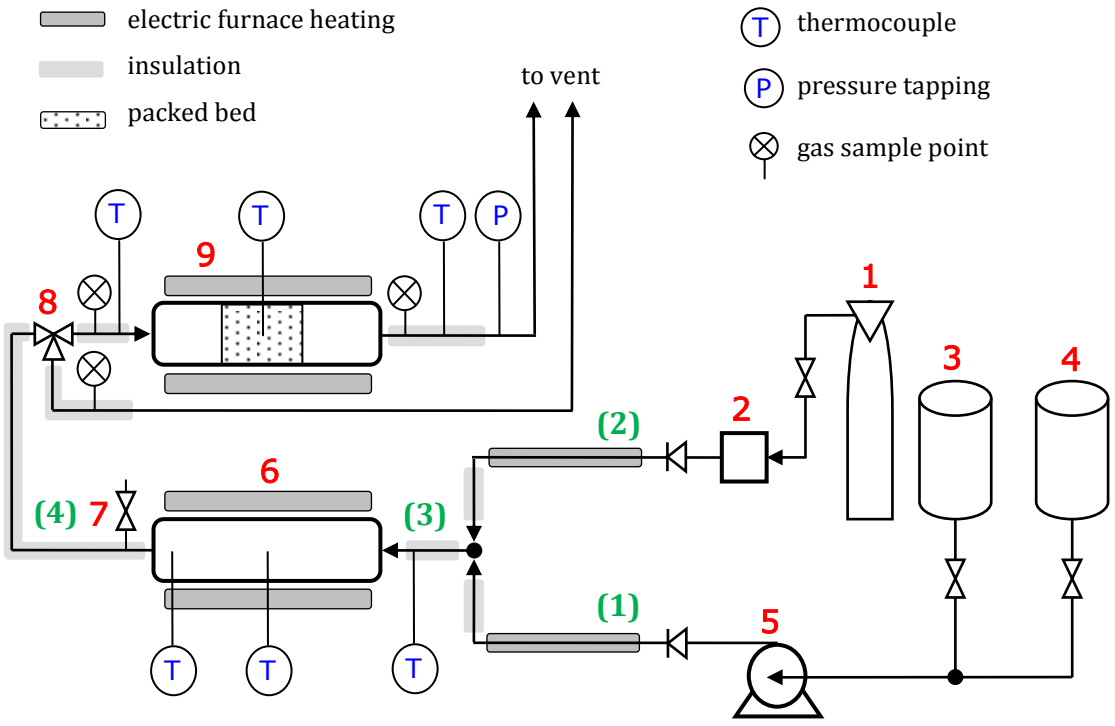

Figure 7.10: Process Flow Diagram: 1. Oxygen cylinder, 2. Mass flow controller, 3. Methanol tank, 4. Sulphur mixture tank, 5. Peristaltic pump, 6. Gasifier, 7. Pressure relief valve, 8. 3-way valve, 9. Desulphurization reactor. The green numbers are the stream numbers.

14. Safety in design

This apparatus has a number of dangerous aspects. The major risks would be:

- Toxic and flammable gas and liquid leaks
- Chemical spills
- Fire: chemicals and equipment
- Pressure explosion: cylinders and system
- Electrical hazards

- Equipment failure due to reaction conditions: high temperatures and corrosive atmosphere

14.1 High temperature

The desulphurization reactor was housed in a commercial laboratory tube furnace. This had excellent thermal insulation. It also had a guard plate. The gasifier furnace, which was custom made, was still extremely hot and thus extra insulation was added.

All contact with the hot equipment must avoided. For example, a material may touch a hot tube, melt or burn and catch fire. A chemical may vaporize instantaneously, ignite etc., and the backflow of hot gas down to the feed tanks was also a concern.

The following measures were taken to address the high temperature problems:

- Insulation: both thermal and electrical. Glass wool was liberally used to cover all exposed pipes and valves. This included the desulphurization reactor ends when they were disconnected. Thus there were no exposed metallic areas when the apparatus was started, apart from the vent line from the knock out pot. The system was electrically earthed from a few points to prevent static build up and possible sparks.

- Pressure: a pressure relief valve was placed after the gasifier, before the desulphurization reactor.

- Non-return valves: were installed on the fuel feed and the oxygen feed line.

- Safety signs: were placed by the apparatus.

14.2 Toxic and flammable gases and liquids

Flammable and toxic liquids: Both methanol and *i*-propanthiol are flammable. In addition, gloves and safety glasses must be worn when handling the liquids.

Flammable gas: Hydrogen, hydrogen sulphide and methane were present in the system. These are flammable gases and hence all sources of ignition or contact with oxygen must be removed or controlled to ensure the gas is outside the flammability region. There was no contact with oxygen (as it was all reacted in the gasification reactions) until the syngas was vented. At this point, it was diluted significantly with the air in the extractor fan.

Toxic gas: all the gases are toxic in one form or another. From Perry and Green (1999), these range from the simple asphyxiants (nitrogen, helium) which 'displace' oxygen supply to the lungs, to the chemical asphyxiants (carbon monoxide, hydrogen sulphide) which physically 'block' oxygen to the lungs.

Hydrogen sulphide has the interesting property that one can detect it by its characteristic 'rotten egg' smell. It is when one stops smelling it (i.e. the senses have been deadened) that it is now lethal and one can literally pass out at any moment.

Liquid odour: As is well known, the mercaptan has an extreme odour. Short term exposure does not have severe health risk.

The safety measures employed were:

- The experiment took place in its own room.
- All pipe connections and fittings were rigorously checked for leaks.
- The draught caused by the extractor fan was quite strong, meaning air was continually being taken out the building.
- All sources of ignition were removed. This was a particular concern for the liquid fuels.

Lastly, it is noted for the experiment, once the flammable gas products were formed in the gasifier, by definition, there was no oxygen present for combustion.

14.3 Other hazards

Electrical: The heating lines were electrically heated. This consisted of nichrome wire in a sheath, wrapped around the pipe to be heated. A large current passed through the wire to heat up the pipe. This must be turned off when connecting or disconnecting the wires.

The electrical connections to the gasifier furnace also had a large current supplied to the heating element. As a result, the entire apparatus was earthed from a number of places.

Oxygen and hydrogen cylinders: These are major fire risks should a flame develop and travel in a pipe line.

High pressure cylinders: The gas cylinders must be fitted with the proper regulators to prevent leaks or explosions.

Connection fittings: All fittings were leak tested.

Over pressure: a pressure relief valve was installed after the gasifier, before the sorbent bed, with a release pressure of 3 bar.

15. Instrumentation

Temperature: (Thermocouples: all type K)

- Gasifier reactor inlet (mixing point)
- Gasifier reactor centre

- Gasifier reactor exit
- Desulphurization reactor inlet
- Desulphurization reactor centre (in sorbent)
- Desulphurization reactor exit

Pressure:

- Differential pressure gauge on sample line to GC
- Pressure display on mass flow controller for oxygen gas feed

Flow:

- Gas mass flow controller for inlet gas
- Calibrated peristaltic pump for inlet fuel
- Bubble flow meter for total gas flow before venting

16. Process control

Temperature control

- Gasifier reactor centre
- Desulphurization reactor centre (in sorbent)
- Heating line with variac

Flow control

- Gas mass flow controller for oxidising gas
- Peristaltic pump: settings calibrated for fluid being pumped

17. Layout and construction

The layout of the equipment was carefully thought out in order to reduce piping and heat loss. The main uncertainty was the degree of cooling that the gas would experience between the gasifier and the desulphurization reactor. Secondly, the sampling points for the GC had to be considered. As mentioned, the gas temperature could be extremely high (>600 °C) after leaving the gasifier. The effectiveness of the insulation was not tested in this project.

17.1 Layout

It was thus decided to have the furnaces above each other with a pipe length of about 70 cm between them. This also helped to reduced the 'footprint' of the system. The liquid pump was placed on the same table as the desulphurization furnace, with the two pot tanks about 30 cm above the pump inlet to ensure there were no air bubbles and that there was always a head of pressure (NSPH) available.

The gas mass flow controller was attached at a convenient location. This was not particularly important as the gas was supplied at high pressure (200 kPa) from a cylinder, and the gas would later mix with the fuel.

As mentioned, the fuel line was pumped around the gasifier to serve as a vaporizer. The ¼ inch pipe was wrapped around the furnace. Due to the low flowrate, there was plenty of time for heat transfer and achieved satisfactory vaporization of the feed.

Electrical heating wire was installed on the sample lines to maintain the gas above 100 °C to prevent water condensation. The apparatus also had to be located in close proximity to an extractor fan. The gases, once passed through the bubble flowmeter, continued straight vertically into the extractor hood.

The gas cylinders were set up in a cylinder bank on the adjacent wall. There were 7 cylinders in total: He, Air Zero and H_2 (for the GC), O_2, N_2 for the apparatus, CH_4 and H_2S for calibration.

17.2 Pipe sizing

Due to the low flows of both gas and liquid, and the corrosive atmosphere, all pipes were ¼ inch stainless steel. The only exception was the pipe joining the two reactors, which was ½ inch to account for the higher volumetric gas flow. This scheme also simplified fittings, as fewer adapter fittings were needed. These were standard sizes. Most joints were compression or NPT fittings.

17.3 Materials

As mentioned, stainless steel was used in most cases. There was, however, one particular material problem: valves. The high temperature of the gas, and its corrosiveness made the seals and o-rings in valves subject to damage. Although the catalogue gave a temperature rating of 120 °C, it was quite possible that the temperatures were significantly above this. The equipment later developed quite a large pressure drop of about 10 kPa, and it is thought that valve blocking may have been the cause.

17.4 Construction

The gasifier furnace was manufactured by GM Heating (pty) Ltd. The unit was leak and pressure tested to 3 bars.

Connection to the GC was a modification of the instrument itself: the carrier gas line was cut open and connected to the sample valve. The line returning from the valve was reconnected to the carrier gas, which then continued to the injector port. These connections were by silver-solder, whereas the valve fittings were compression fittings.

A range of photos of the equipment is shown below in Figures 11 to 14, including some of the construction phase.

Figure 7.11: Photograph of gasifier furnace. The inlet thermocouples and vapour mixing point are clearly seen. The pipes have also been wrapped around the furnace to vaporize the liquid fuel. This was before insulation was added.

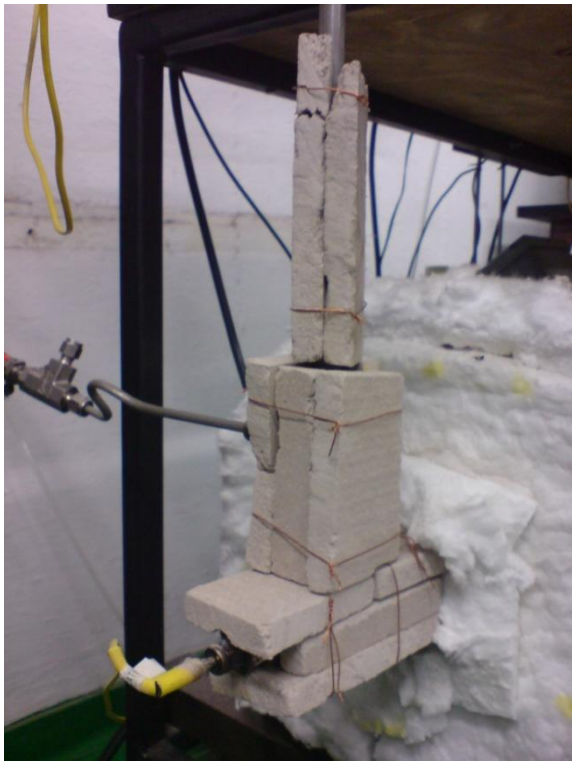

Figure 7.12: Photograph of the outlet of the gasifier. Insulation board was used for insulation. The thermocouple is visible, as is the pressure relief valve. The gas travelled up the pipe to the desulphurization reactor.

Figure 7.13: Photograph of the desulphurization reactor. The inlet thermocouple is still attached. The support grid is in the centre of the tube, secured on the thermocouple. The spacer maintains the integrity of the sorbent bed. The reactor tube was threaded to allow the sockets to be screwed on.

Figure 7.14: Final apparatus setup on laboratory

18. Mass and energy balances

From all the above considerations, the mass balance model used is given below.

18.1 Gasifier Reactor

Residence time in gasifier reactor: $\tau = V/Q$

Reactor volume: D = 4.2 cm, L= 60 cm $\rightarrow$ V = 831.27cm^3.

Flowrate at high temperature of 835 °C: Q = 6380 $cm^3.min^{-1} \rightarrow \tau$ = 7.8 s
Flowrate at STP: Q = 1571 $cm^3.min^{-1} \rightarrow \tau$ = 31.7 s

This shows that a minimum time in the reactor is 7.8 s.

Table 7.10: Mass balance over gasifier reactor, including results from MATLAB calculation and ASPEN simulation. The stream numbers refer to Figure 7.9.

STREAM		**1**	**2**	**3**	**4**	**4**
Mole Fractions					MATAB	ASPEN
Methanol	CH_3OH	0.9341	0.00	0.8845	0.0000	0.0000
i-propanethiol	C_3H_8S	0.0659	0.00	0.0606	0.0000	0.0000
Oxygen	O_2	0.00	1.00	0.0549	0.0000	0.0000
hydrogen	H_2	0.00	0.00	0.00	0.6157	0.6088
carbon monoxide	CO	0.00	0.00	0.00	0.3278	0.3346
carbon dioxide	CO_2	0.00	0.00	0.00	0.0068	0.0062
Water	H_2O	0.00	0.00	0.00	0.0119	0.0116
methane	CH_4	0.00	0.00	0.00	0.0181	0.0177
hydrogen sulphide	H_2S	0.00	0.00	0.00	0.0203	0.0204
Quality		Liquid	Gas	Gas/vapour	Gas	Gas
Temperature	C	25.00	25.00	70.00	835.00	835.00
Pressure	bar g	0.20	0.20	0.20	0.00	0.00
Mole flow	$mol.s^{-1}$	0.000364	0.000036	0.0004	0.0012	0.0011
Mass flow	$g.s^{-1}$	0.0127	0.0012	0.0139	0.0154	0.0154
Density	$g.cm^{-3}$	0.7940	0.00157	0.00148	0.00015	0.00015
Volumetric flow	$cm^3.min^{-1}$	0.961	44.131	564.358	6379.79	6258.74
Pipe Diameter	cm	0.3	0.3	0.3	1.26	1.26
Velocity	$cm.s^{-1}$	0.2267	10.4055	133.0673	85.2755	83.6575
Density at STP	$g.cm^{-3}$ (STP)	0.7940	0.0014	0.0015	0.0006	0.0006
Volumetric flow STP	$cm^3.min^{-1}$ (STP)	0.96	48.41	537.85	1571.92	1542.09

19. Process simulation on ASPEN Plus and comparison

To check the equilibrium model, ASPEN Plus was used to simulate the process. The same components were fed to ASPEN's 'Gibbs Reactor' simulator at the identical conditions. The results of the simulation are shown below in Figure 7.15.

The solid lines are the ASPEN results, and the marker lines are the MATLAB program results. As can be seen, there is excellent agreement. Small deviations can be accounted for due to small differences in thermodynamic data (heat capacities and heats of formation).

Some other components were included in the ASPEN simulation, namely SO_2, COS, CH_3OH and C_3H_7SH. For SO_2, CH_3OH and C_3H_7SH, the mole fractions were below 1×10^{-9}. However, for

COS, the average mole percent was 0.025 mol %. Although very small, it should be acknowledged.

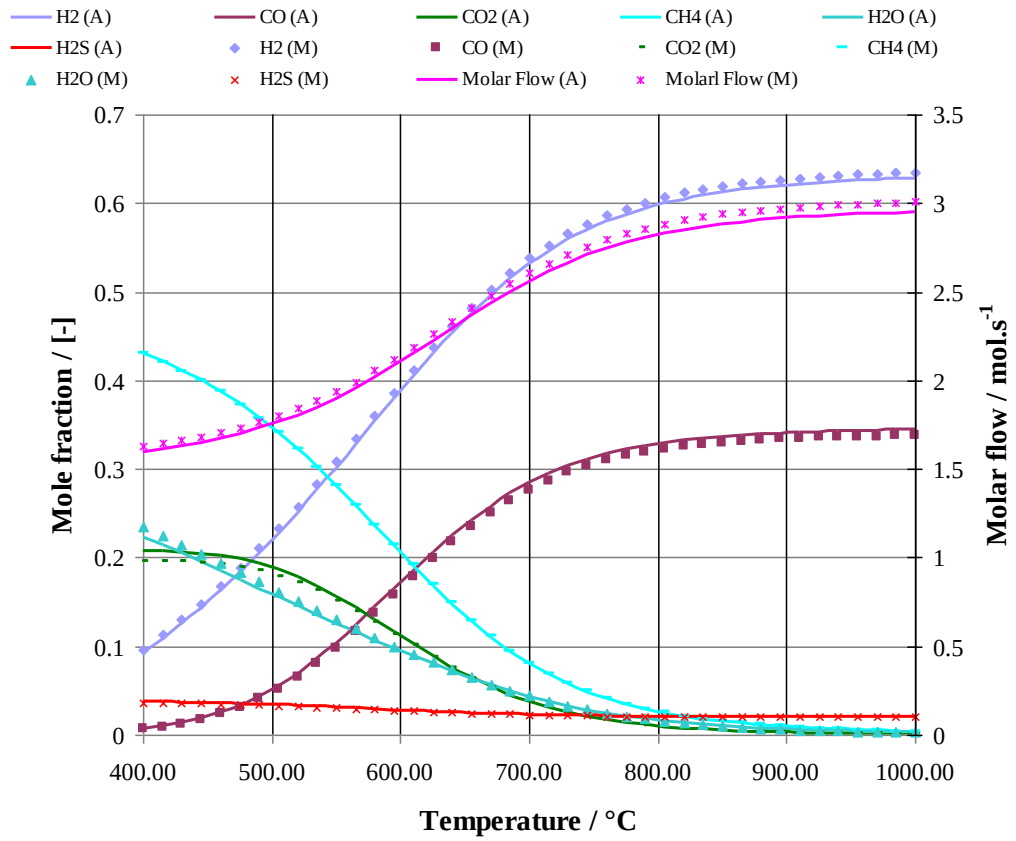

Figure 7.15: Comparison of MATLAB (M) and ASPEN (A) gasifier equilibrium compositions for a feed of 85 mol % CH_3OH, 6 mol % C_3H_7SH and 9 mol % O_2 at a total of 1 $mol.s^{-1}$ at 1.01325 bar a.

As can be seen, there was excellent agreement between the simulation and the MATLAB programme. This validates the use of the MATLAB programme for all equilibrium calculations.

Chapter 8

Experimental Work

1. Introduction

This chapter details the work performed on the equipment. The design has been implemented and it was time to see how the apparatus actually functions. The equipment was tested before two sets of experiments were carried out. The first set varied temperature and particle size and allowed for any shortcomings to be identified and rectified before embarking on the main investigation of the effect of temperature, particle size and flowrate on the gas-solid reaction.

2. Aims of the experimental work

The aims of experimental work were as follows:

1. Test that the equipment actually works. Modify accordingly should problems arise.

2. Develop a procedure to perform the gas-solid reaction investigations in order to obtain meaningful results.

3. Perform a set experimental runs. This was to establish the equipment's performance over a prolonged period of use. It was imperative that the equipment functioned consistently throughout the programme of runs.

4. Evaluate that the experimental outcomes defined in the experimental design could be achieved practically.

5. Establish all possible sources of error (experimental uncertainty) and try to quantify them.

6. Compare the results to reaction models.

7. Suggest areas of improvement to the equipment, to the method, identify limitations and determine any missing data and how it could be obtained. This again links back to the equipment design.

The results of proceeding through these aims provide the basis for the remaining chapters.

3. Apparatus development

3.1 Initial testing of equipment

There were a number of initial tests to conduct to check that the apparatus would work appropriately.

- Connection of desulphurization reactor: reliability of seals and fittings under repeated testing.
- Loading and unloading sorbent: determine degree of sorbent loss, if any.
- The gasifier temperature: ability to maintain isothermal conditions.
- Desulphurization temperature: ability to maintain isothermal conditions.

Secondly, the instrument calibrations had to be performed. This was for the peristaltic pump and for the GC. Finally, the GC analysis with the syringe was ultimately changed to using a sample valve. However, there would be a number of experiments to ascertain the effectiveness of using a gas syringe.

3.2 Modifications of equipment

These were performed after the first set of experiments, without composition analysis.

- Installation of bypass line and associated valves: around the desulphurization reactor
- Gas bubbler (also to collect condensate)
- Installation of gas flowmeter
- GC online connection: heated valve and sample lines to avoid condensate
- Filter of glass beads in desulphurization reactor to prevent carbon deposits
- Level gauge on pot feed tank
- Increased insulation

3.3 Final apparatus

From the equipment development, i.e. after the initial designs and subsequent modifications, the final apparatus consisted of the following units, as given in Table 8.1.

Technical details including operating ranges and error ranges are given in later in Section 9, Table 8.7. For details on the actual operating principles of the apparatus, refer to the Appendix, Section A.5.

Table 8.1: Final apparatus and their manufacturing details

Item	**Model / Manufacturer**
Horizontal tube furnace – gasifier	Custom made by GM Heating
Horizontal tube furnace – desulphurization	Carbolite MTF 400/38
Reactor tube – gasifier	Custom made by workshop
Reactor tube – desulphurization	Custom made by workshop
Pot storage tanks, 3 litre volume (2)	Custom made by workshop
Gas mass flow controller	Alicat Scientific
Peristaltic pump, 0-99 rpm	Watson Marlowe
3 way valves, ¼ inch (3)	Whitey
6 port gas sample valve	Shimadzu
1 m*l* gas sample loop	Shimadzu
Heating wire (nichrome)	[-]
Sheaths for heating wire	[-]
Variac: variable voltage supply	[-]
Knock out condenser	[-]
Miscellaneous piping and fittings	[-]

The desulphurization reactor consisted of the following parts, as detailed in the equipment design and shown previously in Figure 7.4:

- Reactor tube
- Inlet socket (including thermocouple)
- Outlet socket
- Centre thermocouple for sorbent
- Wire mesh particle support plates (2)
- Spacer

4. Chemicals

Table 8.2: Chemicals used and their respective purities

Chemical	**Manufacturer**	**Purity**
Methanol	Saarchem (Merck)	99.5 mole % (min. assay)
i-propanthiol	Fluka (Sigma-Aldrich)	98.9 mass % (COA)
Zinc oxide	M. R. Zinc Oxide (pty) Ltd.	99.5 mass % (COA)
Glass beads	Promark Chemicals	[-]
Oxygen	Afrox	Technical grade
Nitrogen	Afrox	Technical grade
Helium (for GC)	Afrox	Instrument grade
Hydrogen (for GC)	Afrox	Instrument grade
Air zero (for GC)	Afrox	Instrument grade

5. Analysis equipment

The analysis equipment consisted of the following instruments.

- Gas Chromatograph (Shimadzu GC-2014)
- Mass balance (Mettler Toledo)
- Gas analyzer (Bacharach ECA-450)
- Scanning Electron Microscope

5.1 Analysis of solid

The solid was analysed by weighing (before and after each experiment) and the surface was examined using scanning electron microscope.

5.2 Analysis of gas

The accurate determination of a gas mixture's composition was difficult. A sample must be taken from the process stream which was representative of the total gas flow and reproducible. The first problem was to identify the components present. Secondly, there was the problem of quantifying the components into some meaningful number, such as a mole fraction. Further problems would include the sensitivity of the detection method, the detector's range of operation and the time taken for analysis of a sample.

The gas analysis method depends upon two main factors: the actual component to be measured and the expected concentration (and associated accuracy). In addition, there is the constraint of the *amount* of sample available to analyze.

Bear in mind that the main components of syngas are: H_2, CO, CO_2, H_2O, CH_4 and H_2S. Implicit in this list is the absence of O_2 (as it was assumed that it has reacted completely), and hence it can be considered an extra component. Thus there are 7 gases to detect and quantify.

The focus of this study was desulphurization. Hence the detection and quantification of H_2S was the most important area of investigation. The gas analysis is discussed in detail in the Appendix, Sections A.3 and A.4.

6. Experimental procedure

6.1 Introduction

The experimental procedure described here gives the method used to conduct a gas-solid reaction at high temperature in a fixed bed. It was important to note exactly what experimental variables had to be kept constant, which variables could be changed and what information could be gathered as results from these changes. These defined the outcomes of each experiment.

In general, there were two desired outcomes from each experiment:

- Conversion of sorbent under set reaction conditions
- Corresponding breakthrough curve of H_2S, if indeed there was breakthrough

The conversion of the sorbent could be found by the change of mass. The breakthrough curve could be found from the gas analysis of the outlet stream as the experiment progressed.

6.2 Summary of experimental procedure

The experimental procedure is best described by summarizing the 'main steps' before expanding into details associated with each step. The general procedure for a typical gas-solid reaction experiment was as follows:

i. Load the reactor with fresh sorbent and reconnect to the system.
ii. Turn on furnaces and heat up the system to a steady temperature, under a flow of nitrogen to flush out remaining gases.
iii. Check the system for leaks and sample the gas to check system was indeed clean.
iv. Start the flow of fuel and oxygen to create syngas with H_2S. Ensure that this flow bypassed the sorbent reactor while steady state was being reached. Inlet gas samples are taken to determine the steady state gas composition.
v. Start the reaction by switching over the bypass valve to the sorbent reactor.
vi. Take regular exit gas samples for gas composition.
vii. After a set time, switch the valve back to bypass to stop the reaction.
viii. The fuel and oxygen flows were changed to a sulphur free fuel before being stopped altogether and turning on a nitrogen flow to purge the system.
ix. Once the system has cooled down, unload the reactor and weigh the sorbent mass.

6.3 Sorbent preparation

The zinc oxide sorbent was bought from M. R. Zinc (pty) Ltd as a 25 kg bag with varying pellet sizes. The pellets were of uniform shape (spherical). These pellets were chosen because they were of acceptable purity (>99 % ZnO) and they were in the correct size range for the reactor, namely between 0.5 mm and 2 mm.

There were two slight disadvantages. Firstly, the pellets required sieving to obtain a desired size fraction. Secondly, the pellets were quite soft. This meant that they could disintegrate into a powder simply by rubbing them on one's hand. Careful handling of the sorbent was thus very important.

6.4 Fuel preparation

The liquid fuel was prepared by mixing organic liquids in order to achieve the correct molar ratio of carbon to hydrogen to oxygen to sulphur (C:H:O:S). This was determined by both the

mass balance and the equilibrium model, as given in Chapter 7. From the model, both the flowrates and the mole fractions of the fuel and oxygen were set.

Methanol was mixed with *i*-propanthiol (a mercaptan) on a mass balance in a 1 litre glass flask, under a fume hood. In general, a 715.00 g mixture was prepared consisting of 615.00 g methanol and 100.00 g mercaptan. The large mixture reduced any error from mixing (e.g. liquid remaining on the funnel, slight fluctuations on balance reading due to extractor fan) as these losses/uncertainties would be very small compared to the total mass measured.

Once mixed in the flask, the fuel was poured into the correct tank on the apparatus as required. Each run required about 100 g of the mixture.

Methanol was also poured into its own tank as required. Usually about an additional 100 g methanol per run was needed.

6.5 Loading the reactor with sorbent

The design of the reactor allowed for the sorbent to be loaded and unloaded from the reactor relatively easily. The desired mass of sorbent was weighed out using a mass balance to 0.001 g, by pouring the pellets into a beaker on the balance. Typically, 30 g was used.

The wire mesh support must be correctly positioned on the thermocouple. This was to ensure that the sorbent bed was in the centre of the reactor, which was accordingly in the centre of the furnace. This could be calculated by using the sorbent's mass and density to find the volume that the sorbent would occupy in the reactor. The support was tightened onto the thermocouple with a grub screw.

The furnace had a constant temperature length of 10 cm, where according to the manufacturer the temperature is +/-5 °C of the set point. In order for the reaction to be considered isothermal, the sorbent must be in this zone otherwise there would be an axial temperature profile along the sorbent bed, simply due to non-uniform heating from the furnace.

It was found that there could be some carbon deposits on the sorbent. With a second wire mesh support, there was an option of having an inert bed before the sorbent bed. Glass beads were used as a filter to prevent the carbon from depositing on the sorbent. A 10 cm bed depth with 4 mm glass beads was used. Practically, another wire mesh support was placed on the thermocouple, obviously before the support for the sorbent.

The socket with the thermocouple and wire mesh support(s) could now be screwed onto the reactor tube. The thermocouple was inserted about halfway down, and the glass beads were added. The wire mesh support was then lowered and tightened again with a grub screw. Now that the glass beads were secured, the thermocouple was inserted completely.

High temperature anti-seize grease was applied to the reactor tube's threads to aid with unscrewing the socket after the experiment. Using a torch, the seal of the wire mesh with the inside of the reactor tube, and thermocouple, was checked to ensure the sorbent particles could not pass through any small holes.

The reactor tube was tilted and the sorbent particles were carefully poured into the reactor, from the glass beaker. The tube was secured vertically in a vice. A torch was used to check that the thermocouple was completely covered by the sorbent. The spacer was gently lowered down onto the sorbent using a wire with a hook on the end. The spacer was heavy enough to maintain the integrity of the bed without having to be fastened down.

While still vertically positioned in the vice, anti-seize grease was applied to the reactor outlet tube's threads, the outlet socket was screwed on and tightened. The reactor tube was slowly brought to the horizontal position, slid into the furnace and reconnected to the system at the inlet and outlet.

6.6 Unloading the reactor

The reactor was disconnected from the system at each end. The reactor tube was placed horizontally in the vice and the outlet end socket was unscrewed. The spacer was gently pulled out. Extreme care was taken to ensure that no sorbent was caught/become stuck onto the spacer's wire mesh covering. Hence, a glass beaker was held underneath the reactor tube to catch any sorbent that may fall out as the spacer is removed.

The reactor tube was carefully lifted to empty all the sorbent into the glass beaker. Using a torch, the tube was inspected to see if any particles had been trapped on the wire mesh and thermocouple support. These could be removed by tapping the tube with a shifting spanner to ensure all sorbent was literally knocked out. It was critical not to adjust the thermocouple in the centre of the reactor as this could cause the sorbent to be crushed, caused by the wire mesh being rotated or was moved forward or backwards. Once the sorbent was collected in the glass beaker, it was weighed on mass balance, again to 0.001 g.

6.7 Cleaning the reactor

This was not necessary after each run. However, after some time (usually 10 hours of use), there was a thin layer of soot deposited (carbon deposits) on the reactor tube walls and fittings. This was removed by simply cleaning with soap, water and cleaning brushes.

6.8 Start up of apparatus

The limiting step with starting up the apparatus was the gasifier furnace, as it took the longest time to heat up, and for the heat to conduct through the system to reach a steady state with respect to temperature.

- The gasifier was turned on to the set point (usually 830 °C).

- Nitrogen flow was set to 0.5 SLPM (standard litre per minute), and passed through the gasifier, through the bypass line, through the sample line and loop, and back through to the vent.
- The variac (to supply current to the heating wires around the sample lines) was set to 180 V.
- The system was left for 2 hours.
- During this time, the desulphurization reactor was loaded with fresh sorbent and reconnected to the system, as described above.
- Insulation was re-applied to the reactor's inlet and outlet.
- The desulphurization furnace was turned onto the set point (usually 550 °C).

The next step was to check if the system was clean of all gases.

Note that nitrogen was still flowing through the system. An inlet sample was taken for analysis by the GC. If there was a trace amount of H_2S or methane, a second sample was taken. This second sample was almost certainly a blank result. This meant that the gas lines from the inlet to the gasifier and the inlet sample line were 'clean' of all detectable gases.

The bypass valve was changed to allow the nitrogen gas through the sorbent bed, and through the exit valve into the sample line. Again one or two samples were taken to check for any trace gases that may have been in the line from the reactor to the exit sample point. Of main concern was obviously the presence of H_2S.

Once the system was clean, the flow of fuel and oxidiser could start to begin the production on syngas.

- Valve from the methanol tank was opened.
- Methanol flow was set by the calibrated peristaltic pump (usually 18 rpm).
- Oxygen flow was set by the gas mass flow controller (usually 0.044 SLPM).
- The gas would flow through the sorbent bed.
- This was left for 1 hour to allow the temperatures of the system to reach a new steady state. The higher flow of gas resulted in better heat transfer from the reactor walls and hence the temperatures increased accordingly through the system.

After this hour, the fuel was switched from the methanol tank to the mercaptan mixture tank. The methanol valve was closed before the mercaptan valve was opened, otherwise there would be mixing between the tanks due to the difference in liquid level heights. The bypass valve was also changed to prevent the syngas with H_2S from passing over the sorbent.

It took an estimated 6 minutes for the liquid to be pumped from the tank to the gasifier, through the pre-heating section and into the gasifier. However, to allow for the effects of the two feeds mixing, the inlet was sampled only after 20 minutes, and again at 30 minutes. If the gas compositions were the same, the experiment could now start.

- The bypass valve was changed to send the syngas over the sorbent, and the timer was started.
- Gas was sampled from the outlet 20 minutes from the start and then at approximately 10-15 minute intervals.
- Temperatures were recorded every time the gas was sampled, and the flowrate was measured with the bubble flowmeter.

After a pre-determined time the experiment was stopped by changing the reactor inlet to the bypass. As an option, further inlet samples could be taken to compare to the original inlet samples taken at the beginning of the experiment.

The valve to the mercaptan tank was closed, and the valve to the methanol tank was opened to flush the mercaptan out of system. This was left on for 1 hour.

6.9 Shutdown

After the methanol had been through the system for 1 hour, the pump was turned off and gas flow controller was set to zero. The furnaces and the heating line were turned off. Once the desulphurization reactor had cooled down, the insulation was removed, the reactor disconnected and the sorbent mass was found. Refer to Section 8.6, 'Unloading the reactor'.

6.10 Safety aspects

The safety of the apparatus and various precautions was addressed in Chapter 7, Section 12.

7. Sources of experimental uncertainty

The extent to which the result of an experiment represents the true value in the physical world is determined by the extent of the experimental error. A source of error implies that something in the experiment was knowingly incorrect. A better term to use is source of uncertainty. Most sources of uncertainty were a result of a measurement being performed on a process.

The sources of uncertainty fall into two categories, as from Montgomery and Runger (1999). Determinate errors (also known as systematic errors or bias) have an assignable cause and give a measurement that has the same magnitude and direction from the true value, such as a bias. These can theoretically be eliminated since their cause is known. Indeterminate errors arise from uncertainties in a measurement and are a result of 'random noise'. They can be minimized but not eliminated since their exact cause is unknown.

Before examining the sources of uncertainty, it is important to define some terms, also from Montgomery and Runger (1999).

- Accuracy: the degree to which repeated measurements of a known quantity agree with the *actual value*.

- Precision: the degree to which repeated measurements of a known quantity agree with the *each other*.

- Repeatability: the amount of variation expected when almost all external sources of measurement error have been controlled and held fixed. It is the repeated measurement of a *single* item using the same instrument and method.

- Reproducibility: the amount of variation when several parts of the measurement system are allowed to vary at the same time. It is repeatability applied to the *whole* measurement system.

Most of the sources of uncertainty listed below have been accounted for in the equipment design. However, some sources would be a result of repeated equipment use and general 'wear and tear'. It was hoped that these would be identified during systematic equipment checks. The different uncertainties were rigorously examined and have been detailed in the following tables, Table 8.3-8.7.

It was found that the most significant source of error was that associated with measuring the mass of sorbent (Table 8.6). When calculating the conversion of the sorbent, a maximum error of 0.2 g for a total change of 3.0 g gives a 6.7 % error. This was significant. The other major error was associated with measuring the exit gas flowrate. Although this was only used to compare against the equilibrium model, an improvement should be made.

Both these errors have been explained in the discussion, Chapter 10, Sections 2.6 and 3. All the other errors were not significant compared to these and were included for completeness.

Table 8.3: Uncertainties relating to raw materials

Source	**Uncertainty**	**Significance**	**Action taken**	**Quantification**
Zinc oxide pellets	Purity, particle shape, particle uniformity, and particle disintegration during handling.	Particles did not have exact constant physical properties.	None. Impractical and not significant	> 99.5 % mole ZnO
Methanol and *i*-propanethiol	Purity of chemical.	Source of possible contamination.	None. Purity >98%.	Methanol: >99.5 % mole *i*-propanethiol: >98.9% mole (COA)
Gases	Purity of gas from cylinders.	Source of possible contamination.	None. Purity	> 99.999 % mole

Table 8.4: Uncertainties relating to equipment

Source	Uncertainty	Significance	Action taken	Quantification
Peristaltic pump	Accuracy and consistency of liquid fuel flow.	The pump must deliver a constant flowrate for every experiment that does not vary over time.	Calibration. This should be performed periodically to check that the desired was set.	See instrument data.
Gas mass flow controller	Accuracy and consistency of gas flow.	The controller must deliver a constant flowrate for every experiment that does not vary over time.	None. Manufactured instrument.	See instrument data.
Temperature measurements	Accuracy and consistency of temperature measurement.	Ensure thermocouple end was in correct location.	Thermocouples where checked to read 0 °C in ice as a basic check and were cleaned periodically due to carbon deposits.	See instrument data.
Pressure gauge	Accuracy and consistency of pressure measurement.	The pressure was required to calculate gas composition. Also, it must be monitored as it was an indication of blockages.	None. Manufactured instrument. Routine checking against a reference gauge recommended.	See instrument data.
Mass balance	The actual mass measurement.	A 0.05 g mass change was significant.	A balance measuring to 0.001 g was used.	See instrument data.
Gas analyzer	Actual measurement and sampling of gas for composition analysis.	According to manufacturer limits. For example 0.1 % for O_2. Sample must be representative of the bulk gas stream	Place probe in centre of gas line for sampling.	See instrument data.
GC sampling and analysis	Refer to section on GC analysis.			

Table 8.5: Uncertainties relating to the process

Source	Uncertainty	Significance	Action	Quantification
Mixing of liquids	Formation of non-homogenous solution.	Fuel feed has variable composition with time.	None. Fluids were mixed easily enough and left in storage tank. Magnetic stirrer recommended to be installed.	Indeterminate
Dead volumes	Accumulation of gas/liquids in pockets of the equipment.	Accumulation leads to inaccurate overall composition.	Minimize dead volumes during equipment design.	Indeterminate
Channelled gas flow in desulphurization reactor	Even distribution of gas to solid particle bed by wire mesh support.	Poor exposure to metal surfaces for heat transfer and to the solid sorbent for reaction.	Minimize channelling during equipment design.	Indeterminate
Leaks	Unknown leak present.	Affects volumetric flow and composition. Dangerous.	Whole system was leak tested during construction. All fittings always leak tested if removed or included.	Indeterminate

Table 8.6: Uncertainties relating to operation of the equipment

Source	Uncertainty	Significance	Action	Quantification
Loading and unloading sorbent	Some sorbent can disintegrate on reactor walls, get stuck in the reactor on the wire mesh.	As for the mass balance, the change in mass was desired. Hence it was imperative not to have any 'losses'.	Careful handling of sorbent. Reactor tube was checked carefully with a torch to see if any particles remained. These were removed by tapping the side with a spanner.	Loss of sorbent less than 0.2 g.
Bubble flowmeter reading	Timing of bubble as it rises past the graduations on the tube.	This directly calculates the volumetric flowrate.	Repeated readings over a large range (40 cm^3) to try and have a time of at least 6s for the bubble to rise. A larger flowmeter is required for larger flows.	Difficult to measure: flowmeter was significantly more accurate at lower flowrates. Approximately 0.5-5 $cm^3.s^{-1}$.

Table 8.7: Instrument operating ranges and reported errors

Instrument	Manufacturer and Model	Unit	Operation Range	Minimum change	Error	Reference
Peristaltic pump	Watson-Marlowe 101U/R	rpm	0-99	1	not available	Manual
		$cm^3.min^{-1}$	0-6.85	0.07	not available	Measured
Gas mass flow controller	Alicat Scientific M-1SLPM-D	SLPM	0-1.024	0.001	0.003 (max)	Manual
		$g.min^{-1}$ O_2	0-1.340	0.0014	0.004 (max)	Manual
Temperature measurements	Type K thermocouples	°C	0-1200	0.1 or 1	1	Manual
Pressure gauge	Airflow Digital Manomenter DM2L	kPa	0-15	0.001	not available	Manual
Mass balance	Mettler Toledo	g	0-120	0.001	0.002	on equipment
Gas analyzer	Bacharach ECA-450	O_2: mol %	0.1-20.9	0.1	0.3	Manual
		SO_2: ppm	0-4000	1	1	Manual

Chapter 9

Results

1. Introduction

The results presented fall into five categories:

1. Equipment calibration
2. Preliminary experiments
3. GC Work for composition analysis
4. Main experimental programme: Factorial design
5. Modelling the gas-solid reaction

There is some discussion presented in this section, where relevant, to point out interesting features. However, most of the commentary will be provided in the discussion.

2. Equipment calibration

2.1 Sorbent conversion and calibration equations

The conversion of the sorbent was calculated from Equation 9.1. This was derived in the Appendix, Section A.2.

$$X[\%] = 100 - \frac{\left[m_{tot} - m_{ZnO} \times M_{ZnS}\right]}{\left(M_{ZnO} - M_{ZnS}\right) m_{ZnO}} \times 100 \qquad (9.1)$$

m_{tot}	total mass at end of experiment	[g]
m_{ZnO}	mass of ZnO at start of experiment	[g]
M_{ZnO}	molar mass of ZnO	[g.mol^{-1}]
M_{ZnS}	molar mass of ZnS	[g.mol^{-1}]

The calibration results have been summarized in Table 9.1.

Table 9.1: Summary of calibration equations obtained during experimental work

Unit	**Measurement**	**Calibration Equation**
Liquid peristaltic pump	Mass flow liquid feed	Mass flow (g.min^{-1}) = 0.055183×W (rpm)
		Molar flow (mol.min^{-1}) = 0.001722×W (rpm)
	Note: These equations applied to methanol (density 0.7878 g.cm^{-3}) and dilute mixtures (less than 20 mass %) *i*-propanethiol (density 0.8334 g.cm^{-3}).	
Gas mass flow controller	Gas mass flow of O_2	Flow O_2 (SLPM) = 1.3088×m_{O2} (g.min^{-1})
	Note: SLPM: volumetric flow of O_2 in *l*.min^{-1} at 25 °C and 14.696 psia	
GC	Methane mole fraction	n_{CH4} (µmol) = 2.280952×10^{-8}×PA (µV.min) + 0.2181375
	Note: The calibration equation for the number of moles of CH_4 was for a range of 0 to 4.0 µmol. The peak area, PA, was available from the GC software package.	

GC calibration details have been given in the Appendix, Section A.5. The GC result for the methane composition was the *number of moles* CH_4 injected into the instrument, n_{CH4}. The mole fraction of methane in the gas sample was found by dividing n_{CH4} by n_t, the total number of moles injected by the sample, as calculated below:

$$y_{CH_4} = \frac{n_{CH_4}}{n_t} = \frac{n_{CH_4}}{\left(\frac{PV_{inj}}{R_g T}\right)} \qquad (9.2)$$

P	pressure of sample (absolute)	[Pa]
T	absolute temperature of sample	[K]
V_{inj}	volume of sample injected	[m^3]
R_g	gas constant	[J.mol^{-1}.K^{-1}]

2.2 Gasifier temperature controller tuning

The temperature control of the gasifier was good: it maintained the temperature setpoint throughout the experiment.

Figure 9.1 shows the *initial* temperature control of the gasifier before and after tuning. The setpoint was 850 °C with fluctuations of 10 °C. The PID settings were changed and the setpoint was also changed to 800 °C. The control was significantly improved, as can be seen. A steady temperature of 800 °C was obtained after 30 minutes, despite the initial overshoot. Note also that the exit temperature is about 90 °C lower.

Initial settings:	P:	3.0 % (of maximum value)	I:	100 s	D:	0 s
Final settings:	P:	1.5 % (of maximum value)	I:	400 s	D:	100 s

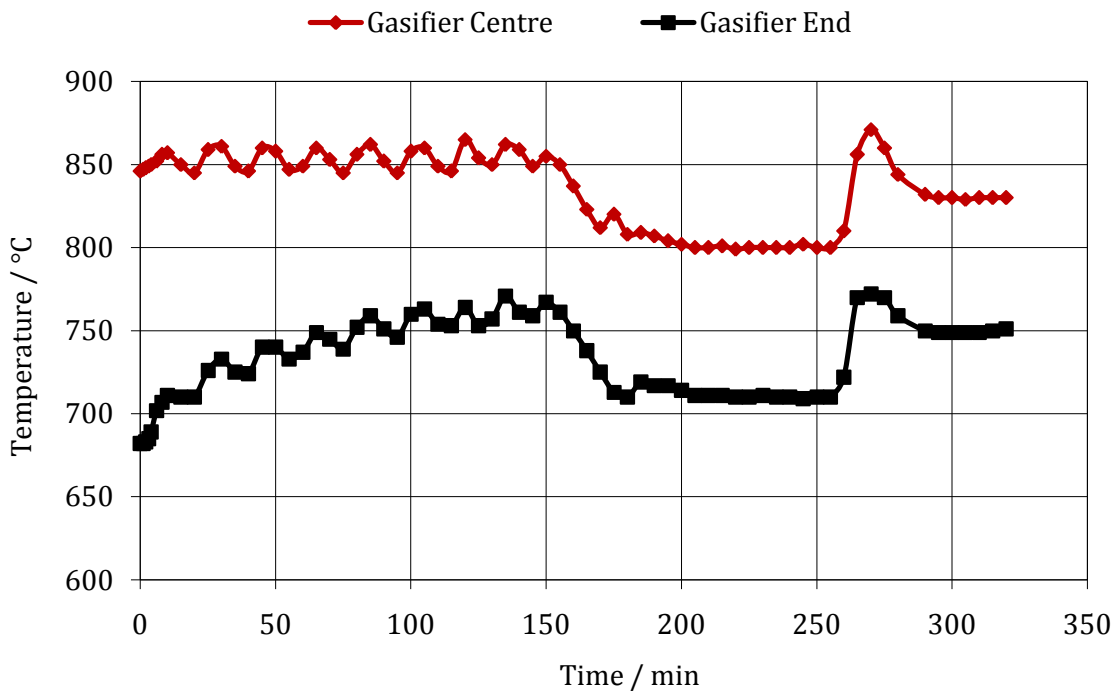

Figure 9.1: Comparison of gasifier controller settings to produce consistent temperature.

3. Preliminary experiments results

The aim of these experiments was to identify and fix any problems that may occur during the actual operation of the equipment, before proceeding to a formal experimental programme.

The first set of experiments varied temperature and particle size. The results have been given in Table 9.2. It was found that there were some deposits of carbon on the sorbent. To see if this was due to the gasification step, an experiment using a gas mixture of 4.18 mol % H_2S in N_2 from a gas cylinder was performed.

3.1 First experimental program

Table 9.2: Summary of experimental conditions and results during first experimental programme. Each result was repeated and the conversion was an average

Pressure: 1 atm Particle density: 1.50 g.cm^{-3} Bulk bed density: 1.07 g.cm^{-3}		**Large Pellets**		**Small Pellets**	
		High Temperature	**Low Temperature**	**High Temperature**	**Low Temperature**
Temperature	°C	540	340	540	340
Diameter sorbent	mm	1.0	1.0	0.5	0.5
Run time	min	120	120	120	120
Flow methanol	g.min^{-1}	0.9068	0.9068	0.9068	0.9068
Flow *i*-propanethiol	g.min^{-1}	0.1416	0.1416	0.1416	0.1416
Mass % methanol	mass %	0.865	0.865	0.865	0.865
Setting fuel pump	rpm	19	19	19	19
Flow oxygen	g.min^{-1}	0.0498	0.0498	0.0498	0.0498
Flow oxygen	SLPM	0.038	0.038	0.038	0.038
Flow syngas (STP *)	cm^3.min^{-1}	1057.63	1057.63	1090.33	1099.93
Inlet H_2S mole %	mol %	3.95	3.95	3.84	3.80
Rate constant †	cm.min^{-1}	0.1334	0.0167	0.1334	0.0167
Volume bed	cm^3	25.28	25.34	26.37	27.20
Superficial velocity	cm.min^{-1}	526	396	526	396
Space velocity (STP)	hr^{-1}	3524	3524	3633	3524
Mass sorbent start	g	27.010	27.079	27.010	27.858
Mass sorbent end	g	30.306	29.169	28.594	28.383
Flow H_2S	g.min^{-1}	0.0634	0.0634	0.0634	0.0634
Ave. H_2S uptake	g.min^{-1}	0.0583	0.0370	0.0280	0.0093
Conversion – actual	%	61.82	39.10	29.70	9.56
Conversion – theoretical #	%	67.25	67.08	67.25	65.21

* 1atm, 0 °C.

based upon all the H_2S reacting with the sorbent for the duration of the run

† taken from Lew *et al.* (1992 a)

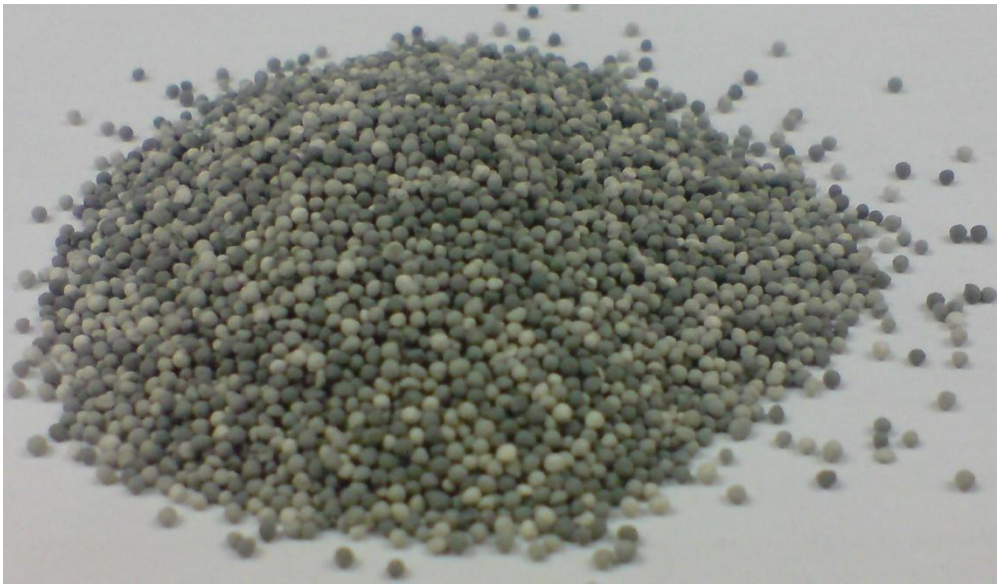

Figure 9.2: 1 mm diameter sorbent after reaction with H_2S in syngas at 550 °C. Note the grey colour indicating some form of carbon deposit.

3.2 Experiment with H_2S in N_2 mixture from gas cylinder

This experiment was to see the sorbent conversion under carbon free conditions. From Figure 9.3, it can be seen that the sorbent turned a pale yellow colour. The conclusion here was that the grey colour observed in Figure 9.2 was not the H_2S-ZnO reaction product.

Table 9.3: Experimental conditions for H_2S/N_2 experiment

Operating condition	**Value**
Temperature	540 °C
Time of reaction	30 minutes
Composition	4.15 mole % H_2S in N_2
Flowrate	not measured but quite high
Mass before	25.2463 g
Mass after	28.8113 g
Conversion	71.53 %

Figure 9.3: Photograph of 1 mm diameter sorbent after reaction with 4.15 mole % H_2S in N_2 at 540 °C. Note the pale yellow colour with no carbon deposits.

3.3 Modifications performed after initial testing

These preliminary experiments showed the need for some modifications, detailed below and explained further in the discussion.

- Installation of a bypass line around desulphurization reactor, including associated valves.
- Installation of a bubble flowmeter on gas exit line for gas flow measurement.
- Installation of a bubbler (a conical flask with water) to collect condensate and provide visual representation of gas flow.
- Installation of gas sampling lines with associated valves.
- GC online analysis: including the heated valve.
- A filter of glass beads in desulphurization reactor to prevent carbon deposits.
- A level gauge on mercaptan mixture fuel tank.
- Increased insulation of equipment.

Lastly, the preliminary experiments excluded gas composition analysis. Before the main experimental programme was started, the gas analysis by GC had to be implemented.

4. GC work for gas composition analysis

Many experiments were performed to develop the GC analysis procedure. These have been documented in the Appendix, Section A.4 and A.5. A typical chromatogram is shown in Figure 9.4, along with peak areas and retention times given in Table 9.4.

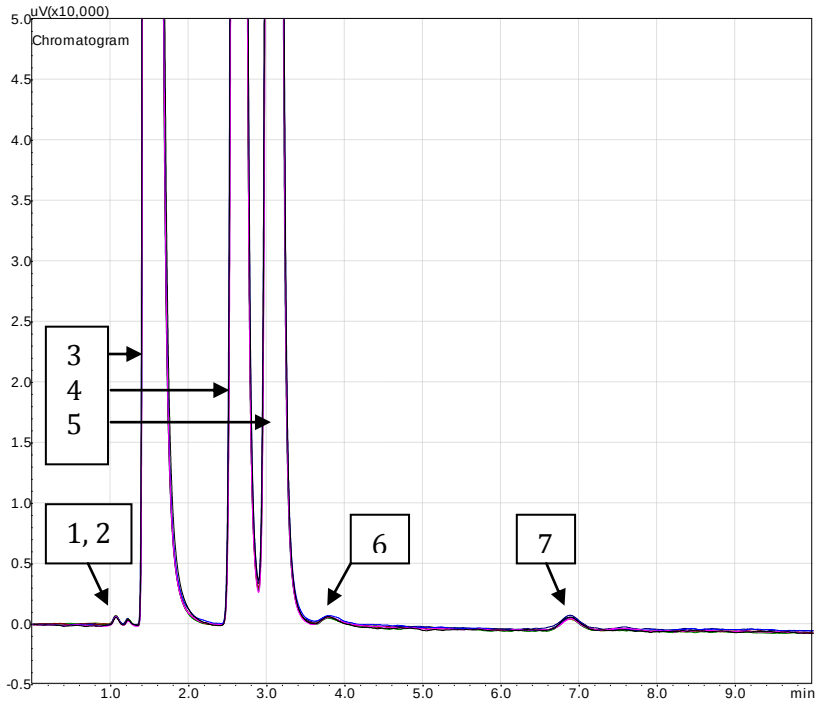

Figure 9.4: A typical chromatogram (from experiment 6). There have been 6 chromatograms overlaid here. The H_2S peak was at 3.8 minutes.

Table 9.4: Species and elution times for identification on chromatogram. Peak numbers refer to Figure 9.4.

Peak number	Component	Elution time / min
1	Unknown (very small)	1.2
2	Unknown (very small)	1.4
3	CH_4	1.5
4	C_2H_8	2.5
5	Unknown – possibly C_3H_{10}	3.0
6	H_2S	3.8
7	Unknown	6.8
	Methanol	8.0

Note that the unknown peaks could be identified by trial and error by injecting pure components under the same GC settings.

The main species of concern were H_2S and CH_4, which were correctly separated and identified.

Figure 9.5 shows that the FID detector H_2S response was very weak compared to CH_4, as expected. However, there was a clear difference between the inlet and the outlet of the reactor.

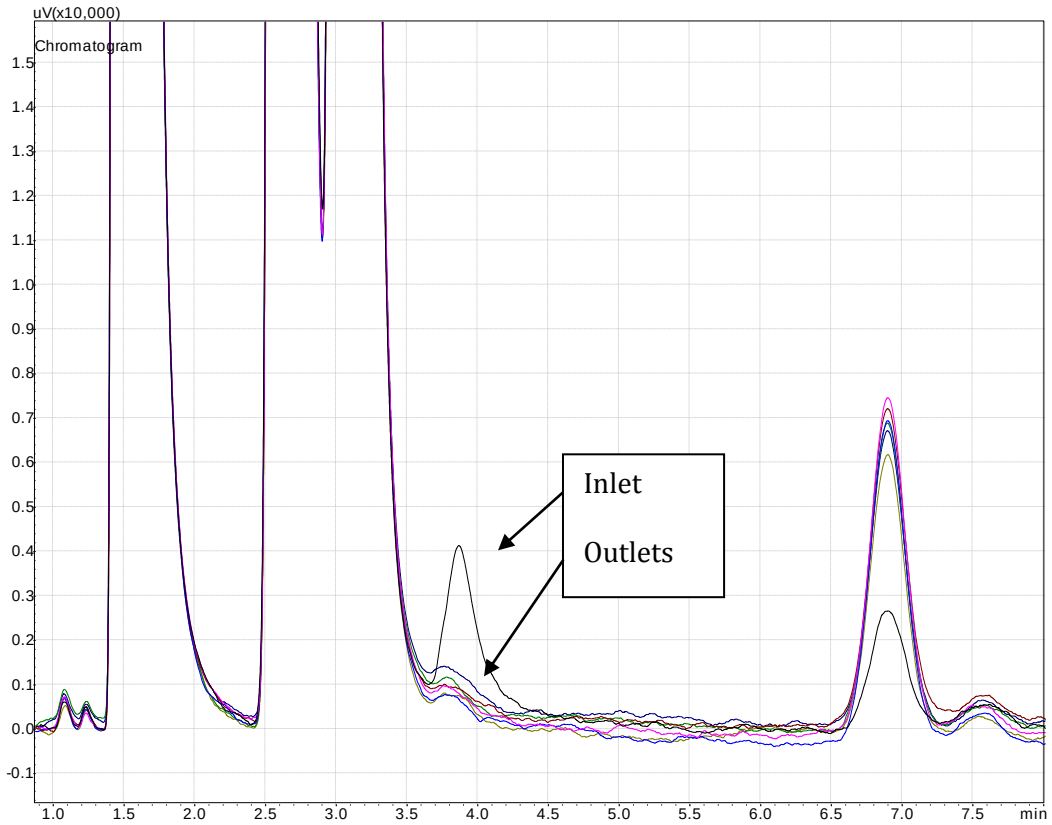

Figure 9.5: The detection of H_2S on the inlet and outlet of the desulphurization reactor. The peak is at 3.8 minutes.

5. Main experimental programme: Factorial design

The desulphurization experiment was performed under eight different conditions by using two levels (high and low) of temperature, sorbent particle size and gas flowrate. Each experiment under a specific condition was repeated giving a total of 16 results. The actual conditions used have been given in Table 9.5.

Table 9.5: High and low levels for temperature, particle size and flowrate

	Low	**High**
Temperature	346 °C	550 °C
Particle size	1 mm	1.4 mm
Total feed flowrate	1.051 $g.min^{-1}$	1.519 $g.min^{-1}$

The other process conditions have been given in Table 9.6. Note that the high flowrate was 1.44 times greater than the low flowrate. In addition, the conditions listed in Table 9.6 were the same for both high and low levels of temperature and particle size.

The measured or calculated variables for the experiment have been given in Table 9.7. the superficial velocity was found by using the ideal gas law to calculate the flowrate at the

reaction temperature (from the measured flowrate at room temperature) and dividing by the cross sectional area of the reactor. The molar flow of H_2S was assumed to be equal to the molar flow of *i*-propanethiol. The total concentration was found from the ideal gas law and the mole fraction of H_2S by dividing the H_2S concentration by the total concentration.

Table 9.6: Process conditions for factorial design

		Low flow	**High Flow (=1.44×low)**
Mass fraction methanol	[-]	0.86	0.86
Setting on pump	rpm	18	26
Flow methanol	$g.min^{-1}$	0.8542	1.2339
Flow *i*-propanethiol (= flow H_2S)	$g.min^{-1}$	0.1391	0.2009
Setting on controller	SLPM	0.044	0.064
Flow oxygen	$g.min^{-1}$	0.0576	0.0838
Flow syngas (STP)	$cm^3.min^{-1}$	667.25	955.57
Space velocity (STP)	hr^{-1}	2002	2867
Mass sorbent	g	30	30
Expected conversion after 120 min	%	55	80

Table 9.7: Conditions for factorial design experiments. Note that the particle size did not affect the values calculated below.

		Low flow		**High flow**	
		High temperature	**Low temperature**	**High temperature**	**Low temperature**
Pressure	bar	1.03	1.03	1.03	1.03
Temperature	°C	550	346	550	346
Total flowrate (at temperature)	$cm^3.min^{-1}$	1987	1498	2845	2145
Superficial velocity	$cm.min^{-1}$	332	250	476	359
Molar flow of H_2S	$mol.min^{-1}$	1.826×10^{-3}	1.826×10^{-3}	2.637×10^{-3}	2.637×10^{-3}
Concentration H_2S	$mol.cm^{-3}$	9.189×10^{-7}	1.219×10^{-7}	9.268×10^{-7}	1.229×10^{-6}
Total concentration	$mol.cm^{-3}$	1.524×10^{-5}	2.021×10^{-5}	1.524×10^{-5}	2.021×10^{-5}
Mole fraction H_2S	mole %	6.03	6.03	6.03	6.03

The conditions for each are summarized in Table 9.8. Also in this table are the conversions of the sorbent. It can be seen that there was some variation between the repeated runs.

Note that the 'Run Numbers' in the first column of Table 9.8 will be used as references in Figures 9.7, 9.8 and 9.9.

Table 9.8: Conversion results of ZnO to ZnS for factorial design

Run Number	Factor			Conversion 1	Conversion 2	Conversion Average
	A	B	C			
	Temper-ature	Particle Size	Flowrate	%	%	%
1 and 9	Low	Low	Low	2.2284	3.3365	2.7824
2 and 10	High	Low	Low	2.7410	3.6631	3.2021
3 and 11	Low	High	Low	2.0578	3.8925	2.9751
4 and 12	High	High	Low	4.1516	4.2713	4.2114
5 and 13	Low	Low	High	8.5336	10.2785	9.4061
6 and 14	High	Low	High	10.0610	10.3671	10.2141
7 and 15	Low	High	High	12.2085	9.8895	11.0490
8 and 16	High	High	High	9.2727	10.3562	9.8145

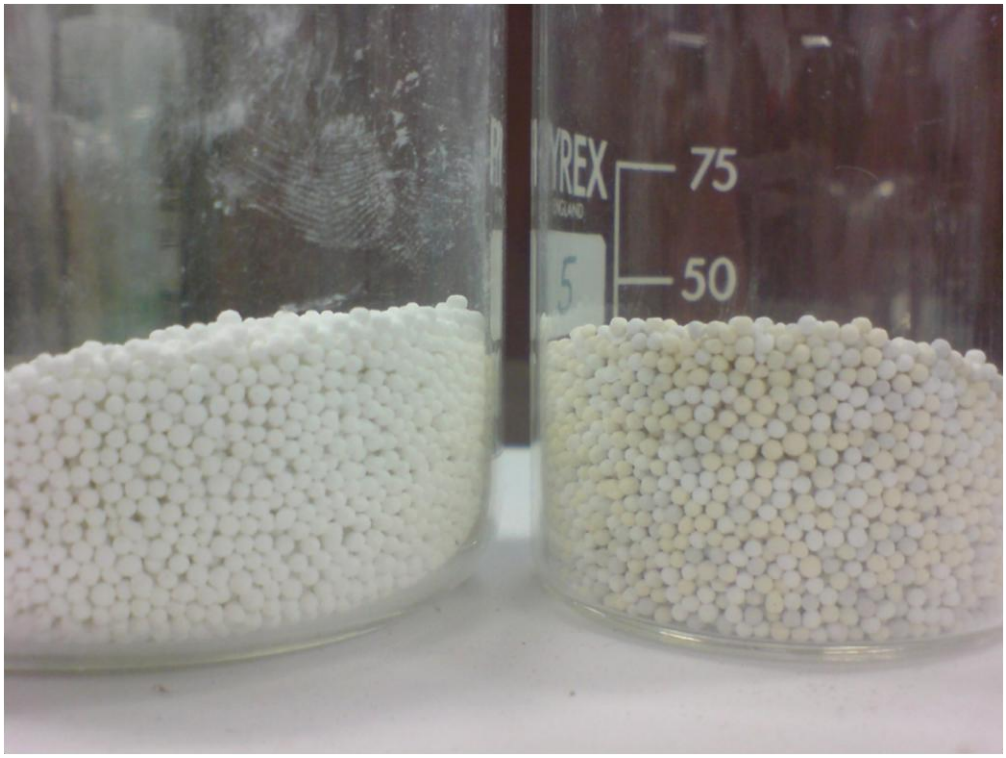

Figure 9.6: 1 mm diameter sorbent before reaction (white particles) and after reaction (white and pale yellow particles).

5.1 Desulphurization reactor temperature

Figures 9.7 and 9.8 show the variation in desulphurization reactor temperature over all experiments. There was a small increase in temperature before a gradual decrease. They show very good consistency under all conditions.

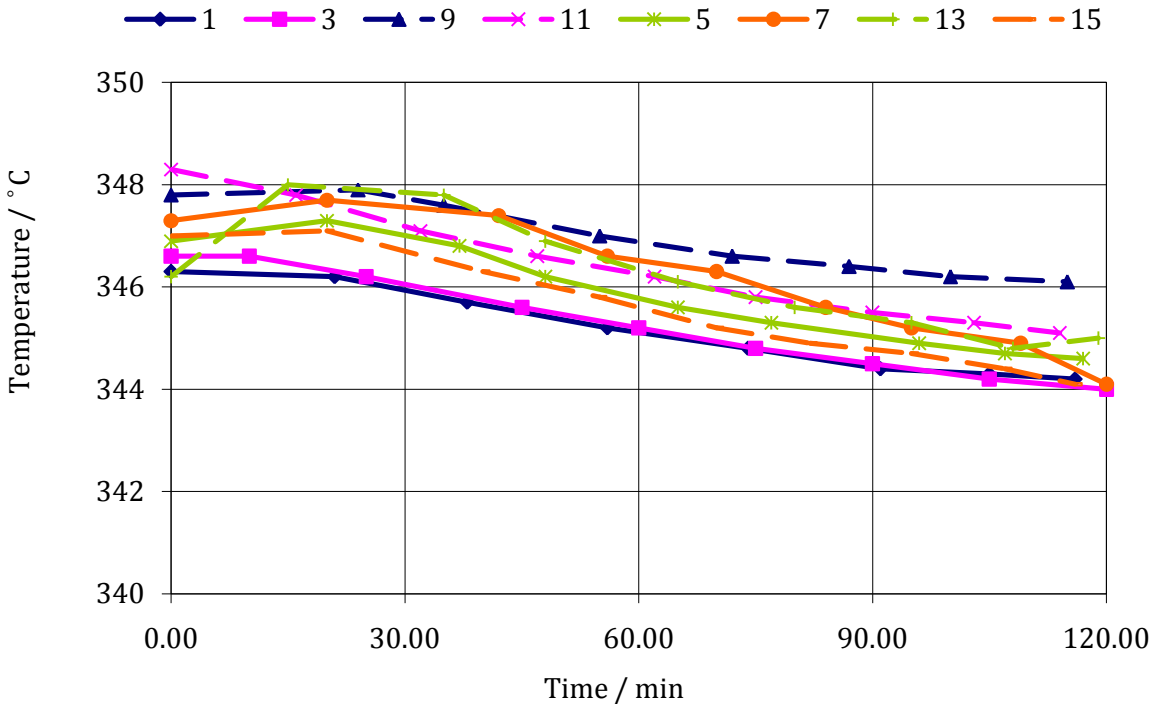

Figure 9.7: Temperature in desulphurization reactor at low temperature. Note that the dashed lines of the same colour were the repeated readings.

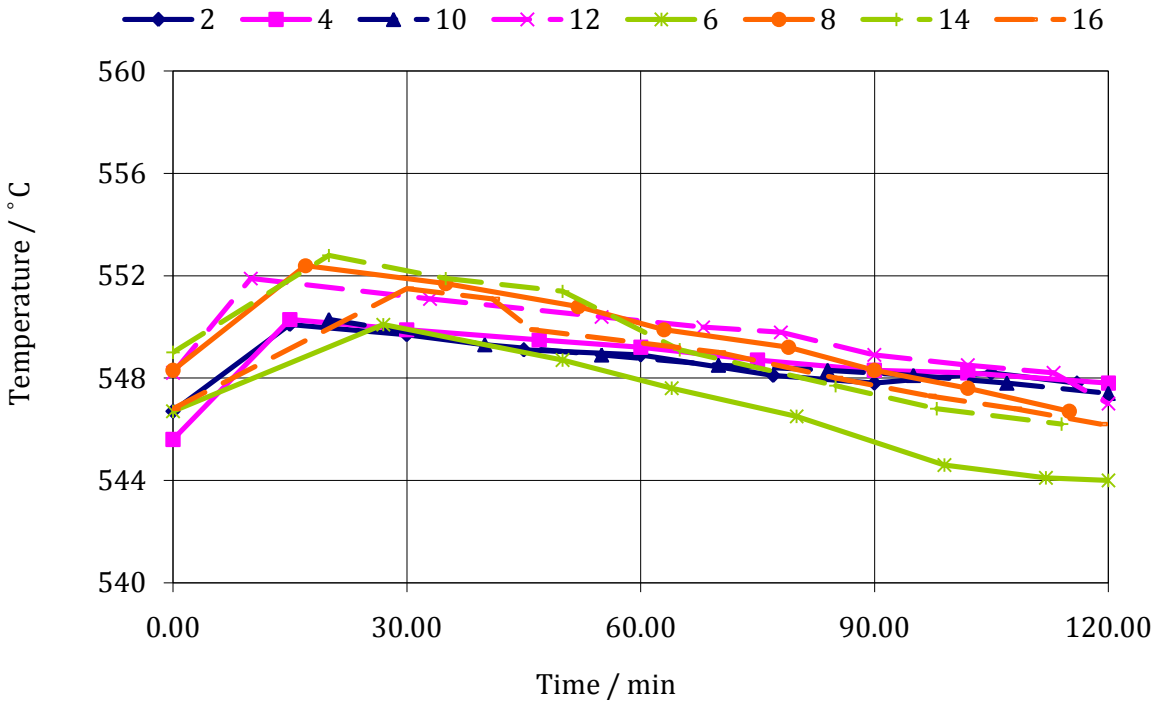

Figure 9.8: Temperature in desulphurization reactor at high temperature. Note that the dashed lines of the same colour were the repeated readings.

5.2 Methane composition in syngas

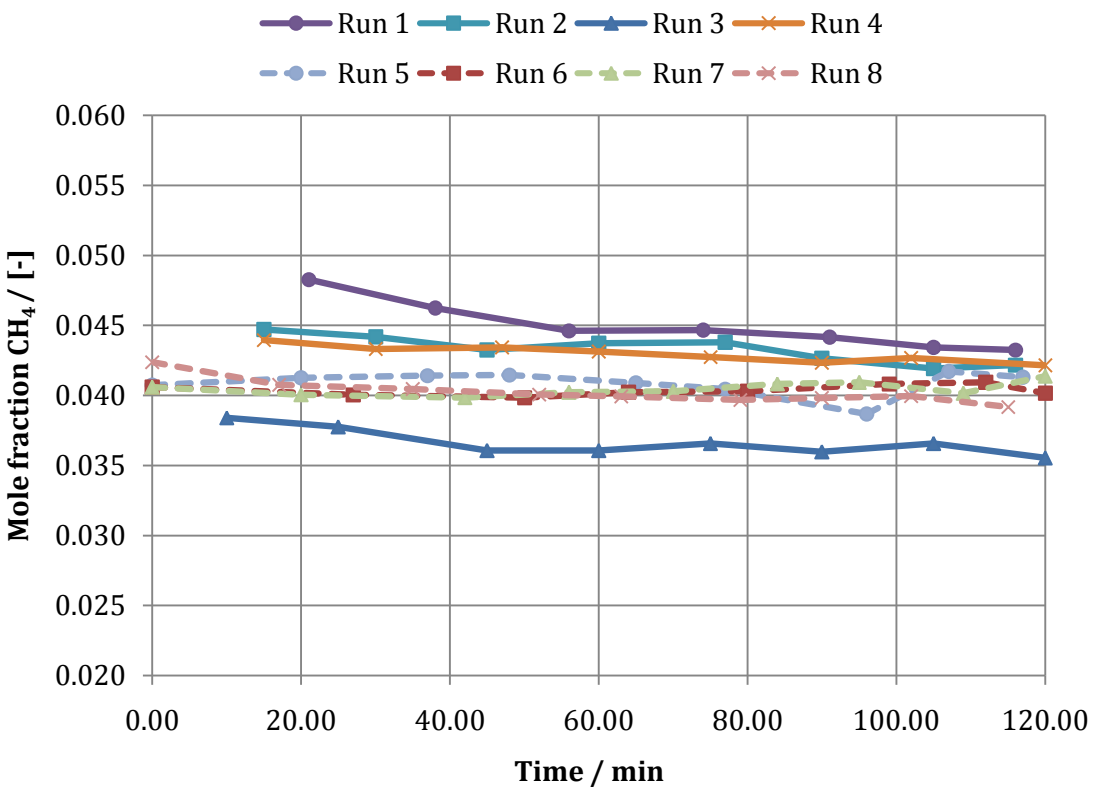

Figure 9.9: Mole fraction of methane over course of experiments. Dotted lines were the higher flowrates and the dashed lines correspond to the low flowrates.

It is important to note that there was very little variation in the gas composition over each experiment. Secondly, there was little variation in the gas composition over all the experiments. This was especially the case with the higher gas flowrate.

The notable exception in Figure 9.9 was Run 3. This was lower than the other runs, although constant throughout the experiment. A possible explanation for this was that the fuel composition was slightly different causing a change in the gas composition.

5.3 Scanning Electron Microscope Images

The images in Figures 9.11 and 9.12 were taken at the Electron Microscope Unit at the University of KwaZulu-Natal. Figure 9.11 was typical of zinc oxide and resembled other images previously published, for example, Lew *et al*. (1992 a). Figure 9.12 shows the extent of reaction, with a clearly defined ash layer and unreacted core.

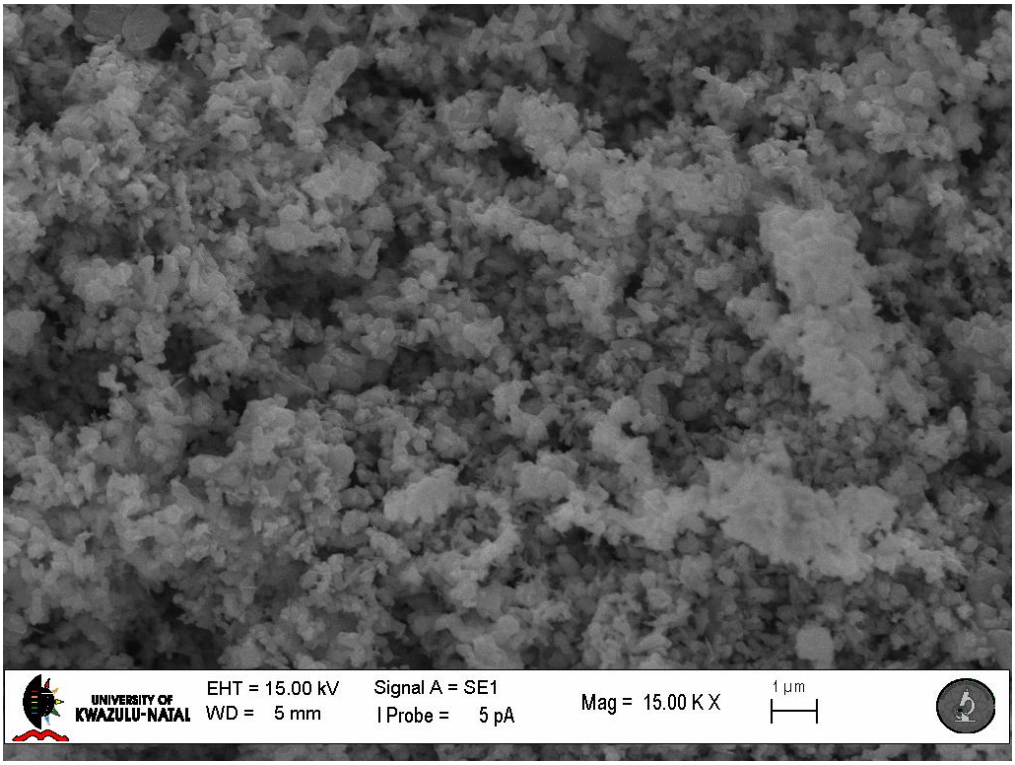

Figure 9.10: Unreacted zinc oxide surface at 15 000 X magnification. The small non-porous grains are clearly visible.

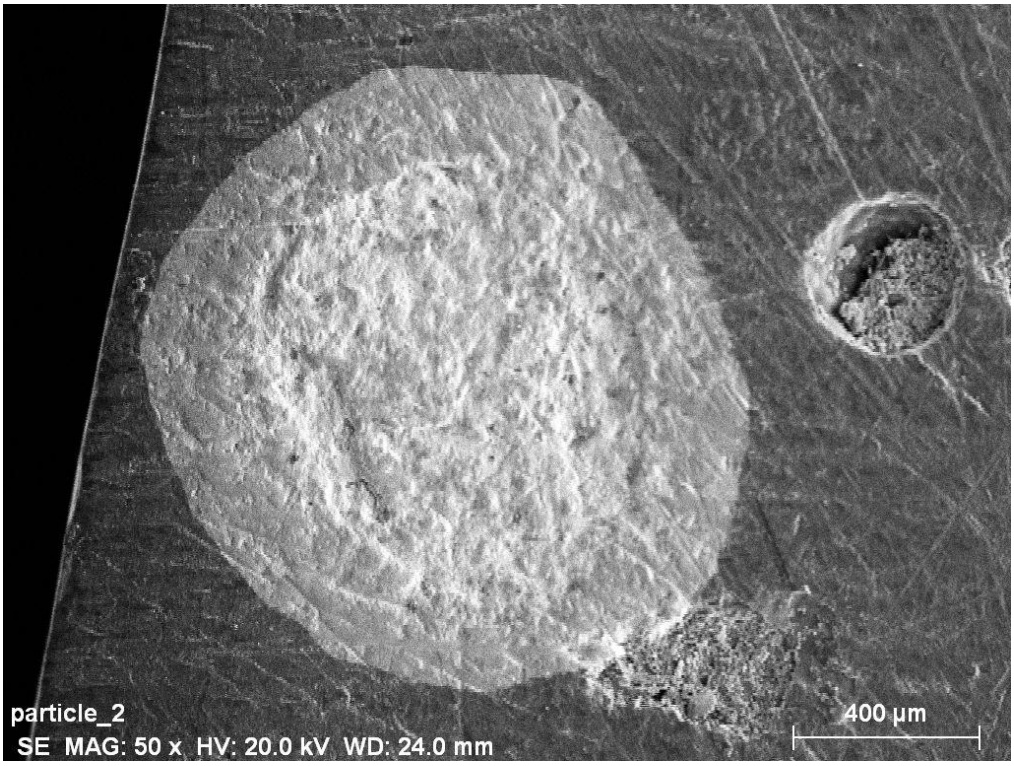

Figure 9.11: Cross section of partially reacted zinc oxide pellet at 50 X magnification. Note the clear difference between an outer product 'ash' shell and the unreacted core.

6. Modelling the gas-solid reaction

6.1 Evaluation of process parameters

The parameters given in Table 9.9 were all required to use the packed bed reactor model given in Chapter 5. The source of the values used has also been included.

Table 9.9: Typical process parameters for evaluation of the packed bed reactor model

Parameter	Symbol	Value	Unit	Source
Reactor conditions				
Temperature	T	550	°C	set
Pressure	P	1.01325	bar	set
Gas constant	R_g	8.314	J.mol^{-1}.K^{-1}	[-]
Gas flowrate STP	Q_{STP}	1.60×10^{-5}	m^3.s^{-1}	measured
Gas flowrate	Q	4.82×10^{-5}	m^3.s^{-1}	measured
Molar flowrate H_2S	n_{H_2S}	4.40×10^{-5}	mol.s^{-1}	set
Mass sorbent	m	30	g	set
Volume sorbent	V	2.00×10^{-5}	m^3	$=m/\rho_p$
Time of reaction	t	120	min	set
Reaction				
Stoichiometric coefficient	ν	1	[-]	reaction
Frequency factor	k_0	0.012	m.s^{-1}	Westmoreland *et al*. (1977)
Activation energy	E	30 300	J.mol^{-1}	Westmoreland *et al*. (1977)
Rate constant	k_s	1.43×10^{-4}	m.s^{-1}	Calculated from rate data
Initial bulk gas concentration	C_{Ab}^o	9.11×10^{-1}	mol.m^{-3}	$=n_{H_2S}/Q$
Particle properties				
Molar mass sorbent	M_B	81.390	g.mol^{-1}	[-]
Particle density	ρ_p	1.50×10^6	g.m^{-3}	measured
Crystalline density	ρ_C	5.60×10^6	g.m^{-3}	Perry and Green (1999)
Particle radius	R	0.0005	m	measured
Bed porosity	ε_b	0.29	[-]	$=1-\rho_B/\rho_p$
Solid concentration	C_B^o	68804	mol.m^{-3}	$=\rho_C/M_B$
Reactor properties				
Diameter reactor	D	0.026	m	set
Cross sectional area	S	5.31×10^{-4}	m^2	set

Parameter	Symbol	Value	Unit	Source
Superficial velocity	u	0.15	m.s^{-1}	$=Q/S$
Bed density	ρ_B	1.07×10^{6}	g.m^{-3}	measured
Length of bed	z	0.053	m	$=m/\rho_B S$
Model parameters				
Dimensionless time	t^*	0.102	[-]	From model
Dimensionless distance	z^*	0.443	[-]	From model

6.2 Evaluation of mass transfer and diffusion coefficient

For the evaluation of the diffusion coefficient in the product layer, values from previous researchers were looked at for a reasonable estimate. Particle size and rate constants are included for comparison. Note that D_e is the diffusion of H_2S through the product ash layer. The parameters used have been given below.

Table 9.10: Values for parameters in packed bed reactor model

D_e	m^2.s^{-1}	1.5×10^{-6}	typical value, from Chapter 4.
k_s	m.s^{-1}	1.43×10^{-4}	Westmoreland *et al*. (1977)
k_g	m.s^{-1}	0.004	Jothimurugesan and Harrison (1990)
R	mm	0.5	experiment
φ	[-]	0.535	calculated

6.3 Solution of packed bed reactor model

Figure 9.12 gives the conversion as a function of dimensionless time and dimensionless distance. The shrinking core model was used to describe the reaction in the sorbent particle.

In the shrinking core packed bed model, the only parameters required are z^*, t^* and then R, k_s, k_g and D_e for evaluation of φ.

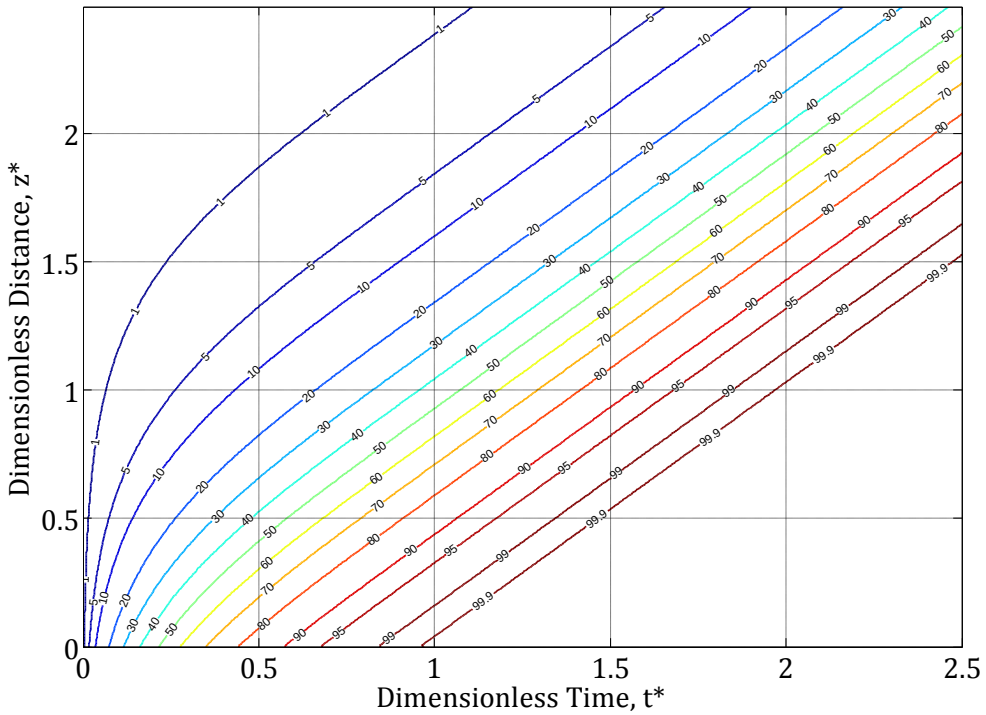

Figure 9.12: Solution of packed bed reactor model with shrinking core model. The contour lines represent conversion of sorbent. Parameters: k_s = 1.43×10^{-4} m.s^{-1}, k_g = 0.004 m.s^{-1}, D_e = 1.5×10^{-6} m^2.s^{-1} and φ = 0.5.

$$t^* = \frac{bk_s C_{Ab}}{\rho_p R} t \tag{9.3}$$

$$z^* = \frac{(1-\varepsilon_b) k_s C_B^o}{u \rho_p R} z \tag{9.4}$$

$$\varphi^2 = \frac{3Rk_s}{D_e} \tag{9.5}$$

b	stoichiometric coefficient of gas species A reacting	[-]
ε_b	porosity of the bed	[-]
ρ_p	molar particle density	[mol.m^{-3}]
R	radius of spherical particle	[m]
u	superficial gas velocity	[m.s^{-1}]
C_{Ab}	concentration of gaseous reactant A in bulk gas stream	[mol.m^{-3}]
C_B^o	concentration of solid reactant B initially	[mol.m^{-3}]
k_s	surface reaction rate constant	[m.s^{-1}]
k_g	mass transfer coefficient	[m.s^{-1}]
D_e	effective diffusion coefficient	[m^2.s^{-1}]
t	time of reaction	[s]
z	bed length	[m]

7. Validation of process models

7.1 Equilibrium model for syngas composition gas flowrate

There were two measurements that could be used from the experiment to compare to the equilibrium model for syngas composition and gas flowrate: the methane mole fraction and the gas flowrate. Since the same composition was used for all the experiments, the methane composition should be the same.

The gas flowrate would depend upon the high or low level used for the feed. The low flowrate runs were 1-4 and the high flowrate runs were 5-8.

Table 9.11: Average mole % CH_4 and syngas flowrate (during an experiment) for each experiment

Run	Mole % CH_4 / mol %			Syngas flowrate / $cm^3.s^{-1}$ (STP)		
	Experiment	**Model**	**Absolute difference**	**Experiment**	**Model**	**Absolute difference**
1	4.49	1.81	2.68	9.55	10.54	0.99
2	4.33	1.81	2.52	9.98	10.54	0.56
3	3.66	1.81	1.85	13.32	10.54	2.78
4	4.30	1.81	2.49	10.83	10.54	0.29
5	4.09	1.81	2.28	14.11	15.23	1.12
6	3.89	1.81	2.08	16.81	15.23	1.58
7	4.05	1.81	2.24	17.10	15.23	1.87
8	4.02	1.81	2.21	16.83	15.23	1.60

7.2 Packed bed reactor model

The packed bed model was used by calculating z^* and t^* for each experimental run condition. By interpolating the results of Figure 9.12, the conversion was found. Note this interpolation was performed in MATLAB using all the data points and not simply based upon the contour lines of Figure 9.12.

From the results in Table 9.12, there was some agreement with between the model and the experimental data. The maximum absolute difference was 7.4 %, although most differences were below 3.0 %.

Table 9.12: Model results compared to experiment

Run	Temperature	Particle Size	Flowrate	z^*	t^*	Model Conversion	Actual Conversion	Absolute Difference
				[-]	[-]	%	%	%
1	low	low	low	0.23	0.04	5.37	2.23	3.14
2	high	low	low	0.74	0.12	4.27	2.74	1.52
3	low	high	low	0.16	0.03	4.62	2.06	2.56
4	high	high	low	0.53	0.08	5.42	4.15	1.27
5	low	low	high	0.14	0.03	6.00	8.53	2.53
6	high	low	high	0.44	0.10	8.40	10.06	1.66
7	low	high	high	0.10	0.02	4.80	12.21	7.41
8	high	high	high	0.32	0.07	8.43	9.27	0.85
9	low	low	low	0.23	0.04	5.37	3.34	2.03
10	high	low	low	0.74	0.12	4.27	3.66	0.60
11	low	high	low	0.16	0.03	4.62	3.89	0.73
12	high	high	low	0.53	0.08	5.42	4.27	1.15
13	low	low	high	0.14	0.03	6.00	10.28	4.28
14	high	low	high	0.44	0.10	8.40	10.37	1.97
15	low	high	high	0.10	0.02	4.80	9.89	5.09
16	high	high	high	0.32	0.07	8.43	10.36	1.93

Chapter 10

Discussion

1. Introduction

The primary aim of this study was to develop apparatus to conduct experiments on the high temperature H_2S removal from syngas. This aim was achieved and the focus of this discussion will be upon the main findings of the study along with a critical analysis of the equipment, the experimental procedure and the results obtained. Through this analysis, both the strengths of the study and conclusions drawn will be highlighted. Since this is the first project in this field of chemical engineering at the School, there will of course be areas for future improvement.

2. Experimental equipment

2.1 General equipment performance and achievements

The equipment functioned very well. The design aspects have been covered and discussed in Chapters 8 and 9. After conducting the experiments, there were many achievements associated with the equipment design and operation, as detailed below.

To the author's best knowledge, this is the first apparatus in hot gas desulphurization (HGD) studies to use pure *liquid* hydrocarbons as a fuel source for gasification. As mentioned in Chapter 7, Section 2, the use of liquids had some practical advantages (flow control, composition control) and the study gave an opportunity to evaluate the method's effectiveness as a laboratory technique for gasification processes.

The industrial representation of a typical gas treatment process was successfully replicated on a laboratory scale, by having both gasification and desulphurization units operating in series. Perhaps of primary significance was the equipment's relatively large size. The desulphurization reactor had an internal diameter of 27 mm and used a sorbent mass of 30 g. Most of the studies in the literature had diameters of 10 mm or less with a sorbent mass of 1-3 g, as detailed in Chapter 3, Table 3.2.

In addition, almost all the studies used synthetic gas compositions, created by mixing pure gases from cylinders. With this study, the syngas with H_2S for desulphurization was created consistently and easily by gasification of the hydrocarbon liquid mixture.

The entire apparatus was able to operate at stable temperature setpoints, which was highly desirable in order to maintain constant gas composition. Once the apparatus had heated up, it remained at its steady state temperatures. The gasifier did take some time (30 minutes) to respond and to reach the new steady state. However, this form of operation was not necessary as the setpoints would not be changed during the course of an experiment.

An important part of the design was that apparatus was remarkably simple to operate. The most complicated part was loading and unloading the sorbent from the reactor and using the bubble flowmeter to make a gas flow reading.

In addition, the design allowed for a significant operating *range* available for different experiments. The gasifier could have a temperature from 700 °C to 900 °C. Lower temperatures than 700 °C should not be used since the methanol was not completely reacted; the methanol was detected by the GC when the lower temperatures were used (this result was not included).

In terms of pressure, if a back pressure valve/regulator was installed, higher pressures of up to 5 bar could easily be obtained. Both the peristaltic pump and the mass flow controller would operate under 5 bar pressure. Obviously leak detection of the fittings around the desulphurization reactor would have to be rigorous.

The gas composition could be changed simply by changing the fuel mixture. The equilibrium model developed for predicting syngas composition could be used as a guideline. Combinations of methanol, water, other alkanes and mercaptans could be used as fuel mixtures. The success of the equilibrium model will be discussed in Section 5. In this study, oxygen was used as the oxidising agent for gasification, but air could very easily be used by simply changing the gas cylinder.

2.2 Establishing a breakthrough curve

The detection of H_2S by the FID detector on the GC was achieved. The main outcome here was that a higher H_2S concentration on the reactor inlet was observed and a marked reduction in concentration was observed at the outlet. This was shown clearly in Figure 9.5. However, the detector was not ideal and it was determined that it had a lower limit of about 0.1 mol %, as calculated in the Appendix, Section A.4.

The breakthrough curve of (typical) industrial interest is in the range 0-500 ppm, with a limit of 50-100 ppm to define the breakthrough point. With the use of FID, perhaps the 'end' of the breakthrough curve could be found, as shown by the blue line in Figure 10.1. However, the region of interest for this gas-solid reaction has been given by the red line, and as shown it was a very small part of the breakthrough curve.

The time frame for breakthrough could correspond to the mass balance designed for the conversion of sorbent. Here, it was a theoretical sorbent conversion of 55 – 80 %. This conversion did not *guarantee* breakthrough of the gas from the bed. Rather, this theoretical conversion was used as a point to fix the experiment time for investigation of process conditions. This is explained in more detail in Section 4.3.

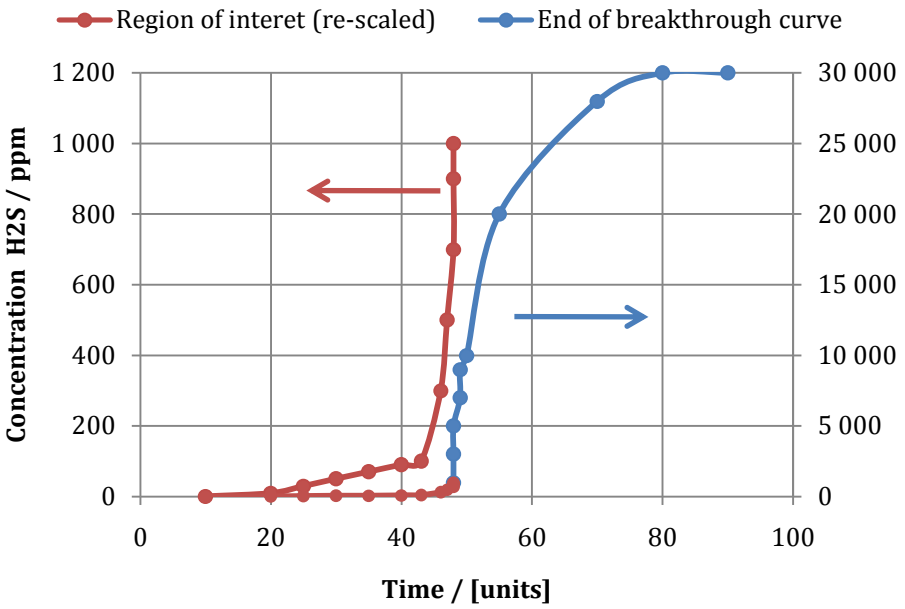

Figure 10.1: Illustration of breakthrough curves, with initial H_2S concentration of 3 mole %.

Since completing the experiments, an FPD (flame photometric detector) has been ordered and will be installed. This would detect H_2S from 10 000 ppm to about 200 ppb, i.e. the red line in Figure 10.1. The experiment could continue without a fixed time to ensure breakthrough was detected.

2.3 Establishing a stable gas composition

There were some aspects of the equipment where careful design and engineering was needed. The first of these was to ensure a stable gas composition.

The apparatus had two fuel tanks, each having different chemical compositions (one with sulphur, the other was pure methanol). This was to prevent excessive use of the mercaptan mixture during start-up and shutdown and to allow for cleaning the system. A small difference in the *fuel* composition could make a large difference to the *gas* composition, especially with respect to the H_2S concentration. The feed was vapourized to ensure that good mixing with oxygen could occur in the gas phase before entering the gasifier.

The feed was adequately vaporized by wrapping the feed lines around the gasifier. This method introduced a lag time between the fuel tanks and the mixing point. Since the flowrate was about 1 $cm^3.min^{-1}$, it took about 6 minutes for the fuel to be pumped into the gasifier. Thus, a recommended modification would be to minimize the length of these pipes and

vaporize the liquid using electrical heating. Note that this lag time was not a problem; it should simply be kept in mind when looking at the feed flowrates.

2.4 Gas sampling for GC analysis

Heating lines were employed for the GC sample lines to maintain a temperature greater than 100 °C, to prevent water condensation from the syngas in the sample lines. The gas sample temperature and gas volume must be known for the composition calculations. This calculation was described in Chapter 9, Section 2. The water must be in the gas phase for correct representation of the overall gas concentration. Once the sample was taken, further heating was not required.

There were some limitations on the valves. The three 3-way valves operated at about 120-160 °C. The manufactures recommended maximum temperatures of 85 °C due to the material of the seals in the valves. During the course of the experiments, the line pressure increased from 3 kPa to 12 kPa and this may be attributed to blockages in the valves caused by either some kind of deposits or damage to the seals.

2.5 Carbon deposits

The deposits, shown on the sorbent in Figure 9.2, were due to the gasification step. With any form of high temperature reaction involving hydrocarbons, small deposits of carbon could be expected. The desulphurization reactor was modified to incorporate a bed of 4 mm glass beads to act as a filter before the sorbent. The deposits would most likely be in the first valve due to the gas passing through a filter of glass beads before reaching the subsequent valves. The issue of carbon deposits will be discussed in Section 4. It was hence recommended to replace these valves with ones more suited to the conditions.

2.6 Flowrate measurement

The bubble flowmeter on the gas exit line was useful but required improvement for more accurate readings. While it gave readings of about 12-20 $cm^3.s^{-1}$, the error of up to 1-2 $cm^3.s^{-1}$ was significant. The error was due to the difficulty in reading, relying on the operator's judgement. An improvement would be to source a flowmeter with a large diameter (with total volume, say, 200 cm^3 instead of the 50 cm^3) or use a universal gas flowmeter instrument.

The flowrate measured was on a 'water free' basis since the gas passed through the gas bubbler before the flowmeter. This meant that the gas would have some degree of saturation with water due to bubbling it through 2 cm height of water. This was assumed to be very small as there was no visible further condensation on the outlet pipes.

Despite removing the water, the flowrate reading is still fairly accurate, since the amount of water collected throughout the experiment in the bubbler was very small, typically less than

10 cm^3, over the course of 2 hours (~0.1 $cm^3.min^{-1}$). This was expected, as the Equilibrium Model gave a composition of 1.2 mole %, or approximately 0.01 $cm^3.min^{-1}$.

The water flow was, however, never measured to a high degree of accuracy and hence is a recommendation for further apparatus improvement. As a direct result, the Degree of Freedom analysis, in Chapter 7, Section 3, could not be implemented to solve for the remaining components (namely H_2, CO and CO_2) as the system was still underspecified by one variable.

2.7 Sulphur deposits

At one stage during equipment testing, there were noticeable deposits of sulphur on the outlet thermocouple from the desulphurization reactor. At this stage, the gas analyzer was being used and detected about 500 ppm SO_2. The explanation was that sulphur may have been forming via the Claus reaction: $2H_2S + SO_2 \rightarrow 3S + 2H_2O$. This indicated that there was an excess of oxygen available in the system (to enable the formation of SO_2). Hence the molar amount of oxygen fed into the system was reduced and the sulphur deposits were eliminated.

2.8 Industrial syngas

An interesting recommendation would be to connect and use a raw syngas mixture available in a cylinder from an industrial source (for example, from Sasol). This could be connected to the system directly for desulphurization experiments with the necessary gas flow control instrumentation.

Thus, it can be concluded that a novel gasification-desulphurization apparatus was successfully designed and constructed.

3. Experimental procedure

In general, there were no major procedural changes that occurred throughout the experiments; the procedure had been carefully planned. As noted, establishing a stable gas composition was imperative and much of the procedure was associated with this in mind.

Nitrogen was used to flush out the system to ensure that it was clean. The fuel tank with pure methanol was then reacted with oxygen in the gasifier to produce 'clean', H_2S free syngas. When the flowrate through the gasifier changed, this affected the gasifier's temperature and the time to re-establish the correct temperature could be up to 10 minutes. These temperature changes would affect the gas composition. Hence it was important to limit the changes to the flowrate, justifying the flow of H_2S free syngas prior to switching over to the other mercaptan-methanol fuel mixture and using the bypass line.

Perhaps only one fuel tank was necessary, whereby the bypass line for the desulphurization reactor was used. However, this would result in the significant use of the mercaptan, which

was relatively expensive (20 times the price of methanol) and for long time periods (about 1.5 hour extra per run). Nitrogen would then have been used to purge the system.

GC gas analysis took 10 minutes and hence gas samples were obviously limited to this time interval. The experiment had been designed to be 120 minutes long, which offered about 10 gas samples. It was hoped that this would provide a decent breakthrough curve. However, this was not possible due to the FID detector being out of range of the low H_2S concentration levels. Again, the 120 minutes was set from a mass balance to, ideally, achieve a conversion of 60-90% of the sorbent, as discussed further in Section 4.3.

The introduction of the 6 port valve, as designed, gave much improved results in terms of sampling consistency. Initially, using a gas syringe, it proved to be impossible to reproduce a gas sample taken from the system. The result of using the 6 port valve was shown in Figure A.6 and Table A.6, in the Appendix, with a coefficient of variation between the samples of 1 %.

In essence, full gas analysis required a very large capital expense and professional expertise. For a full discussion of H_2S detection and quantification methods, please refer to the Appendix, Section A.3 and A.4, including the reasons for choosing GC as a composition analysis method.

It must be highlighted that calculating the conversion of the sorbent depended (critically) upon the full recovery of sorbent from the reactor. The maximum error was estimated at 0.2 g per 30 g sample. With a maximum sorbent mass change of about 3 g, this was an error of 6.7 %. However, the loss from attrition was checked by simply loading and unloading the reactor and typically a loss of 0.1 g was found (results not included). This gave an minimum error of 3.3 %.

The analysis of the conversion of the sorbent under different conditions leads to the nature of the experimental programme. From an optimization point of view, finding the conditions that gave the highest conversion (while maintaining the outlet concentration of H_2S under the breakthrough limit) was desirable.

The experimental programme was designed to test the effect of three variables, namely temperature, particle size and flowrate. Obviously, the conversion results should differ by an amount greater than the experimental error of 3 % to be able to draw specific conclusions.

As an important part of the procedure, experiments were conducted in a random order to reduce the chance of a systematic error occurring. The statistical analysis aspects of the procedure will be discussed in lieu of the actual results obtained.

4. Discussion of results from experiments

4.1 Calibration of equipment

Calibration experiments were required for the flowrate of fuel from the peristaltic pump and the gas composition from the GC. All other readings could be taken directly. The calibration of the pump was straightforward and, as mentioned in the Appendix, Section A.5, could actually be modelled. The calibration of the GC for detecting CH_4 and H_2S was far more challenging.

The GC calibration has been discussed at length in the Appendix, Section A.4. The calibration for CH_4 was acceptable. The conclusion with respect to H_2S was that an accurate quantification of a peak area into a concentration value was unfortunately not possible.

After tuning, the gasifier temperature control was very good, as seen in Figure 9.1. It was important to maintain an isothermal gasifier since the composition of the syngas was a function of temperature and it had to remain constant throughout the desulphurization experiment time. In general, the gasifier temperature fluctuated periodically by 1 °C.

4.2 Initial experiments

From the first set of experiments, it became apparent that certain modifications to the apparatus were necessary. This was part of the purpose of the experiments: to identify and correct any problematic areas.

The preliminary results provide interesting reading, in particular, the conversions of the sorbent. These ranged from 9.56 % (small pellets, low temperature) to 61.82 % (large pellets, high temperature). The surprising result was that the smaller pellets had lower conversions, which was contrary to the reactor theory, as given in Chapter 4. Smaller particles have a larger surface area to volume ratio and hence there would be more surface area available for reaction.

These conversion results, however, have been compromised by a layer of carbon deposit that formed on the particle. This is evident by the dark particles shown in Figure 9.2. The result of the carbon deposit was that the mass measured obviously included the mass of carbon. The amount of carbon would be very difficult to quantify. Hence the true conversion from ZnO to ZnS would be less than that calculated.

To ensure that this was not, in fact, the true reaction product, an experiment was performed with a gas mixture of 4.18 mol % H_2S in N_2, free from carbon based compounds. The result was that the white ZnO was converted to a pale yellow ZnS, as shown in Figure 9.3. It would not be possible to form other compounds since the only species present are ZnO, ZnS, H_2S, H_2O and N_2.

The carbon could either be 'soot' (residue from incomplete reaction in the gasifier), or it could be formed, for example, by the reverse Boudouard reaction: $C + CO_2 \leftrightarrow 2CO$. The exploration of these possibilities was outside the scope of the study.

The soot formation could be due to the specific fuel composition being fed to the gasifier. Li *et al.* (2001) published a very useful ternary diagram of the C-H-O system at equilibrium with the carbon formation boundary, as a function of temperature. Although the experiments were conducted at compositions and temperatures outside the carbon formation range, the formation could still be possible due to the axial temperature variations in the gasifier.

In this study, it was not desirable to have carbon deposits and hence a filter of glass beads was introduced. These worked well to 'trap' the carbon before the gas flowed into the sorbent bed. The beads were 4 mm silica glass, hence inert, and generally formed a 10 cm bed. The glass beads had to be replaced every 3 runs.

The effect of temperature, whereby larger conversions were obtained at higher temperatures, could be explained due to the reaction rate constant: simply the reaction *rate* is higher at higher temperatures. Since the reaction was not equilibrium limited (the equilibrium constant is very large, 2.71×10^4 at 550 °C), and heat effects are small (the reaction is very mildly exothermic, $\Delta H°_{rxn}$ = -106.1 kJ.mol^{-1}), one can conclude that increasing the temperature would certainly increase the reaction rate. The rate constant increased almost tenfold from 0.0167 to 0.1334 cm.min^{-1} from 346 to 550 °C, based upon data from Lew *et al.* (1992 a).

The last finding from the initial tests was that it was difficult to recover all of the smaller particles (0.5 mm diameter) from the reactor. During the experiments, there was minor loss of sorbent through attrition as it turned into a powder. This was estimated at 0.5 g for the small particles. For future tests, 1 mm is recommended as the smallest particle size, unless the sorbent type is changed.

Now that many of the initial problems had been identified and rectified, the final aim of the study was a detailed experimental programme to test the performance of the unit over a prolonged time period.

4.3 Main experimental work

4.3.1 Experimental conditions

During this main programme, the effect of temperature, particle size and flowrate upon sorbent conversion was investigated. The first decision was to select the range of the process variables over which the experiment could be performed. For temperature, the range of 350-550 °C was selected since below 350 °C the temperature would be too low for the process and above 550 °C, the ZnO starts to become unstable, with the vaporization of Zn occurring from 600 °C.

Particle size was determined by the type of sorbent. Sizes of 1 mm and 1.4 mm were used. There was some distribution amongst these fractions, i.e. every pellet was not exactly 1 mm. As mentioned, a minimum diameter of 1 mm was recommended for this sorbent.

For the flowrate, careful thought was required. With a higher gas flow, breakthrough of the gas would occur earlier and there would be an associated conversion of the sorbent. This could *not* be compared directly to conversion at lower flowrates as the sorbent has not been exposed to the same amount of H_2S flowing past it.

The flowrate affects the mass transfer resistance of the H_2S into the pellet and hence could have an effect on the overall reaction rate. In order for a more useful comparison of conversion at different flowrates, it was proposed to use a 'relative conversion', defined as the actual conversion (from experiment) divided by the theoretical conversion (if all the H_2S entering the reactor had reacted during the time of the experiment, from the mass balance). With a *constant* reaction time, the relative conversions values could be compared to one another and would give an indication of the better operating condition.

For this reason, the experiment was designed that under both flowrates, a maximum conversion of about 55 % and 80 % would be achieved for 120 minute operation. Note that the 60 % also gave a significant mass change of about 1.5 g for a 30 g sample. This mass balance was given in Table 9.6.

It must be re-iterated that the aim of this experimental programme was to investigate the effect of process variables on the *conversion* of the sorbent. Hence, the time of reaction had to be set. The breakthrough would not necessarily be guaranteed for this reaction time and it was of course part of experimentation to see if it would occur, despite the limitations of the FID detector.

In Table 9.7, an inlet concentration for H_2S of 6.03 mol % was calculated. The equilibrium model predicted a concentration of 2.03 mole %. The reason for the high value was probably due to the uncertainties with the measurement of the volumetric flowrate. Hence this value should certainly be treated with caution and has definite scope for improvement. As mentioned, the flowrate was measured on a water free basis, although this difference was considered negligible.

4.3.2 Sorbent conversion

The most interesting part of the results were the low conversions of 2-12 %. This was surprising since, firstly, higher conversions of up to 60 % had been obtained for the preliminary experiments and secondly, there had been ample time for reaction according to the mass balance.

From the results in Table 9.8, it can be seen that higher conversions were obtained at higher flowrates. This would simply be due to more H_2S being available to react with the sorbent during the experimental time.

One fact, that was characteristic to this reaction, is that the molar volume of the solid product, ZnS, was significantly larger than the reactant. ZnS has a crystalline molar density of 23.85 $cm^3.mol^{-1}$ compared to 14.88 $cm^3.mol^{-1}$ of ZnO, from Perry and Green (1999). The surface reaction of zinc oxide to suphide would result in the narrowing and blocking of pores due to the increase in molar volume. This would inhibit H_2S diffusion further into the pellet. In others words, there would be significant ash layer resistance to the reaction.

Furthermore, it could be seen by visual inspection that there was a large amount of ZnO that had not reacted – there were still many white particles, as seen in Figure 9.6. This supports the fact that low conversion was in fact a true result.

From Table 9.12, the packed bed model gave comparable results for the sorbent conversion to the measured results from the experiment. The model ranged from 4.27 % to 8.43 % and the differences to the experiment ranged from 0.60-7.41 %.

A conclusion that can be drawn was that there was a definite effect of temperature, particle size and flowrate. Due to the variation in reproducibility (with respect to sorbent conversion), the 'relative' conversion comparison was not implemented.

The GC work showed a definite drop in H_2S detection between the inlet and outlet of the reactor, as indicated by Figure 9.5. With only 2-12 % sorbent conversion, it would be expected that the inlet and outlet peaks would be very similar (since the H_2S has simply not reacted).

Another possibility was that less H_2S was formed in the gasifier than anticipated and it did in fact react. This would be an unlikely scenario as feed products were set to ensure a highly reducing atmosphere and the temperature was high enough to ensure complete gasification of the reactants.

The only way to resolve this inconsistency (of having low conversion of sorbent, while the gas analysis showing definite reaction) would be to improve both the analysis and the experimental procedure. The gas analysis was for more important. With a new GC detector, a proper breakthrough curve could be obtained along with an accurate value for the inlet concentration.

A closing remark concerning the obtained conversions is that these values were very likely the correct values. It was due to the complex nature of trying to reconcile both gas phase and solid phase analysis that provided cause to critically examine the results, as discussed above.

What was evident from the conversion results was the reproducibility of the experiments. There were variations of up to 2.3 % under the same experimental conditions. This could be acceptable if the all the conversion results were spread over a much larger range. Again, this is an area where there is scope for future improvement.

4.3.3 Gas composition

The positive aspect of the GC analysis was with respect to CH_4. The result of the CH_4 composition analysis was shown in Figure 9.9. There was stable CH_4 composition over the course of the entire experiment, with a fluctuation of less than 1 mol %.

Importantly, the results were consistent over *all* the experiments. In particular, the experiments with higher gas flowrates proved to be even more consistent, with fluctuations of less than 0.5 mole % throughout all experiments.

This was a major finding in the study: the establishment of a stable, reproducible syngas mixture from the gasification of liquids. Obviously it would have been desirable to detect other gases, notably H_2 and CO. However, due to the high sensitivity of the FID detector with CH_4, it could be concluded that the entire gas composition was constant.

This was further supported in that the concentrations of other species, notably C_2H_6, were constant. This was visibly evident by over-laying chromatograms and confirmed by checking that the actual peak area values were indeed very similar, as seen in Figure 9.5 and in the Appendix, Section A.4.

4.3.4 Reactor temperature

Figures 9.7 and 9.8 show the temperature profiles in the desulphurization reactor sorbent bed, for the high and low temperatures respectively. It must be noted that the thermocouple associated with the furnace temperature *controller* was placed on the outside wall of the reactor. This could not be changed, as it invalidated the manufacturer's warranty of furnace.

The difference between the setpoint of the furnace and the temperature reading of the thermocouple in the temperature bed was about between 3-5 °C depending upon the temperature. The need for temperature measurement *in* the bed was thus apparent.

For the low temperature experiments, the temperature in the bed decreased by about 2 °C over 120 minutes. In general, all the experiments were very consistent and within a maximum of 4 °C of each other.

From Figure 9.7 at high temperature, when the gas was switched from the bypass line to pass through the reactor, the temperature initially increased. This showed that with the hot gas flow, there was very good heat transfer between the gas and the sorbent. The increase was about 3-5 °C and only occurred with the experiments at 550 °C.

It could be argued that the maintaining of a constant reactor temperature was a success, due to very little fluctuations below 5 °C, bearing in mind that this was a flowing system. However, it could also be argued that it was not good enough. An obvious improvement would be to have the controller using the signal from the sorbent bed thermocouple, rather than the outside reactor wall.

4.4 Scanning electron microscope images

The Scanning Electron Microscope (SEM) images added an exciting dimension to the project. It was noted that literally weeks could be spent studying the reaction using these images, along with elemental analysis. However, this was simply outside the scope of this study.

The important result was that excellent images could be obtained and can provide very useful information, when required. This includes grain size and structure, an insight into pore structure, reaction evolution (from partially reacted particles) and element distribution within a particle. This allows for comparison with other published images and structural results presented in the literature.

Figure 9.10 shows the surface of unreacted ZnO. It can be clearly seen that the surface is in fact made up of small grains, with an average diameter 0.1-1.0 μm. It seems that there was a mixture of spheres and cylinders and quite a wide distribution of grain sizes. This highlighted the fact that the grain model would be most appropriate for gas-solid reaction modelling involving this sorbent.

The other image of Figure 9.11 shows a cross section of a partially reacted pellet. The image shows the reacted ash layer and an unreacted core. The uniformity of the ash layer suggests that the unreacted core model would be appropriate to use for single particle reaction modelling. This is detailed in the following section.

5. Modelling results and comparison

5.1 Equilibrium model for syngas composition and flowrate

The equilibrium model for the gasifier has been compared to experimental results in Table 9.11 for CH_4 composition and the volumetric flowrate.

The model gave an expected CH_4 mole percent of 1.81 mol %. Hence, the gasifier equilibrium model under-predicted the experiment by 1.85-2.68 mol % on an absolute basis. This was a very promising result.

The volumetric flowrate from the experiment did not agree as well as the methane composition, possible due to the uncertainty of the bubble flowmeter readings. Differences ranged from 0.29-2.78 $cm^3.s^{-1}$ (STP) between the model and experimental results. The encouraging result was that the model and experiment were certainly in range of each other.

5.2 Packed bed reactor model for sorbent conversion

The modelling solution procedure for sorbent conversion has been given in the Appendix, Section A.6. The model incorporated the shrinking core model for single particles and applied it to a packed bed of particles.

Table 9.9 shows all the process parameters required to evaluate the model and Table 9.12 displays the results along with the experimental conversions. The packed bed reactor model was also within the same range as the experiments. The differences ranged from 0.60-7.41 %. The model results showed interesting trends when evaluated with the experimental operating conditions, as detailed below.

With low values for particle size and flowrate as inputs for the model, increasing the temperature decreased conversion by 1.1 %. However, with particle size and flowrate at the higher values, increasing the temperature increased conversion from 4.8 to 8.4 %. Changing the temperature has an effect on the reaction rate constant, k_s, gas velocity, u, the bulk gas concentration and diffusion coefficient.

For the particle size, by decreasing the particle size, the model's conversion result was increased while at low temperature and flowrate. However, if the temperature was increased, the effect was reversed, and there was higher conversion with larger particles at the high temperature. The same trends were observed at the higher flowrate, with slightly higher conversions.

Lastly, for the different flowrates, it could be seen that in general higher conversions were obtained from the model at the higher flowrates. This was probably due to the increase in superficial gas velocity. A higher gas velocity, u, would decrease the value of z^* and according to the conversion relationships in Figure 9.12, in that range of z^*, the conversion would increase.

Perhaps the most remarkable result was that there was certainly interaction between the variables. For instance, decreasing the particle size does not necessarily result in a higher conversion, for example, at high temperature and low flowrate.

Since the conversion results from the model were in range of those in the experiment, this supports the argument that the reaction is controlled by diffusion through the ash layer. The shrinking core model cannot be applied to porous particles if the reaction rate is the limiting step. The reaction interface becomes diffused and the homogenous model is more applicable.

Here, despite having porous particles, the shrinking core provides reasonable agreement, indicating that the reaction is not controlled by the chemical reaction. Since ash diffusion is usually much more significant than gas film mass transfer, it suggests that it is indeed the controlling mechanism. In addition, the SEM image of Figure 9.11 clearly shows a uniform ash layer. While it was shown that the grain model can be applied to the packed bed, this has been left for future work.

The interesting result is that the model gives better agreement to the experimental data under the high temperature conditions. The difference (absolute) ranged from 0.60 – 1.97 % conversion, compared to 0.73 – 7.41 % conversion for the low temperatures. The explanation here is that perhaps the *values* of the model parameters (diffusion and mass transfer

coefficient, rate constant) have smaller errors (from estimation or correlations) at the higher temperature, and hence the values provide a better representation of the physical process.

Ideally, single particle experiments would be used, in the same reactor environment (temperature, pressure, gas composition and flowrate) to determine the kinetic parameters, diffusion coefficient and mass transfer coefficient, by the regression of a conversion-time profile to a particular gas-solid reaction model. Secondly, accurate measurements for the sorbent's physical properties (crystalline and particle density, porosity and grain size) would be made and applied to the packed bed model.

5.3 Statistical analysis

Since the conversion results from the experiment were, firstly, in a narrow range of 2-12 % and secondly had some variation in repeatability, they were not suited for a full statistical analysis to obtain the interaction effect parameters.

In addition, the error associated with the conversion was about 3 %. Hence, some of the results were too close to each other to discern a definite trend. Simultaneously, the fact that they are so close to each other is indeed a result. Ultimately, as mentioned, the repeatability of each experiment needs to be improved.

Should the experimental conditions be changed providing results in a much larger range, than this analysis would be appropriate, along with the simplex optimization experimental design, as discussed in Chapter 6. This would provide useful information such as the effect of operating conditions on sorbent conversion and breakthrough curve characteristics under these conditions that could be utilized for industrial gas-solid reactor design.

6. Final recommendations

From the discussion above, a number of recommendations have been made and these have been detailed below for ease of reference. They include useful further experiments.

- Installation and calibration of new FPD detector for the GC for low level H_2S measurement.
- Improvement to gas flow measurement.
- Replacement of 3 way valves with valves suitable for high temperature operation.
- Change of desulphurization reactor temperature controller thermocouple.
- Measurements of sorbent density, porosity, pore size distribution and surface area using specialist equipment.
- Further validation of equilibrium model using different fuel compositions and flowrates.
- Application of the grain model to the packed bed reactor model.
- Investigation of the effect of carbon deposits by removing the filter.

The last point of this discussion is to note that all the aims of the experimental work were achieved. The equipment worked, a procedure was developed and the results have been critically examined.

It is hoped that, with slightly more reproducible experimental results and the establishment of accurate breakthrough curves, more conclusions can be made as to the nature of this gas-solid reaction. These can be compared to other studies and applied to industry using the methods developed in this study.

Chapter 11

Conclusions

This study has successfully completed the design, construction of apparatus and development of a procedure to conduct experiments into Hot Gas Desulphurization (HDG). It was evident from the literature that HDG is an area of great engineering interest worldwide, with many other studies focussing on the development of new materials, equipment and processes for industrial application.

The conclusions from this study were:

- A new apparatus and method of syngas production for HGD, using liquid fuels for gasification was designed and constructed.

- The use of pure liquids for the laboratory production of syngas has not been implemented elsewhere. It was found that the liquid fuel feed gave a consistent syngas composition. This bypassed the need for a bank of gas cylinders and flow controllers and allowed for gasification to be included in the desulphurization experiments. This was more representative of a typical industrial process.

- The construction of the equipment had many challenges, including establishing isothermal conditions and gas analysis by GC. A FID detector was available which was calibrated for methane. It was able to detect hydrogen sulphide to about 0.1 mole %, although an actual calibration was unable to be satisfactorily completed. A new FPD detector has since been ordered for future studies.

- A factorial experimental design for determining the interaction effects of the variables was employed. This focussed upon the variation of temperature (346 and 550 °C), particle size (1.0 and 1.4 mm), and flowrate (1.051 and 1.519 $g.min^{-1}$) to ascertain the interaction effects upon conversion. There was some variation in the

repeated results. Hence, the full statistical analysis was not implemented. An optimization procedure was proposed and can be implemented in future studies.

- The conversion results of ZnO to ZnS ranged from 2-12 % by mole for the factorial design experiments.

- The equilibrium model of the gasifier gave good agreement (for syngas composition and flowrate) with the experimental results, while the model under-predicted the experiment by methane composition by 1.85-2.68 mol %.

- The packed bed reactor model (for sorbent conversion) gave promising results. Although it was based upon the shrinking core model, it can be extended to use the grain model. The difference between the model and the experiment ranged from 0.60-7.41 % for the sorbent conversion.

- Improvements to the apparatus and incorporating the new GC detector will allow further studies into this reaction and the possibly the use other sorbents for HGD.

References

Abbasian J, Bachta RP, Wangerow JR, Mojtahedi W and Salo K (1994). "Advanced High-pressure Bench-Scale Reactor for Testing with Hot Corrosive Gases", *Industrial and Engineering Chemistry Research*, **33 (1)**, 91-95

Alonso L, Palacios JM and Moliner R (2001). "The Performance of Some ZnO-Based Regenerable Sorbents in Hot Coal Gas Desulfurization Long-Term Tests Using Graphite as a Pore-Modifier Additive", *Energy & Fuels* , **15 (6)**, 1396-1402

Altafini CR, Wander PR and Barreto RM (2003). "Prediction of the working parameters of a wood waste gasifier through an equilibrium model", *Energy Conversion and Management*, **44**, 2763–2777

ASTM (2009 a) "ASTM D2420 - 07 Standard Test Method for Hydrogen Sulfide in Liquefied Petroleum (LP) Gases (Lead Acetate)", [online]. Available from: http://www.astm.org/Standards/D2420.htm, [Accessed 6 October 2009]

ASTM (2009 b) "ASTM D4323 – 84 (2009) Standard Test Method for Hydrogen Sulfide in the Atmosphere by Rate of Change of Reflectance", [online]. Available from: http://www.astm.org/Standards/D4323.htm, [Accessed 6 October 2009]

Bagajewicz MJ, Tamhankar SS, Flytzani-Stephanopoulos M and Gavalas GR (1988). "Hydrogen sulfide removal by supported vanadium oxide", *Environmental Science & Technology*, **22**, 467-470

Bu X, Ying Y, Ji X, Zhang C and Peng W (2007). "New development of zinc-based sorbents for hot gas desulfurization", *Fuel Processing Technology*, **88**, 143–147

Cal MP, Strickler BW and Lizzio AA (2000 a). "High temperature hydrogen sulfide adsorption on activated carbon I. Effects of gas composition and metal addition", *Carbon*, **38**, 1757–1765

Cal MP, Strickler BW and Lizzio AA and Gangwal SK (2000 b). "High temperature hydrogen sulfide adsorption on activated carbon II. Effects of gas temperature, gas pressure and sorbent regeneration", *Carbon*, **38**, 1767–1774

Cook CS, Gal E, Furman AH and Ayala R (1992). "Integrated Operation of a Pressurized Fixed Bed Gasifier and Hot Gas Desulfurization System", *In: Ninth Annual Coal-Fueled Heat Engines, Advanced Pressurized Fluidized Bed Combustion (PFBC) and Gas Stream Cleanup Systems Contractors Review Meeting*, 27-29 October 1992, Morgantown, West Virginia

Devore J and Farnum N (2005). "Applied Statistics for Engineers and Scientists", 2nd edition, Thomson Brooks/Cole, Belmont, California

Do DD (1982). "On the validity of the shrinking core model in gas solid reaction", *Chemical Engineering Science*, **37 (10)**, 1477-1481

Doraiswamy LK and Sharma MM (1984). "Heterogeneous reactions: Analysis, examples and reactor design. Volume I: Gas-solid and solid-solid reactions", John Wiley & Sons, New York

Efthimiadis EA and Sotirchos SV (1993). "A Partially Overlapping Grain Model for Gas-Solid Reactions", *Chemical Engineering Science*, **48 (7)**, 1201-1212

Elseviers WF and Verelst H (1999). "Transition metal oxides for hot gas desulphurisation", *Fuel*, **78**, 601–612

Engelbrecht AD, North BC and Hadley TD (2008). "Clean coal technology: Gasification of South African coals", *In:* T. Hadley and P. Smit , eds. *IFSA 2008, Industrial Fluidization South Africa*, 19-20 Novenmber 2008 Johnannesburg. Johannesburg: The Southern African Institute of Mining and Metallurgy, 188-202

Evans JW and Ranade MG (1980). "The grain model for reaction between a gas and a porous solid - a refined approximate solution to the equations", *Chemical Engineering Science*, **35**, 1261-1262

Evans JW and Song S (1974). "Application of a Porous Pellet Model to a Fixed, Moving, and Fluidized Bed Gas-Solid Reactors", *Industrial and Engineering Chemistry Process Design and Development*, **13 (2)**, 146-152

Feng W, Kwon S, Borguet E and Vidic R (2005). "Adsorption of hydrogen sulfide onto activated carbon fibers: Effect of pore structure and surface chemistry", *Environmental Science and Technology*, **39 (24)**, 9744-9749

Fogler HS (2006). "Elements of Chemical Reaction Engineering", 4th Edition, Pearson Education, Inc, Upper Saddle River, New Jersey

Froment GF and Bischoff KB (1990). “Chemical Reactor Analysis and Design”, 2nd Edition, Wiley, New York

Gangwal SK, Gupta R and McMichael WJ (1995). "Hot-gas cleanup-sulfur recovery technical, environmental, and economic issues", *Heat Recovery Systems & CHP*, **15 (2)**, 205-214

Gangwal SK, Portzer JW, Roberts GW and Kozup SC (1998). "Engineering Evaluation of Hot-Gas Desulphurization with Sulfur Recovery", Final Report, DOE Award Number: DE-AC21-94MC31258

Gil J, Aznar MP, Caballero MA, Francés E and Corella J (1997). "Biomass gasification in fluidized bed at pilot scale with steam-oxygen mixtures. Product distribution for very different operating conditions", *Energy & Fuels*, **11 (6)**, 1109-1118

Harrison DP, Groves FR, Huang W-N, Lopez Ortiz A, White JD, Zeng Y and Zhang S (1998). "Advanced Sulfur Control Concepts for Hot-Gas Desulfurization Technology", Final Report, DOE Award Number: DE-AC21-94MC30012 -18

Hobbs ML, Radulovic PT and Smoot LD (1992). "Modeling Fixed-bed Coal Gasifiers", *American Institute of Chemical Engineers Journal*, **38 (5)**, 681-702

Horazak DA, Newby RA, Smeltzer EE, Slimane RB, Vann Bush P, Aderhold Jr JL and Bryan BG (2005). "Novel gas cleaning/ conditioning for integrated gasification combined cycle.Volume I - Conceptual commercial evaluation", Final Report, DOE Award Number: DE-AC26-99FT40674

Huiling F, Yanxu L, Chunhu L, Hanxian G and Kechang X (2002). "The apparent kinetics of H_2S removal by zinc oxide in the presence of hydrogen", *Fuel*, **81**, 91-96

International Sensor Technology (2008), Solid-State Gas Sensors [online]. Available from: http://www.intlsensor.com/, [Accessed 5 October 2009]

Ishida M and Wen CY (1968). "Comparison of Kinetic and Diffusional Models for Solid-gas Reactions", *American Institute of Chemical Engineers Journal*, **14 (2)**, 311-317

Ishida M and Wen CY (1971). "Comparison of zone-reaction model and unreacted-core shrinking model in solid-gas reactions - I Isothermal analysis", *Chemical Engineering Science*, 26, 1031-1041

Jothimurugesan K and Gangwal SK (1998). "Regeneration of zinc titanate H_2S sorbents", *Industrial and Engineering Chemistry Research*, **37 (5)**, 1929-1933

Jothimurugesan K and Harrison DP (1990). "Reaction between H_2S and zinc oxide-titanium oxide sorbents. 2. Single-Pellet Sulfidation Modeling", *Industrial and Engineering Chemistry Research*, **29 (7)**, 1167-1172

Jun HK, Lee TJ, Ryu SO and Kim JC (2001). "A Study of Zn−Ti-Based H_2S Removal Sorbents Promoted with Cobalt Oxides", *Industrial and Engineering Chemistry Research*, **40 (16)**, 3547-3556

Jung SY, Lee SJ, Lee TJ, CK Ryu and Kim JC (2006). "H_2S removal and regeneration properties of Zn-Al-based sorbents promoted with various promoters", *Catalysis Today*, **111**, 217–222

Karayilan DK, Dogu T, Yasyerli S and Dogu G (2005). "Mn−Cu and Mn−Cu−V Mixed-Oxide Regenerable Sorbents for Hot Gas Desulfurization", *Industrial and Engineering Chemistry Research*, **44 (14)**, 5221-5226

Khan AR and Bowen JH (1992). "A theoretical analysis of reaction zone thinkness and concentration profile in non-catalytic, gas-solid reactions", *Trans IChemE,* **70 Part A***, 265-275*

Ko T-H, Chu H and Liou, Y-J (2007). "A study of Zn–Mn based sorbent for the high-temperature removal of H_2S from coal-derived gas", *Journal of Hazardous Materials*, **147**, 334–341

Kohl A and Riesenfeld F (1979). "Gas Purification", 3rd edition, Gulf Publishing Company, Houston, Texas

Kramreiter R, Url M, Kotik J and Hofbauer H (2008). "Experimental investigation of a 125 kW twin-fire fixed bed gasification pilot plant", *Fuel Processing technology*, **89**, 90-102

Kuramochi H, Wu W and Kawamoto K (2005). "Prediction of the behaviors of H_2S and HCl during gasification of selected residual biomass fuels by equilibrium calculation", *Fuel*, **84**, 377–387

Kwon KC, Park YK, Gangwal SK and Das K (2003). "Reactivity of Sorbents with Hot Hydrogen Sulfide in the Presence of Moisture and Hydrogen", *Separation Science and Technology*, **38 (12&13)**, 3289–3311

Leibold H, Hornung A and Seifert H (2008). "HTHP syngas cleaning concept of two stage biomass gasification for FT synthesis", *Powder Technology*, **180**, 265-270

Levenspiel O (1979). "Chemical Reactor Omnibook", OSU Book Stores

Levenspiel O (1999). "Chemical Reaction Engineering", 3rd edition, John Wiley & Sons, New York

Lew S, Jothimurugesan K and Flytzani-Stephanopoulos M (1989). "High-Temperature H_2S Removal from Fuel Gases by Regenerable Zinc Oxide-Titanium Dioxide Sorbents", *Industrial and Engineering Chemistry Research*, **28 (5)**, 535-541

Lew S, Sarofim AF and Flytzani-Stephanopoulos M (1992 a). "Sulfidation of Zinc Titanate and Zinc Oxide Solids", *Industrial and Engineering Chemistry Research*, **31 (8)**, 1890-1899

Lew S, Sarofim AF and Flytzani-Stephanopoulos M (1992 b). "Modeling of the sulfidation of zinc-titanium oxide sorbents with hydrogen sulfide", *American Institute of Chemical Engineers Journal*, **38 (8)**, 1161-1169

Li X, Grace JR, Watkinson AP, Lim CJ and Ergüdenler A (2001). "Equilibrium modeling of gasification: a free energy minimization approach and its application to a circulating fluidized bed coal gasifer, *Fuel*, **80**, 195-207

Li Y, Guo H, Li C and Zhang S (1997). "A Study on the Apparent Kinetics of H_2S Removal Using a ZnO-MnO Desulfurizer", *Industrial and Engineering Chemistry Research*, **36 (9)**, 3982-3987

Lipták BG (editor) (2003). "Instrument Engineers' Handbook Volume 1: Process measurement and analysis", 4th edition, CRC Press LLC, USA

Lodge JP (editor) (1988). "Methods of Air Sampling and Analysis", Lodge JP (editor), 3rd edition, Lewis Publishers

Lucas C, Szewczyk D, Blasiaka E and Mochida S (2004). "High-temperature air and steam gasification of densified biofuels", *Biomass and Bioenergy*, **27**, 563–575

Lurgi (2009). "The Rectisol Process" [online]. Available from: http://www.lurgi.com/website/fileadmin/user_upload/1_PDF/1_Broshures_Flyer/englisch/0308e_Rectisol.pdf, [Accessed 5 December 2009]

McKendry P (2002). "Energy production from biomass (part 3): gasification technologies", *Bioresource Technology*, **83**, 55–63

Melgar A, Pérez JF, Laget H and Horillo A (2007). "Thermochemical equilibrium modelling of a gasifying process", *Energy Conversion and Management*, **48,** 59–67

Montgomery DC and Runger GC (1999). "Applied Statistics and Probability for Engineers", 2nd edition, John Wiley & Sons, New York

Mutasher EI, Khan AR and Bowen JH (1989). "A generalized diffuse interface model of gas-solid non-catalytic reaction in a fixed bed", *Chemical Engineering Research and Design*, **67**, 66-75

Nowacki P (1981). "Coal gasification processes ", Noyes Data Corporation, Park Ridge, New Jersey

Park HC, Kimura S, Sakai Y, Tone S and Otake T (1984). "An unsteady state analysis of packed bed reactors for gas-solid reactions", *Journal of Chemical Engineering of Japan*, **17 (3)**, 269-274

Park N-K, Lee JD, Lee TJ, Ryu SO and Chang CH (2005). "The preparation of a high surface area metal oxide prepared by a matrix-assisted method for hot gas desulphurization", *Fuel*, **84**, 2165–2171

Pawlak Z and Pawlak AS (1999). “Modification of iodometric determination of total and reactive sulfide in environmental samples”, *Talanta*, **48**, 347-333

Perry HP and Green DW (editors) (1999). "Perry's Handbook of Chemical Engineering", 7th edition, McGraw Hill, New York

Pineda M, Palacios JM, Alonso L, García E and Moliner R (2000). "Performance of zinc oxide based sorbents for hot coal gas desulfurization in multicycle tests in a fixed-bed reactor", *Fuel*, **79**, 885–895

Poling BE, Prausnitz JM and O’Connell JP (2001). "The Properties of Gases and Liquids", 5th edition, McGraw-Hill, New York

Prasannan PC, Ramachandran PA and Doraiswamy LK (1985). "A model for gas-solid reactions with structural changes in the presence of inert solids", *Chemical Engineering Science*, **40 (7)**, 1251-1261

Quinn R, Dahl TA and Toseland BA (2004). "An evaluation of synthesis gas contaminants as methanol synthesis catalyst poisons", *Applied Catalysis A: General*, **272**, 61–68

Raal JD and Mühlbauer AL (1998). “Phase Equilibriua; Measurement and Computation”, Taylor and Francis, Bristol, Pennsylvania

Rajagopalan V and Amiridis MD (1999). ""Hot Coal Gas" Desulfurization by Perovskite-type Sorbents", *Industrial and Engineering Chemistry Research*, **38 (10)**, 3886-3891

Ramachandran PA and Smith JM (1977)."A Single-Pore Model for Gas-Solid Noncatalytic Reactions", *American Institute of Chemical Engineers Journal*, **23 (3)**, 353-361

Ranade MG and Evans JW (1980). "Reaction between a gas and a solid in a nonisothermal packed bed-simulation and experiments", *Industrial and Engineering Chemistry Process Design and Development*, **19 (1)**, 118-123

Ranade PV and Harrision DP (1979). "The Grain Model Applied to Porous Solids with varying structural properties", *Chemical Engineering Science*, **34**, 427-432

Rezaiyan J and Cheremisinoff NP (2005). "Gasification Technologies", Taylor and Francis Group, Boca Raton, Florida

Ruggiero M and Manfrida G (1999). "An equilibrium model for biomass gasification processes", *Renewable Energy*, **16,** 1106-1109

Ryu SO, Park N-K, Chang CH, Kim JC and Lee TJ (2004). "Multicyclic Study on Improved Zn-Ti-Based Desulfurization Sorbents", *Industrial and Engineering Chemistry Research*, **43 (6)**, 1466-1471

Sánchez JM, Ruiz E and Otero J (2005). "Selective Removal of Hydrogen Sulfide from Gaseous Streams Using a Zinc-Based Sorbent", *Industrial and Engineering Chemistry Research*, **44 (2)**, 241-249

Sánchez-Hervás JM, Otero J and Ruiz E (2005). "A study on sulphidation and regeneration of Z-Sorb III sorbent for H_2S removal from simulated ELCOGAS IGCC syngas", *Chemical Engineering Science*, **60**, 2977 – 2989

Sasaoka E, Hirano S, Kasaoka S and Sakata Y (1994). "Stability of zinc oxide high-temperature desulfurization sorbents for reduction", *Energy & Fuels*, **8 (3)**, 763-769

Sasaoka E, Iwamoto Y, Hirano S, Azhar Uddin A and Sakata Y (1995). "Soot Formation over Zinc Ferrite High-Temperature Desulfurization Sorbent", *Energy & Fuels*, **9 (2)**, 344-353

Seader JD and Henley EJ (2006). "Separation Process Principles", 2nd edition, John Wiley & Sons, New York

Slimane RB and Abbasian J (2000 a). "Copper-Based Sorbents for Coal Gas Desulfurization at Moderate Temperatures", *Industrial and Engineering Chemistry Research*, **39 (5)**, 1338-1344

Slimane RB and Abbasian J (2000 b). "Regenerable mixed metal oxide sorbents for coal gas desulfurization at moderate temperatures", *Advances in Environmental Research*, **4**, 147-162

Smith JM, van Ness HC and Abbott MM (2001). "Introduction to Chemical Engineering Thermodynamics", 6th edition, McGraw-Hill, Singapore

Sohn HY and Szekely J (1972). "A structural model for gas-soild reactions with a moving boundary - III A general dimensionless representation of the irreversible reaction between a porous solid and a reactant gas", *Chemical Engineering Science*, **27**, 763-778

Sotirchos SV and Yu H-C (1985). "Mathematical Modelling of Gas-Solid Reactions with Solid Product", *Chemical Engineering Science*, **40 (11)**, 2039-2052

Sotirchos SV and Yu H-C (1987). "Mathematical Modelling of Gas-Solid Reactions with Solid Product", *American Institute of Chemical Engineers Journal*, **33 (3)**, 382-393

Sotirchos SV and Yu H-C (1988)." Overlapping Grain Models for Gas-Solid Reactions with Solid Product", *Industrial and Engineering Chemistry Research*, **27 (5)**, 836-845

Sotirchos SV and Zarkanitis S (1989). "Pellet-Model Effects on Simulation Models for Fixed-Bed Desulfurization Reactors", *American Institute of Chemical Engineers Journal*, **35 (7)**, 1137-1147

Sun J, Modi S, LiuK, Lesieur R and Buglass J (2007). "Kinetics of Zinc Oxide Sulfidation for Packed-Bed Desulfurizer Modeling", *Energy & Fuels*, **21 (4)**, 1863-1871

Szekely J and Evans JW (1970). "A structural model for gas-solid reactions with a moving boundary", *Chemical Engineering Science*, **25**, 1091-1107

Szekely J and Evans JW (1971). "A structural model for gas-soild reactions with a moving boundary - II The effect of grain size, porosity and temperature on the reaction of porous pellets ", *Chemical Engineering Science*, **26**, 1901-1913

Szekely J, Evans JW and Sohn HY (1976). "Gas-solid reactions", Academic Press, New York

Tamhankar SS, Bagajewicz MJ, Gavalas GR, Sharma PK and Flytzani-Stephanopoulos (1986). "Mixed-oxide sorbents for high-temperature removal of hydrogen sulfide", *Industrial and Engineering Chemistry Process Design and Development*, **25 (2)**, 429-437

Torres W, Pansare SS, and Goodwin Jr JG (2007). "Hot Gas Removal of Tars, Ammonia, and Hydrogen Sulfide from Biomass Gasification Gas", *Catalysis Reviews*, **49**, 407-456

Tsukada M, Abe K, Yonemochi Y, Ameyama A, Kamiya H, Kambara S, Moritomi H and Uehara T (2008). "Dry gas cleaning in coal gasification systems for fuel cells using composite sorbents", *Powder Technology*, **180**, 232–238

Turton R, Berry DA, Gardner TH and Miltz A (2004). "Evaluation of Zinc Oxide Sorbents in a Pilot-Scale Transport Reactor: Sulfidation Kinetics and Reactor Modeling", *Industrial and Engineering Chemistry Research*, **43 (5)**, 1235-1243

UOP (2009). "The Rectisol Process" [online]. Available from: http://www.uop.com/objects/97%20Selexol.pdf, [Accessed 5 December 2009]

Valco Instruments Co. Inc. (2009). "Sample injection with a 6 port valve" [online]. Available from: http://www.vici.com/support/app/app11.php, [Accessed 5 December 2009]

Villa LT Quiroga OD and Morales GV (1992). "The shrinking core model for non-catalytic gas-solid reactions with arbitrary order with respectr to the gaseous reactant and general boundary conditions", *Trans IChemE*, **70 Part A**, 276-281

Wakker JP, Gerritsen AW and Moulijn JA (1993). "High temperature H_2S and COS removal with MnO and FeO on γ-alumina acceptors", *Industrial and Engineering Chemistry Research*, **32 (1)**, 139-149

Wen CY (1968). "Non-catalytic Heterogenous Solid Fluid Reaction Models", *Industrial and Engineering Chemistry*, **60 (9)**, 34-54

Wender I (1996). "Reactions of Synthesis Gas", *Fuel Processing Technology*, **48,** 189-297

Westmoreland PR and Harrison DP, (1976). "Evaluation of candidate solids for high-temperature desulfurization of low-Btu gases", *Environmental Science & Technology*, **10 (7)**, 659-661

Westmoreland PR, Gibson JB and Harrison DP, (1977). "Comparative Kinetics of High-Temperature Reaction Between H_2S and Selected Metal Oxides", *Environmental Science & Technology*, **11 (5)**, 488-491

Wheelock TD, Doraiswamy LK and Constant KP (2003). "Engineering Has a New Material for Hot Gas Cleanup", Final Report, DOE Award Number: DE-FG26-99FT40587

Woods MC, Gangwal SK, Jothimurugesan K and Harrison DP (1990). "Reaction between H_2S and zinc oxide-titanium oxide sorbents. 1. Single-pellet kinetic studies", *Industrial and Engineering Chemistry Research*, **29 (7)**, 1160-1167

Yasyerli S (2008). "Cerium–manganese mixed oxides for high temperature H_2S removal and activity comparisons with V–Mn, Zn–Mn, Fe–Mn sorbents", *Chemical Engineering and Processing*, **47**, 577–584

Yumura M and Furimsky E (1985). "Comparison of CaO, ZnO, and Fe_2O_3 as H_2S adsorbents at High Temperatures", *Industrial and Engineering Chemistry Research*, **24 (4)**, 1165-1168

Zainal ZA, Ali R, Lean CH and Seetharamu KN (2001). "Prediction of performance of a downdraft gasifier using equilibrium modeling for different biomass materials", *Energy Conservation and Management*, **42**, 1499-1515

Zhang J, Wang Y and Wu D (2003). "Effect investigation of ZnO additive on Mn–Fe/*y*-Al_2O_3 sorbents for hot gas desulfurization", *Energy Conversion and Management*, **44**, 357–367

Appendix

A.1 Gasification equilibrium model

There are two mainstream methods to determine the equilibrium composition of a multi-reaction system, and both methods are thermodynamically rigorous. The first is based upon mass balances and known reactions, and the second upon minimisation of the total Gibbs free energy of the system. The methods have been adapted from Smith *et al.* (2001).

1.1 Reaction based method

This assumes an understanding of the exact, *independent* set of reactions occurring, and the number of moles of each species entering the system. There are 2 possible ways to model the system:

(i) Based upon the extent of reaction ε_j

For species i of N components in reaction j of R reactions, the mole fraction of i in the gas phase is expressed by:

$$y_i = \frac{n_{i0} + \sum_{j=1}^{R} \upsilon_{i,j}\varepsilon_j}{n_0 + \sum_{j=1}^{R} \upsilon_j \varepsilon_j} \qquad \text{(A.1.1)}$$

n_{i0} moles component i at start
n_0 moles total system at start
$\upsilon_{i,j}$ stoichiometric coefficient of component i in reaction j of R total reactions
υ_j = $\sum_{i=1}^{N} \nu_{i,j}$ overall stoichiometric coefficient for reaction j

ε_j extent of reaction j (unknown)

This gives N equations with (N+R) unknowns variables (y_i and ε_j). The remaining equations are the R equilibrium relationships, one for each independent reaction:

$$\prod_{i=1}^{N} \left(y_i \varphi_i\right)^{\upsilon_i} \left[\frac{P}{P^\circ}\right]^{\upsilon} = K_E = \exp\left(\frac{-\Delta G^o_{rxn,j}}{R_g T}\right) \qquad \text{(A.1.2)}$$

P pressure
P^o standard pressure (1 atm)
K_E equilibrium constant
R_g gas constant
T absolute temperature
$\Delta G^\circ_{rxn,j}$ Gibbs energy of reaction j
φ_i fugacity coefficient of component i

At high temperature and low pressure, the fugacity coefficient can be set to 1, and ideal gases considered. The values of $\Delta G^\circ_{rxn,j}$ can be found from calorific data.

For a solution, the expressions given in (A.1.1) can be substituted into the reactions of (A.1.2) and solved for ε_j by a numerical technique due to the non-linearities. The corresponding y_i can be found from (A.1.1).

(ii) Based upon mass balance

A general reaction is written such as:

$$\text{Reactant} \rightarrow n_1 \text{ Product 1} + n_2 \text{ Product 2} + n_3 \text{ Product 3} + \ldots \qquad \text{(A.1.3)}$$

Atomic balances are written for each atomic species resulting in (A+1) balance equations for unknowns n_1, n_2, n_3 … The remaining equations are the independent equilibrium constants, as for Equation (A.1.2) above. This should provide a unique set of equations, providing the input is not over specified. An energy balance is also required and a numerical solution.

1.2 Minimization of the Gibbs Free Energy

This method uses the fact that at equilibrium, the total Gibbs energy of the system is at minimum value. From first principles of solution thermodynamics, at constant pressure and temperature, the total Gibbs energy of a single phase system is:

$$\left(G^t\right)_{T,P} = f\left(n_1, n_2, n_3, \ldots n_N\right) \tag{A.1.4}$$

The problem is essentially trying to find a set of $\{n_i\}$ that minimises the above function, i.e. constrained optimization. The best method of solution is to use Lagrange Undetermined Multipliers.

Smith *et al.* (2001) present an excellent derivation of the required equations, via the chemical potential and Gibbs energy of formation. The resulting equation is:

$$\Delta G^{\circ}_{f_i} + RT \log\left(\frac{y_i \hat{\varphi}_i P}{P^{\circ}}\right) + \sum_{k=1}^{E} \lambda_k a_{ik} = 0 \tag{A.1.5}$$

$\Delta G^{\circ}_{f_i}$ Gibbs energy of formation of species *i* at *T*, and = 0 for an element
λ_k Lagrange multiplyer for element *k* of total *E* elements
a_{ik} number of atoms of *k* per molecule species *i*

This gives *N* equations for *N* species present at equilibrium with (*N+E+1*) unknowns. The extra '1' is for the total number of moles of the system, *n*. A_k is the total number of atoms of element *k* in the system.

$$\sum_{i=1}^{N} n_{i,k} = A_k \tag{A.1.6}$$

$$\sum_{i=1}^{N} n_i = n \tag{A.1.7}$$

The remaining *E* equations are atom balances (A.1.6) and a total mole balance (A.1.7), and this fixes the system. Again, a numerical solution is required. Note that this assumes a knowledge of which chemical species are expected to be present at equilibrium.

1.3 Implementation of the equilibrium model

A program was written in MATLAB to perform this calculation, requiring the inputs:

- Temperature range of interest
- Pressure
- Either atomic flows or component flows

The output from the program gives the mole fraction, component flows, total flowrate, volumetric flowrate and H_2:CO ratio as a function of the temperature range. The following components were possible:

H_2, CO, CO_2, H_2O, CH_4, N_2, H_2S and COS.

The program calculated the "atomic flow" of each element, C, H, O, S and N and solved the set of equations above. The Newton-Raphson method was used. The program included finding the derivatives analytically for evaluating the Jacobean matrix as part of the solution method.

The program was tested against Example 13.14 given in Smith *et al.* (2001) and the results are given below.

Table A.1: Comparison of results from Example 13.14 from Smith *et al.* (2001) and the MATLAB calculation

1000 K, 1 bar	**ΔG_{rxn}**		**Absolute difference ΔG_{rxn}**	**y_i**		**Absolute difference y_i**
	Example	MATLAB		Example	MATLAB	
	J.mol^{-1}	J.mol^{-1}	J.mol^{-1}	[-]	[-]	[-]
CH_4	19 720	19 437	283	0.0196	0.0202	0.0006
H_2O	-192 420	-192 545	125	0.0980	0.0986	0.0006
CO	-200 240	-200 261	21	0.1743	0.1737	0.0006
CO_2	-395 790	-395 940	150	0.0371	0.0373	0.0002
H_2	0	0	0	0.6710	0.6702	0.0008
Sum	-	-	-	1.0000	1.0000	0.0028

The very small differences in mole fractions can be attributed to the very small differences in the calculation of ΔG_{rxn}. Since this was the quantity being minimised, a difference here would affect the overall result. It was not stated how Smith calculated their ΔG_{rxn} values, however, the same method given in the book, with their constants for heats of formation and heat capacities, was used in MATLAB.

There were two primary limitations of the program:

- Only species mentioned above are considered.
- The program is moderately sensitive to the initial guess: this may have to be changed if there is no convergence for a particular initial composition.

This shows the program works well. In addition, a comparison was made with ASPEN and this was given in Figure 7.14.

A.2 Calculating conversion of sorbent

2.1 Definitions

In reactor analysis, there are three indicators of a reaction, each with slightly different meanings, namely conversion, selectivity and yield.

The **Conversion** of a particular reactant is defined as the ratio of the number of moles of reactant that reacted to the number of moles of reactant initially. In terms of the reactant ZnO, this is expressed as:

$$X[\%] = \frac{[ZnO]_s - [ZnO]_e}{[ZnO]_s} \times 100 \qquad \text{(A.2.1)}$$

$$X[\%] = \left(1 - \frac{[ZnO]_e}{[ZnO]_s}\right) \times 100 \qquad \text{(A.2.2)}$$

Where $[ZnO]_s$ and $[ZnO]_e$ are the number of moles of ZnO at the start and end of experiment.

The **Selectivity** of a product, when considering multiple reactions, is the ratio of the number of moles of a *specific* product to the number of moles of reactant that reacted. Here the desired product is ZnS from ZnO and this is expressed as:

$$S[\%] = \frac{[ZnS]_e}{[ZnO]_s - [ZnO]_e} \times 100 \qquad \text{(A.2.3)}$$

This is a useful indicator when there is more than one reaction product.

The **Yield** of a reaction is the ratio of the number of moles of product to the number of moles reactant. For example, the yield of ZnS from ZnO. This is expressed as:

$$Y[\%] = \frac{[ZnS]_e}{[ZnO]_s} \times 100 \qquad \text{(A.2.4)}$$

$$Y[\%] = X[\%] \times S[\%] / 100 \qquad \text{(A.2.5)}$$

For a single reaction, the Selectivity is 100 % (i.e. there is only one desired product), and hence the Conversion is the equal to the Yield.

2.2 Using the data from experiment

The reaction is as follows:

$$ZnO_{(s)} + H_2S_{(g)} \longrightarrow ZnS_{(s)} + H_2O_{(g)} \qquad \text{(A.2.6)}$$

Initially, there is a measured mass of pure ZnO placed in the reactor. This is $[ZnO]_s$. At the end of the experiment, the solid content's mass is measured again. This is now a *mixture* of ZnO and ZnS, namely $[ZnO]_e$ and $[ZnS]_e$.

This total mass at the end can be expressed as products of molar masses (M_{ZnO} and M_{ZnS} for oxide and sulphide) and the number of moles of each component:

$$m_{tot} = [ZnO]_e \times M_{ZnO} + [ZnS]_e \times M_{ZnS} \qquad \text{(A.2.7)}$$

The key is to realise that at any point during the reaction, the total number of moles must be constant, as the reaction is equi-molar.

$$ZnO \longrightarrow ZnS \qquad \text{(A.2.8)}$$

$$ZnO + ZnS = \text{constant} = [ZnO]_s \qquad \text{(A.2.9)}$$

Hence

$$[ZnS]_e + [ZnO]_e = [ZnO]_s \qquad \text{(A.2.10)}$$

$$[ZnS]_e = [ZnO]_s - [ZnO]_e \qquad \text{(A.2.11)}$$

Thus the equation for the total mass, where all terms except $[ZnO]_e$ are known, becomes:

$$m_{tot} = [ZnO]_e \times M_{ZnO} + \left([ZnO]_s - [ZnO]_e\right) \times M_{ZnS} \qquad \text{(A.2.12)}$$

Rearranging

$$[ZnO]_e = \frac{m_{tot} - [ZnO]_s \times M_{ZnS}}{M_{ZnO} - M_{ZnS}} \qquad \text{(A.2.13)}$$

Hence the conversion can now be found from Equation (A.2.2):

$$X[\%] = 100 - \frac{\left[m_{tot} - m_{ZnO} \times M_{ZnS}\right]}{\left(M_{ZnO} - M_{ZnS}\right) m_{ZnO}} \times 100 \qquad \text{(A.2.14)}$$

A.3 Detection methods for H_2S

The industrial sectors where the measurement of H_2S is most common are the petrochemical (fuel or natural gas) industry and for environmental assessment. The environmental methods measure H_2S in the very low concentration range (down to ppb levels) for atmospheric monitoring and environmental regulation control. The petrochemical side is concerned with a broader range (ppb to ppm, and even up to percent) levels for both the safety of the personnel and to meet process or product specifications.

3.1 Titrations

The sulphur content of H_2S can be found by titration, whereby the concentration of the suphide ion S^{2-} is measured. However, this method is complicated when the H_2S is being measured from the gas phase, as opposed to measuring the H_2S that has been dissolved in a liquid phase. For example, H_2S present in a liquid fuel or even crude oil. The H_2S must be absorbed from the gas phase into the liquid phase, and a titration can then be carried out. For the absorption step, the flowrate of the gas must be known and controlled. Traditionally, the titration is iodometric or potentiometric.

(i) Iodometric

The H_2S is reacted by absorption in a cadmium sulphate ($CdSO_4$) solution to form cadmium sulphide (CdS). This is quantified by iodometric titration.

(ii) Potentiometric

This uses a voltage across an electrolyte to determine the neutralisation point of a titration, instead of using an indicator. Specific electrodes are also required. A graph of voltage against volume titrant will show the end point by an inflection in the voltage-volume curve.

The problems with both titration methods are:

- Require large sample volume from the gas phase
- Take a long time
- The procedure is not conducive for easily repeating readings

Reference: Pawlak and Pawlak (1999).

3.2 Spectrophotometry

Spectrophotometry uses the measurement of an electromagnetic wave as it passes through a solution to quantify the concentration of a species, since the species present will absorb the wave at a particular wavelength. The wave can be light, infra-red or ultra violet. With H_2S

measurement, the gas must be absorbed or reacted into a solution before it can be placed in the spectrophotometer. This is the idea behind the popular Methylene Blue Method.

The Methylene Blue Method has 2 parts. Firstly, H_2S is collected by passing a measured volume of gas through an alkaline suspension of cadmium hydroxide, reacting to form cadmium sulphide, as for the titration methods. Secondly, this sulphide is collected and reacted with dimethyl-*p*-phenylenediamine and iron (III) chloride at a pH of 0.4-0.7 to form methylene blue. This solution is then placed in a spectrophotometer and compared to a calibration chart for a concentration value of H_2S. This method is used primarily for the measurement of atmospheric H_2S.

According to Lodge (1988), it is used for 0.7 to 8.4 $\mu g.m^{-3}$, which is about 0.5 ppb (volume) to 6 ppb (volume). Other concentration ranges are possible by changing the flowrate of gas and concentration of $CdSO_4$ solution.

Reference: Lodge (1988).

3.3 Solid state sensors

These are metal oxide sensors that, in the presence of a gas, cause the gas to dissociate into charged ions or complexes. The result is a transfer of electrons and can be measured by a change in electrical conductivity. This conductivity change is measured by a pair of biased electrodes, which is thus proportional to the gas concentration. They are temperature dependent. The sensors have a long life span and are quite robust.

Reference: International Sensor Technology (2008).

3.4 Electrochemical cells

The principle here is that the gas is reacted with an electrolyte and sensing electrode. A typical electrochemical cell reaction occurs, where the working electrode is exposed to both the gas and the electrolyte. A resistor is placed between the anode and the cathode and the current produced is proportional to the gas concentration. The selection of electrodes is dependent upon the type of gas to be measured. The cells usually have a limited range of operation, but greater than solid state sensors.

Reference: International Sensor Technology (2008).

3.5 Lead acetate tape method

This is a common method in the process industry. A sample gas stream is bubbled through a solution of 5 % acetic acid and water to saturate the gas. It is then passed over some tape that has been soaked with lead acetate. There is a reaction between the lead acetate and the H_2S which leaves a brown lead sulphide stain. The rate of change of staining of the tape is proportional to the H_2S concentration. The tape is automatically moved forward by a motor.

The sensor is a photocell. This has an output as a voltage which is calibrated accordingly to references.

Reference: Lipták BG (2003).

3.6 Standard H_2S test methods

These are available for purchase from the ASTM. Two examples are given below.

ASTM D2420 - 07 Standard Test Method for Hydrogen Sulfide in Liquefied Petroleum (LP) Gases (Lead Acetate).

ASTM D4323 – 84 (2009) Standard Test Method for Hydrogen Sulfide in the Atmosphere by Rate of Change of Reflectance.

Reference: ASTM (2009 a) and ASTM (2009 b).

3.7 Gas chromatography

By far the majority of experiments examined have used a gas chromatograph (GC) to determine the concentration of H_2S. It is important to outline the principles of gas chromatography before expanding on the application to H_2S measurement for this study.

(i) Background to gas chromatography

Chromatography is a method for the separation of multi-component mixtures into their constituent parts. Gas chromatography is named due to the separation of components occurring in the gas phase. Note that this can include liquids by vaporization of the sample. The sample is injected into the gas chromatograph (GC). At the injection point, the sample is heated to a high temperature to ensure complete vapourization. It is also mixed with an inert carrier gas. The sample then travels down a long tube, packed with a stationary phase.

The components in the sample will adsorb onto the stationary phase (i.e. the packing), and desorb. The *rate* of this continuous process of adsorption and desorption is dependent on the actual chemical compound. Hence, separation of all the compounds in the mixture is possible.

Upon leaving the column, the sample passes through a detector that gives an electronic signal. For most detectors, the amount of sample is proportional to the time integral ('peak area') of the reading given by the detector. The result is a chromatogram, with a series of peaks corresponding to each component that has been separated from the mixture. The peak area is calculated by an electronic integrator that is part of the GC software.

There are different detectors for different compounds (based on chemical or physical properties), and the columns suitable for different mixtures. In addition, the temperatures of injector, column and detector affect the adsorption and desorption process.

The main advantages of GC analysis are:

- Accuracy of measurement
- Repeatability
- Small sample size required, and sample can be gas or liquid
- Analysis can be very quick (10 minutes)
- One instrument for multi-component mixture
- The GC can be connected directly to the experimental apparatus
- There is the possibility of measuring high and low concentrations without significant change to the procedure.

The main disadvantages of GC analysis are:

- Calibration of instrument with known samples
- Inability of instrument to *identify* samples if no reference is available
- Analysis can be very long (1 hour)
- Totally unknown systems are very difficult to quantify
- Different detectors / columns / programs per system
- Presence of 'hidden' peaks due do large peaks overlapping smaller ones

(ii) Relating "Peak Area" to a useful concentration measurement

As described above, quantative gas analysis by GC is based on the principle that the detected peak area of an individual component is proportional (not necessarily linear) to the number of moles injected into the machine.

For an unknown number of moles of a component, the peak area can be compared to a prepared calibration, and hence the number of moles is found. In practice, the number of moles injected is not a very helpful result. A reference component, or additional information, is required to express the quantity as a fraction or concentration, which is scientifically meaningful. This can be done in several ways:

- Measure the total number of moles, mass or volume introduced to the GC.
    - The mole fraction is the number moles detected divided by the total injected (requires some kind of measurement of total number of moles).
    - The concentration is the number of moles detected divided by the volume injected.
    - The concentration is the number of moles detected divided by the mass injected (difficult on a practical scale, but possible by weighing syringe etc.)

- Internal standard method. This requires the addition of a known quantity of a new, detectable component.
- Internal normalization method. This requires all components to be detected, and the detector to have an equal response to each.

Raal and Mülbauer (1998) have covered the important aspects of GC calculations.

In general, the GC detector will be linear over a certain range of sample, mathematically: $n_i = A_i F_i$. The proportionality constant is called the response factor, F_i. A_i is the area and n_i is the number of moles of i. It can be difficult to repeat the measurements, i.e. obtain the same area for the same sample injected. Hence is advised to use ratios:

$$\frac{n_1}{n_2} = \left(\frac{A_1}{A_2}\right)\left(\frac{F_1}{F_2}\right) = \frac{n_1/n_{tot}}{n_2/n_{tot}} = \frac{x_1}{x_2} \qquad \text{(A.3.1)}$$

Note x is the mole fraction. This is very useful for binary mixtures, and the principle can be extended to multi-component mixtures.

1. Absolute method:

As described above, the number of moles of a specific component is related directly to the peak area. In order to have a fraction, the total number of moles must be known. For gases, this can be found from an equation of state, such as the ideal gas equation. Here, the temperature, pressure and volume of the sample injected must be known.

2. Internal standard:

Sometimes a component cannot be detected or calibrated. A useful solution is to add an additional component (internal standard) to the sample, and use the peak area ratio:

$$\frac{n_1}{n_S} = \left(\frac{A_1}{A_S}\right)\left(\frac{F_1}{F_S}\right) \qquad \text{(A.3.2)}$$

Where n_S is the number of moles of known standard. This can be extended to multi-components using A_i/A_S.

The mole fraction is found by a mass balance. The whole sample is weighed to give m_T, i.e. the total mass. This is made up of the individual masses of the original mixture, m_i and the standard mass m_s. All the m_i and m_s are available from the addition, and the GC result. Hence the mass and moles fractions are easily found using m_T. This method is more suited to liquid mixtures due to the measurement of the total mass.

3. Internal normalization:

This can be utilized when all the components are detected, and the detector response is consistent for all species. The ratio concept is extended:

$$x_i = \frac{n_i}{n_{tot}} = \frac{\left(\frac{A_i}{A_R}\right)\left(\frac{F_i}{F_R}\right)}{\sum_{i=1}^{N}\left(\frac{A_i}{A_R}\right)\left(\frac{F_i}{F_R}\right)} \qquad \text{(A.3.3)}$$

For N components, where R is a pre-determined reference component. Obviously the response factors F_i/F_R would be required from calibrations. The reference component is in the mixture already.

(iii) Application of GC technology to H_2S and syngas composition measurement

1. Selection of a detector

Different detectors use different measuring techniques based upon the chemical or physical properties of the type of species. For example, the Thermal Conductivity Detector is based upon measuring the thermal conductivity of a species compared to a reference species (usually helium). The problem is that the only 'universal detector', the TCD has a sensitivity of about 0.1 mole % (or 0.001 mole fraction). This does not reach the ppm range. The main types of detectors are shown in the following table:

Table A.2: Summary of GC detectors and their performance with various chemical species

Type of detector		**Applicable compounds**	**Detector performance**			
			Hydro-carbons	H_2S	H_2O	Inorganic Gases (O_2, N_2, H_2, CO, CO_2)
TCD	Thermal Conductivity	Universal detector	Average	Average	Average	Average
FID	Flame Ionization	Hydrocarbons	Good	Poor	[-]	[-]
FPD	Flame Photometric	Sulphur and phosphorus	[-]	Good	[-]	[-]
SCD	Sulfur Chemi-luminescent	Sulphur compounds	[-]	Excellent	[-]	
ECD	Electron Capture	Halogenated compounds	[-]	[-]	[-]	[-]

Note that sulphur compounds are H_2S, SO_2, COS, CS_2 and mercaptans.

Note that there are other detectors on the market. In addition, the SCD and ECD are specialist detectors. In particular, the ECD uses a radioactive source and generally permits are required to operate one.

The lower limit of the FPD is about 200 ppb, although limits of 50 ppb have been reported. The SCD can reach a limit of 1 ppb. Both detectors can detect all sulphur species, providing they can be separated from each other in the column.

For H_2S measurement, the ideal situation is to have dual detectors: a thermal conductivity detector for concentrations of 0.1 to 5 mol %, and a FPD for 1 to 10 000 ppm. An SCD is optional for extreme low levels.

The problem is that the FPD has a maximum operating limit of about 10 000 ppm, hence the need for the TCD. This also assumes that the analyst has a prior idea of which range of H_2S concentration is expected. The FID has a limited detection range of H_2S, to about 1 mole %. With the TCD, all other major components (H_2, CO, CO_2, H_2O, CH_4) can also be detected. Again, it is required that they are first separated in the column, which can be difficult.

The final problem is that of calibration. Some strategy has to be employed to relate the peak area to the mole fraction, as related earlier.

2. Selection of a column

The column determines the separation of the components. There are two types: packed or capillary. Columns are then classified according to their polarity. Columns are selected based upon the type of mixture to be separated. These can range from light hydrocarbons, to pesticides. The problem here was to find a column that could handle some water present in the sample, and be selective for H_2S and other components in the mixture, such as methane.

3. The GC program

An associated “program method”, or set of operating conditions of the GC is essential for the column to function properly for the separation.

i. Volume of sample injected
ii. Temperature of injector port
iii. Split ratio of sample (usually for capillary columns)
iv. Carrier gas type (usually Helium or Nitrogen)
v. Carrier gas flowrate *or* pressure *or* linear velocity
vi. Purge gas flowrate
vii. Initial oven temperature (i.e. column temperature)
viii. Oven temperature profile – rate(s) of increase in °C/min, holding times
ix. Final oven temperature
x. Detector temperature

There are guidelines as to what settings to use for a specific system, and they are generally available from the GC suppliers.

A.4 Application of GC analysis in this study

1. GC system available

The GC System available was a Shimadzu GC-2010, a modern standard GC. Unfortunately, it only had an FID detector. This meant that it was expected to detect CH_4 and H_2S only. A packed column was ordered with the specific intention of separating H_2S and H_2O.

In terms of calibration gas cylinders, CH_4 was available gas cylinders at 99.5 mol % and H_2S at 5.0 mass %. The calibration results have been given in Section 3.2.

The disadvantages of using FID are that the detection of H_2S was poor, and limited to above 0.5 mole % and important components such as H_2 and CO could not be measured. However, the minor advantage of using FID is that a number of components (H_2, CO, CO_2 and H_2O) are simply not detected, and hence the analysis of the chromatogram is simplified. The development of a program to separate a complex mixture can be extremely difficult.

There are only two ways to identify an unknown sample peak when only GC is available:

- Comparison of the retention time of the unknown peak with a reference chromatogram where the same operating conditions have been used.

- Comparison of the retention time of the unknown peak with a known gas. Here, the component is assumed, for example, CH_4. A sample that is known to be CH_4 is then injected and the results are compared.

Lastly, a combustion gas analyzer was available, as mentioned in Section 8.4 of Chapter 7. Although many of the components were outside the range of analyzer (CO, CO_2), the useful readings were O_2 and SO_2. These were typically 0.1 mol % for O_2 (the lowest reading) and below 50 ppm for SO_2, typically below 10 ppm.

2. Calibration Method

For calibration, there was an option of calibrating with a ratio of H_2S to CH_4 as they would both be detected. However, this required specialist gas mixing and due to the limitations of the detector with respect to H_2S, this was not pursued. An apparatus for gas mixing to create accurate calibration mixtures has been developed by Raal and Mülhbauer (1998).

For a first attempt at quantification, the absolute calibration method was used. Since gases were being analyzed, it was straightforward to measure the temperature, pressure and volume of the sample. Thus, the *total* number of moles injected could be found from the ideal gas law.

When measuring from the system, the inclusion of a compressibility factor *Z* was impossible, as the calculation of *Z* is dependent on composition and associated mixing rules. Since the entire gas composition could not be found, this could not be evaluated. Should it be possible, there would be some iteration involved (assume composition, calculate *Z*, evaluate new composition from GC and compare to assumed and iterate).

Initially, a gas tight syringe was used for both calibration and sampling from the system. A calibration chart was prepared by simply changing the volume of the gas injected. A low gas flow was set from the cylinder and a sample was taken via a septum. The pressure in the gas line and the temperature was measured.

It was found that the procedure was difficult to perform practically and was thus susceptible to significant error. This included measuring the correct volume to inject. The results showed the inconsistency in taking a repeated sample.

The installation of online sampling via a 6 port valve and sampling loop solved these problems. The repeatability of samples for calibration was extremely good. The only problem was that one was now limited to a calibration of two points i.e. two sample loops of different volumes, and these were not necessarily in the range to be encountered in the experiment.

To widen the calibration range, dilution of the gas mixtures was required. This could not be performed due to time constraints and the fact that it was known that the detector was limited with respect to H_2S.

3. GC Gas Syringe Calibration

3.1 Range of Calibration

The GC must be calibrated in the expected range of gas composition to avoid extrapolation. The expected range was calculated below.

From the equilibrium composition calculation, the syngas was expected to have a CH_4 mole fraction of between 1 and 20 %, depending on the temperature of gasification and the ratio of the fuel to oxygen feed. Using a calibration standard of 99.5 mol % methane, also at ambient conditions, this corresponds to injecting a range of volumes from 5 to 100 µl at 25 °C and atmospheric pressure.

The expected H_2S mole fraction was 5 % and 10 ppm (0.001 %). This is the inlet and outlet to the desulphurization reactor respectively. It was unclear at this stage whether the FID detector would actually detect this lower limit of H_2S.. This corresponded to volumes of 60 ml to 10 µl using a calibration standard of 5.0 mass % H_2S in nitrogen (4.15 mol %).

Although the method of using gas syringes and variable volumes has quite large uncertainties, it was a simple method to try before moving on to more sophisticated techniques.

3.2 Results of Syringe Calibration

Figure A.1 shows the calibration for CH_4 from 0.2 µmol to 3.6 µmol. The linearity over this range is fair. It shows that the syringe method is not completely repeatable. In total, 54 measurements were taken to generate the calibration. The number of moles of CH_4 was calculated by the ideal gas equation with the compressibility factor *Z*. For CH_4 at 25 °C and 1 atm, *Z* is 0.9982 Perry and Green(1999). The small differences in the number of moles were due to small changes in the gauge pressure measured.

Table A.3: Calculation of calibration range

Expected range during experiment		**CH_4**		**H_2S**	
		Maximum	Minimum	Maximum	Minimum
Mole fraction	[-]	0.2	0.01	0.05	0.00001
Absolute pressure	bar	1.01	1.01	1.01	1.01
Volume of syringe	ml	0.5	0.5	0.5	0.5
Temperature	°C	25	25	25	25
Total moles sample	µ mol	20.3726	20.3726	20.3726	20.3726
Moles CH_4 or H_2S	µ mol	**4.0745**	**0.2037**	**1.0186**	**0.0002**
Relating experiment to syringe volume requited					
Purity of cylinder	mol %	99.5	99.5	0.0415	0.0415
Moles CH_4 or H_2S	µ mol	4.0745	0.2037	1.0186	0.0002
Volume of sample for the same number of moles above	ml	0.1005	0.0050	60.2410	0.0120
	µl	**100.50**	**5.03**	**60240.96**	**12.05**

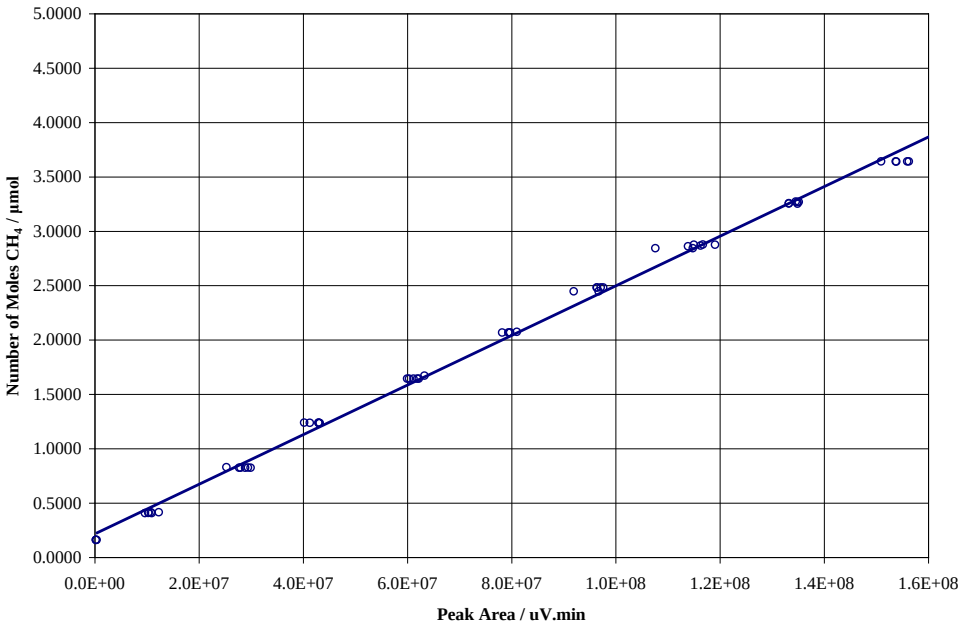

Figure A.1: Gas syringe calibration for CH_4

The calibration equation was:

$$y \text{ (moles } CH_4 \text{ [µmol])} = 2.280952\times10^{-8}\, x \text{ (peak area [uV.min])} + 0.2181375 \qquad \text{(A.4.1)}$$

Note that the trendline did not pass through the origin, which by definition was a requirement of the calibration. If there is no species present in the sample, then there cannot be any 'peak area' showing the detection. Once again, this highlights the difficulties of using the syringe method.

The result for the low range of H_2S is shown in Figure A.2. The detector response is of the order of 10^4 compared to 10^8 for CH_4, highlighting the difficulty in detecting H_2S with an FID.

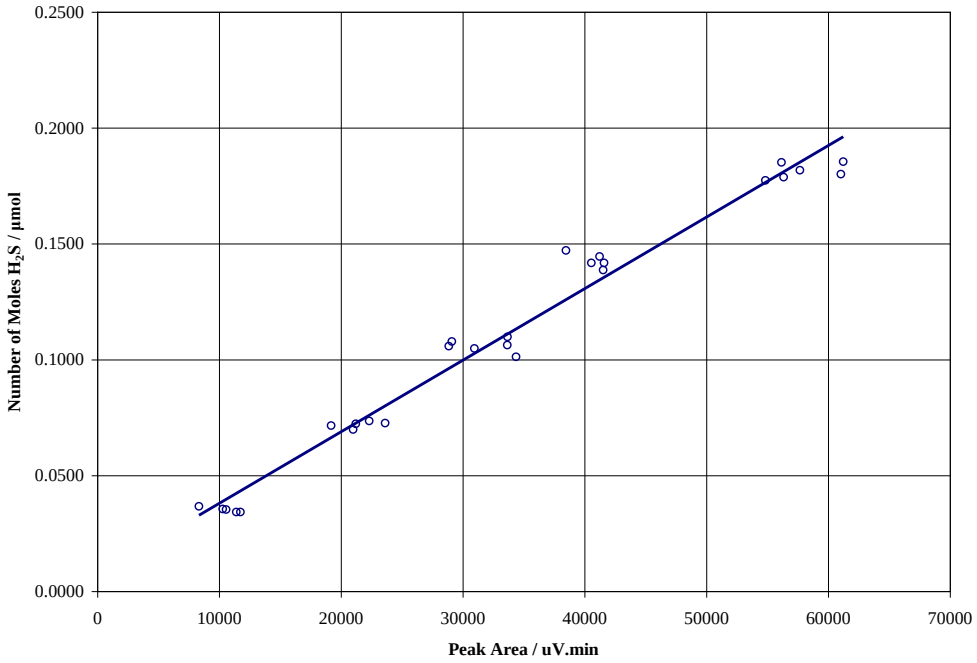

Figure A.2: Gas syringe calibration for H_2S: low number of moles range

The calibration equation was:

$$y \text{ (moles } H_2S \text{ [µmol])} = 3.087029\times10^{-6}\, x \text{ (peak area [uV.min])} + 7.223579\times10^{-3} \qquad \text{(A.4.2)}$$

Figure A.2 shows a fairly linear relationship. However, when the range was extended, the results were not very satisfactory. The calibration chart for larger number of moles is shown in Figure A.3. The larger range calibration equation was:

$$y \text{ (moles } H_2S \text{ [µmol])} = 1.361796\times10^{5}\, x \text{ (peak area [uV.min])} + 0.2101 \qquad \text{(A.4.3)}$$

The larger number of mole measurements (the blue points on Figure A.3) were performed on a different day with a different syringe. This highlights the inconsistency of using a gas syringe. Not only is there significant scatter, but there is also poor agreement with the other

measurements (the pink points). The orange points are the samples taken using the sample valve and loop and are included here for comparison.

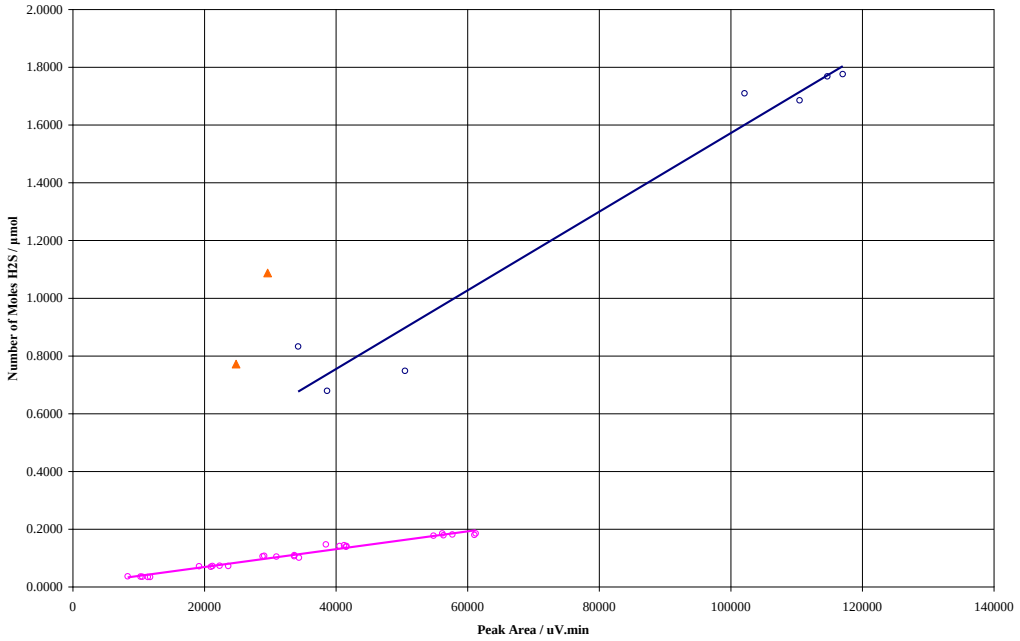

Figure A.3: Gas syringe calibration for H_2S with different syringes. The 2 orange points were those obtained using the online sample valve.

The temperature and pressure of the sample were carefully measured. It is acknowledged that there is some error associated with the volume, as it is extremely difficult to inject the same volume for each sample. This further strengthened the need for the sample loop and valve.

The graph also shows the limit of H_2S detection. The peak area of 10 000 uV.min corresponded to a detected amount about 0.05 µmol H_2S. If a 1 ml sample loop at 25 °C and 1 atm was used, there were 40.90 µmol total. Hence, the limit was 0.05/40.90 = 0.12 mol %.

4 Experiments Conducted to Test Online GC Performance

4.1 Introduction

The GC had been connected to the reactor system directly. This allowed samples to be taken from the flowing process streams and be sent to the GC simply by turning the 6 port sample valve. There were a number of experiments conducted to test the consistency of the system. These are described below, after a description of the experimental apparatus.

4.2 Equipment Setup

There are sample points at the inlet and outlet of the reactor. The sampling method involves directing the flow of gas through a series of 3 way valves to the 6 port sample valve. At this point, it can be sent to the GC.

On the inlet side, the gas flow bypassed the reactor i.e. no gas flow to the reactor at all; it passed through the 6 port valve before returning to be vented. On the outlet side, the gas can be directed through the sample loop to the 6 port valve and then it is vented, or it can be vented directly. Essentially, the gas can be vented from inlet or outlet, and sampled when required. Refer to Figure A.4 below. The correct combination of the 3 way valves is given in Table A.4.

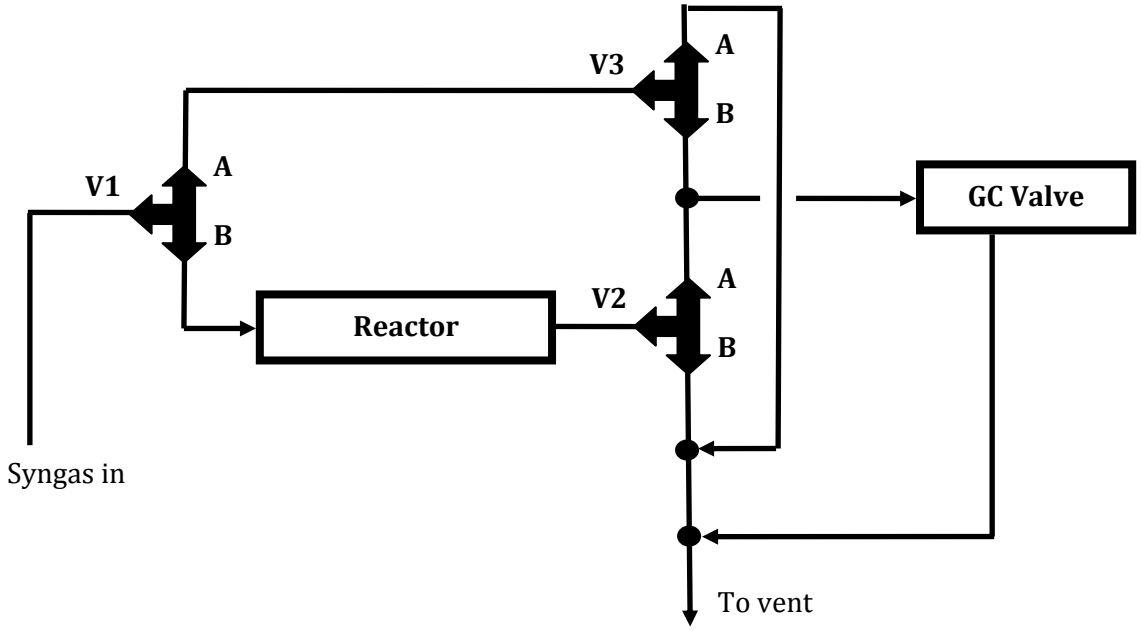

Figure A.4: Gas sampling piping and valves

Table A.4: Valve positions for gas sampling

Action	**V1**	**V2**	**V3**
To bypass reactor and vent gas	A	Closed	A
To sample inlet gas	A	Closed	B
To vent gas after reactor	B	B	Closed
To sample exit gas	B	A	Closed

The 6 port GC valve operated by changing the flow path of the carrier gas. Initially, the 'process stream' to be sampled must flow through the sample loop, as in Position 1 of Figure A.5. When the valve was switched into Position 2, the carrier gas from the GC now flowed through the sample loop and took the contents of the loop into the GC. The process stream bypassed the loop in this position. For the next sample, the valve was turned back to Position 1 to fill the sample loop again.

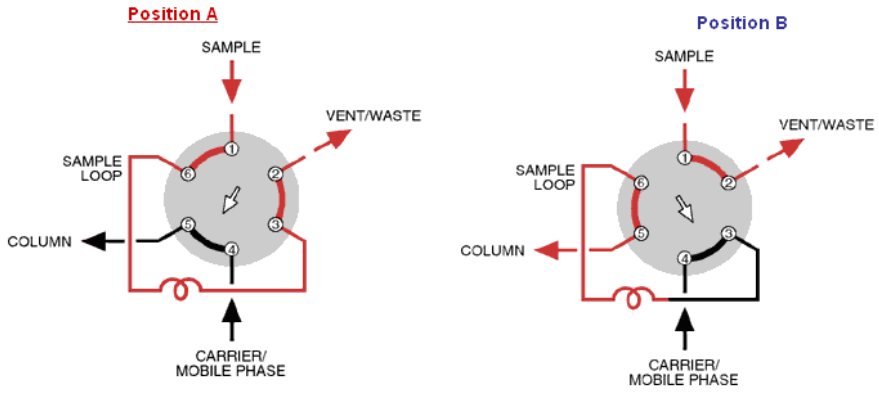

Figure A.5: Valve positions for sample collection (Position A) and sample analysis (Position B). From Valco Instruments Co. Inc. (2009).

4.3 Experiments

These have been summarized in Table A.5.

4.3.1 Experiment 1

The reactor was loaded with sorbent and nitrogen was passed over the sorbent. Samples were taken from the inlet and outlet of the reactor. There were unidentified peaks on the GC, indicating some unknown species were present. The sorbent was removed, and the reactor was cleaned, re-connected and purged with nitrogen. This leads to Experiment 2. Note that the FID is very sensitive to the organic compounds and will detect CH_4, CH_3OH at trace level.
Conclusions:

- The sorbent was possibly not pure or had been contaminated
- The system was not purged of trace gases: this was possible since the sample lines had previous been used with pure methane for the calibration of the GC
- Simplify the testing procedure to rule out contamination from the sorbent while the analysis procedure is being developed.

4.3.2 Experiment 2

The reactor was connected with no sorbent loaded i.e. an empty reactor, and nitrogen was blown through. After some time, the GC showed no response.

Conclusions:

- The system must be checked that there are no traces of gases before conducting the experiments. This is particularly significant for H_2S, as it has a small response compared to the other gases that can be detected.

Table A.5: Summary of experiments and qualitative results

Number	Test	Objective	Result	Next Step
1	N_2 over sorbent	Check for no peaks from GC	There were small strange peaks at random times.	Clean reactor and simplify testing procedure
2	N_2 in empty reactor	Check for no peaks from GC	After some time, no peaks: system is clean.	Try syngas first with no sorbent to simplify the analysis.
3	Syngas in empty reactor.	Gas separation from syngas and consistency.	Clean syngas chromatogram	Repeat and check location of methanol peak.
4	Vapourize methanol, syngas in empty reactor	Identify methanol peak. Compare inlet and outlet samples	Methanol peak at 8 minutes. Good consistency after time and inlet sample agreed the outlet.	Introduce H_2S into gas mixture.
5	Syngas with H_2S in empty reactor	Consistency and separation of gases to isolate H_2S peak	Good consistency, H_2S peak identified.	Check location of H_2S using pure gas cylinder
6	H_2S peak	What is the H_2S retention time?	H_2S is detected at 3.9 minutes (under current settings)	This agrees with experiment 5. Add the sorbent to the reactor.
7	Syngas, no H_2S, sorbent in the reactor	Check the response with sorbent loaded		Add the mercaptan to produce H_2S.
8	Syngas with H_2S with sorbent	Difference in H_2S in the inlet and the exit Consistency of composition	Good consistency. Difference in H_2S peaks between exit and inlet.	

4.3.3 Experiment 3

Since the apparatus has been purged prior to gasification, the GC response would be an accurate analyse of the gasification products. Pure methanol was gasified with oxygen, to produce 'clean syngas' i.e. no H_2S. The emphasis was now on consistency over time. Secondly, when the H_2S is introduced, it should be a new peak on the chromatogram generated from this experiment.

Conclusions:

- Consistent gas compositions are possible at constant feed flowrates and system temperatures. It takes time of about 1 hour from when the fuel is switched on.
- A baseline chromatogram is available with 'clean' syngas to compare against syngas with H_2S.

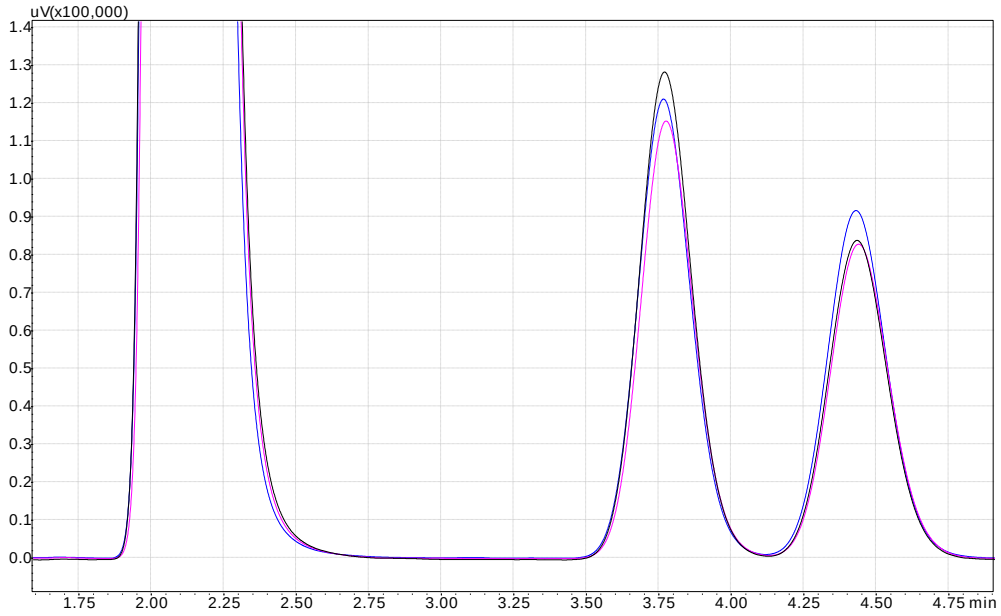

Result 3.1: Clean syngas chromatogram. The first peak is methane (very large), the second is ethane, and the third is not known. The samples very taken 10 minutes apart. There was another very small peak at 8 minutes (methanol).

4.3.4 Experiment 4

Methanol was vapourized (not gasified) and a sample was taken. This was to identify the peak caused by pure methanol.

The reactor was connected with no sorbent loaded. Syngas was produced and flowed through the empty reactor and sampled from the exit and inlet. This checked that the same gas flowing through two difference routes gave the same result. This was essentially a repeat of Experiment 3.

Note that one setting was changed on the GC, and hence the peak position times are different to those in Experiment 3.

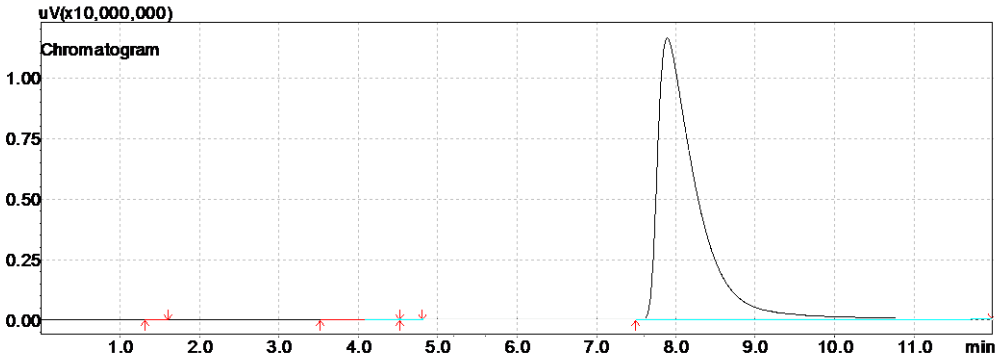

Result 4.1: Methanol identification. There was very large and unmistakable methanol peak at 7.9 minutes.

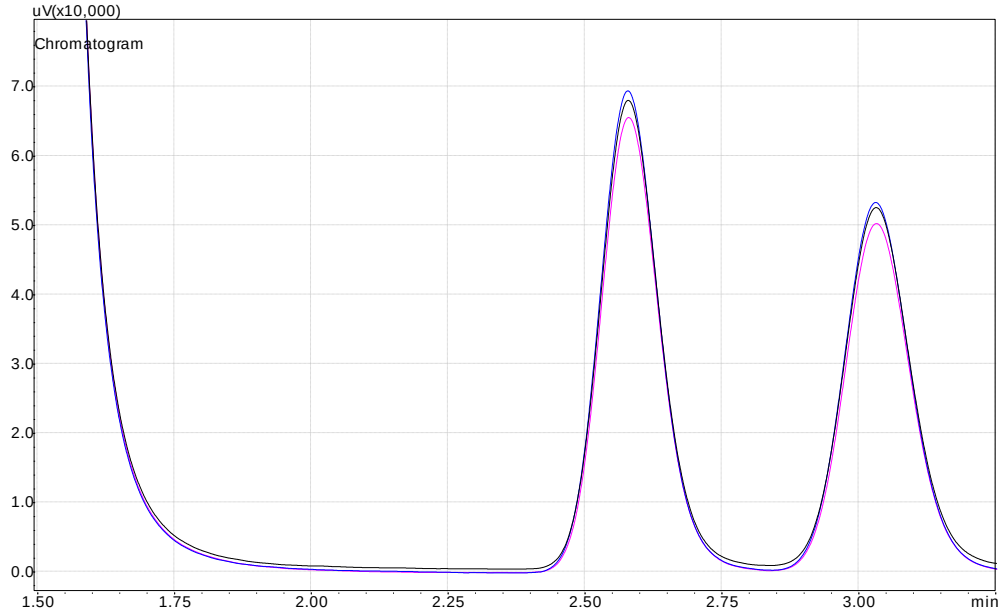

Result 4.2: Consistency of gas composition. This is after 1 hour after switching on the flow, and these are exit samples. The time *order* is black line, pink line and then blue line at 10 minute intervals. Note these two are very small peaks, but they show the consistency very well.

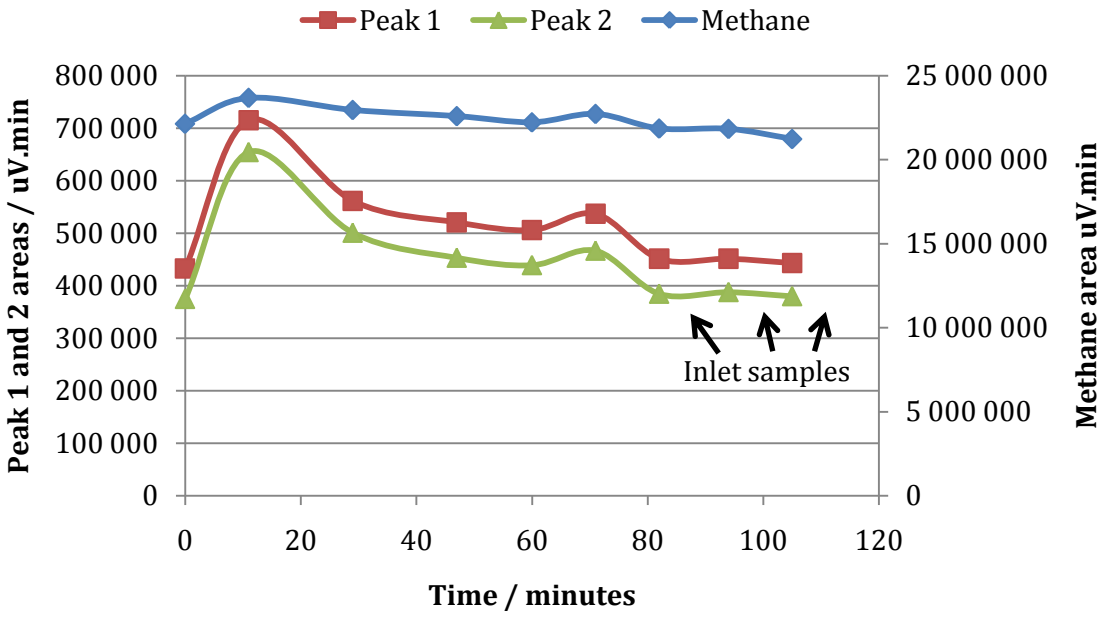

Figure A.6: Methane composition from inlet and exit of reactor over time

Table A.6: Actual peak area values for 3 predominant peaks

	Peak 1 (methane)	**Peak 2**	**Peak 3**	**Relative Error (%)** |reading-average| / average *100		
	Area / uV.min	**Area / uV.min**	**Area / uV.min**	**Peak 1**	**Peak 2**	**Peak 3**
exit_1	22 592 863.6	520 773.4	453 344.3	0.35	0.11	0.05
exit_2	22 223 948.7	506 171.7	439 269.5	1.29	2.91	3.06
exit_3	22 724 104.2	537 161.8	466 779.9	0.93	3.03	3.01
Average	22 513 638.8	521 369.0	453 131.2			
Std deviation	259 319.0	15 504.0	13 756.0			
Coefficient of Variation % (Std dev / average) ×100	1.15	2.97	3.04			

That the small difference between the inlet and exit (shown by dotted lines) can be attributed to the pressure of the sample loop. The pressure will be different due to the different piping lines connecting the sampling points to the sample loop. A difference of 1 kPa is significant.

Note that maintaining isobaric conditions to within 1 kPa is not essential; as long as the pressure is recorded at the time the sample is taken.

The effect of temperature is smaller and a change of 1 degree can be tolerated without a great change in GC response. This is because the detector response is proportional to the number of moles injected via the sample loop.

Due to the large magnitude of the numbers, the results can be misleading – a difference of 200 000 uV.min is possibly very large. Hence the visual representation with the chromatograms overlayed is useful.

The coefficient of variation is a measurement of the 'normalised dispersion of a probability distribution'. This measures the extent of variability relative to the mean, and allows comparison between different data sets.

Conclusions:

- Identification of the methanol peak elution time from the GC
- Consistency of the syngas composition over time, on both the inlet and exit to the reactor, shown by low values for coefficient of variation

4.3.5 Experiment 5

The reactor was connected, again with no sorbent loaded. Syngas with H_2S was produced and flowed through the empty reactor and sampled from the exit and inlet. This checked that the same gas flowing through two difference routes gave the same result. Some of the GC settings were changed in an attempt to improve the response. There was no improvement and the settings were changed back to the original ones.

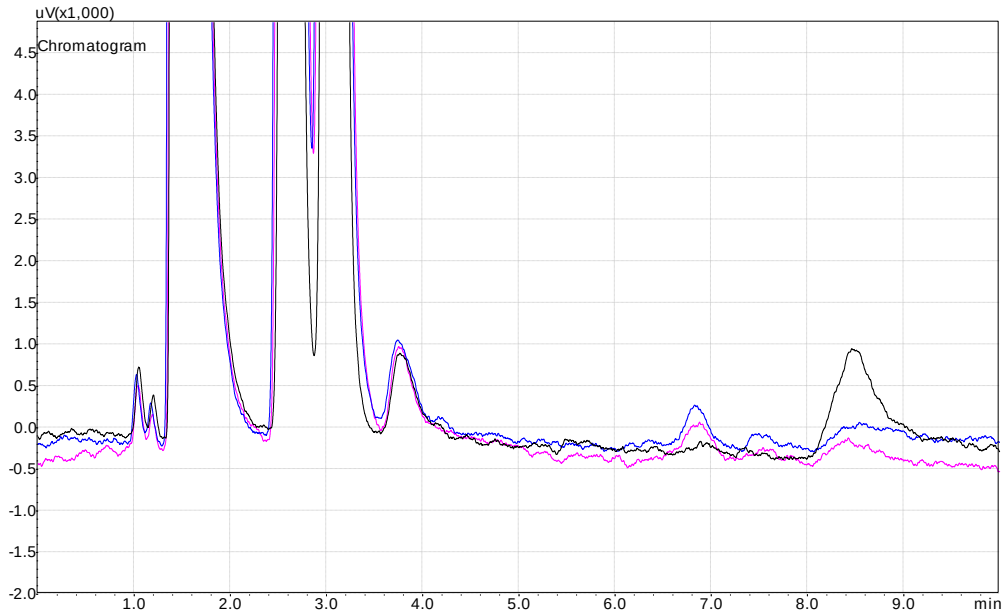

Result 5.1: The H_2S peak was identified, as expected at 3.8 minutes. This would be confirmed during experiment 6. The H_2S peak is much smaller at 3.8 minutes, but still consistent. The peak just before 7 minutes is unknown, and the one just after 8 minutes is methanol.

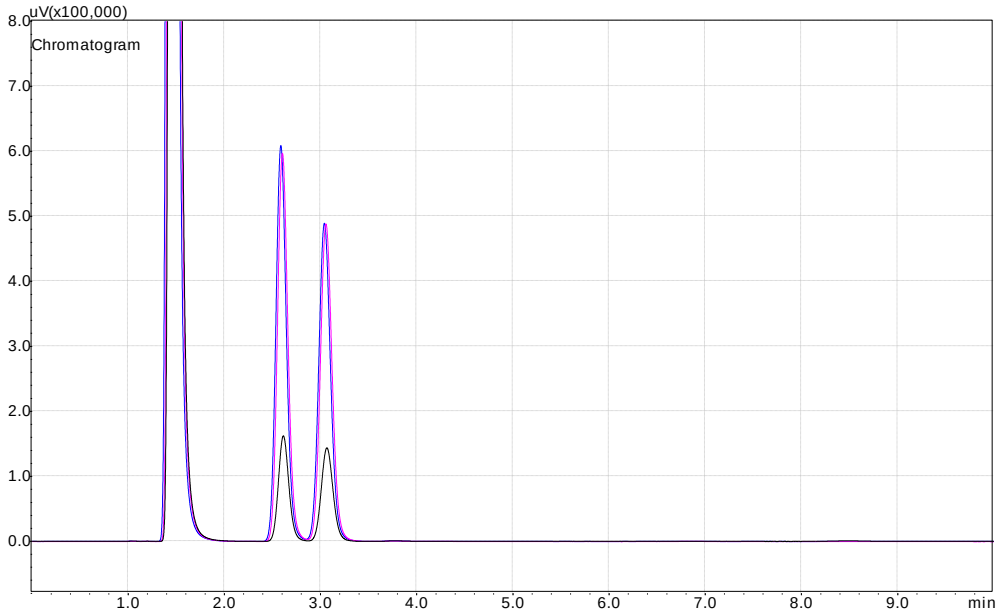

Result 5.2: The consistency of the sampling: 3 samples at 10 minute intervals. Black line: still reaching steady state, blue and pink lines are very similar.

4.3.6 Experiment 6

The mercaptan-methanol was vapourized and sent to the GC. This was to ensure that none of the mercaptan overlapped the CH4 or H2S peaks. Both components had far longer elution times – about 8 minutes. In addition, a pure 5% by mass H2S in N2 mixture from the cylinder was sampled to check the location of the H2S peaks. This was confirmed at 4 minutes.

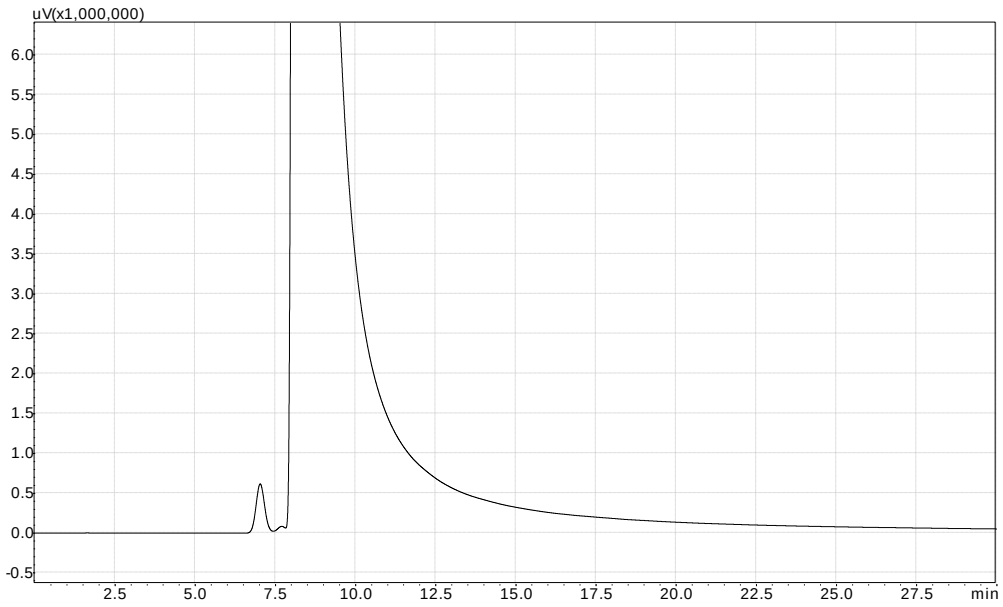

Result 6.1: The mercaptan / methanol peak. No GC response before 7 minutes.

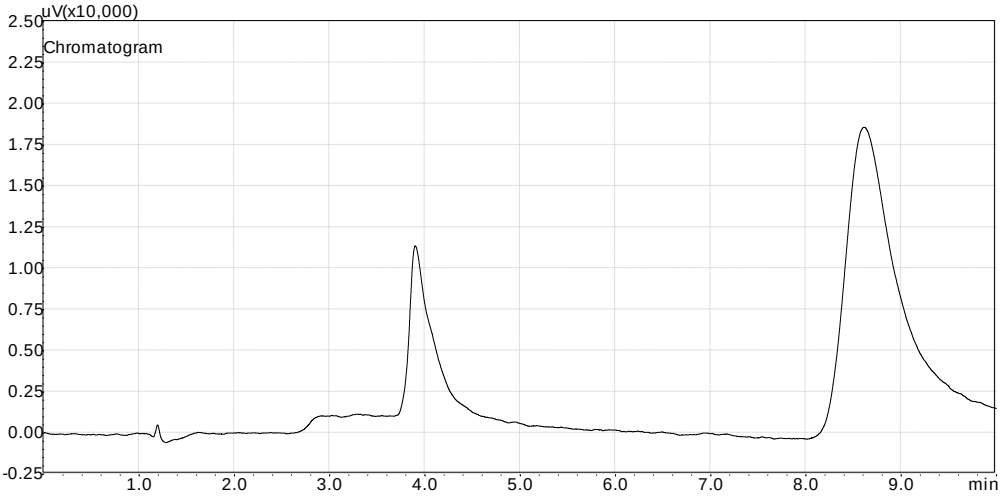

Result 6.2: The H_2S peak at 3.9 minutes. The 2nd peak at 8 minutes was residual methanol.

Note that the peak is well defined, but very small, even at this high percentage of 5% by mass.

4.3.7 Experiment 7

The reactor was loaded with the sorbent. Clean, H_2S free, syngas was passed through the reactor.

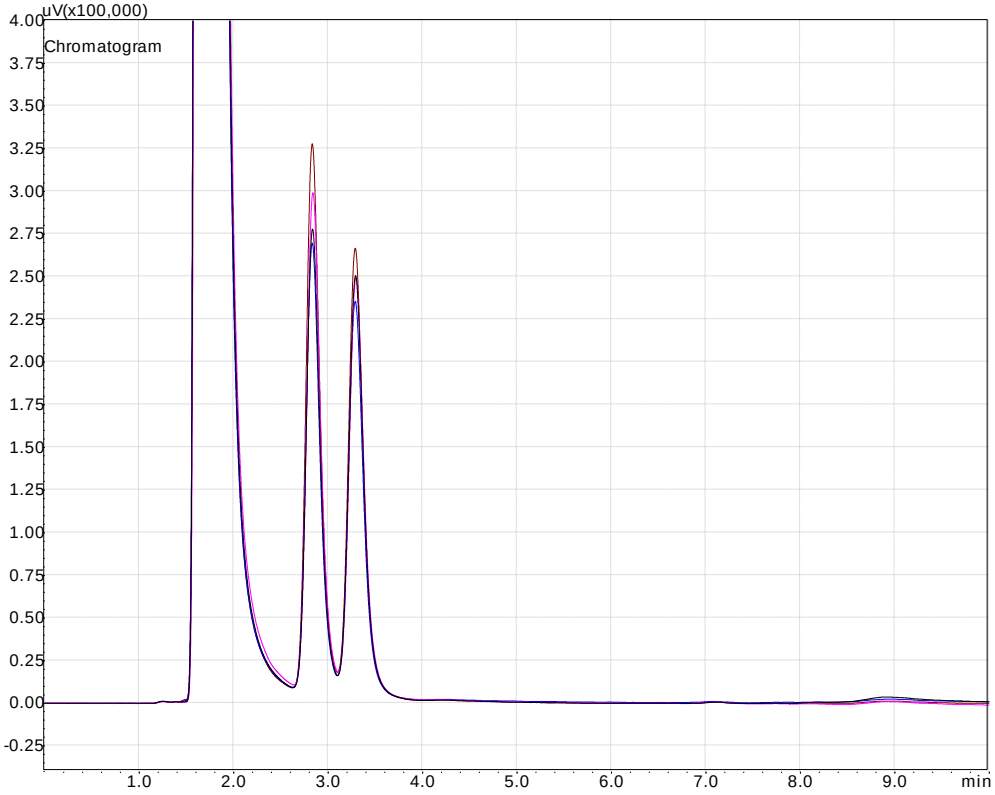

Result 7.1: Consistent Gas Composition. Order of samples: Black, pink, blue, brown.

Table A.7: Further peak area comparisons with actual peak area values

	Time of sample / min	**Peak 1 (methane)**	**Peak 2**	**Peak 3**	**Relative Error (%)** |reading-average| / average ×100		
		Area / uV.min	**Area / uV.min**	**Area / uV.min**	**Peak 1**	**Peak 2**	**Peak 3**
exit_1	0	126 119 027	2 823 632	2 782 589	0.96	5.47	0.17
exit_2	13	126 681 128	3 050 835	2 767 670	1.41	2.14	0.37
exit_3	32	122 519 517	2 730 526	2 598 711	1.92	8.59	6.45
exit_4	44	124 343 572	3 343 046	2 963 024	0.46	11.92	6.66
Average		124 915 811	2 987 010	2 777 998			
Std deviation		1 882 707	272 832	148 892			
Coefficient of Variation % (Std dev / average) ×100		1.5	9.13	5.36			

The results show excellent consistency over the course of the experiment. The first exit sample was given a time of 0 minutes.

It is also noted that the 'relative error' is not the best statistic to use, but it provides some kind of ball park figure to gauge the variation in response.

Lastly, the mass of the sorbent changed by less than 0.02 g. This shows that a complete recovery of the sorbent out the reactor is possible. It is aimed at having an uncertainty in the mass readings of 0.1g. This is well within the overall change expected during the reaction:

4.3.8 Experiment 8

The reactor was loaded with the sorbent. The syngas was produced from a methanol and mercaptan mixture.

There were initially some problems with the GC and it was realised that some settings had been inadvertently changed. Once these were changed back, the results were good, as detailed below.

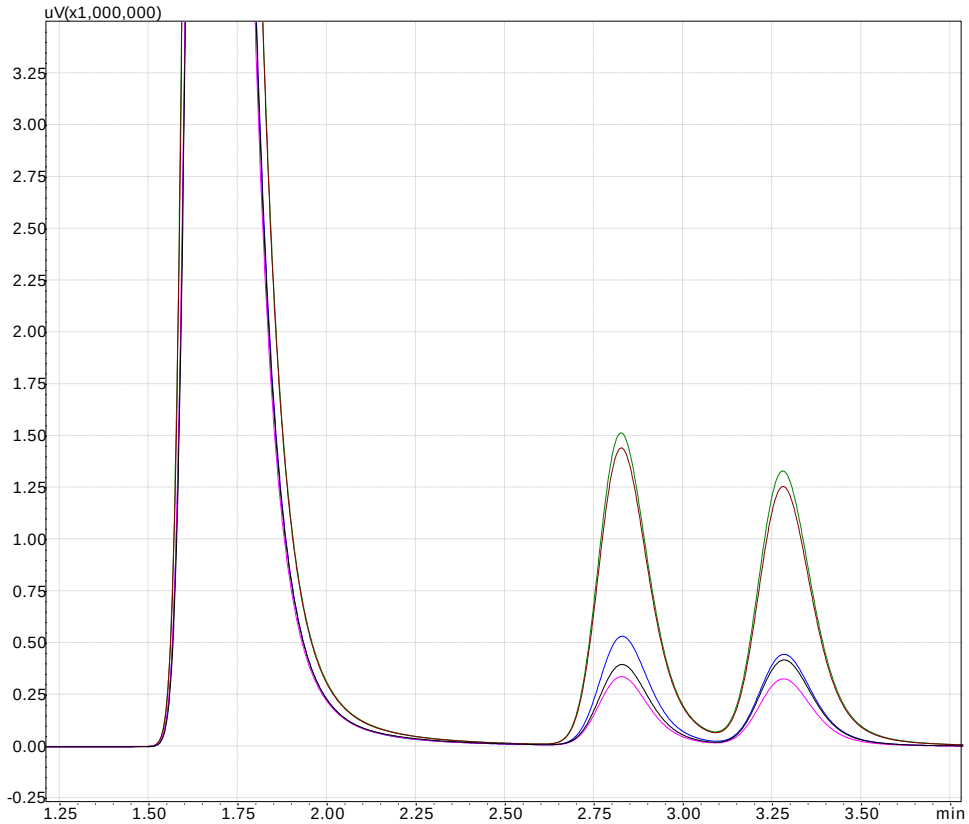

Result 8.1: Consistency of system under 2 different conditions. Note that this figure does *not* show the H_2S peak. This highlights the time taken for the composition to stabilise once the feed has been changed.

Table A.8: Legend for Result 8.1

Time / min	Condition	Line colour	Comment
0	Methanol feed, exit	Black	Quite consistent
13	Methanol feed, exit	Pink	
29	Mercaptan feed, exit	Blue	Still reaching steady state
40	Mercaptan feed, exit	Brown	Good consistency of composition
52	Mercaptan feed, exit	Green	

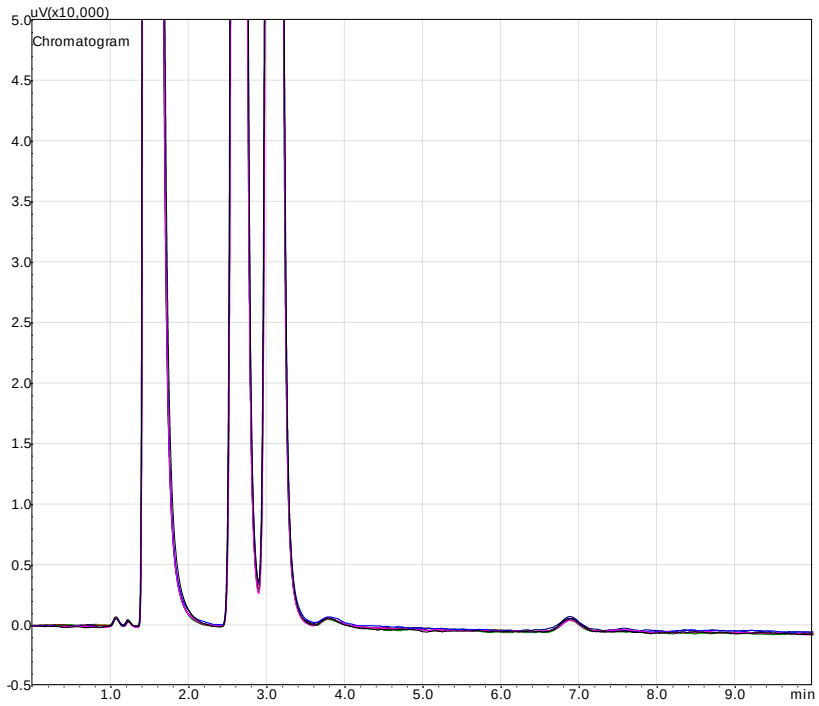

Result 8.2: Consistency of gas composition over time, at the exit.

There are actually 7 chromatograms overlayed here. The total time difference was 1 hour and 15 minutes. The small H_2S peak can be seen at 3.8 minutes. See the next chromatogram below for a closer look.

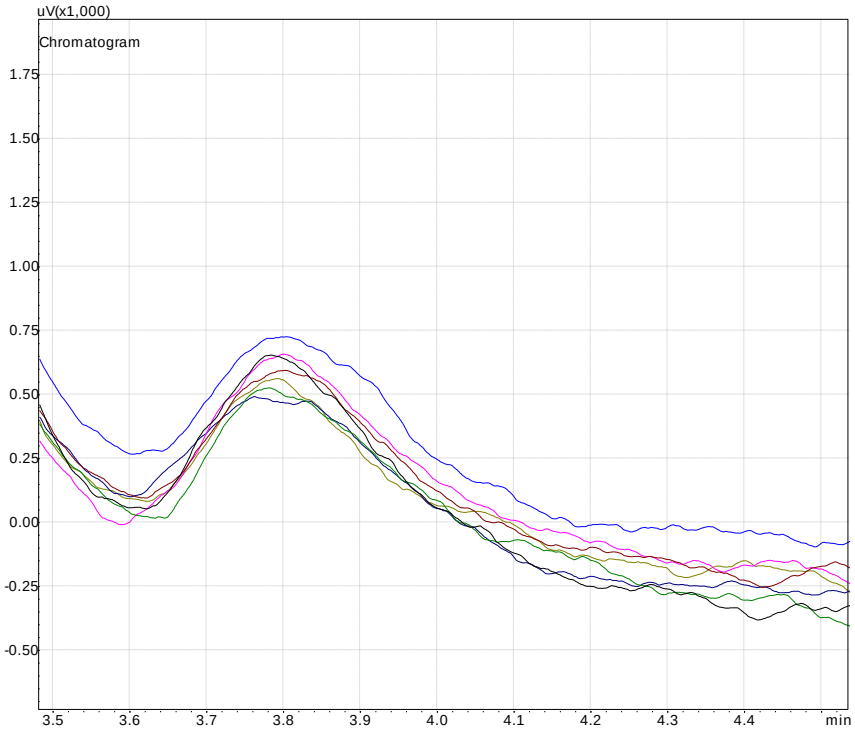

Result 8.3: Magnification of H_2S peak on reactor inlet

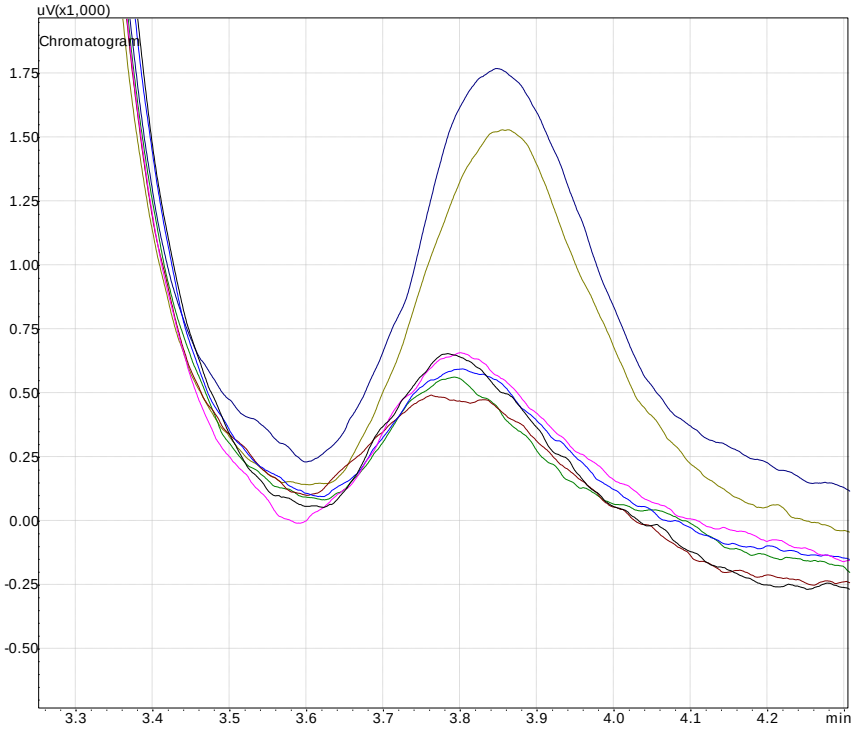

Result 8.4: Comparison of inlet and exit peaks. Obviously, the composition of the gas should be the same, with the exception of the reacted H_2S. The next chromatogram does show excellent consistency.

The inlet samples were taken at the end of the experiment. Note that the inlet concentration was relatively small, and hence there is not a large difference between the inlet and exit peaks. However, the difference is large enough to show the effect of the reaction.

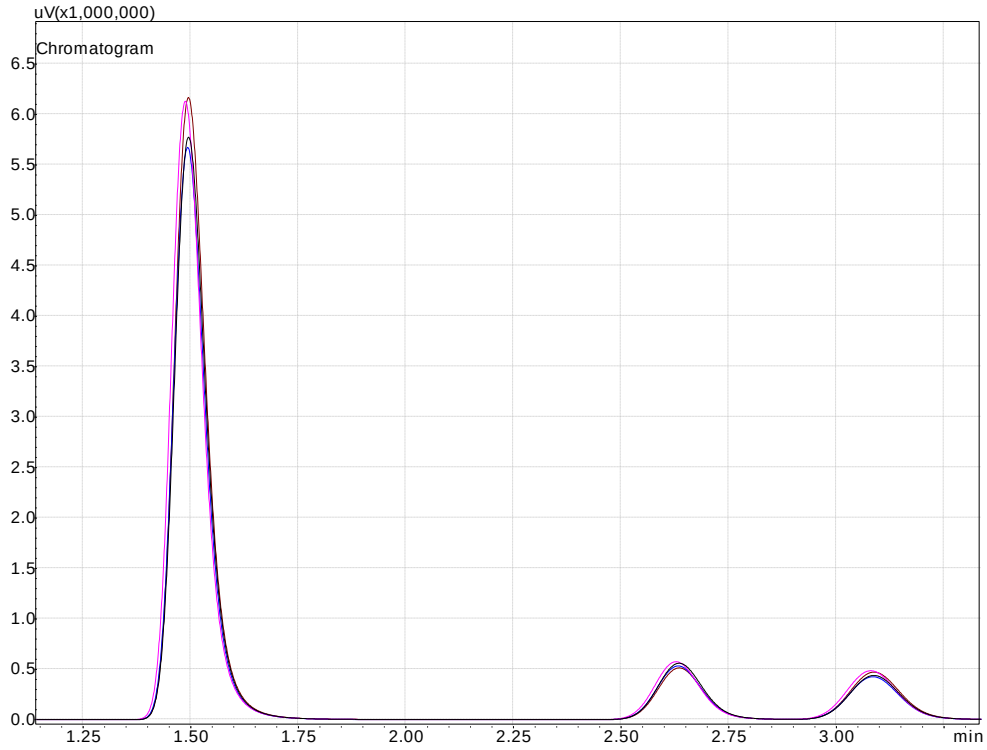

Result 8.5: Overlaid chromatograms over the course of the experiment

5. GC online calibration results

A sample valve and sample loop was installed in the apparatus. Methane from a gas cylinder flowed through the sample line and through the sample loop for the analysis.

Using the 1 and 0.2 sample loop volumes, there was excellent repeatability with methane.

Table A.9: Results of online calibration for methane using two syringe volumes

Sample volume / m*l*	**1**	**0.2**
Number of moles / µmol	**41.036**	**8.277**
Sample 1	1.0473×10^{9}	4.7395×10^{8}
Sample 2	1.0503×10^{9}	4.7463×10^{8}
Sample 3	1.0495×10^{9}	4.7440×10^{8}
Sample 4	1.0501×10^{9}	4.7473×10^{8}
Sample 5	1.0485×10^{9}	
Average	1.0491×10^{9}	4.7443×10^{8}
Standard deviation	1.0824×10^{6}	3.4708×10^{5}
Coefficient of variation (%)	0.10	0.07

Unfortunately, the number of moles sample range of 8.2-41.0 µmol was significantly out of the calibration range of 0.2-4.0 µmol. Secondly, as shown by the graph below, detector response was certainly not linear.

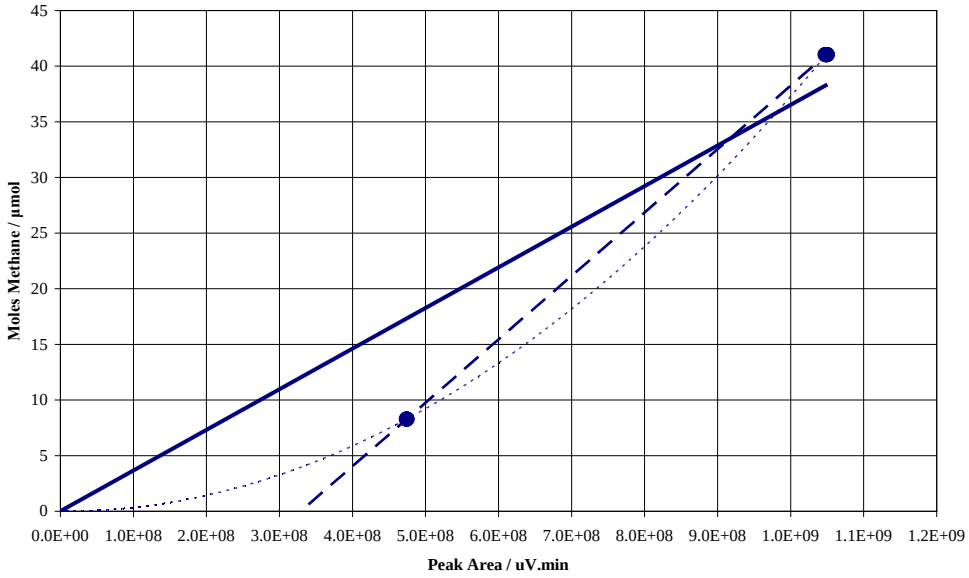

Figure A.7: The two calibration points for methane using the sample loops of 1 and 0.2 ml volume. The 'points' were made up of 5 and 4 points respectively. The solid line is a straight line through the origin, the dashed line is a linear relationship and the dotted line is a 2nd order polynomial through the origin.

Thus it could be concluded that the sample valve showed excellent repeatability, at least for CH_4. However, the calibration points were out of range to be used for the actual experiments. Since the 0.2 ml sample was the smallest available, the CH_4 gas would have to be diluted to achieve lower sample amounts.

Comparing the response with the gas syringe, the non linearity was clear.

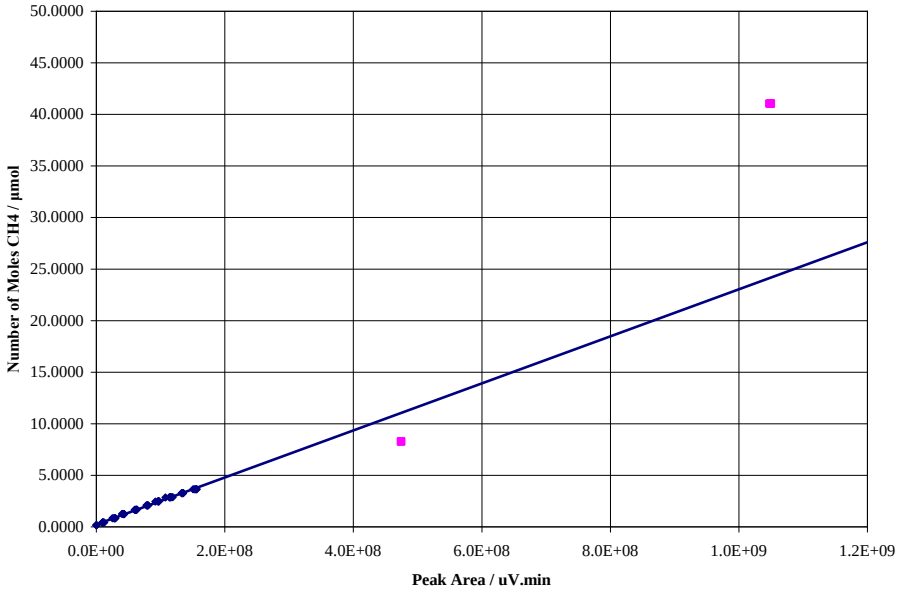

Figure A.8: Gas syringe calibration and trend line (blue) and online calibration (pink points)

Calibration for H_2S was with the 0.2 ml loop. As with the syringe the results were inconsistent, as shown above in Figure A.8. Only 2 points were used as there were problems associated with the other experimental points, such as residual methane in the sample loop and ensuring that the flow of the H_2S was steady during sampling.

Compared to the high repeatability of the methane, the H_2S response was very poor. This could be attributed to the FID detector. The CH_4 result showed that the experimental procedure worked.

6. Final Conclusions from GC calibration work

- The gas syringe method worked in principle but was inconsistent due to practical difficulties of sampling, injection and volume measurement.

- The online sample valve and loop made a dramatic improvement to the consistency of the results for CH_4.

- The FID cannot be used as a reliable measure of H_2S concentration. Perhaps there are ways of improving the detection method with respect to H_2S. This was outside the scope of the project.

- The FID can be used to check for the *presence* of H_2S in a gas stream, i.e. used as a qualitative measurement.

- The FID detection limit of H_2S was calculated at approximately 0.1 mol %.

- The need for calibration in the range of expected results is essential.

7. Final GC Operational Settings

Sample size:	1.0	m*l*
Injector temperature:	160	°C
Column temperature:	130	°C (constant)
Detector temperature:	240	°C
Pressure:	150	kPa
Purge flow:	0.5	ml/min
Carrier flow:	He	
Split ratio:	0	

Column: 3m x 1/8 inch Stainless Steel packed with HayeSep D, 100/120 mesh

Further column details from column suppliers:

"Hayesep D is a high-purity divinylbenzene polymer with 80 % highly-crosslinked DVB (no liquid stationary phase required). It combines high surface area with a high operating temperature. Hayesep D polymers offer superior separation characteristics for light gases e.g. CO and CO_2 from room air at ambient temperatures and the separation of acetylene prior to other C_2's. It is highly recommended for the separation of water and hydrogen sulphide."

A.5 Equipment related information

1. Pump calibration

The peristaltic pump gave a speed reading in rpm. It was calibrated by pumping a fluid onto a mass balance and recording the time. In this case, the fluid was methanol. The result is shown in Figure A.9.

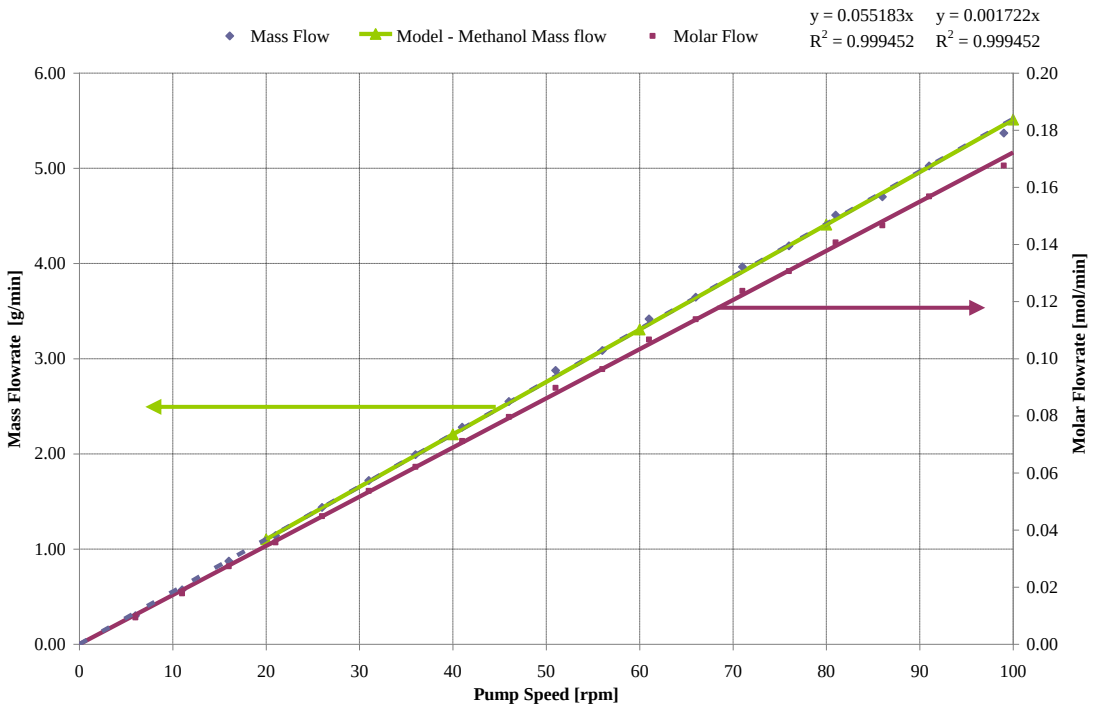

Figure A.9: Peristaltic pump calibration

The calibration equations were:

Mass flow (g.min^{-1}) = 0.055183×*W* (rpm)
Molar flow (mol.min^{-1}) = 0.001722×*W* (rpm)

These equations applied to methanol with a density of 0.7878 g.cm^{-3} and dilute mixtures (less than 20 mass %) *i*-propanethiol with a density of 0.8334 g.cm^{-3}.

2. Pressure drop calculation

Input Parameters			
Inlet pressure	P_1	2.00	bar
Inlet temperature	T	300	°C
Flowrate at temperature	Q	3 200	$cm^3.min^{-1}$
Velocity at temperature	u_0	0.09315	$m.s^{-1}$
Diameter of reactor	D	0.027	m
Length of packing	L_b	0.1	m
Mass of sorbent	m	61.26	g
Particle Properties - measured			
Particle density of sorbent	ρ_P	1500	$kg.m^{-3}$
Volume reactor	V	5.73×10^{-5}	m^3
Volume sorbent	V_s	2.00×10^{-5}	m^3
Bed porosity (spheres)	ε	0.4	[-]
Sphericity (sphere)	Φ_s	1	[-]
Particle Diameter (minimum)	D_p	0.005	m
Fluid Properties - from Perry and Green (1999)			
Gas constant	R_g	8314	$J.kmol^{-1}.K^{-1}$
Fluid		Nitrogen	[-]
Viscosity at temperature	μ	1.5866×10^{-5}	Pa.s
Density at temperature, pressure	ρ	1.1752	$kg.m^{-3}$
Ergun Equation			
Pressure drop	ΔP	29.96	Pa

The Ergun Equation, from Szekely *et al*. (1976) is:

$$\Delta P = \frac{150\mu u_0 L_b}{\Phi_s^2 D_p^2}\frac{(1-\varepsilon_b)^2}{\varepsilon_b^3} + \frac{1.75\rho u_0^2 L_b}{\Phi_s D_p}\frac{(1-\varepsilon_b)}{\varepsilon_b^3} \qquad \text{(A.5.1)}$$

Thus, a maximum pressure drop of 100 Pa (0.1 kPa) was accounted for.

3. Equipment description and operation

This section explains how the units in the apparatus physically function. It includes their basic operating principle and some advantages or disadvantages associated with their use and how they are integrated into the apparatus.

a. Mass flow controller

Flow range: 0-1.024 SLPM or 0-1.3088 $g.min^{-1}$ oxygen.

The controller takes gas from storage (for example, from a gas cylinder) and delivers a constant mass flow rate of the gas. The gas supply pressure must be above the discharge pressure. The controller moves a valve to ensure that the flow is constant.

The controller used was based upon the principle of a Laminar Flow Element and uses the Hagen-Poiseuille equation. By measuring the pressure drop, and by including the viscosity of the fluid (as a function of temperature), the pipe diameter, the volumetric flow is calculated.

$$Q = \frac{(P_1 - P_2)\pi r^4}{8\mu L} \qquad \text{(A.5.2)}$$

This is corrected to standard conditions using the measured pressure, temperature and compressibility factors.

$$\frac{Q_1}{Q_2} = \frac{Z_1}{Z_2}\frac{T_1}{T_2}\frac{P_2}{P_1} \qquad \text{(A.5.3)}$$

Where 1 is standard conditions and 2 is measured condition. The standard conditions used were 25 °C and 1 atm (6.996 PSI). The unit of Q_1 would be 'standard volumetric', such as standard litre. Finally, the mass flow is found by multiplication by the density (taken at the standard conditions).

Note that the controller performs all these calculations bar the last one i.e. the output is as standard litres per minute, SLPM. Also note that the gas type must be known as it is required for the calculation of the viscosity and the compressibility factors.

The advantage of this controller was that a very accurate mass flow was delivered. The controller could also account for variations in temperature and pressure on the inlet and outlet. For example, if the pressure on the outlet increased, the mass flow delivered would stay constant. A minor disadvantage was that the controller had a relatively limited range of 0.000 to 1.024 SLPM. However, increasing the flow meter's range decreased its accuracy of flow measurement.

b. Bubble flowmeter

A very simple flowmeter was used to measure the volumetric flowrate of the gas before it was discharged to the atmosphere (via an extractor fan). The gas passed upwards through a marked glass tube, similar to a burette. At the base there was a small reservoir of soap solution in a rubber teat. The teat is squeezed and a soap bubble was generated which was carried up the tube by the gas. The gas flowrate was simply the volume travelled by the bubble in a certain amount of time, for example, 30 cm^3 in 30 seconds is 1 $cm^3.s^{-1}$.

The bubble flowmeter was very simple to setup and use, and was independent of gas composition. However, it was dependent on the operator's ability to judge the movement of the bubble as it passed up the tube. It was estimated that the error is less than 1 $cm^3.s^{-1}$, which is about 10%.

c. Peristaltic pump

Flow range: 0-99 rpm: 0-5.46 $g.min^{-1}$ or 0-6.97 $cm^3.min^{-1}$ methanol.

The peristaltic pump has a very simple operation whereby flexible tubing was compressed by a roller that displaces liquid as it moved in a circular direction.

The flowrate of the pump was determined by the speed of the roller rotation, the diameter of the tubing and (to a far lesser extent) the density of fluid. The pump used had various speeds available, where the speed was measured in revolutions per minute (rpm). It thus had to be calibrated according to the fluid being pumped so that the rpm value corresponded to a mass flow unit such as grams per minute.

The calibration was performed easily enough. However, the flowrate could also be calculated from the geometry. The volumetric flowrate was given by the volume of the tube displaced during the time it takes the rollers to rotate. Then the mass flow can be found using the density of the fluid.

$$\dot{m} = \rho \dot{V} = \rho SL \times \text{rpm} = \rho\left(\pi r^2 D\right) \frac{1}{2}\pi D \ \omega \qquad \text{(A.5.4)}$$

$$\dot{m} = \frac{\rho \pi^2 D^2 r^2}{2}\omega \qquad \text{(A.5.5)}$$

Where S is the tube cross sectional area, L is the tube length, r is the tube radius, D is diameter of roller and ω is the speed, in rpm.

A criticism of peristaltic pumps is that they can deliver a 'pulsed' flow due to there being two rollers. However, they give very consistent and accurate average flow because the same volume is always displaced. They can pump against a high back pressure of up to 5 bar.

Assuming that the liquids are incompressible, the density is constant and hence the volumetric flowrate is directly proportional to the mass flowrate.

A major advantage of the pump is that can deliver very low flows (of the order of less than 1 m*l* per minute), which was in the range required for this experiment. Also, no contamination or corrosion occurs as the fluid was only in contact with the tubing material.

d. Gas analyzer

The gas analyzer, Bacharach ECA 450, was designed for combustion gas analysis. Composition analysis was performed using electrochemical cells. Although it could analyze CO and CO_2, it was out of range for CO and the CO_2 reading was via a calculation whereby the combustion fuel (natural gas, coal etc.) was required. The oxygen reading, which was usually zero, was useful.

The analyzer worked by connected a sample probe to the gas stream .This took a gsa sample to the instrument for analysis. The probe included a thermocouple and a pressure gauge.

e. Heating wire

Since water was produced in the gasification reactions, it was essential to keep all subsequent gas piping above 100 °C to keep the water in the gas phase and prevent condensation in the system.

The heating was to an extent ad hoc. A variac supplied a current to the heating wire. The length of the wire determined its resistance and hence the voltage required to be set. The important aspect was determining the maximum voltage to ensure that the wire did not literally burn out. It was found that one variac was sufficient to heat all the sample lines to above 100 °C.

The temperature used was that of the sample loop. This temperature was required for calculations involving the GC composition analysis. It was usually about 110 °C.

4. A note on gas concentration units

A major problem was the definition of the H_2S concentration, as it is a function of temperature and pressure. The following relationships hold:

$$C_{H_2S} = \frac{n_{H_2S}}{Q} \qquad \text{(A.5.6)}$$

C_{H_2S}	concentration of H_2S	[$mol.m^{-3}$]
n_{H_2S}	molar flowrate of H_2S	[$mol.s^{-1}$]
Q	total volumetric flowrate at temperature T	[$m^3.s^{-1}$]

Although n_{H_2S} is constant, the volumetric flowrate changes according to an equation of state:

$$Q = \frac{n_t \times Z \times R_g \times T}{P} \qquad \text{(A.5.7)}$$

n_t	total molar flowrate	[$mol.s^{-1}$]
Z	compressibility factor	[-]
R_g	gas constant	[$J.mol^{-1}.K^{-1}$]
T	absolute temperature	[K]
P	pressure	[Pa]

If there are reactions, the n_t value would change as well.

It made practical sense to refer to the concentration at STP conditions, under constant gas composition.

The mole fraction of H_2S, y_{H2S}, assuming ideal gases, can be found as:

$$y_{H_2S} = \frac{n_{H_2S}}{n_t} = \frac{n_{H_2S}}{\frac{Q_0 P_0}{R_g T_0}} \qquad \text{(A.5.8)}$$

Where Q_0 was evaluated at P_0 and T_0, i.e. standard conditions, assuming there was no reaction.

Hence
$$C_{H_2S} = y_{H_2S} \frac{P}{R_g T} \qquad \text{(A.5.9)}$$

It is possible have the same *concentration* of H_2S at different pressure and temperature conditions by changing the mole fraction of the gas.

Since the mole fraction does not depend upon the process conditions, but simply on molar flowrates, it is the best indicator to use for H_2S composition.

To express the concentration of H_2S in a fluid solution in a mixture as ppm by mass, multiply by molar mass of H_2S and by the inverse of the density of the mixture. Unfortunately, if the density of the gas is unknown, this cannot be expressed.

$$C_{H_2S}\ \frac{\text{mol H}_2\text{S}}{\text{m}^3\text{ mix}} \times M_{H_2S}\ \frac{\text{g H}_2\text{S}}{\text{mol H}_2\text{S}} \times \frac{1}{\rho}\ \frac{\text{m}^3\text{ mix}}{\text{g mix}} \times 10^6 \rightarrow \text{ppm}\ \frac{\text{g H}_2\text{S}}{\text{g mix}} \qquad \text{(A.5.10)}$$

Note that the density of the mixture could be estimated by:

$$\rho = \frac{M_r P}{R_g T} \qquad \text{(A.5.11)}$$

Where M_r is the average molecular mass of the mixture, but this is unknown unless the exact mixture composition is known.

To express the concentration as ppm by volume, take the mole fraction and multiply by one million. This assumes that the gas is ideal. This is the most common measurement of dilute gas mixtures.

$$y_{H_2S}[\text{-}] \times 10^6 \rightarrow \text{ppm}\left[\frac{\text{m}^3\text{ H}_2\text{S}}{\text{m}^3\text{ mix}}\right] \qquad \text{(A.5.12)}$$

A.6 Packed bed reactor model

1. Conversion of the solid sorbent

The conversion of a particular reactant is defined as the ratio of the number of moles of reactant that reacted to the number of moles of reactant initially, as explained in Section A.2. This analysis has been adapted by the author from Levenspiel (1999).

$$X = \frac{n_B^o - n_B}{n_B^o} = 1 - \frac{n_B}{n_B^o} \qquad \text{(A.6.1)}$$

X	conversion of solid B	[-]
n_B^o	initial number of moles of solid B	[mol B]
n_B	number of moles of solid B at some reaction time	[mol B]

Differentiating Equation (A.6.1) with respect to time,

$$\frac{dX}{dt} = -\frac{1}{n_B^o}\frac{dn_B}{dt} \qquad \text{(A.6.2)}$$

The reaction of gaseous species A with solid B can be expressed as

$$A_{(g)} + bB_{(s)} \xrightarrow{k_s} \text{Products} \qquad \text{(A.6.3)}$$

Reaction rate B

$$-\frac{dn_B}{dt} = -N_B \qquad \text{(A.6.4)}$$

Reaction rate A

$$-N_A = \frac{-N_B}{b} \qquad \text{(A.6.5)}$$

N_A	single particle reaction rate of A	[mol.s^{-1}]
N_B	single particle reaction rate of B	[mol.s^{-1}]
b	stoichiometric coefficient, defined by Equation (A.6.3)	[-]
k_s	surface reaction rate constant	[m.s^{-1}]

Note, b is defined as a *positive number*. Note the negative signs in Equation (A.6.4) and (A.6.5) are to show the *consumption* of A and B. Combining (A.6.2) with (A.6.4) and (A.6.5),

$$\frac{dX}{dt} = \frac{-1}{n_B^o} N_B = \frac{-b}{n_B^o} N_A \qquad \text{(A.6.6)}$$

Using the physical properties of the solid, the number of moles of solid can easily be found via the molar density, for spherical particles,both initally and at some reaction time *t*.

$$n_B^o = V_p \times \rho_p = \frac{4}{3}\pi R^3 \rho_p \qquad \text{(A.6.7)}$$

$$n_B = V_p \times \rho_p = \frac{4}{3}\pi R_C^3 \rho_p \qquad \text{(A.6.8)}$$

V_p	volume of solid (non-porous) spherical particle	[m^3]
ρ_p	molar density of solid reactant particle	[mol. m^{-3}]
R	particle radius	[m]
R_C	particle radius of unreacted core	[m]

Note that this assumes that the density of reactant and product is constant. The conversion can be expressed in terms of the particle's radius, from Equations (A.6.1), (A.6.7) and (A.6.8).

$$X = 1 - \frac{\frac{4}{3}\pi R_C^3 \rho_p}{\frac{4}{3}\pi R^3 \rho_p} = 1 - \left(\frac{R_C}{R}\right)^3 \qquad \text{(A.6.9)}$$

Hence $$R_C = (1 - X)^{1/3} R \qquad \text{(A.6.10)}$$

Equation (A.6.6) and (A.6.7) are combined into the form to describe the extent of reaction.

$$\frac{dX}{dt} = \frac{-b}{\left(\frac{4}{3}\pi R^3 \rho_p\right)} N_A \qquad \text{(A.6.11)}$$

Now an expression for N_A that describes the reaction of species *A* through the particle is required. This is available from an appropriate single particle model.

2. The shrinking core model

The following Equations (A.6.12) to (A.6.14) are expressions for the various resistances that occur in the reaction, from Doraiswamy and Sharma (1984).

As mentioned, since *A* is being consumed, the particle reaction rate is negative, as below.

Note that these are only applicable for *spherical* particles with kinetics of the *first order*.

External mass transfer through gas film

$$-N_A = 4\pi R^2 k_g \left(C_{Ab} - C_{Ai}\right) \qquad \text{(A.6.12)}$$

Diffusion through ash layer

$$-N_A = \frac{4\pi D_e}{\left(\frac{1}{R_C} - \frac{1}{R}\right)} \left(C_{Ai} - C_{As}\right) \qquad \text{(A.6.13)}$$

Chemical reaction

$$-N_A = 4\pi R_C^2 k_s \left(C_{As}\right) \qquad \text{(A.6.14)}$$

k_g	mass transfer coefficient	[m.s^{-1}]
D_e	effective diffusion coefficient	[m^2.s^{-1}]
k_s	surface reaction rate constant (first order)	[m.s^{-1}]
C_{Ab}	concentration of reactant gas *A* in bulk gas	[mol *A*.m^{-3}]
C_{Ai}	concentration of reactant gas *A* at solid interface	[mol *A*.m^{-3}]
C_{As}	concentration of reactant gas *A* at reaction interface	[mol *A*.m^{-3}]

The equations can be rearranged. Secondly, by the conservation of mass, the relations can be added to each other.

Mass transfer through gas film

$$C_{Ab} - C_{Ai} = \frac{-N_A}{4\pi R^2 k_g} \qquad \text{(A.6.15)}$$

Diffusion through ash layer

$$C_{Ai} - C_{As} = \frac{-N_A}{4\pi D_e}\left(\frac{1}{R_C} - \frac{1}{R}\right) \qquad \text{(A.6.16)}$$

Chemical reaction

$$C_{As} = \frac{-N_A}{4\pi R_C^2 k_s} \qquad \text{(A.6.17)}$$

Addition

$$C_{Ab} = -N_A \left[\frac{1}{4\pi R^2 k_g} + \frac{\left(\frac{1}{R_C} - \frac{1}{R}\right)}{4\pi D_e} + \frac{1}{4\pi R_C^2 k_s} \right] \qquad \text{(A.6.18)}$$

$$-N_A = \left[\frac{1}{R^2 k_g} + \frac{\left(\frac{1}{R_C} - \frac{1}{R} \right)}{D_e} + \frac{1}{R_C^2 k_s} \right]^{-1} 4\pi C_{Ab} \qquad \text{(A.6.19)}$$

Equation (A.6.10) can be substituted into (A.6.19) to account for R_C in terms of X,

$$-N_A = \left[\frac{1}{R^2 k_g} + \frac{1}{RD_e}\left((1-X)^{-1/3} - 1 \right) + \frac{1}{R^2 k_s}(1-X)^{-2/3} \right]^{-1} 4\pi C_{Ab} \qquad \text{(A.6.20)}$$

This expression of N_A is most useful and can be inserted into the conversion Equation (A.6.11) to relate to N_A and dX/dt,

$$\frac{dX}{dt} = \frac{-b}{\left(\frac{4}{3}\pi R^3 \rho_p \right)} N_A$$

$$\frac{dX}{dt} = \frac{b 4\pi C_{Ab}}{\left(\frac{4}{3}\pi R^3 \rho_p \right)} \left[\frac{1}{R^2 k_g} + \frac{1}{RD_e}\left((1-X)^{-1/3} - 1 \right) + \frac{1}{R^2 k_s}(1-X)^{-2/3} \right]^{-1}$$

$$\frac{dX}{dt} = \frac{3b}{\rho_p} \left[\frac{R}{k_g} + \frac{R^2}{D_e}\left((1-X)^{-1/3} - 1 \right) + \frac{R}{k_s}(1-X)^{-2/3} \right]^{-1} C_{Ab} \qquad \text{(A.6.21)}$$

This can be more conveniently expressed as

$$\frac{dX}{dt} = \beta(X) C_{Ab} \qquad \text{(A.6.22)}$$

where

$$\beta(X) = \frac{3b}{\rho_p} \left[\frac{R}{k_g} + \frac{R^2}{D_e}\left((1-X)^{-1/3} - 1 \right) + \frac{R}{k_s}(1-X)^{-2/3} \right]^{-1} \qquad \text{(A.6.23)}$$

Note that Equations (A.6.22) and (A.6.23) have been given in Doraiswamy and Sharma (1984) without the complete derivation given here.

Also note that the units of $\beta(X)$ are $m^3.mol^{-1}.s^{-1}$.

3. Model of Packed Bed Reactor

A standard model of a packed bed reactor is derived as follows. A gaseous species *A* reacts with a solid *B*. The assumptions are: plug flow, no axial dispersion and isothermal conditions. The unsteady gas phase mass balance across a control volume of reactor, $S\Delta z$, is:

Moles *A* in:	$F_A\|_z \times \Delta t$
Moles *A* out:	$F_A\|_{z+\Delta z} \times \Delta t$
Moles *A* reacted:	$\hat{r}_A \times (S\Delta z) \times \Delta t$
Moles *A* accumulated:	$\varepsilon_b (S\Delta z) \times \Delta C_{Ab}$

F_A	molar flow of *A*	[mol.s^{-1}]
C_{Ab}	concentration of *A* in bulk gas	[mol.m^{-3}]
$\hat{r}_A$	reaction rate of *A* per volume reactor	[mol *A*.m^{-3}.s^{-1}]
S	cross sectional area of reactor	[m^2]
Δt	differential time	[s]
Δz	differential bed distance	[m]
ε_b	bed voidage	[-]
u	superficial velocity	[m.s^{-1}]
Q	gas flowrate	[m^3.s^{-1}]

The balance is: *Moles A in – Moles A out – Moles A reacted = Moles A accumulated*

$$F_A|_z \times \Delta t - F_A|_{z+\Delta z} \times \Delta t - \hat{r}_A \times (S\Delta z) \times \Delta t = \varepsilon_b (S\Delta z) \times \Delta C_{Ab}$$

Dividing by $-\Delta z \Delta t$ and rearranging,

$$\frac{F_A|_{z+\Delta z} - F_A|_z}{\Delta z} + \varepsilon_b S \frac{\Delta C_A}{\Delta t} = -\hat{r}_A S$$

Taking the limit of $\Delta z \longrightarrow 0$, $\Delta t \longrightarrow 0$, $\Delta C_A \longrightarrow 0$,

$$\frac{\partial F_A}{\partial z} + \varepsilon_b S \frac{\partial C_{Ab}}{\partial t} = -\hat{r}_A S$$

Since $$F_A = Q \times C_A = u \times S \times C_{Ab}$$

Simplifying $$uS \frac{\partial C_{Ab}}{\partial z} + \varepsilon_b S \frac{\partial C_{Ab}}{\partial t} = -\hat{r}_A S$$

Finally, $$u \frac{\partial C_{Ab}}{\partial z} + \varepsilon_b \frac{\partial C_{Ab}}{\partial t} = -\hat{r}_A \qquad \text{(A.6.24)}$$

With the pseudo-steady state assumption,

$$\frac{\partial C_{Ab}}{\partial t} = 0 \qquad \text{(A.6.25)}$$

The reaction in a *particle* must be related to the reaction occurring in the *bed* as a whole. The volume of a differential element of the packed bed, is simply $dV = Sdz$, The volume of this element occupied by solids, dV_s, is a fraction of this (determined by the bed voidage).

$$dV_s = (1-\varepsilon_b)dV \qquad \text{(A.6.26)}$$

By definition $$dN_A^t = \hat{r}_A dV \qquad \text{(A.6.27)}$$

and $$dN_A^t = (-N_A)d\lambda \qquad \text{(A.6.28)}$$

N_A^t	total effect of reaction of A present in dV	[mol A.s^{-1}]
N_A	particle reaction rate of A	[mol A.s^{-1}]
$d\lambda$	number of particles in dV	[-]
dV_s	volume of solids in dV	[m^3]
V_B^o	initial volume of 1 particle	[m^3]

$$\text{number of particles} = \frac{\text{total solid volume}}{1\,\text{particle volume}} = \frac{dV_S}{V_B^o} = d\lambda \qquad \text{(A.6.29)}$$

Hence $$dN_A^t = -N_A \frac{(1-\varepsilon_b)}{V_B^o} dV \qquad \text{(A.6.30)}$$

And with comparison to Equation (A.6.27), the expression for $\hat{r}_A$ is

$$-\hat{r}_A = N_A \frac{(1-\varepsilon_b)}{V_B^o} \qquad \text{(A.6.31)}$$

And comparison of Equation (A.6.31) to Equation (A.6.6), to express in terms of conversion,

$$\frac{dX}{dt} = -\frac{b}{n_B^o} N_A \qquad \text{(A.6.6)}$$

(rearranged) $$N_A = \frac{V_B^o(-\hat{r}_A)}{(1-\varepsilon_b)} \qquad \text{(A.6.31)}$$

Combined
$$\frac{dX}{dt} = -\frac{b}{n_B^o}\frac{V_B^o\left(-\hat{r}_A\right)}{\left(1-\varepsilon_b\right)}$$

Hence
$$-\hat{r}_A = \frac{\left(1-\varepsilon_b\right)n_B^o}{-bV_B^o}\frac{dX}{dt} \qquad \text{(A.6.32)}$$

With the initial concentration of solid *B* defined as

$$C_B^o = \frac{n_B^o}{V_B^o} \qquad \text{(A.6.33)}$$

$$-\hat{r}_A = \frac{\left(1-\varepsilon_b\right)}{-b}C_B^o\frac{dX}{dt} \qquad \text{(A.6.34)}$$

Combination of Equation (A.6.34) with (A.6.22) gives

$$\frac{dX}{dt} = \beta(X)C_{Ab} \qquad \text{(A.6.22)}$$

$$-\hat{r}_A = \frac{\left(1-\varepsilon_b\right)}{-b}C_B^o\beta(X)C_{Ab} \qquad \text{(A.6.35)}$$

This is suitable for inserting into the reactor equation, Equation (A.6.24),

$$u\frac{dC_{Ab}}{dz} = \frac{\left(1-\varepsilon_b\right)}{-b}C_B^o\beta(X)C_{Ab} \qquad \text{(A.6.36)}$$

The variables can easily be separated for integration. The boundary conditions are:

At $z = 0$: $C_{Ab} = C_{Ab}^o$ (initial bulk concentration of *A*)

At $z = z$: $C_{Ab} = C_{Ab}$ (bulk concentration of *A* at a point *z* in the bed)

$$\int_{C_{Ab}^o}^{C_{Ab}}\frac{dC_{Ab}}{C_{Ab}} = \frac{\left(1-\varepsilon_b\right)}{-bu}C_B^o\int_0^z\beta(X)dz \qquad \text{(A.6.37)}$$

$$\ln\left[\frac{C_{Ab}}{C_{Ab}^o}\right] = \frac{\left(1-\varepsilon_b\right)}{-bu}C_B^o\int_0^z\beta(X)dz \qquad \text{(A.6.38)}$$

Let
$$\xi = \frac{\left(1-\varepsilon_b\right)}{bu}C_B^o \qquad \text{(A.6.39)}$$

Hence
$$C_{Ab} = C_{Ab}^{o} \exp\left\{-\xi \int_{0}^{z} \beta(X) dz\right\} \tag{A.6.40}$$

Equation (A.6.40) is recombined with Equation (A.6.22),

$$\frac{dX}{dt} = \beta(X) C_{Ab}^{o} \exp\left\{-\xi \int_{0}^{z} \beta(X) dz\right\} \tag{A.6.41}$$

Note that Equation (A.6.40) is dimensionally correct, of course.

4. Numerical solution procedure

It is easier to consider Equation (A.6.41) as being the combination of the two original equations, Equation (A.6.22) as the conversion-time profile, and Equation (A.6.36) as the gas concentration-bed length profile. Hence, there is a system of two partial differential equations.

$$\frac{\partial C_{Ab}}{\partial z} = -\xi \beta(X) C_{Ab} \tag{A.6.42}$$

$$\frac{\partial X}{\partial t} = \beta(X) C_{Ab} \tag{A.6.43}$$

The boundary conditions are expressed as

$$C_{Ab}(t, 0) = C_{Ab}^{o} \tag{A.6.44}$$

$$X(0, z) = 0 \tag{A.6.45}$$

A discretization is applied to the derivative in Equation (A.6.42) and to the conversion, *X*, shown as Equations (A.6.46) and (A6.47). Equation (A.6.47) is then treated as an initial value problem, and is integrated at the discrete points. The results are then updated for new evaluation of (A.6.46) which can be stepped forward by Δ*z*.

$$\frac{C_{Ab}^{i} - C_{Ab}^{i-1}}{\Delta z} = -\xi \beta\left(X^{i-1}\right) C_{Ab}^{i-1} \tag{A.6.46}$$

$$\frac{\partial X^{i}}{\partial t} = \beta\left(X^{i}\right) C_{Ab}^{i} \tag{A.6.47}$$

$$X^{i}(0) = 0 \tag{A.6.48}$$

5. Dimensionless form of the model

A useful procedure is to present the results in dimensionless form. This was achieved as follows.

From (A.6.23)
$$\beta(X)=\frac{bk_s}{\rho_p R}\left[\frac{k_s}{3k_g}+\frac{Rk_s}{3D_e}\left(\left(1-X\right)^{-1/3}-1\right)+\frac{1}{3}\left(1-X\right)^{-2/3}\right]^{-1}$$

Let
$$\varphi^2=\frac{3Rk_s}{D_e} \qquad \text{(A.6.49)}$$
$$\frac{Rk_s}{3D_e}=\frac{\varphi^2}{9}$$

and
$$\beta(X)=\frac{bk_s}{\rho_p R}\left[\frac{k_s}{3k_g}+\frac{\varphi^2}{9}\left(\left(1-X\right)^{-1/3}-1\right)+\frac{1}{3}\left(1-X\right)^{-2/3}\right]^{-1}$$
$$\beta(X)=\frac{bk_s}{\rho_p R}\hat{\beta}(X) \qquad \text{(A.6.50)}$$

where
$$\hat{\beta}(X)=\left[\frac{k_s}{3k_g}+\frac{\varphi^2}{9}\left(\left(1-X\right)^{-1/3}-1\right)+\frac{1}{3}\left(1-X\right)^{-2/3}\right]^{-1} \qquad \text{(A.6.51)}$$

Defining dimensionless concentration as

$$\hat{C}_{Ab}=\frac{C_{Ab}}{C^o_{Ab}} \qquad \text{(A.6.52)}$$

Equations (A.6.42) and (A.6.43) become

$$\frac{\partial \hat{C}_{Ab}}{\partial z}=-\xi\frac{bk_s}{\rho_p R}\hat{\beta}(X)\hat{C}_{Ab} \qquad \text{(A.6.53)}$$
$$\frac{\partial X}{\partial t}=\frac{bk_s C^o_{Ab}}{\rho_p R}\hat{\beta}(X)\hat{C}_{Ab} \qquad \text{(A.6.54)}$$

Defining dimensionless time and reactor distance as

$$t^*=\frac{bk_s C^o_{Ab}}{\rho_p R}t \qquad \text{(A.6.55)}$$

$$z^* = \xi \frac{bk_s}{\rho_p R} z = \frac{(1-\varepsilon_b) C_B^o k_s}{u \rho_p R} z \tag{A.6.56}$$

Note that these parameters, t^* and z^* have no physical meaning and are simply a result of the combination of physical properties. The advantage is that the equations are simplified.

These definitions result in the following equations:

$$\frac{\partial X}{\partial t^*} = \hat{\beta}(X) \hat{C}_{Ab} \tag{A.6.57}$$

$$\frac{\partial \hat{C}_{Ab}}{\partial z^*} = -\hat{\beta}(X) \hat{C}_{Ab} \tag{A.6.58}$$

The boundary conditions become

$$\hat{C}_{Ab}(t^*, 0) = 1 \tag{A.6.59}$$

$$X(0, z^*) = 0 \tag{A.6.60}$$

For solution, the same discretization as earlier applies.

$$\frac{\hat{C}_{Ab}^i - \hat{C}_{Ab}^{i-1}}{\Delta z^*} = -\hat{\beta}\left(X^{i-1}\right) \hat{C}_{Ab}^{i-1} \tag{A.6.61}$$

$$\frac{\partial X^i}{\partial t^*} = \hat{\beta}\left(X^i\right) \hat{C}_{Ab}^i \tag{A.6.62}$$

$$\hat{C}_{Ab}^{i=1}(t^*, 0) = 1 \tag{A.6.63}$$

$$X^{i=1}(0) = 0 \tag{A.6.64}$$

The solution was completed using a programme in MATLAB. Refer to Figure 9.12 for a solution with φ = 0.5.